UNIVERSITÄT ZU LÜBECK

From the Department of Infectious Diseases and Microbiology
of the University of Lübeck
Director: Prof. Dr. Jan Rupp

"Investigating the phenotypic plasticity and functional potential of gut bacteria to various IBD relevant stressors"

Dissertation
for Fulfillment of Requirements
for the Doctoral Degree
of the University of Lübeck

from the Department of Natural Sciences

Submitted by
Kathrin Schäfer
from Wiesbaden, Germany

Lübeck 2024

First referee: Prof. Dr. Jan Rupp

Second referee: Prof. Dr. Stefanie Derer-Petersen

Date of oral examination: 09.10.2024

Approved for printing. Lübeck, 03.06.2025

Table of Content

List of figures

List of tables

List of abbreviations

Abbreviation	Long Term
µg	micro gram
µl	micro litre
µm	micro meter
°C	degree Celsius
5-ASA	5-aminosalicylic acid
AIEC	adherent invasive *E. coli*
AMP	antimicrobial peptide
APC	Antigen presenting cell
$Aqua_{dest}$	aqua destillata: distilled water
ARTE	rapid antigen-specific T-cell enrichment
ATP	adenosine-tri-phosphate
B. longum	*Bifidobacterium longum*
B. hydrogenotrophica	*Blautia hydrogenotrophica*
B. producta	*Blautia producta*
B. thetaiotaomicron	*Bacteroides thetaiotaomicron*
BHI	brain heart infusion
BSA	Bovine serum albumin
CD	Crohn's disease
CFU	colony forming units
CO_2	carbon dioxide
COS	Columbia Agar with 5% Sheep Blood
cpm	cycles per minute
Cq	Cycle of quantification
DFG	Deutsche Forschungsgemeinschaft
DNA	desoxyribonucleic acid
DPBS	Dulbecco's Phosphate Buffered Saline
Dps	DNA-binding protein in starved cells
DSMZ	Deutsche Sammlung von Mikroorganismen und Zellkulturen
DTT	Dithiothreitol
E. coli	*Escherichia coli*
E. faecalis	*Enterococcus faecalis*
EAEC	enteroaggregative *E. coli*
Edta	Ethylenediaminetetraacetic Acid
EHEC	enterohemorrhagic *E. coli*
EM	electron microscopy
EPEC	enteropathogenic *E. coli*
EV	extracellular vesicle
FMT	faecal microbiota transplant
g/l	gram per litre
GIT	gastro intestinal tract
GO	Gene orthologous (data base)
H_2	hydrogen
h	hours
HEPES	4-(2-hydroxyethyl)-1-piperazineethanesulfonic acid

IBD	inflammatory bowel disease
IL	interleukin
LAB	lactic acid bacteria
LB	lysogeny broth
LPS	lipopolysaccharide
M. formatexigens	*Marvinbryantia formatexigens*
MA plot	M (log ratio) and A (mean average) plot
mg	milli gram
mg/ml	milli gram per millilitre
min	minutes
miTarget	Microbiome as therapeutic Target in IBD (research unit group)
ml	millilitre
mM	milli Molar
MPR	Multiplate Reader
N_2	nitrogen
NaCl	sodium chloride
NaOH	sodium hydroxide
ng/ml	nano gram per millilitre
nm	nano meter
NMR	Nuclear magnetic resonance
OD	optical density
OD_{max}	maximum optical density
OMV	outer membrane vesicle
OPLS-DA	Orthogonal Partial Least Square Discriminant Analysis
PBS	Phosphate Buffer Saline
PBMC	Peripheral blood mononuclear cells
PEB	PBS, 2 mM EDTA, 0.5% BSA
R. intestinalis	*Roseburia intestinalis*
rcf	relative centrifugal force
roc	regulator of colonization
ROK	repressor, open reading frame, kinase
RT	Room temperature
PCA	principle component analysis
PCR	polymerase chain reaction
Pfam	Protein families (data base)
PLP	pirin-like protein
rpm	rotes per minute
PBS	phosphate-buffered saline
PEP	phosphoenolpyruvic acid
pH	negative decimal logarithm of the H+ ion concentration
PVX	Chocolate agar PolyViteX
RNA	ribonucleic acid
SCFA	short chain fatty acids
SEP	sORF-encoded protein
SHIP	Src homology 2 (SH2)-containing inositol-5-phosphatase
SIHUMIx	extended simplified human intestinal microbiota
SNPs	single nucleotide polymorphisms
sORF	short open reading frame
T mem	Memory T-cell

T reg	regulatory T-cell
TEM	transmission electron microscopy
TFA	Trifluoracetic acid
TLR4	Toll-like-receptor 4
TSP	sodium trimethylsilyl propionate
UC	ulcerative colitis
UKSH	Universitätsklinikum Schleswig Holstein
vs	versus
v/v	volume in volume
x *g*	standard gravity
YCFA	yeast extract, castione and fatty acids (medium)

Abstract

Inflammatory bowel diseases (IBD) are characterized by chronic inflammations of the gastrointestinal tract. These multifactorial diseases are distinguished by an imbalanced immune response, the loss of tolerance to the resident gut bacteria and a reduced microbial diversity. Altered microenvironments in the diseased gut leads to functional shifts in the resident bacteria, therefore potentially shaping the microbial community, influencing single bacteria and the inflammation process. Hence, the aim of the project is to investigate the phenotypic plasticity and functional potential of three gut bacteria exposing them to various IBD relevant stressors. Growth experiments revealed that *B. thetaiotaomicron* and *B. producta* were negatively affected in acidic conditions, while *B. longum* was more affected by a higher pH. Additionally, the morphology of *B. thetaiotaomicron* was strongly affected in the acidic stress condition, while the other two bacteria did not display acidic specific morphological adaptations. Combining these phenotypic observations with functional assays and -omics methods this project elucidates comprehensive insights into the functional potential of bacteria. Observing the transcriptome of *B. thetaiotaomicron* grown in acidic conditions, the potential activation of multiple protection mechanisms of this bacterium grown in stressful conditions could be revealed. Metabolomic analyses of the three tested gut bacteria lead to the discovery of additional stress protection mechanisms. It was shown that the metabolome production was strain and pH dependent, identifying the potential key metabolite inositol, which is important in inflammation processes. Additionally, with proteomic analyses of *B. producta* grown in differently composed media, the production of SEPs in monoculture was discovered. Previously described to be only produced by this bacterium in community, this opens new interpretations concerning the role *B. producta* in the community and the potential function of SEPs. Furthermore, using the ARTE Assay the immunogenic potential of pathogenic *E. coli* and stressed *B. thetaiotaomicron* was investigated. While the *E. coli* provoked a T-cell reaction, *B. thetaiotaomicron* grown in pH 6 did not activate T-cells. Discovering the plasticity and reaction patterns of bacteria to different IBD-relevant conditions should elucidate potential functions of single bacteria and key metabolites or proteins which can be implied to a greater system, influencing the host, the disease or the bacterial community.

Zusammenfassung

Chronisch entzündliche Darmerkrankungen (CED) sind durch anhaltende Entzündungen des Magen-Darm-Trakts gekennzeichnet. Diese multifaktoriellen Erkrankungen zeichnen sich durch eine vermehrte pro-inflammatorische Immunantwort, den Verlust der Toleranz gegenüber den ansässigen Darmbakterien und eine verringerte mikrobielle Vielfalt aus. Es wird davon ausgegangen, dass sich durch übergeordnete physiologische Veränderungen, wie z.B. einer Verschiebung des pH-Wertes, die Zusammensetzung des intestinalen Mikrobioms ändert und dadurch Entzündungsprozesse nicht mehr kontrolliert werden können. Ziel des Projekts ist es daher, die phänotypische Plastizität und das funktionelle Potenzial von den drei Darmbakterien *B. producta*, *B. thetaiotaomicron* und *B. longum* zu untersuchen und sie CED-relevanten Stressfaktoren, wie beispielsweise einen sauren pH, auszusetzen. Die Wachstumsexperimente ergaben, dass *B. producta* und *B. thetaiotaomicron* in sauren Wachstumsbedingungen negativ beeinflusst wurden, während *B. longum* durch einen höheren pH-Wert im Wachstum beeinträchtigt wurde. Darüber hinaus wurde die Morphologie von *B. thetaiotaomicron* durch die sauren Stressbedingungen stark beeinflusst, während die anderen beiden Bakterien keine säurespezifischen morphologischen Anpassungen zeigten. Durch die Kombination dieser phänotypischen Beobachtungen mit funktionellen Assays und -omics Methoden liefert dieses Projekt umfassende Einblicke für das funktionelle Potenzial von Bakterien. Durch die Beobachtung des Transkriptoms von *B. thetaiotaomicron*, das in sauren Bedingungen gezüchtet wurde, konnte die mögliche Aktivierung mehrerer Schutzmechanismen dieses unter Stressbedingungen gezüchteten Bakteriums aufgedeckt werden. Metabolomische Analysen der drei getesteten Darmbakterien führte zur Identifizierung zusätzlicher Stressschutzmechanismen. Es zeigte sich, dass die Metabolomproduktion Stamm- und pH-abhängig war und führte zu der Identifizierung des potenziellen Schlüsselmetaboliten Inositol, welches bei Entzündungsprozessen wichtig ist. Zusätzlich konnte mit Hilfe von proteomischen Analysen von *B. producta*, welches in unterschiedlichen Medien gezüchtet wurde, die Produktion von SEPs in Monokultur entdeckt werden. Bisher wurde beschrieben, dass *B. producta* diese nur in bakterieller Gemeinschaft produziert. Dies eröffnet neue Interpretationen hinsichtlich der Rolle des Bakteriums in der Gemeinschaft und der möglichen Funktion von SEPs. Außerdem würde mit dem ARTE-Assay das immunogene Potenzial von pathogenen *E. coli* und gestresstem *B. thetaiotaomicron* untersucht. Während *E. coli* immer eine T-Zell-Reaktion hervorrief, aktivierte bei pH 6 gezüchtetes *B. thetaiotaomicron* keine T-Zellen.

Eine detailliertere funktionelle Charakterisierung von CED-relevanten Bakterien trägt dazu bei, die Pathogenese der Erkrankung besser zu verstehen und daraus Rückschlüsse auf mögliche therapeutische Interventionen ziehen zu können.

1. Introduction

1.1 Gastrointestinal system and the gut microbiome

1.1.1 The gastrointestinal tract is central component for overall health

The human gastrointestinal tract (GIT) is a central component for health and well-being. It harbours a complex microbial ecosystem consisting of bacteria, archaea and eukaryotes. Gut health and the gut microbiota are important for the function of the immune system and immune homeostasis, which displays a scientific area of clinical importance. The gut is inevitable interconnected to other organ systems by the microbiota and the immune system, for example via the gut-brain axis, the gut-skin axis or the gut-lung axis. Skin conditions are strongly dependent on the gastro-intestinal health and the gut microbiome through the gut-skin axis; several skin diseases such as Atopic Dermatitis, Acne vulgaris or Psoriasis are connected to gut microbiota dysbiosis or reduced microbial diversity (De Pessemier et al., 2021). There is strong evidence that between the gut and the nervous system a bidirectional interaction exists (gut-brain axis). While the brain has an important role influencing gut functions and conclusively modulating the microbiota compositions (Carabotti et al., 2015), on the other hand the microbiota is also able to communicate with the brain for example via the vagus nerve (Bravo et al., 2011). Due to the close proximity of the gut and the lung, this specific axis allows intensive interactions between the resident microbiome in the respective organs, allowing both microbial and immune interactions, to influence host health and diseases (Enaud et al., 2020).

1.1.2 Gut microbiome composition and importance for the host

Bacteria can be found everywhere in the human body and have a great influence on our life. The gut microbiome is crucial to the host's physical and mental health (Sarkar et al., 2018) (C. Liu et al., 2021). The number of bacterial cells in the human body is in fact the same order as the number of human cells, with a total biomass of about 0.2 kg. The greatest number of bacterial cells can be found in the colon with 10^{11} cells/ml content (Sender et al., 2016). The gut microbiota is essential for the host digestion, since the resident bacteria help e.g. to sustain the mucosal barrier integrity, provide nutrients or protect against pathogens. Bacteria can ferment non-digestible substrates like dietary carbohydrates or dietary fibre and produce short-chain fatty acids (SCFA) (Wong et al., 2006). One of the mainly produced SCFAs is butyrate, which is the main energy source for human colonocytes. Colonocytes play an important role in the human health, since they can induce apoptosis of colon cancer cells or have favourable effects on glucose and energy homeostasis (De Vadder et al., 2014).

For the hosts health it is crucial to maintain the balance in the immune system of eliminating pathogens, but maintaining self-tolerance to avoid autoimmunity (Wu and Wu, 2012). In a mouse

model it was demonstrated, that bacterial antigens are important for the generation and expansion of regulatory T cells (Tregs), which influence and regulate other cells in the immune system in a healthy individual, hence bacterial colonization is crucial for maintaining the immunological balance (Strauch, 2005). The microbiota appears to be a natural adjuvant for spontaneous T cell proliferation and the development of chronic intestinal inflammation (Erridge, 2010).

The early colonization of the infant GIT by microbes is an essential process in human life, since bacteria-host interactions have an important influence on human health and disease. After birth, the human intestine is rapidly colonized by a variety of microorganisms; this colonization is influenced by a multiple factors including diet, mode of birth, sanitation or antibiotic treatment (Rodríguez et al., 2015). The gut microbiota mostly consist of strict anaerobic or facultative anaerobic bacteria (Bull and Plummer, 2014). 16S DNA sequencing, meta-omics and microbial culturing allowed an extensive insight into the gut microbiota composition. The major bacterial taxa of the intestines of a healthy adult person are Firmicutes (*Lachnospiraceae* and *Ruminococcaceae*), *Bacteroidetes* (*Bacteroidaceae*, *Prevotellaceae*, and *Rikenellaceae*), Actinobacteria (*Bifidobacteriaceae* and *Coriobacteriaceae*) *Proteobacteria, Fusobacteria,* and *Verrucomicrobia;* while Firmicutes and Bacteroidetes are the prevailing members (Syromyatnikov et al., 2022) (Rinninella et al., 2019). The microbial composition varies along the gastrointestinal system. Due to different physiological properties of the organs along the GIT, the bacteria are also unevenly distributed. Several microenvironments, such as different pH or nutrient availability, exist across the intestine, hence the microbiota in the lumen of the intestine also differs in its composition from the ones in close proximity or attached to the epithelium (Swidsinski, 2005). Nevertheless, the gut microbiome also has an individual composition among different hosts and the metabolic activity of the gut microbiota is essential to sustain the host homoeostasis and health (Thursby and Juge, 2017). Investigating microbiome differences amongst humans from different ethnicities, genes from gut microbiomes of African, Asian and European were extracted and compared. Here, the different composition of the gut microbiome was potentially influenced by eating habits, the living environment and antibiotic usage (Chen et al., 2016).

1.1.3 Influencing factors on the healthy gut microbiome and community dynamics

Gut bacteria and the microbial composition in the human intestine are challenged by the host and environmental factors. Those internal and external selective pressures can include the hosts diet, the use of antibiotics, the hosts lifestyle, microenvironmental changes along the gastrointestinal tract and competition within the microbiota (Fig. 1).

The gastrointestinal system isn't a uniform environment, observing the pH along the GIT a great variation can be found. While the gastric pH is highly acidic and generally doesn't exceed a value of pH

2, the pH in the proximal small intestine is mostly around 6.6. In the following terminal ileum, the pH increases up to 7.5, followed by a sharp decrease in pH to 6.4 within the caecum. The pH in the colon was up to a final pH of 7 (Evans et al., 1988), while subsequently rising from the colon to the rectum up to pH 8 (Nugent, 2001).

Long-term diet influences the structure and activity of gut bacteria, but also short-term consumption of specific diets affects the compositions of the microbial community (David et al., 2014). It is reported that the microbiome can change between herbivorous and carnivorous functional profiles, which may reflect past selective pressures during the human evolution. For example, an animal-based diet increased the abundance of bile-tolerant microorganisms (e.g. *Bacteroides*) and decreased the levels of Firmicutes, which are able to metabolize dietary plant polysaccharides (David et al., 2014). In addition to the type of diet, obesity manipulates the diversity of the gut microbiota. Studies in mouse models comparing obese and lean mice revealed a reduction in *Bacteroidetes* and a greater abundance of Firmicutes in the obese mice (Ley et al., 2005). In another study, a bacterium with diet specific adaptations was investigated in a mouse model with diet-induced obesity, identifying diet as selective pressure. It was found, the human gut-associated *Eubacterium dolichum* (Firmicute) has distinct features that potentially provide competitive advantages in hosts consuming the Western diet, including import and processing of simple sugars (Turnbaugh et al., 2008).

Research has shown that exercise also acutely affects the gut microbiota. It was found that performing sports on a regular basis leads to physiological adaptions like the release of stress hormones, gastrointestinal hypoxia and hyperfusion. This eventually results in an increased intestinal permeability and oxidative stress in the GIT, which can influence the microbial composition in it. Having an active lifestyle also affects the mitochondria and their function, since it was shown that the gut microbiota and mitochondria communicate bidirectionally (Clark and Mach, 2017). Being physically active and paying attention to nutrition leads to less health complication due to pathogens. After a trial period, researchers also reported that probands ingesting protein supplements after exercising had an average of 33 % fewer medical visits, including 28 % less visits assignable to bacterial or viral infections (Campbell et al., 2007). Another example for the influence of lifestyle on the gut microbiota is smoking. In mouse experiments, smoking led to a microbial dysbiosis with differential abundance of bacterial species altering gut metabolites, which can cause an impairment of the gut barrier and is linked to the development of colorectal cancer (Xiaowu Bai et al., 2022).

The use of antibiotics is a major challenge for the gut microbiome. Antibiotics can induce changes in microbial composition, exerting a negative implication on the hosts health by changing bacterial functional attributes and potentially causing the formation of antibiotic-resistant strains. This can lead to short- and even long-term effects on the microbial balance, including a decrease in the richness and

diversity of the intestinal community (Thursby and Juge, 2017). A problem with the use of antibiotics is, that they do not only operate against pathogens, but also target commensal bacteria, causing microbial dysbiosis (Maier et al., 2021). In a study of Huang et al., a combination of four antibiotics decreased the diversity of the microbiota. It was shown that the antibiotics themselves were a threat for the resident gut bacteria, as well as the competition between different bacterial communities induced by the dysbiosis. It was observed that the diversity of the intestinal microbiota recovered after discontinuing the antibiotics. Nevertheless, the microbiota composition was persistently altered compared to before the treatment. Those changes that appear to be permanent, may also lead to the development of resistant species, reducing the abundance of potentially beneficial bacteria, and increasing the abundance of genera with pathogenic potential (Huang et al., 2022).

The microbial community can also be a challenging factor itself; competition and mutualism of the community members forcing additional selective pressures on each other. The bacterial community can encounter diversification of the microbial population by events like mutation or lateral gene transfer. The establishment of new bacterial functions promotes niche variation, creating a feedback loop in which a stronger diversification can occur (Thursby and Juge, 2017). Bacterial competition and niche occupation are also strain dependent. In various experiments, it was shown that during gut colonization of *C. elegans* with strains of *A. muciniphila* showed severe competitive exclusion, while *B. vulgatus* strains coexisted (Segura Munoz et al., 2022). *A. muciniphila* strains, have restricted and most likely overlapping niches, whereas *B. vulgatus* strains likely have a broader niche partitioning, while still showing ecological interactions pointing to competition (Segura Munoz et al., 2022).

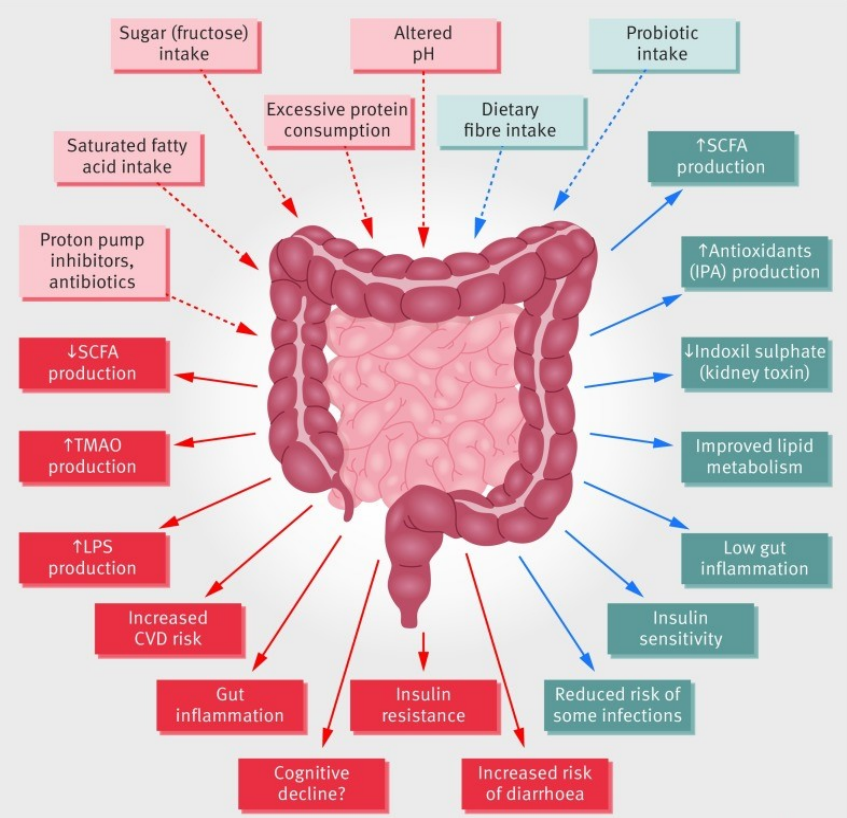

Figure 1: Interplay between environmental factors and microbiota in the gut. Summary of different factors (dotted arrows) acting on gut microbiota and their role in a healthy (blue arrows) or diseased (red arrows) gut. CVD=cardiovascular disease; IPA=indolepropionic acid; LPS=lipopolysaccharide; SCFA=short chain fatty acids; TMAO=trimethylamine N-oxide (Valdes et al., 2018).

1.2 Inflammatory bowel disease and microbiome

1.2.1 Chronic disease with a worldwide prevalence

Inflammatory bowel diseases (IBD) are chronic and relapsing diseases of the GIT. There are two main types of IBD, Crohn's disease (CD) and ulcerative colitis (UC) (Fig. 2). CD can occur anywhere between the mouth and the rectum with a patchy inflammation pattern occurring in all the layers of the bowel walls. In contrast, in UC the inflammation starts at the rectum and displays a continuous inflammation, affecting mostly the inner lining of the colon (Yang et al., 2019).

Globally, 4.90 million cases of IBD were reported in the year 2019 (Fig. 3), which displays an increase of 47.5 % compared to 1990 (Rui Wang et al., 2023). In 2013, there were about 320,000 IBD patients in Germany, the cases are distributed closely even between CD and UC patients. In most cases, IBD developed in young patients at age 15-35 (Bokemeyer et al., 2013) (Prenzler et al., 2011). Patients with IBD suffer from severe and painful symptoms concerning the GIT, but also extraintestinal manifestations of IBD can be noticed (Rothfuss et al., 2006). The symptoms of IBD include for example the passage of mucus and blood with bowel movement, diarrhoea and passage of blood from the anus.

Additionally, most patients experience anxiety, e.g. about the bathroom distance (Perler et al., 2019). The occurrence of these symptoms can be different comparing CD and UC. The most common health complications in CD were tiredness/fatigue and abdominal pain, while for UC most commonly the passage of blood with bowel movements and watery bowel movements were observed (Perler et al., 2019). Both, patients with UC and patients with CD have an increased risk to develop colorectal cancer (Jess et al., 2012) (Olén et al., 2020).

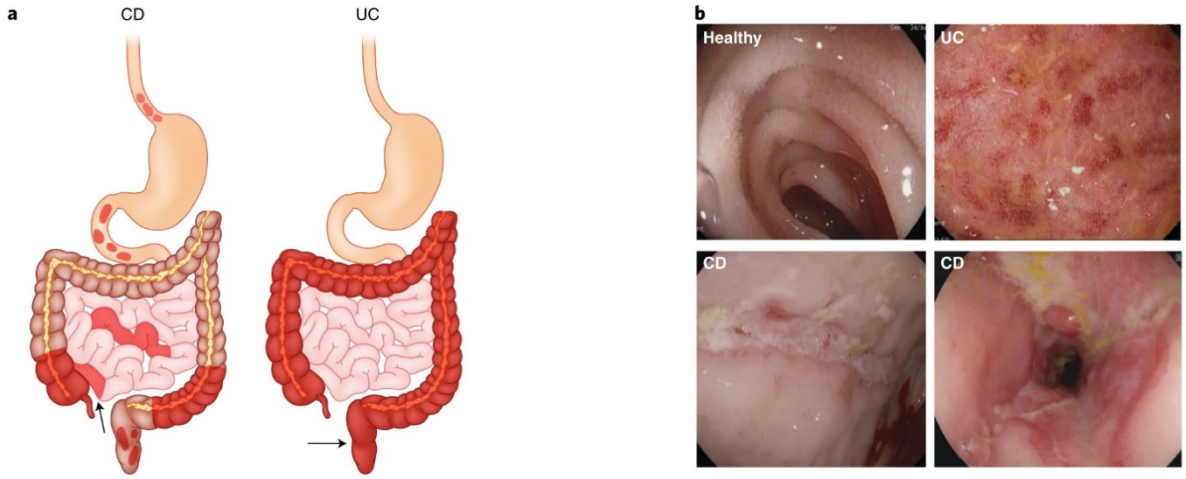

Figure 2: IBD lead to inflammation in the gastrointestinal tract. (a) Crohn's disease (CD, left) leads to a patchy inflammation across the whole gastrointestinal tract. Ulcerative Colitis (UC, right) causes a continues inflammation in the colon, starting from the rectum (b) Endoscopic pictures of a healthy, unaffected gut (left upper corner) and with CD (lower row) or UC (right upper corner) diseased guts (Neurath, 2019 (modified))

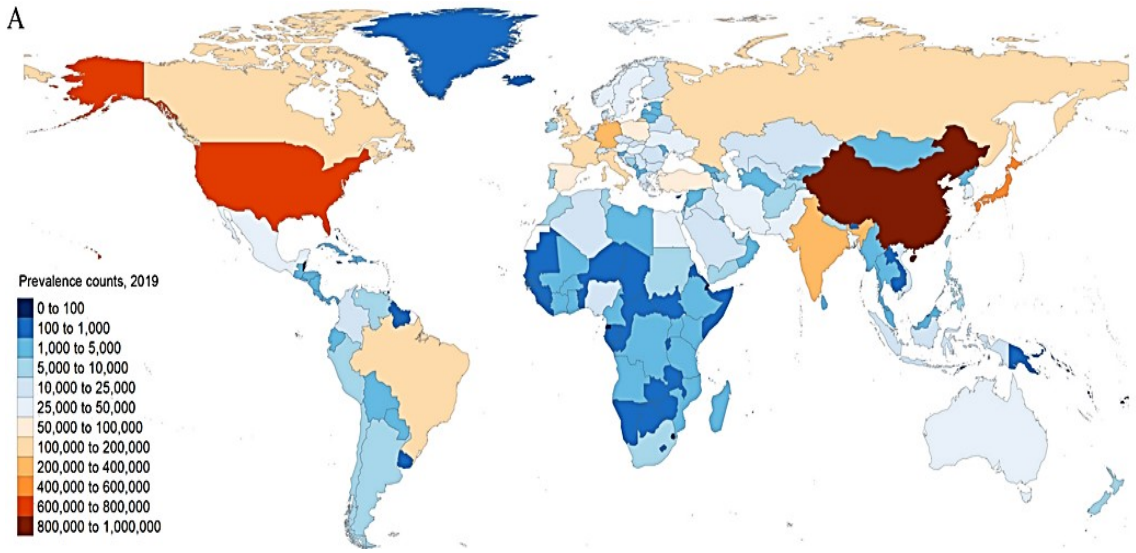

Figure 3: Global absolute number of Inflammatory bowel diseases prevalent cases in 204 countries and territories in the year 2019 (Rui Wang et al., 2023 (modified))

1.2.2 Causes of IBD and therapeutic approaches

While IBD is a multifactorial disease, many causes and reasons for the development of IBD are under investigation, but not completely elucidated yet. Parameters like genetic predisposition, the immune system, bacterial dysbiosis, antibiotic use and some environmental influences are in the discussion of being causes and risk factors of IBD. Additionally, a viral infection-induced autoimmunity is discussed as a pathology for IBD, especially in CD (Yang et al., 2019).

Studies have shown that not only the risk of IBD is increased when having relatives suffering from those diseases, but also ethnics seems to play a role. This is stressing the fact, that the development of IBD has a genetic predisposition. In Europeans the standardized prevalence of CD and UC was higher than the prevalence among South Asians and Hindus. The risk of developing UC in first degree relatives of European patients with UC and CD was increased. While the risk to develop disease among relatives of South Asian patients with CD was not increased, the risk of developing UC in relatives of patients with UC was (Probert et al., 1993). In a study enclosing the entire Danish population during 1977–2011, with obtaining information on diagnosis date of IBD and family ties, the risk of IBD is significantly increased in first -, second-, and third-degree relatives of IBD-affected cases. Up to 12 % of all IBD cases are family cases and the risk in young individuals is especially distinct (Moller et al., 2015). In cohort analysis, genome wide association studies, and meta-analyses, multiple UC and CD susceptibility genes could be identified. The identification of single nucleotide polymorphisms (SNPs) recently demonstrated a highly significant association with CD and could also confer genetic susceptibility to UC. This was confirmed for cases from the Australia and New Zealand IBD Consortium and also in multiple European populations (Doecke et al., 2013).

If microbial dysbiosis is a cause or an effect of IBD has not been clarified yet. However, the finding of dysbiosis during IBD and other non-inflammatory chronic immune diseases of the gut indicates that a dysbiosis leads to immune dysregulation. The use of antibiotics changes the gut microbiome, which might affect the risk for IBD or the composition of the gut microbiome. It was revealed that the use of antibiotics before diagnosis of CD occurred in 71 % of cases. Hence, there is evidence provided of an association between antibiotic use and the diagnosis of CD (Card, 2004). Another cohort study of Danish children born from 1995 to 2003 conducted with information on antibiotic prescriptions, IBD and potential other confounding variables also identified an association of antibiotic use and CD development in childhood. The use of antibiotics is a potential environmental risk factor for IBD, since children who were treated with antibiotics are more likely to be diagnosed with IBD (Hviid et al., 2011). Other factors which also influence IBD and the gut microbiome are smoking, oral contraceptive use, cardiovascular and neurological drugs, non-steroids or anti-inflammatory drug use (Bernstein, 2019) (Card, 2004).

IBD is a life-long disease. A lot of treatment options exist, but none of the available approaches appear to be optimal. Most of the medicine used for IBD treatment has side effects like diarrhoea, abdominal pain, headache and nasopharyngitis. Amongst the used drugs for the treatment of IBD are immunosuppressive drugs, biological agents, and antibiotics (Yao et al., 2021). The drug 5-aminosalicylic acid (5-ASA) is commonly used in the treatment of IBD because of its adequate clinical efficacy (Yao et al., 2021). Another option to treat IBD is the use of faecal microbial transplants (FMT) from healthy donors, which successfully used to improve CD (Kunde et al., 2013). The administration of antibiotics in IBD potentially decreases the microbial diversity. In mouse models, the changes in the intestinal microbiota can be observed due to the antibiotics' mechanisms of action, acting against Gram-negative and/or Gram-positive either aerobe or anaerobe bacteria, but also through competition between bacterial communities. The induced intestinal dysbiosis as well as the increased abundance of bacteria with pathogenic potential have been shown to also enhance the host inflammatory response (Huang et al., 2022). In some cases, surgery and stomas are treatment options in IBD. However, in patients with permanent or temporary stomas an increased anti-depressants use was noticed, probably due to elevated anxiety and depression (Blackwell et al., 2022).

1.2.3. Reduced microbial diversity in IBD

Various studies revealed changes of the intestinal microbiota composition during chronic gut inflammation and an overall reduced microbial diversity in patients with IBD. Mucosal inflammation in IBD is associated with a loss of the usually resident anaerobic gut bacteria. Here, the composition of the intestinal bacterial microflora seems to be more relevant for IBD pathogenesis rather than the occurrence of specific pathogens (Ott, 2004). In general, the abundance of Gram-positive bacteria is decreased, while an increase of Gram-negative bacteria can be observed in IBD patients (Loh and Blaut, 2012). By investigating faecal specimen and gut biopsies taken from diseased and healthy individuals, an imbalance of the four major bacterial phyla including Firmicutes, Bacteroidetes, Proteobacteria and Actinobacteria could be identified (Fig. 4). Interestingly, the bacterial groups which were changed in IBD patients were groups, which do not co-exist well with the resident commensal gut microbiota (Alam et al., 2020).

While UC and CD share many common features, some investigations suggest that two distinct subtypes on the microbiome level can be observed for the two subtypes of IBD (Fig. 4). For example, analysis indicated that in UC the extent differentially modulated the abundance of *Bifidobacteriaceae*, *Rikenellaceae*, *Christensenellaceae*, *Marinifilaceae*, *Desulfovibrionaceae*, *Lactobacillaceae*, *Streptococcaceae* and *Peptostreptococcaceae* families, while CD influenced the abundance of *Christensenellaceae*, *Marinifilaceae*, *Rikenellaceae*, *Ruminococcaceae*, *Barnesiellaceae* and *Coriobacteriaceae* families (Teofani et al., 2022). By investigating faecal samples of patients from four European countries applying 16S rRNA sequencing, dysbiosis was found to be significantly greater in

patients with CD than with UC. This was indicated by a more reduced diversity, a more altered microbiome and a less stable microbial community and leading to an identification of a specific microbial signature for CD allowing to discriminate CD from non-CD. While for example *Faecalibacterium prausnitzii* was decreased, *Escherichia coli* had an increased abundance in CD (Victoria Pascal et al., 2017).

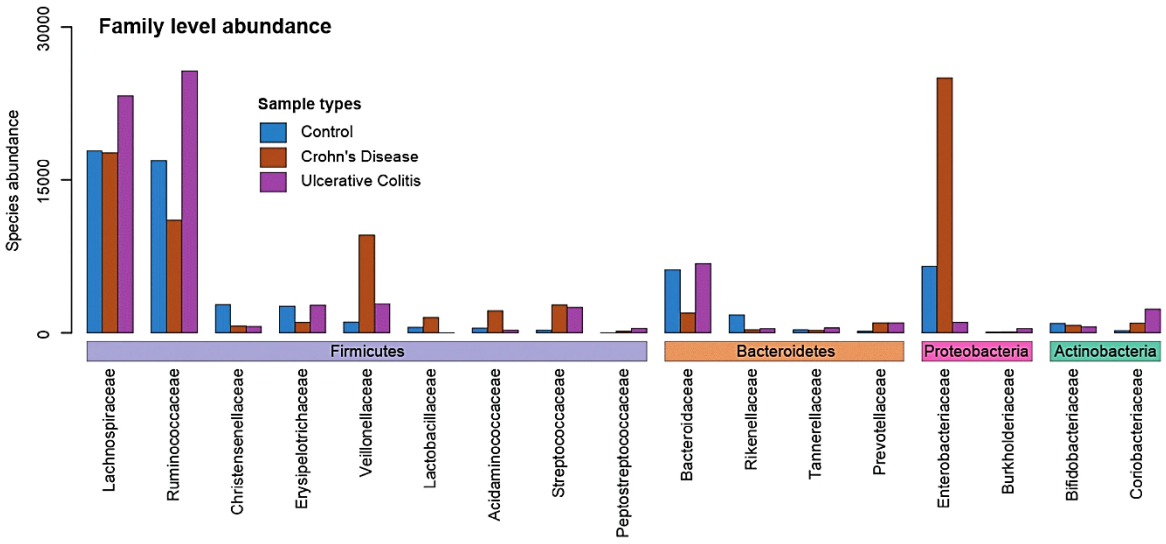

Figure 4: Abundance of bacterial families during IBD. Species abundance in the microbiome of Chron's Disease (brown), Ulcerative Colitis (purple) and in healthy controls (blue) (Alam et al., 2020 (modified))

1.2.4. Risk factors and changed microenvironmental conditions in a diseased gastrointestinal tract

Living organisms react to their environment. During a disease like IBD, the gut environment changes with inflammation flares. While the host can indirectly influence the gastrointestinal environment for example by following a specific diet, there are some factors like pH or the accumulation of bacterial metabolites, which are less easy to control, but have strong influences on the commensal bacteria in the intestinal environment.

Diet plays a crucial role in IBD development and the course of the disease. It is suggested that the intake of short sugars predisposes to colitis and increases its pathogenesis by microbiota modulation in mice (Khan et al., 2020). IBD is a modern disease with an increasing abundance due to the Western lifestyle and diet. The Western diet is characterized by the extensive consumption of high-fat/high-sugar products and fewer dietary fibres derived from plants (Cordain et al., 2005). Consuming high amounts of short chain sugars, such as glucose, fructose and sucrose results in changes in the microbial gut community and potentially lead to further increase of inflammation during disease. Hence, a high-sugar diet might be a critical trigger for IBD. While it was observed that the short-term intake of high-glucose/-fructose diet did not trigger inflammatory responses in a healthy gut, the gut microbiota

composition was already influenced, with increasing abundance of mucus-degrading bacteria such as *Akkermansia muciniphila* and *Bacteroides fragilis* (Khan et al., 2020). In addition to that, it was discovered that in mouse models the consumption of the complex saccharide beta-glucan reduced the level of inflammatory markers, recovered the signalling pathways and histological changes. Conclusively, dietary oat beta-glucans potentially reduce colitis and improve CD remission (Żyła et al., 2021).

The pH in the gut of patients with IBD is altered, but only little information is available. Studies suggest that the pH in patients with UC is generally lower compared to healthy controls, nonetheless for both, patients with UC and CD, the findings are inconsistent. For example, CD patients had comparable pH values in the small bowel and colonic segments to those of the healthy controls (Press et al., 1998). Similar observations were made for pH values in the proximal small intestine and in the left colon in patients with UC (Press et al., 1998). In contrast, other studies showed drastic acidic colonic environments in patients with active or inactive CD with a minimum colonic pH of 0.6 - 5.3 pH in the patients (Sasaki et al., 1997). In patients with UC a low intraluminal pH was observed, potentially due to higher concentrations of lactate, which occur in an active disease and was detected in the faeces. Hence, a low pH might be an indicator of severe activity of the disease (Fallingborg et al., 1993a). In severe colitis a lower faecal pH could be observed as well, additionally to very high lactate levels, high amounts of bicarbonate, potassium, sodium, chloride, and low short-chain fatty acid levels could be detected. In this case, it was suggested that the decrease of the intraluminal pH forces the bacterial metabolism to shift from short-chain fatty acid to lactate production, which might be the reason for the intraluminal accumulation of lactate (Vernia et al., 1988). A pH shift during IBD potentially has implications for the microenvironments, such as lower pH conditions, and the resident microbiota.

1.3 Single bacteria and their properties

1.3.1 Properties and functions of potentially beneficial and harmful bacteria in the GIT and in IBD

In a healthy gut the microbiota are regulators of digestion and maintaining the intestinal epithelium integrity. Commensal bacteria play an important role in the biosynthesis and absorption of nutrients and metabolites, such as lipids, glycans, amino acids, vitamins, and SCFA. Additionally, they have an important role against pathogen colonization by inhibiting their growth, consuming available nutrients or producing bacteriocins (Rinninella et al., 2019) (Gill et al., 2006). In a diseased gut, common bacteria are not able to fulfil their symbiotic function.

Potentially harmful bacteria in IBD showed the production of pro-inflammatory molecules and/or invasive properties. The changed microbial composition in IBD leads to species producing higher

amounts of bacterial antigens, such as lipopolysaccharides (LPS), subsequently leading to the recognition by the immune system and enabling pro-inflammatory responses (Loh and Blaut, 2012). Moreover, during CD remission a high number of *Enterobacteriaceae* with adhesion properties were observed (Seksik, 2003). This was also observed in paediatric IBD patients, where specific mucosa-associated species with increased invasive capacities were detected (Armstrong et al., 2019). On the other hand, some bacteria demonstrate preventive or favourable effects in IBD. For example, when lactic acid bacteria (LAB) and bifidobacteria are used as probiotics, which are able to produce lactic acid and have a tolerance to acidity, they can provide an improvement of clinical symptoms in IBD. They displayed beneficial effects such as the production of SCFAs and lactate, inhibiting the growth of potentially pathogenic organisms and influences the adherence of bacteria to the intestinal wall (Saez-Lara et al., 2015). Furthermore, in IL-10 gene-deficient mice, *Lactobacillus* sp. could limit the bacterial colonization of the intestine by exerting an antagonistic effect against pathogenic bacterial species, preventing their growth and mucosal adherence (Madsen et al., 1999).

1.3.2 Bacterial interactions with the Host: Metabolites, Vesicles and small Proteins

Bacteria have a variety of possibilities to interact with each other, the host and the hosts immune system mediated via nucleic acids, small molecules, metabolites, vesicles, or proteins. Metabolites are biomolecules that play a role in energy production and conversion. The gut microbiota is able to produce metabolites impacting the host, hence microbial species and their metabolic functions are proposed to possess an important role in the gut-systemic metabolic interplay (Visconti et al., 2019). Bacteria in the gut produce metabolites such SCFA, tryptophan catabolites, and polyamines, which are able to migrate widely into the host tissue, mainly through the small intestine (Zhang et al., 2023). So far, in microbiome studies, where the emphasis is mostly directed towards the impact of individual microbial taxa on human health, the metabolic potential of bacteria has been mostly overlooked (Visconti et al., 2019).

Bacterial vesicles are spherical nanosized particles, serving a plethora of biological functions. Vesicles derived from the outer membranes of Gram-negative bacteria are called outer membrane vesicles (OMVs). OMVs are packed with different proteins, virulence factors, lipopolysaccharides, phospholipids, peptidoglycan or enzymes, which are involved for example in the cleavage of complex polysaccharides. Therefore, they have been suggested to also have favourable functions within bacterial communities, providing the growth of other bacterial species due to releasing polysaccharide breakdown products into the lumen (Valguarnera et al., 2018). Considering the host interactions, OMVs can migrate across the epithelial barrier and mediate microbe-host cell crosstalk (Durant et al., 2020). Gram-positive bacterial extracellular vesicles (EV) are derived from the cytoplasmic membrane containing mainly proteins, lipoteichoic acid and peptidoglycan. Besides bacteria-bacteria interaction,

EVs are involved in immune evasion, host-cell modulation and have suspected pathophysiological functions (Kim et al., 2015) (Bose et al., 2020). In contrast to the whole bacteria itself, OMVS and EVs can cross from the gut lumen through the epithelial barrier, reach organs and tissues beyond the GIT, e.g. interacting with the immune system and helping to sustain intestinal homeostasis (Durant et al., 2020).

Bacterial sORF-encoded polypeptides (SEP) consisting of 50 - 100 amino acids were undiscovered for a long time, since they are difficult to detect using the conventional bottom-up proteomics. Additionally, SEP are encoded in small open reading frames (sORFs) which are over-looked in gene annotations, due to genome annotation algorithms applied with a 100 codon cut-off for annotation to reduce the error rate (Petruschke et al., 2020). They have several biological functions and are associated with larger membrane proteins, such as transmembrane proteins, to regulate their levels or activities or affecting the activity of transcription regulators (Gray et al., 2022). Additionally, it is reported that they are involved in stress responses, metabolic regulation, regulating membrane thickness/fluidity, pathogenicity, and adjusting metabolic activity to nutrient availability (Steinberg and Koch, 2021). Furthermore, they are suggested to have important functions in bacterial communities, like the human gut microbiome in the intestinal tract. For the bacterial community "simplified human intestinal microbiota" (SIHUMIx) several unknown SEPs were identified and investigated by Petruschke et al. Novel SEPs were discovered for *B. producta* within the SIHUMIx community, potentially harbouring antimicrobial properties. Therefore, SEPs contribute to shape the microbial community (Petruschke et al., 2021). Bacterial antimicrobial peptides (AMPs), also called bacteriocins, are oligopeptides with antimicrobial properties, which enter their bacterial target via nutrient-uptake systems, most frequently iron-uptake systems. Inside the target cell, they compromise a variety of essential processes, such as translation or ATP production. AMPs are secreted by both prokaryotic and eukaryotic cells as a defence mechanism (Steinberg and Koch, 2021).

1.3.3 B. thetaiotaomicron has a plethora of favourable features

Bacteroides thetaiotaomicron (*B. thetaiotaomicron*) is a Gram-negative anaerobic gut bacterium, firstly described in 1912 by Arcangelo Distaso (Rangarajan et al., 2020). It is a common member of the healthy human distal small intestinal and colonic microbiota (Xu et al., 2003). *B. thetaiotaomicron* may shape the metabolic milieu of the intestinal ecosystem and is known to break down several types of dietary plant polysaccharides, which is an otherwise difficult accessible source of nutrients for the human host. *B. thetaiotaomicron* has a variety of mobile genetic elements, which potential contribute to horizontal transfer of DNA between *B. thetaiotaomicron* and other bacteria, hence promoting microevolution (Xu et al., 2003). *B. thetaiotaomicron* has a genetic distinctiveness and a large

evolutionary distance to other phyla of bacteria such as Proteobacteria and Firmicutes. Some of the genetic distinctiveness could be related to the challenging environment in which it evolved and the competition with other bacterial species for survival in the colonic environment (Comstock and Coyne, 2003).

For *B. thetaiotaomicron* it was confirmed, to produce substantial amounts of OMVs (Fig. 5). Those particles allow ecological interactions within bacterial communities and are as well involved in host-bacteria relationships, in particular concerning the development of the host immune system (Valguarnera et al., 2018). Furthermore, the OMVs produced by *B. thetaiotaomicron* are reported to be able to transmigrate through epithelial cells. Jones et al., discovered that within hours of oral administration, vesicles produced by *B. thetaiotaomicron* can be detected in systemic tissues *in vivo*. Hence, these OMVs may be a long-distance microbiota-host communication system and interact with cells of the GIT through several endocytosis pathways (Jones et al., 2020). Another key role for *B. thetaiotaomicron* OMVs is mediating a balanced immune response to components of the microbiota locally and systemically during health; this mechanism is altered in IBD patients (Durant et al., 2020). These regulatory immune responses involve a balance of host protective Interleukin-6 (IL-6) and regulatory Interleukin-10 (IL-10) produced by dendritic cells. In IBD patients, there is a loss of regulatory IL-10 responses towards *B. thetaiotaomicron* OMVs which may contribute to the inflammation of the intestine and the development of CD and UC (Durant et al., 2020).

It is reported that *B. thetaiotaomicron* can have anti-inflammatory properties, may enhance the mucosal barrier function and limits pathogen invasions. A study of Delday et al., showed that treatment with *B. thetaiotaomicron* has protective effects in models of colitis in mice and rats, displayed by significant improvement of symptoms such as weight loss, colon shortening, histopathological damage and immune activation. Additionally, pirin-like proteins (PLP) of *B. thetaiotaomicron* reduced pro-inflammatory NF-κB signalling in Caco-2 epithelial cells. The data indicate that living bacteria or their products may be a new therapeutic approach to the current treatments for CD (Delday et al., 2019). For patients with UC, *Bacteroides* species are suggested as microbial biomarkers, opening the possibility for a non-invasive and accurate method to monitor this disease by observing the microbiome. In a study from Nomura et a., *Bacteroides* species displayed significantly lower relative abundance in patients with UC compared to healthy controls. Twelve key Bacteroidetes species could be identified, demonstrating negative correlations with UC activity. The loss of these species is suggested to be caused by UC exacerbation, since Bacteroidetes species may be unable to inhabit the niche of the damaged mucosa in highly severe UC (Nomura et al., 2021).

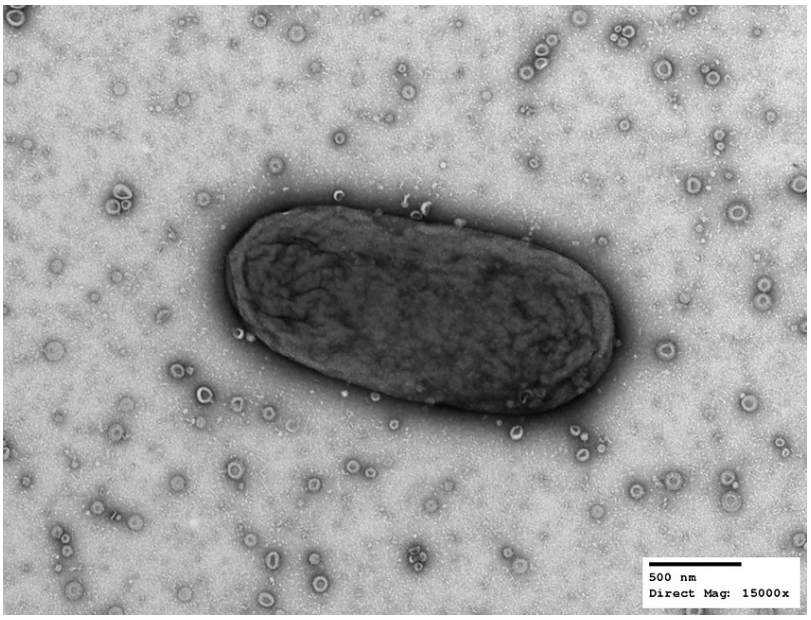

Figure 5: Transmission Electron microscopy picture of *B. thetaiotaomicron* with its produced OMVs. The direct magnification was 15,000, the scale bar represents 500 nm (Valguarnera et al., 2018)

1.3.4 B. producta ameliorates inflammation

The strictly anaerobic Gram-positive gut bacterium *Blautia producta* (formerly: *Ruminococcus productus, Peptostreptococcus productus* or *Streptococcus productus*) is mostly cocci-shaped and occurs solitary, in pairs or in short chains (Ezaki et al., 1994) (Liu et al., 2008). It is described to from colonies on blood agar that are 0.5 to 1.0 mm in diameter, circular, greyish white in colour and with a smooth surface. Growth of *B. producta* is stimulated by fermentable carbohydrates and carbon monoxide. Strains of *B. producta* are isolated from human faeces, since it is one of the dominant members of the human intestinal flora. Occasionally, it is also associated with bacteremia (Ezaki et al., 1994). *B. producta* DSM 2950 has been considered as a potential probiotic (X. Liu et al., 2021). It positively relieves inflammatory and metabolic diseases, and has antimicrobial mechanisms against some microorganisms. In a previous study, a multifaceted safety assessment of this strain was performed, which detected no safety concerns. Hence, it possesses the potential to be safe for human consumption (X. Liu et al., 2021). Just recently, a *B. producta* strain was discussed as a functional probiotic for colitis. In DSS-induced colitis mouse models, the oral administration of *B. producta* D4 could relieve inflammation by inhibiting the secretion of pro-inflammatory cytokines, reducing oxidative stress, preventing the damage of the intestinal barrier, regulating the TLR4/NF-κB signalling pathway, and reshaping intestinal microbiota (Mao et al., 2023).

1.3.5 B. longum is a known probiotic, which has the ability to improve inflammation

Bacteria within the genus *Bifidobacterium* are obligate anaerobes and belong to the high G+C Gram-positive *Actinomycetales.* They are one of the first bacterial colonizers of the GITs of new-borns and

predominate in breast-fed infants until weaning (Schell et al., 2002). They are represented in only to 3 - 6 % of adult faecal flora. Nevertheless, their presence is connected to advantageous health effects, such as prevention of diarrhoea, improvement of lactose intolerance and influence of host physiology, such as the immune response, by interfering with a regulatory serine protease (Schell et al., 2002). Currently, *Bifidobacteria* are used in the food industry as health-promoting microorganism. The species *Bifidobacterium longum* (*B. longum*) is a strict fermentative anaerobe (Yuan et al., 2006), which appears observed under a light microscope in different and irregular shapes such as irregular rods, V-shaped, Y-shaped, or clubbed rods (Young Park et al., 2011). This bacterium has a crucial role in maintaining the balance of common intestinal flora by producing lactic and acetic acids, which in turn avert the colonization of pathogens. One of its most important metabolic activities is the deconjugation of bile salts, which is important for the hosts bile acid metabolism (Yuan et al., 2006).

B. longum is able to reduce the symptoms of colitis and relieve chronic inflammation in mouse experiments and can be stably colonized in the human intestine (Yao et al., 2021). Lin et al. demonstrated that pre-treatment of *B. longum* BAA2573 improved symptoms and histopathological damage in DSS-induced colitis mice by altering the gut microbiota and downregulating harmful and opportunistic pathogens (Lin et al., 2023).

1.3.6 E. coli, a common gut habitant and opportunistic pathogen in IBD

The Gram-negative, rod shaped and flagellated *Escherichia coli* (*E. coli*) is a commensal gut bacterium in humans. As a pathobiont *E. coli* is well-studied in IBD, where it potentially plays an important role in IBD and the relapse of the disease, although mostly *in vivo* studies are missing up to this time (Dubinsky et al., 2022). Generally, *E. coli* is reported to be well-adapted to the environment that prevails in the IBD gut. Frequently, during inflammation a higher amount of nitrate can be observed, hence *E. coli* is more often abundant in patients with IBD, where it performs anaerobic respiration and grows faster compared to other bacteria (Dubinsky et al., 2022). Additionally, it was found that in IBD patients *E. coli* strains with a greater prevalence of virulence factors were present (Moustafa et al., 2018).

In CD, it is discussed that the presence of *E. coli* is one potential reason for the onset of disease, since an increased amount of *E. coli* strains with virulence properties were obtained from IBD patients compared to the healthy controls (Mirsepasi-Lauridsen et al., 2019). It could be noticed that bacterial isolates from patients with IBD had adhesive properties, which were similar to those of pathogenic intestinal *E. coli* strains (Burke and Axon, 1988). For UC it was also reported that *E. coli* from patients had adhered properties, which were more adherend to buccal epithelial cells compared to *E. coli* strains obtained from controls in *in vitro* experiments (Burke and Axon, 1987).

1.4 Culturomics, bacterial culturing and microbial characterization as an important complement in health research

Bacteria-host interactions are complex, multifaceted and represent a major current challenge for (medical) researchers. A wide range of bacterial species are still undiscovered or not further described and investigated. Up to 70 % of bacteria comprising the gut microbiota have not been cultured so far and 40 % of their protein-coding sequences have no functional annotations (C. Liu et al., 2021). One tool to acquire information about these missing bacteria is Culturomics. Defined by Greub (2012) as a "method allowing the description of the microbial composition by high-throughput culture" with the ability to detect minority populations cultured from biological samples, Culturomics was established 2012 by Lagier et al. (Greub, 2012) (Lagier et al., 2012). Investigating the human microbiome via Culturomics expands the comprehension concerning the repertoire of human microbes by discovering new taxa and the identification of rare bacteria (Diakite et al., 2020). It displays a strong tool to complement metagenomics in the study of the human gut microbiome (Lagier et al., 2012). Thereby, culturing these bacteria opens possibilities to discover unknown genes of interest and the production of specific metabolites (C. Liu et al., 2021). For example, bacteria can be used as biomarkers in diseases, targeted cultures allow the provision of biological material for *in vitro* experiments in medical research and finally optimizing cultural approaches opens the possibilities for bacteriotherapy (Diakite et al., 2020).

Bioreactors may be a promising strategy for studying the importance of single bacterial isolates in a community, since culture conditions within the bioreactors can be strictly controlled. The use of defined microbial consortia can additionally serve to investigate a system, which allows for manipulation and expand the experimental set up (Oliphant et al., 2019). Nevertheless, it is important to also investigate single bacterial isolates in mono culture. A pure bacterial culture is crucial for the discovery of bacterial virulence, its antibiotic susceptibility and its genome sequence in order to improve the understanding and, in case of pathogenic bacteria, finding possible treatment options of a caused diseases (Lagier et al., 2015). Joining single bacterial culturing, Culturomics with other -omics methods can reveal functional potential of bacteria and provide further insight into bacteria-host interactions. A study combining microbiome and metabolome displayed a promising approach to evaluate host-microbiome interactions (Visconti et al., 2019). Investigating faecal and blood metabolites, the results indicated the role of the microbiome on the faecal and host systemic metabolism, where some key species and microbial functions, are associated with faecal and blood metabolic profiles. Hence, microbial metabolic pathways should be considered not only by their function, but also interpreted as representatives for microbial communities, interacting with their surrounding environment, while looking at functions rather than solely on taxonomy (Visconti et al., 2019).

1.5 Aims and Hypothesis

Altered microenvironments in a diseased gut lead to functional shifts in resident bacteria, consequently shaping the microbial community, potentially opening niches for pathogens and influencing the inflammation process. All of these effects have a direct impact on the host and the course of the disease. Hence, this thesis investigates the impact on bacterial growth and biomass formation of three gut bacteria, exposing them to different media with various stressors. Since a lower pH can be observed in the GIT of patients with IBD during flares of inflammation, the functional potential and plasticity of these bacteria during acidic stress and to other stressors are examined by morphological observations, metabolome analysis, transcriptome shifts, and their immunogenic potential towards T-cell reactions. The aim of this thesis is to characterize and discover the plasticity of the bacteria to different physiological relevant conditions to elucidate potential functions of single bacteria, which can be implied to a greater system. Recognising and characterizing changes in bacteria is important to assign meaning to the single bacterium and its products within a community during changing conditions of a diseased gut. Hence, further this project aims to identify key molecules, which influence the host immune response, the progression of IBD, and the bacterial community within the gut. With this thesis the following objectives were pursued:

I. Investigating the phenotypic plasticity of three bacteria to IBD-relevant stressors such as low pH, the presence or absence of SCFA and carbon sources in growth experiments and with morphological observations.
II. After identifying distinct growth differences or morphology changes to certain stressors, the resulting differentiate gene expression is investigated by transcriptomics. Since changes in the transcriptome subsequently lead to changes in metabolite and protein production, analyses of the intracellular metabolome and proteome are conducted.
III. Establishing qPCR-based culture experiments of *B. producta* and *B. thetaiotaomicron* to discover biological interactions.
IV. The hosts immune reaction and the immunogenic potential of various pathogenic *E. coli* and the potentially beneficial *B. thetaiotaomicron* is tested using the ARTE Assay.

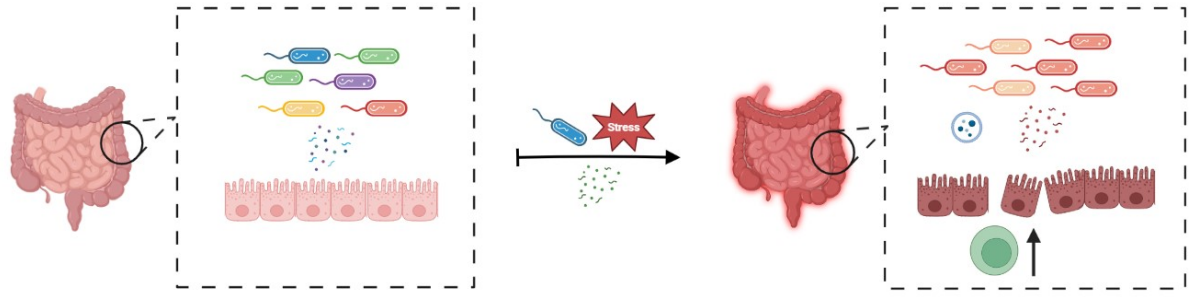

Figure 6: Graphical overview of the project in this thesis. In a healthy state, the host and the gut microbiota existing in a symbiotic state. Changing environment in a diseased gut lead to functional shift of the resident gut microbiota, elevating the hosts immune response and influencing the course of the disease.

2. Methods

2.1 Bacterial strains

For this thesis, the following bacteria were used: *Bacteroides thetaiotaomicron* DSM 2079, *Blautia producta* DSM 2950, *Bifidobacterium longum* NCC 2705, *E. coli* K12 and *Enterococcus faecalis* ATCC 29212 were either purchased from the German Collection of Microorganisms and Cell Cultures GmbH (DSMZ, Leibniz Institute) or taken from the frozen institute internal strain collection. The pathogenic *E. coli* strains with different pathovar SH096, SH038, SH006, SH103, SH114 and SH123 were obtained from faecal samples of patients from the routine diagnostics of the Department of Infectious Diseases and Microbiology, UKSH Lübeck (Tab. 1). Species identity was regularly tested using MADLI-TOF MS (Maldi Biotyper, MBT smart, Bruker Corporation).

Table 1: Pathogenic *E. coli* strains from stool samples

Strain number	SH096	SH038	SH006	SH103	SH114	SH123
Pathovar	EAEC	α-EAEC	EAEC	α-EAEC	EHEC	EPEC

2.2 Medium Preparation

2.2.1 YCFA Medium

The standard YCFA medium was prepared according to the recipe (DSMZ Media 1611) with the following changes: during the boiling step for 10 min, the medium was not gassed. Hemin was solved in 1 M NaOH before added to the media. Depending on the experiment, the pH was adjusted after autoclaving under sterile conditions with 10 M or 1 M NaOH or 25 % HCl to standard pH (pH 6,7-6,8), pH 6, pH 7 or pH 8. For the growth experiments, where the effect of different saccharides was tested, YCFA medium was prepared without any addition of glucose; subsequently different 1 M mono- or disaccharide solutions were added to the glucose free YFCA medium to reach 27.8 mM final concentration. For experiments with polysaccharides, if not stated otherwise, the sugar concentration was 1 % (v/v) in YCFA media. Furthermore, YCFA medium without the addition of the SCFA was prepared. Prior to each experiment, the medium was anaerobically gassed for minimum 24 h in an anaerobic chamber (H35, Don Whitley Scientific Limited, UK) with 85 % (v/v) N_2, 10 % (v/v) CO_2 and 5 % (v/v) H_2.

2.2.2 LB Medium

Lysogenic Broth (LB) medium consisting of 10 g/l peptone/tryptone, 5 g/l yeast extract and 5g/l sodium chloride was used for growth experiments. The pH was adjusted to pH 6 or pH 7 under sterile conditions after autoclaving. For anaerobic growth experiments, this medium was anaerobically

gassed for minimum 24 h in an anaerobic chamber (H35, Don Whitley Scientific Limited, UK) with 85 % (v/v) N_2, 10 % (v/v) CO_2 and 5 % (v/v) H_2.

2.2.3 BHI Medium

Brain-heart infusion (BHI) medium (Carl Roth) was prepared according to the declaration of the product and adjusted to pH 7.0. The BHI media was supplemented either with 2.5 g/l yeast extract, 100 ng/ml LPS (*E. coli* O128:B12, Sigma Aldrich) or the amount of SCFA corresponding to the standard YCFA media. Prior to each experiment, the medium was anaerobically gassed for minimum 24 h in the anaerobic chamber (H35, Don Whitley Scientific Limited, UK) with 85 % (v/v) N_2, 10 % (v/v) CO_2 and 5 % (v/v) H_2.

2.3 Detection of bacterial growth

2.3.1 Growth curves were obtained using a Multiplate reader

Constant maintenance cultures were performed on chocolate agar PolyViteX (Biomérieux) or Columbia agar + 5 % sheep blood (Biomérieux) at 37 °C in an anoxic workstation (H35, Don Whitley Scientific Limited, UK) with 85 % N_2, 10 % CO_2 and 5 % H_2. Bacterial precultures from a single colony were incubated overnight in 5 ml liquid medium in a Hungate tube without shaking. A 96-well microtiter plate (Greiner 96 flat bottom) was prepared with three media blanks. Bacteria were inoculated with 0.1 % (v/v) of the overnight preculture. Five technical replicates of this culture with a total volume of 200 µl were filled into the 96- well plate. Subsequently, the plate was sealed with petroleum jelly and parafilm to ensure anaerobic conditions outside of the anoxic workstation. Bacterial growth was measured every 10 - 20 min at 600 nm wavelength for 20 h or longer, depending on the bacterium, in a multiplate reader (BioTek, Epoch 2), with continuous shaking at a frequency of 237 cpm at 37 °C. Each experimental set up for each bacterium grown in the different conditions was repeated usually two to three times. Data were collected and exported via the Gen5 Version 10.3 program (BioTek, Agilent). The original raw data can be found on the institute server (IFIM), the digital lab book (in the folder “Wachstumskurven”) and on the laboratory Laptop connected to the multiplate readers (Folder “Kathrin”).

Gen5 provides information on the duration of lag phase, the growth rate (named in the program: Max V), the time when the specific growth rate was reached and calculates the linear regression (R^2 value) for each individual growth curve. Gen5 calculates the growth rate Max V using linear regression of the maximum slope. The specific growth rate is calculated by determining the slope of the linear regression obtained after plotting the change in OD against time during exponential phase. The doubling time (generation time of the bacteria) is calculated by the following formula:

$$\frac{\ln(2)}{\text{Max V}} * 60 = \text{doubling time [min]}$$

For further analysis Excel (Microsoft, Office Professional Plus 2019) was used. For each experiment, the bacterial replicates were combined to form the average and the blank was subtracted. The standard deviation was calculated for each measuring point of the growth curve using the command "=STABW.N". A cut-off for the calculation and evaluation of the growth data was made at latest at 40h, since the bacteria were in the stationary phase for a sufficient time.

2.3.2 Growth curves obtained by photometric measurements

For upscaling experiments 25 ml medium was inoculated with 0.1 % (v/v) of the overnight culture, using the same conditions as describe before (2.3.1). Regularly, subsamples were measured in 1.5 ml cuvettes (Sarstaedt) using a nanophotometer (Implen P330) at absorption 600 nm. If bacterial cultures reached an OD of 0.5, the samples were diluted 1:10 in the respective medium. Calculation and analysis were executed as described above (2.3.1).

2.3.3 BactoBox

To distinguish between life and dead bacterial cells the BactoBox® was used to monitor bacterial cell numbers. From a liquid culture a subsample was taken and vortexed vigorously. 101 µL of homogenized bacterial solution was transferred to 10 ml of BactoBox® diluent and vortexed for 15 seconds, generating a 1:100 dilution. Subsequently a 1:10,000 dilution was created as well. Before the actual measurement a clean program with a fresh disinfection vial needs to be performed. The BactoBox® measurements was started on the least concentrated sample. If the measurement was within the range 10,000-5,000,000 total particles/ml the measurement was accepted. If the measurement was not within the range another dilution was measured. The BactoBox provide the intact cell number and the total particle number. For the final results, the measured values need to be multiplied with the used dilution factor.

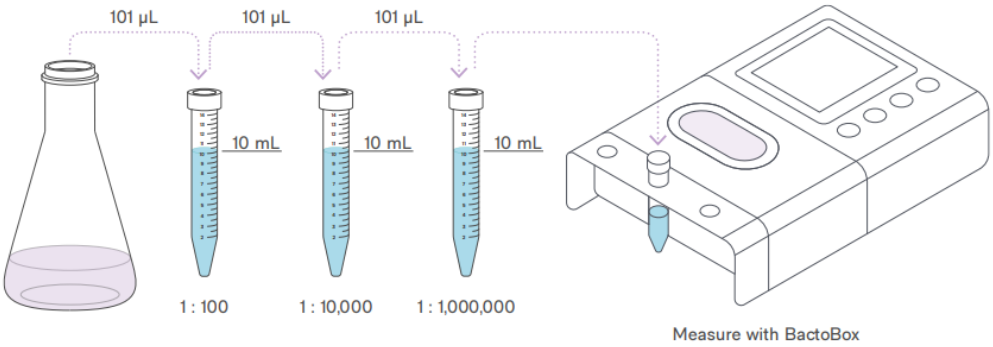

Figure 7: SBT BactoBox protocol. The bacterial culture is subsequently diluted in the diluent and measured with the BactoBox. Latest revision: May 1st 2023

2.3.4 Electron microscopy pictures

For electron microscopy (EM), bacteria were sampled (approx. 1 ml) at the end of exponential phase/ beginning of stationary phase. For each pH condition and bacteria biological duplicates were sampled, some of the experiments were repeated to support previous observations, resulting in either n= 2 or n= 4 sample size. The bacterial solution was centrifuged at 4000 – 6000x *g* for 10 min to settle the bacteria. The supernatant was discarded. The remaining cell pellet should have the size of a small droplet (about 10 µl). It was washed with DPBS and centrifuged down as described previously. Afterwards, the supernatant was discarded again and the cell pellet was resuspended with 1 ml Monti-Graziadei solution (2.5 % glutaraldehyde solution, provided by C. Örün, Institute of Anatomy, Lübeck). The bacteria were preserved in the fixative for at least 2 days at 4 °C. Afterwards, multiple pictures per bacterial sample were taken by Christo Örün from the Institute of Anatomy, University of Lübeck.

2.4 Lysate preparation and proteome analysis

An overnight culture of *B. producta* was prepared in 5 mL of liquid YCFA medium in a Hungate tube. YCFA and BHI media were prepared as described (2.2.1 and 2.2.3). YCFA medium adjusted to pH 6 or pH 7 and without SCFA (pH 7) was prepared; BHI medium adjusted to pH 7 and modified with and without SCFA, with LPS and yeast extract was prepared. 25 mL cultures with the respective media were inoculated with 0.1% (v/v) of a preculture. When the bacteria reached the exponential phase, they were harvested. The cells were centrifuged at 7,000 x g for 10 min at 4 °C (Rotina 38R, Hettich Zentrifugen). The cells were resuspended in pre-prepared lysis buffer (6 M guanidine hydrochloride, 100 mM HEPES, 20 mM NaCl, 1x c-complete protease inhibitor, pH 7.5). Lysis was then performed by a freeze/thaw cycle using a -80°C ethanol bath to freeze the cells for 30 seconds and sonicated in a

water bath for 30 seconds. This cycle was repeated 15 times. The cells were then centrifuged at maximum g (20817 rcf) for 20 min at 4 °C to remove cell debris (5417R, Eppendorf Centrifuge). The supernatant was transferred to a new tube. The cell debris was washed twice more with lysis buffer, the supernatants were combined and further stored at -80 °C.

The samples were sent and analysed by Jerome Genth and Prof. Andreas Tholey from the Institute for experimental medicine (UKSH Kiel), working group Proteomics in cooperation within the DFG research Unit miTarget (P8). The procedure is published in detail in Gent et al. 2023: Protein concentrations of extracted proteins were determined with the BCA assay (Thermo Fisher Scientific). For bottom-up full proteome analysis, the proteins were reduced with 10 mM dithiothreitol (DTT) (56°C, 800 rpm, 1 h) prior to alkylation with 55 mM iodoacetamide (RT, 800 rpm, 30 min). The samples were precipitated with ethanol, suspended in 200 µL digestion buffer (0.1 M TEAB, pH 8.5), digested with trypsin (Promega) at a protease-to-protein ratio of 1:40 (wt/wt) and incubated for 20 h at 37°C. The samples were afterwards acidified to pH 2-3 with 10% trifluoracetic acid (TFA), desalted by solid phase extraction and lyophilized. Peptide samples were suspended in loading solution (3% ACN and 0.1% aqueous TFA) for subsequent measurements. For depletion of high molecular weight proteins, a total of 400 µg of extracted protein was precipitated with ethanol and suspended in 80 µL 210 mM NaCl or 420 mM TEAB. Samples were solubilised, acidic depleted and incubated at 20°C for 1 hour at 1,300 rpm. The samples were centrifuged at 21,000 × g for 20 min at 20°C and the supernatant was transferred to a new tube and dried. For low molecular weight protein bottom-up preparation, proteins were suspended in 200 µL digestion buffer (0.1 M TEAB, pH 8.5), reduced, alkylated, trypsinsed, desalted and suspended in loading solution prior to LC-MS/MS analysis. Liquid chromatography-tandem mass spectrometry (LC-MS/MS) analysis was performed on a Q Exactive plus mass spectrometer coupled to a Dionex U3000 UHPLC (both Thermo Fisher Scientific). Peptides were concentrated on a reverse-phase trap column (Acclaim PepMap100, 2 µm, 100 Å, 75 µm × 20 mm) at 30 µL/min for 5 min with 2% ACN and 0.05% TFA before separation with a linear 120 min gradient of 95% eluent A (0. 1% formic acid [FA]) to 50% eluent B (80% ACN, 0.1% FA). The flow rate was 300 nL/min on a C18 reversed-phase analytical column (Acclaim PepMap100, C18, 2 µm, 100 Å, 75 µm × 500 mm) (both Thermo Fisher Scientific). The mass spectrometer was operated in positive ion mode. MS data were acquired using a data-dependent top10 method, dynamically selecting the most abundant precursor ions from the survey scan (300 to 1800 m/z, resolution: 70,000, automatic gain control (ACG) target: 3e6, maximum injection time (IT): 100 ms) with a 2.0 m/z isolation window for high energy collisional dissociation (HCD) fragmentation. Ions with unassigned and charge states +1 and >+8 were excluded. HCD spectra (resolution: 17,500, AGC target: 1e5, maximum IT: 100 ms, dynamic exclusion: 40 s) used a normalised collision energy (NCE) of 27. Three technical replicates

were used to measure the full proteome samples, while two technical replicates were used to measure the low molecular weight protein samples. For each in vitro culture, two biological replicates underwent full proteome and depletion analysis. The YCFA pH 6.0 condition was processed with full proteome analysis only and was therefore prepared as five biological replicates. MS/MS raw data files for bottom-up proteomics were processed in Proteome Discoverer (PD) (version 2.5, Thermo Fisher Scientific) using the integrated proteogenomics search database (iPtgxDB) for *Blautia producta* ATCC 27340 (accessed 28 November 2022) and 47 sequences of commonly observed laboratory contaminants. The standalone version of Pepquery (v. 2.0.2) was used for bottom-up validation of SEP identifications. This peptide-centric search engine was used to confirm the quality of the PSMs and to determine whether the matched sequences were unique or could be assigned to the *B. producta* proteome. The retrieved MS/MS spectra were converted to MGF format using msconvert from proteowizard. The final PepQuery command line was: java -jar pepquery-2.0.2.jar -db [fasta file] -ms [mgf files] -i [peptid list] -aa -hc TRUE -c 4 -maxVar 4 -itol 0.02 -o [output directory], allowing modification searching and amino acid substitution. The results were subsequently filtered to eliminate any peptides that matched the reference proteomes, leaving only those peptides that matched potential SEPs. The validated peptides were then analysed using the Proteomics Data Viewer and further evaluated against the *B. producta* proteome using NCBI Protein Blast. The peptides with a P value ≤0.01 that passed this filtering process were used to generate a high confidence list that served as the basis for the identification of SEPs. The BLASTp search was performed using the NCBI protein RefSeq database (30 December 2022). Search criteria included an E-value threshold of 1 × 10-5, a minimum sequence identity of 90% and a query coverage of 100%. The reference database used for comparison was the *B. producta* proteome (taxid:33035). To determine sequence conservation, the RefSeq database was searched for bacterial species (taxid:2) using the same E-value threshold, a minimum sequence identity of 50%, and a query coverage of 50%. The sequence coverage of the data was calculated using the protti package in R (v.4.2.2). The UpSet plots were generated using the upsetplot and matplotlib packages in Python (v. 3.11.1).

2.5 RNA Isolation and transcriptome analysis

RNA Isolation was performed with 200 µl subsamples of bacteria, grown in different pH in YCFA liquid culture until the end of exponential phase. The RNA isolation kit (Macherey-Nagel) and protocol "5.2 RNA preparation from up to 10^9 bacterial cells" was used. No changes in the suggested workflow from the protocol were made. The RNA concentration and purity were measured using the nanophotometer (Implen P330). Samples were stored at -80 °C.

For transcriptome analysis, the RNA was sent to the Competence Centre for Genomic Analysis (CCGA) in Kiel. The Illumina stranded total RNA Library was used with NextSeq 500 MID 2x75 bp sequencing. The results were analysed by Dr. Sebastien Boutin (Working group Nurjadi, UKSH Lübeck). The RNA data were analysed as followed: The raw reads were trimmed for quality control using fastp with the parameters -q 30 (cut after quality < 30) and -l 45 (length minimum 45 nt). The reads were afterwards mapped to their respective references using Reademption software to obtain read counts per gene. These gene read counts were normalised and analysed using DEseq2 to compare each group. Significant difference was selected with adjusted p-value < 0.05 and absolute log fold change > 2. For this thesis, the data of transcripts comparing pH 6 vs pH 7 was used, with pH 7 as divisor (reference library) and the data of pH 6 as numerator (comparison library). The original files can be found on the IFIM server in the institute or in the digital Lab book in the folder “Trancriptomics_RNA”.

The significant genes with an adjusted p-value (padjust) of < 0.05 were subsequently analysed using FUNAGE-Pro (http://funagepro.molgenrug.nl/, Anne de Jong, Sept 2022, Department of Molecular Genetics, University of Groningen, 19.01.2024) and FACoP.v2 (http://facop.molgenrug.nl/, May 2023. Anne de Jong. Department of Molecular Genetics, University of Groningen, 19.01.2024). The FUNAGE-Pro analysis regroups the genes into functional groups, which is another test to identify the pathways that are over/under regulated in the bacterium. The final annotation and assigning the molecular functions of the genes were evaluated using the QuickGO (https://www.ebi.ac.uk/QuickGO/, 24.01.24) or InterPro for classification of protein families (https://www.ebi.ac.uk/interpro/entry/pfam/#table, 24.01.24) databases operated by the European Bioinformatics Institute. These two databases were chosen to optimise the interpretation of the results.

2.6 Lysates for metabolome analysis of bacteria grown in different conditions

Of each respective bacterium five biological replicates were grown in 20 ml YCFA with pH 6, pH 7 or pH 8 until the end of exponential phase. Afterwards cells were centrifuged at 7,500x *g* for 10 min at 4 °C (Rotina 38R, Hettich Zentrifugen), followed by two washing steps with 1 ml DPBS using the same centrifuge set up. For the cell lysis, 750 µl ice cold 80 % methanol were added to the cell pellet. Subsequently, the pellet was vortexed and ultrasonicated in an iced water bath for 3*30 sec. The samples were stored at -80 °C. As a blank control for the metabolome analysis, 3*500 µl YCFA media were additionally provided.

The samples were sent and analysed by Dr. Silke Heinzmann and Dr. Alesia Walker, from Helmholtz Zentrum München GmbH, working group Analytical BioGeoChemistry, in cooperation within the DFG research unit miTarget (PZ): The 80 % methanol from the bacterial lysates was evaporated using SpeedVac and the pellet was reconstituted in aqueous NMR buffer. A Nuclear magnetic resonance

spectroscopy was performed. The nuclear magnetic resonance (NMR) spectra were processed, afterwards a normalization was carried out to an internal standard TSP as well as to TSP + bacterial biomass (OD). The datasets were prepared in two approaches: the complete dataset including all datapoints except the residual water peak resulting in 32,637 datapoints, and a dataset after a peak picking algorithm resulting in 418 datapoints. For this thesis, the latter was used for further observation. To discover the maximal variation in the dataset, an unsupervised PCA analysis was performed, using Matlab 2011b (Mathworks) with in-house developed codes. In this PCAs, only the scores plot was used to show the separation of bacterial strains and pH. Additionally, a supervised Orthogonal Partial Least Square Discriminant Analysis (OPLS-DA) analysis was performed, to find effects of pH change. Afterwards, the metabolites that were different in OPLS-DA analysis were identified. An overview of the detected metabolites can be found in the appendix (Fig. 33 - 35) and the raw data, which can be found at Dr. Silke Heinzmanns Lab, Helmholtz Munich and on the institute server (IFIM) or the digital lab book. Furthermore, a graphic summary of the detected metabolites is provided, which was made using Excel (Microsoft, Office Professional Plus 2019).

2.7 Bacterial interspecies interactions

2.7.1. Co-cultures

From an overnight culture, *B. thetaiotaomicron* and *B. producta* were inoculated in relation 50:50 in 25 ml YCFA media, calculating a start OD of 0.1 for each bacterium. 500 µl subsamples were taken every hour for 10 hours and one subsample after 24 hours of co-cultivation the next day. The samples were stored at -80 °C until further processing.

For DNA isolation, the samples were thawed slowly. An internal standard of *Enterococcus faecalis* ATCC 29212 (*E. faecalis*) suspension was added equally to the samples. The DNA Isolation Mini Kit (Qiagen) was used, following the protocol for Gram-positive bacteria, using 20 mg/ml Lysozyme in the first step. The protocol was followed accordingly. Alternatively, the DNeasy PowerSoil Pro Kit (Qiagen) was used for the DNA isolation. After isolation, the DNA concentration was controlled via nanophotometer (Implen P330) and/or Qubit (Invitrogen) using the high sensitive assay. The isolated DNA was stored at -20 °C.

To quantitatively differentiate the relation of the bacteria, a qPCR was conducted. Bacteria specific 16S primer for *B. producta* and *B. thetaiotaomicron* were designed prior with the Pick Primer option from the National Centre for Biotechnology Information (NCBI) and the *E. faecalis* primer were obtained from the internal primer collection of medical doctoral student Tim Wübken (Tab2). The Light Cycler SYBR Green 480 Kit was chosen, using a white 96-well plate with 0.5 µl of each primer and 2 µl DNA in

a total volume of 20 µl. Samples were performed in technical triplicates. A standard row of DNA from the respective bacteria were pipetted additionally. The samples were processed in the LightCylcer 480 (Roche) with the program parameters listed in Table 3. The second derivative calculation was used in the LightCycler® 480 software release 1.5.0, the calculated values were exported and further evaluated with NEBioCalculator (https://nebiocalculator.neb.com/#!/qPCRGen). On this website, for the qPCR quantification standard curve the Slope (m), intercept (b) and R^2 was determined by linear regression of the cycle of quantification (Cq) vs Log(amount). The amount of DNA for the qPCR sample quantification was calculated using the formula:

$$\text{Concentration} = 10^{((Cq - b)/m)}$$

The results were displayed in a graph using Excel (Microsoft, Office Professional Plus 2019).

Table 2: Primers of respective bacteria used for qPCR

	Forward Primer Sequence	Reverse Primer Sequence
B. producta	ggggAgTACgTTCgCAAgAA	CCCAACATCTCACgACACgA
B. thetaiotaomicron	CCgACTTCgTgAAgCTggAT	CTTCCggTACggCTACCTTg
E. faecalis	CgCTTCTTTCCTCCCgAgT	gCCATgCggCATAAACTg

Table 3: Program steps for PCR

Program step	Cycles	Temperature [°C]	Duration
Denaturation	1	95	2 min
Amplification	40	95	15 sec
		55	20 sec
		72	15 sec
Melting curve	1	95	1 sec
		50	30 sec
		95	continuous
Cooling	1	40	15 sec

2.8 Bacteria – Host interactions: ARTE assay

Bacteria were either grown on chocolate agar plates (PVX) or in liquid YCFA or in liquid LB medium, both media with either pH 6 or pH 7 (n = 1). Cells were firstly analysed, using a lysis buffer. After building of sufficient biomass on the plates, cells were harvested by scraping from the plate. For the harvest of liquid culture, OD 600 nm was measured until bacteria reached the end of the exponential phase. Then, the cells were centrifuged at 6000x *g* for 10 min at 4 °C (Rotina 38R, Hettich Zentrifugen) and the supernatant was discarded. After the cell harvest by scraping of the plate or the pellet formation by centrifugation, the bacterial cells were resuspended in 17.4 ml sterile $Aqua_{dest}$. Afterwards, 0.8 ml 1 N NaOH, 0.2 ml 2 N HCl and 2 ml 10×PBS pH 7.5 were added and the suspension was vortexed thoroughly. Samples were stored at -80 °C. To confirm cell death, the lysate was streaked out on a PVX plate and incubated overnight. Another 1 ml of NaOH was added to the lysate until no growth could be observed. Since the NaOH from the lysis buffer interfered with the immune assay, the lysis method was changed to a non-chemical method using heat. After reaching the exponential phase in 250 ml liquid media cells were centrifuged at 7,500x *g* for 10 min at 4 °C (Rotina 38R, Hettich Zentrifugen). The supernatant was discarded and cells were resuspended in 1 ml DPBS, followed by another centrifugation step with the same conditions. Afterwards, the supernatant was discarded, the cell pellet was resuspended in 900 µl sterile water and stored until further processing at -80 °C. Bacteria were lysed at 90 °C for 1.5 hours.

The samples were sent and analysed by Stephan Schneiders and Prof. Petra Bacher from the Institute of Clinical Molecular Biology (UKSH Kiel), Immunology Group, in cooperation with the DFG Research Unit miTarget (P1). The detailed methods are described in S. Schneiders doctoral thesis, a graphical overview is provided in Figure 8: Peripheral blood mononuclear cells (PBMC) were processed, their cell counts and the T-cell frequencies were determined. The PBMCs were stimulated with the bacterial lysates at a protein concentration of 40 µg/ml, pure antibodies were added and the PBMCs were incubated at 37°C and 5% CO2. Each lysate (n = 1) was tested once per donor. After 7 h of antigen stimulation, the PBMCs were harvested. The cells were rinsed with buffer, centrifuged and resuspended with matrix staining containing different concentrations of two anti-CD4 antibodies and incubated for 15 min at RT. In addition, anti-CD154 antibodies in the matrix staining allowed magnetic enrichment of memory T-cells (T mem) and regulatory T-cells (T reg). After a washing step, the cells were pooled and the pellet was resuspended with pre-mixed anti-Biotin and anti-PE MicroBeads and were incubated at 4°C for 15 min. The cells were afterwards washed in PEB and the cell suspension was added to a MACS column to bind magnetically labelled CD154+ and CD137+ cells and the surface was stained for 15 min at RT. The cells were subsequently washed, eluted and then fixed. The staining was stopped by rinsing the column, the enriched cells were eluted in PEB and flow cytometric counting of microbe-reactive CD4+ T-cell populations were acquired on a LRS Fortessa (BD Biosciences, San Jose,

CA, USA) or a Northern Lights 3000 (Cytek Biosciences). Afterwards, additional steps followed such as expansion and restimulation of antigen-reactive T-cells by sorting CD4+ Tmem cells with surface staining, IFN-γ and IL-22 secretion assays using detection kits (both Miltenyi Biotec) and the isolation of CD14+ naïve antigen presenting cells (APC). The data were analysed using GraphPad PRISM 9.4.1 (GraphPad Software, La Jolla, CA, USA). For the data of this thesis, the Kruskal-Wallis with Dunn's post hoc was used to compare multiple bacteria and conditions and the Mann-Whitney was applied to compare the two conditions pH6 vs. pH7 (S. Schneiders, 2024) (Rosati et al., 2022).

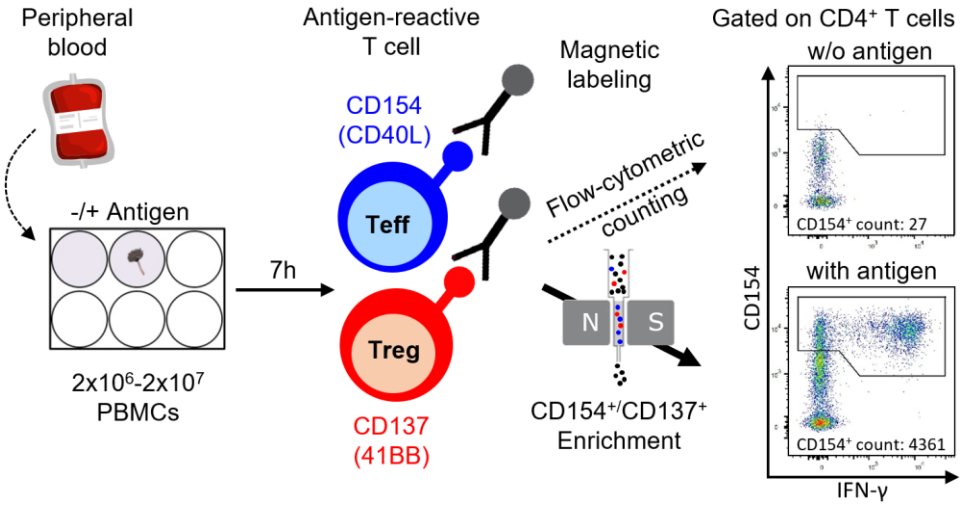

Figure 8: Workflow ARTE Assay. The isolated PBMCs contain T-cells and other antigen-presenting cells. The cells were presented with the processed bacterial lysates and 5-7 h in vitro activated. The activated T-cells express CD154 or CD137. Subsequently, they are labelled, enriched and their intracellular cytokines can be stained. After the cells are enriched and stained, a multiparameter flow cytometric analysis can follow (Doctoral thesis, S. Schneiders, 2024).

3. Results

3.1 Commensal gut bacteria exposed to changing environments

The three gut bacteria *Bacteroides thetaiotaomicron* DSM 2079, *Blautia producta* DSM 2950, and *Bifidobacterium longum* NCC 2705 were grown under different environmental conditions to observe the phenotypic plasticity of the single bacteria isolates. All results in this subsection 3.1 refer to data derived by multiplate reader measurements. The displayed experiments had n= 5 technical replicates, the mean value was used and the standard deviation is depicted. Additional data is given in the tables in the appendix (Tab. 4 - 8).

3.1.1 Bacteria grown in acidic environments displayed a reduced growth rate and biomass formation

All of the tested bacteria showed affected growth in different pH. In most growth experiments, an extended lag-phase, a slower growth rate and a reduced biomass formation could be observed for acidic conditions (Fig. 9).

B. producta had similar growth in media adjusted to pH 7 and pH 8, with a short lag phase which is characterized by no detectable growth, a growth rate of 2.2 h^{-1} respectively 2.8 h^{-1} at 11 h of cultivation and reaching a maximum OD of 0.69. Cultures grown in pH 6 media had an elongated lag-phase of 24 h and a slower growth rate of 0.57 h^{-1}. In general, growth appeared to be very diverse and unpredictable for bacteria at pH 6, which is also depicted by the high standard deviation of all evaluated parameters within the replicates (Appendix, Tab 4). A general maximum OD could not be calculated reliably for all replicates. Some replicates showed a biphasic growth curve (Fig 9 B).

B. thetaiotaomicron also had similar growth comparing cultures grown in pH 7 and pH 8 (Fig. 9 C). Here the growth rate was 2.3 - 2.5 h^{-1} and the maximum OD was 0.94, respectively 0.83. Replicates grown in pH 6 showed no growth, or an elongated lag phase of up to 10.2 h, a slower growth rate (0.77 h^{-1}) and a reduced biomass formation, reaching OD_{max} 0.62 and going into the stationary phase after 20 hours of cultivation.

Cultures from *B. longum* showed slightly different growth in all three tested pH media, with a similar lag phase in all tested conditions (Fig. 9 D). The best growth defined by the fastest doubling time of 18 min was observed in cultures grown in pH 7, whereas highest biomass formation (OD_{max} = 0.73) was observed in cultures grown in pH 6. However, bacteria grown in pH 6 showed a slightly reduced growth rate and doubling time. *B. longum* cultivated in pH 8 showed the highest reduction in the growth rate during exponential growth (Max V = 0.98 h^{-1}; doubling time = 42 min), reaching a OD_{max} of 0.49 h^{-1}. After a relatively short exponential phase, a phase with linear growth was observed.

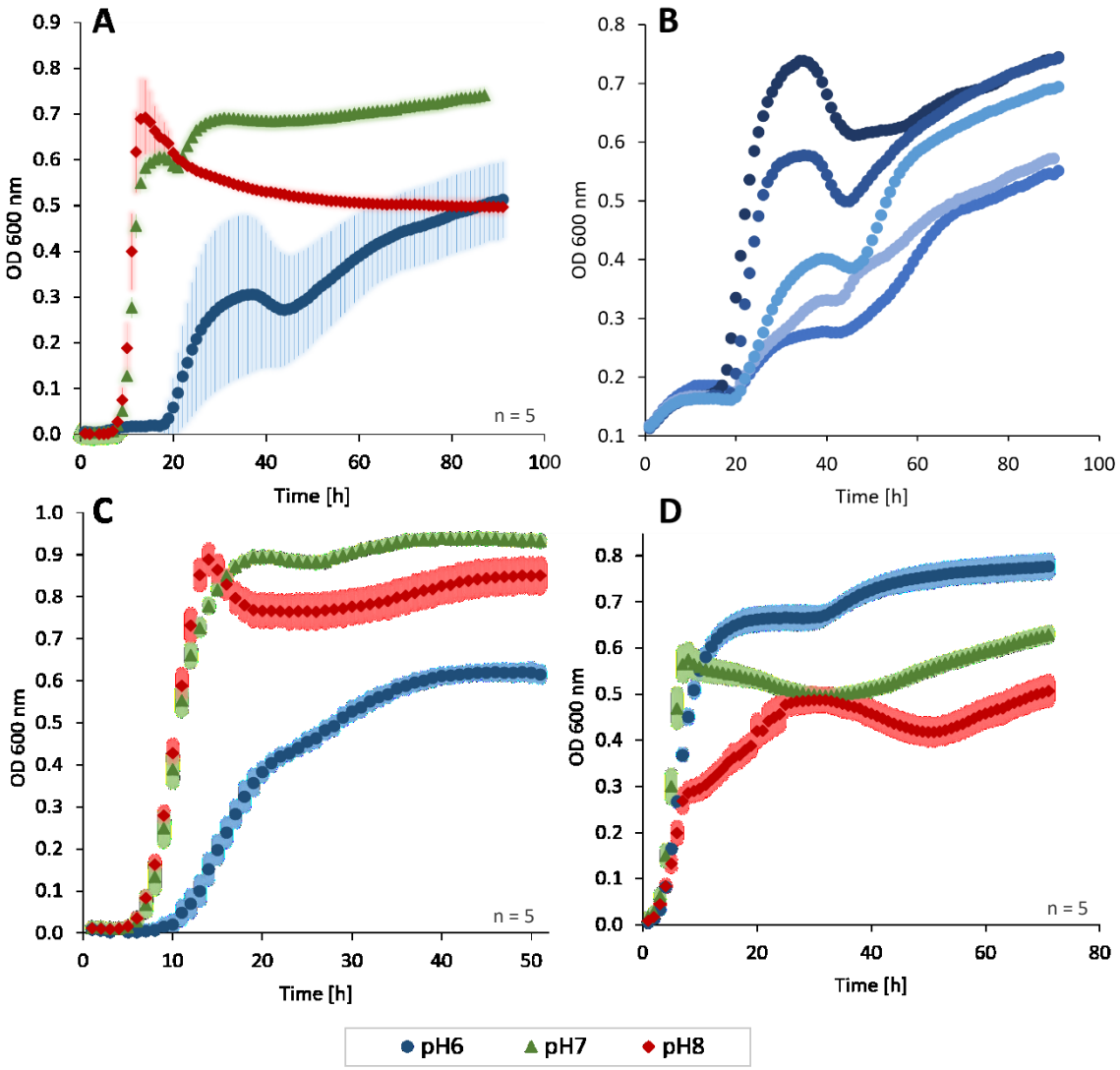

Figure 9: Growth of gut bacteria in YCFA media under 3 different pH conditions measured with the MPR. All conditions and bacteria were tested with n= 5 technical replicates, the mean value of the replicates with the standard deviation is displayed. (A) *B. producta* showed similar growth in pH 7 (green triangles) und pH 8 (red rhombus). In media with pH 6 (dark blue dots) growth was reduced. (B) The replicates of *B. producta* grown in pH6, some showed a biphasic growth (C*) B. thetaiotaomicron* showed good growth in pH 7 (green triangles) und pH 8 (red rhombus) and less sufficient growth with pH 6 (dark blue dots). (D) *B. longum* had the sufficient growth in media with pH 7 (green triangles) and pH 6 (dark blue dots), while replicates grown in pH 8 had an additional linear growth phase before entering stationary phase.

3.1.2 Bacteria grew differently providing various saccharides as main carbon source

The tested bacteria showed variable growth properties while providing mono-, di- and polysaccharides, with no common pattern amongst the three different bacterial species (Fig. 10 - 12). In the following section, all data points in the growth curves of cultures grown with monosaccharides are indicated with rhombuses, a mixture of monosaccharides is depicted by a star, growth with the

disaccharide sucrose is indicated by a dot, growth with polysaccharides is indicated with a square and growth without sugar is depicted with a cross.

B. producta showed better growth with the highest biomass formation of 0.54 - 0.64 in YCFA media supplemented with the disaccharide sucrose, compared to the standard YCFA media with glucose as main sugar source (Fig. 10). In YCFA with glucose, *B. producta* had a growth rate of 0.8 - 1.2 h^{-1}, a doubling time of 35 - 50 min with total biomass formation resulting in an OD around 0.4. Similar biomass formation and similar growth rates could be observed for this bacterium grown with the polysaccharide beta-glucan, and monosaccharide fructose as sugar sources. Noticeably, replicates grown in medium supplemented with the polysaccharide starch showed overly slow growth (growth rate: 0.2 - 0.4 h^{-1}; doubling time: 95 - 223 min) and only little biomass formation with an OD_{max} of 0.1 - 0.2. Comparing the growth kinetics of bacteria grown with starch with replicates grown in YCFA medium without any provided sugar, the growth rate, biomass formation, and growth patterns are similar low.

Since *B. thetaiotaomicron* is known to degrade various polysaccharides, a broader choice of polysaccharides and different saccharide concentrations were tested for this bacterium. Overall, *B. thetaiotaomicron* grew equally well with the polysaccharides laminarin, starch, beta-glucan, and mucin. The growth kinetics seems to be independent of the concentration and type of the given polysaccharide (Fig 11 A and B). After a short lag phase of 2.1 - 4.8 h growth started. The maximum OD for bacteria grown in medium supplemented with mucin was 0.27 - 0.32 for both concentrations, for laminarin 0.23 - 0.29 and for beta-glucan 0.23 – 0.29. More than double of the biomass formation can be observed for replicates grown in media with 0.1 % (v/v) glucose, reaching an OD of 0.63 - 0.66. In the case of bacteria grown with glucose, the concentration of this monosaccharide impacted the growth. Cultures grown in a concentration of 0.01 % showed a reduced growth and biomass formation (OD_{max} = 0.29 - 0.35), which was similar to cultures grown with polysaccharides. In biological replicates of these experiments (Fig 11 C), the growth of all bacteria with the different saccharides appeared to be generally lower. It can be noticed, that for cultures supplemented with the disaccharide sucrose, the growth rate and biomass formation was better compared to growth with the monosaccharides fructose, glucose and a mixture of fructose and glucose. The effect of an increased amount of glucose and sucrose to 0.5 % was tested and it did not affect the growth drastically (Fig 11 D).

Bifidobacterium longum shows consistent growth within the different growth experiments, making results comparable within the plates (Fig. 12). Medium comprising the disaccharide sucrose as main carbohydrate source, led to the best growth of *B. longum.* In all evaluated experiments, an OD_{max} of 0.40 - 0.44 was reached after a relatively short lag phase (2.4 - 3.5 h), a growth rate of 0.9 -1.3 h^{-1} and doubling time of 31 - 46 min. In media with the same amount of glucose bacteria reached only half of

the maximum OD (0.18 - 0.23). The growth rate and doubling time were additionally decreased with 43 - 55 min. In standard YCFA media (0.5 % = 27.8 mM glucose), *B. longum* showed the biggest biomass formation reaching a maximum OD of 0.5 and a doubling time of 27 min. With the polysaccharide beta-glucan bacterial cultures grew only slowly and with little to no biomass formation (OD_{max} 0.04 – 0.08), similar to the cultures grown in YCFA media without any saccharides (OD_{max} = 0.04 - 0.06). Providing starch as polysaccharide, this bacterium showed mostly low biomass formation (OD_{max} = 0.07 - 0.08) and slow growth rate (0.07 - 0.09 h^{-1}). Indistinct growth behaviour could be observed for replicates grown in YCFA medium with monosaccharide fructose.

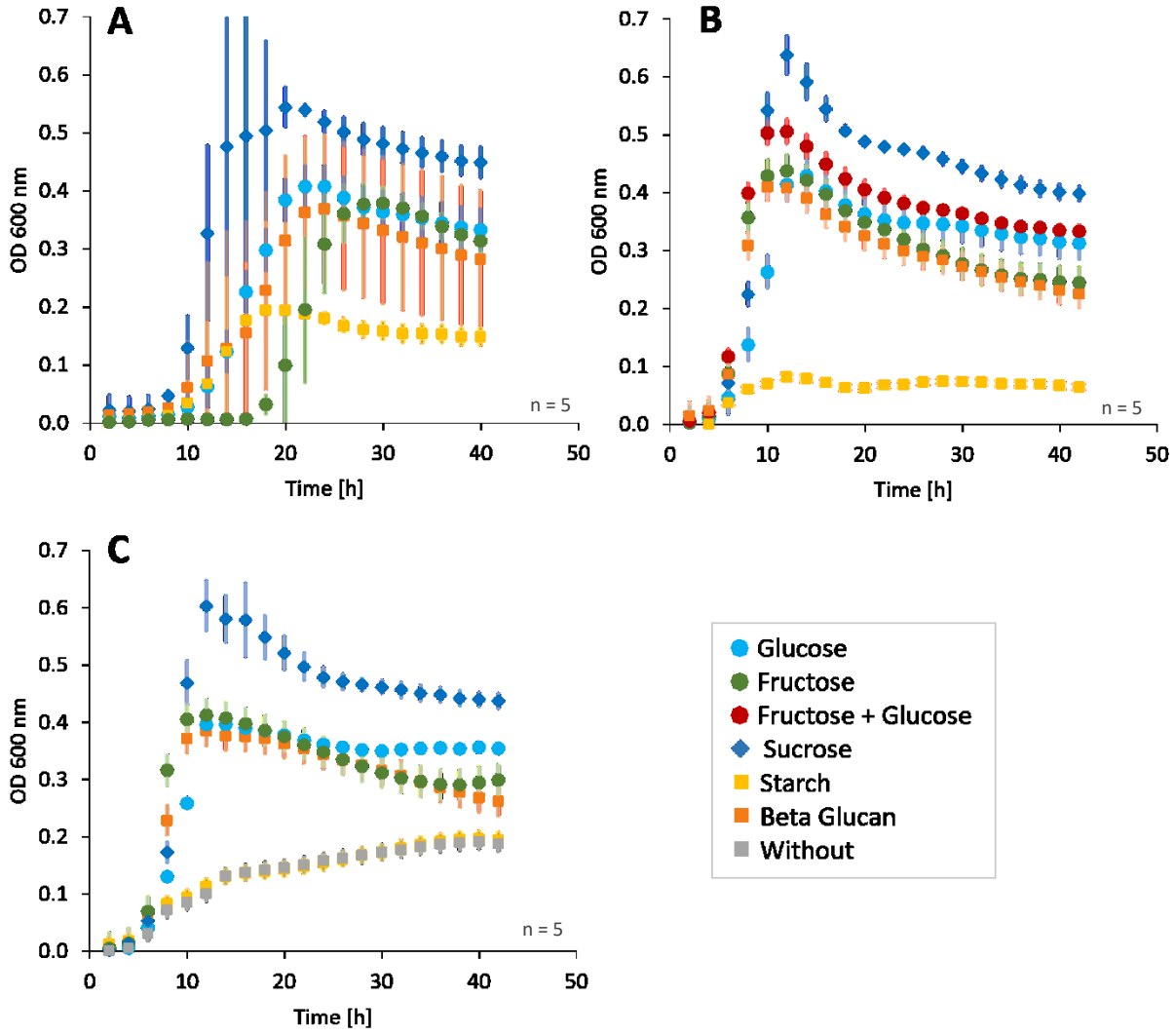

Figure 10: Growth dynamics of *B. producta* grown in YFCA medium with different saccharides a main carbon source. All conditions were tested with n= 5 technical replicates. The mean value with the standard deviation of the replicates is displayed. (A) *B. producta* had the best growth with sucrose provided as saccharide (blue dots). Cultures grown with fructose had a longer lag phase (green rectangle), cultures grown with starch (yellow square) had the least biomass formation and replicates grown in beta-glucan and glucose showed similar growth kinetics. (B) *B. producta* had the best growth with sucrose, cultures grown with starch had the least biomass formation and replicated grown in beta-glucan, fructose and Glucose had comparable growth patterns. (C) *B. producta* had the best growth with sucrose, cultures grown with starch had the least biomass formation, similar to replicates grown without any sugar provided. Cultures grown in beta-glucan, fructose and glucose had comparable growth patterns.

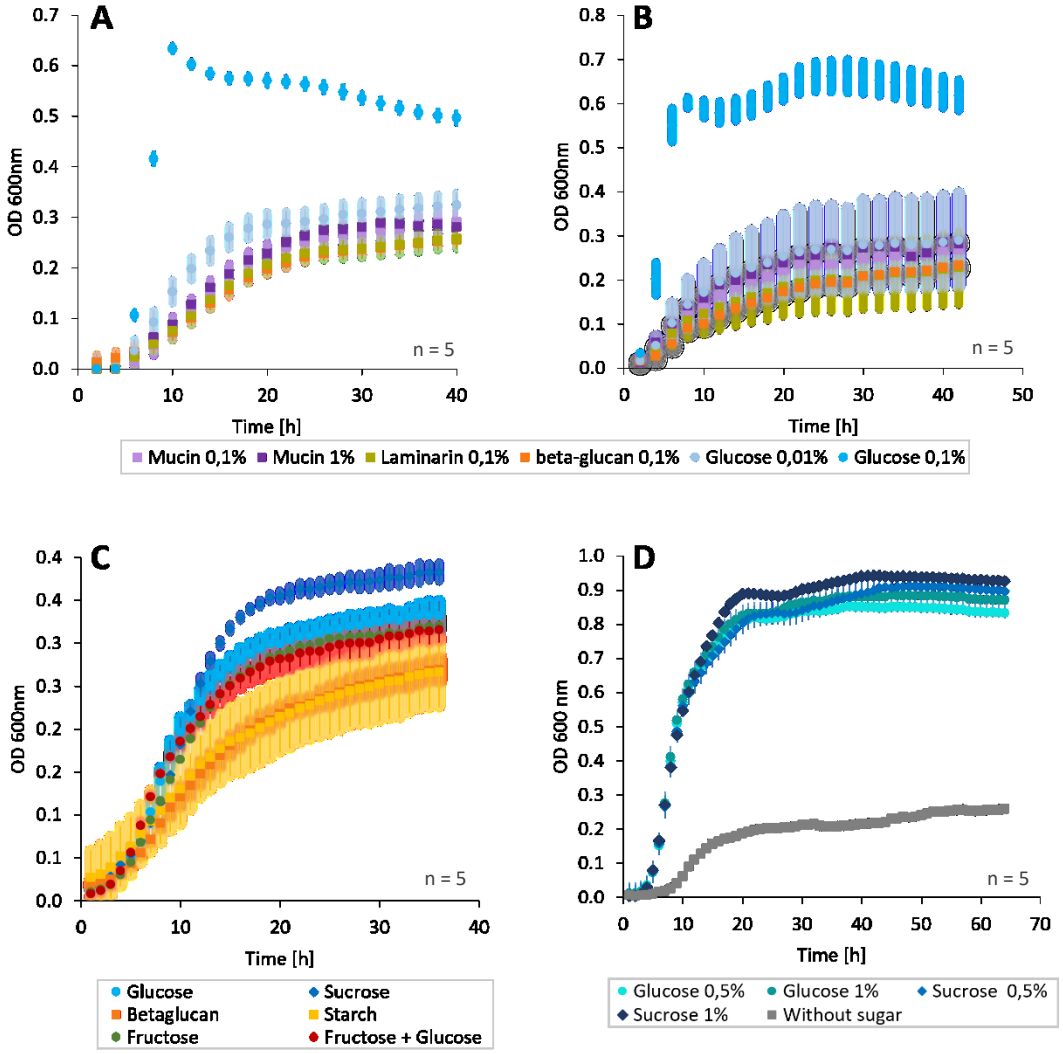

Figure 11: Growth kinetics of *B. thetaiotaomicron* in YCFA medium with different saccharides and in different concentrations. All conditions were tested with n= 5 technical replicates. The mean value with the standard deviation of the replicates is displayed. (A) + (B) Two representative results: The optimal growth conditions provided YCFA medium with 0.1% Glucose, while reducing the glucose concentration results in less biomass formation. All the cultures had a similar growth kinetics in media with the different polysaccharides. (C) The best growth was observed for cultures grown in media with sucrose. Replicates grown in media with Glucose, Fructose and a mixture of glucose and fructose had comparable growth patterns, while the least biomass formation could be observed for cultures grown with polysaccharides. (D) Increasing the concentration of glucose or sucrose did not affect the growth drastically.

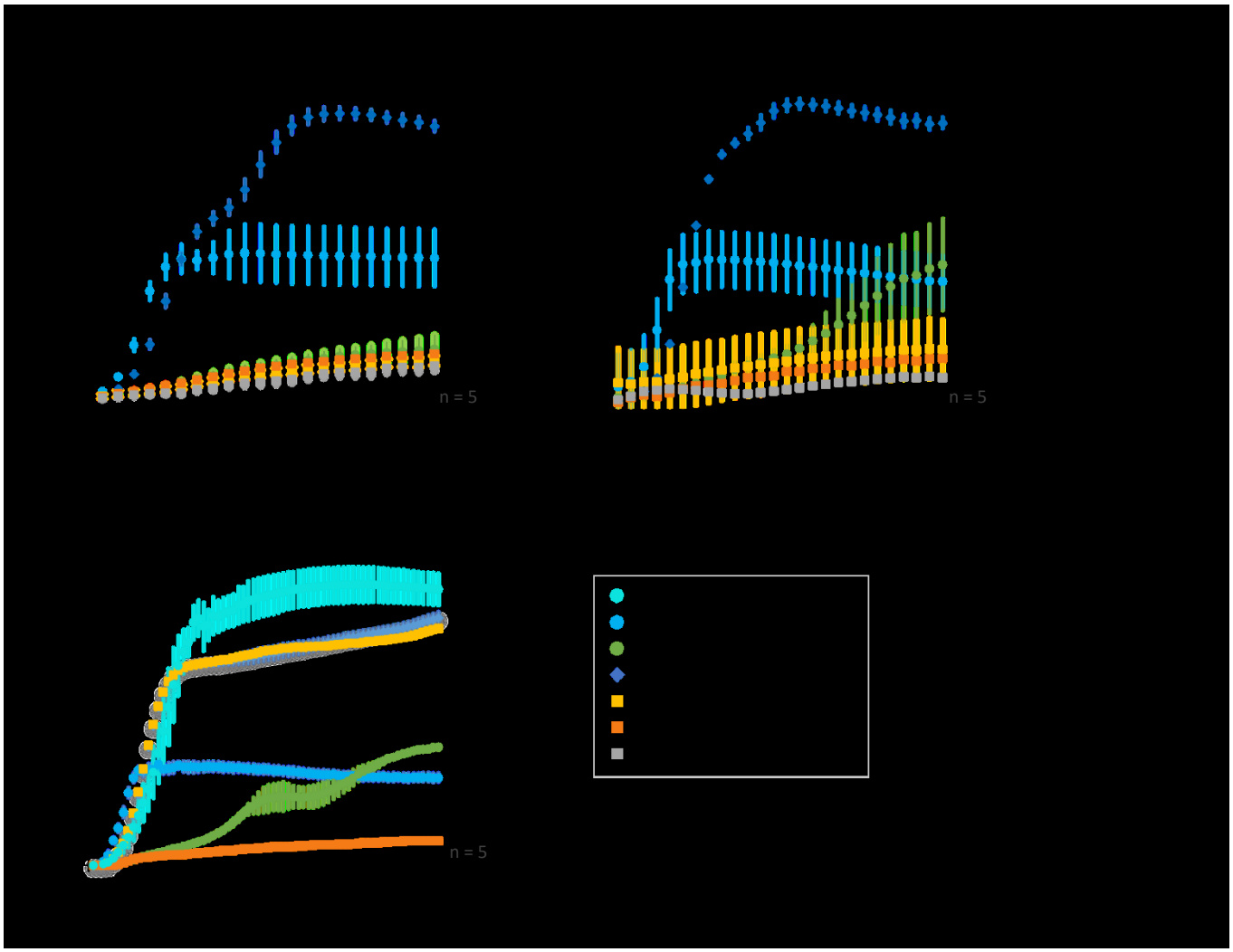

Figure 12: Growth dynamics of B. longum in YCFA medium with different saccharides as main carbon source. All conditions were tested with n= 5 technical replicates. The mean value with the standard deviation of the replicates is displayed. (A) The highest biomass formation was observed for replicates grown in sucrose, roughly half of that biomass formation was reached with media containing glucose. B. longum grown with media containing fructose and polysaccharides showed similar growth to bacteria grown in media without any sugar. (B) Similar observations could be made, besides replicated started to grow with fructose aster 10 h of cultivation time. (C) Increased glucose concentration results in the best biomass formation of B. longum, while replicates grown in sucrose and starch also had sufficient biomass formation. In fructose B. longum showed a biphasic growth pattern and with beta-glucan the least growth was detected.

3.1.3 Bacterial growth in different media types with and without SCFA

In addition to modifying one parameter of the standard YCFA medium, the influence of various additives in different media types was tested (Fig. 13). The standard YCFA medium provided good growth conditions for all the bacteria. The bacteria showed different growth kinetics regarding the absence or presence of short chain fatty acids (SCFA) in YCFA or BHI medium. Other additives in BHI medium did not seem to influence the growth behaviour of the bacteria.

The best growth conditions for *B. producta* are provided by YCFA medium with and without SCFA. In both cases, a short lag phase, the fastest growth rate (3.8 h^{-1} respectively 4.2 h^{-1}), a doubling time of 10-11 min during exponential phase and OD_{max} of 1.3 and 1.2 could be observed (Fig 13 A). Bacterial cultures of *B. producta* showed the same growth kinetics for BHI, BHI + yeast extract and BHI + LPS. In this case, a maximum OD of 0.9 - 1.1 and a growth rate of 2.1 - 2.3 h^{-1} can be found. Noteworthy is the growth behaviour of *B. producta* in BHI medium with added SCFA, where in most cases little to no growth could be detected (OD_{max} = 0.1).

B. thetaiotaomicron shows similar growth patterns in the different media types as *B. producta* (Fig. 13 B). Comparing the different media types, YCFA with and without SCFA provide the best growth conditions for *B. thetaiotaomicron* as well. Here, the maximum OD with 0.92 and 0.86 was reached after a short lag-phase, with growth rates of 2.44 h^{-1} and 1.89 h^{-1}, and a doubling time of 17 and 22 min respectively. Except for bacteria grown in BHI + SCFA, the replicates had similar growth in BHI medium and BHI with LPS and yeast extract. The growth rate of these bacteria grown in BHI with 0.80 - 0.88 h^{-1} was slower than the specific growth rate of bacteria grown in standard YCFA medium. Additionally, the maximal OD in the 3 conditions was comparably lower with 0.4. Bacterial cultures grown in BHI + SCFA had slow growth with little biomass formation (growth rate 0.34 h^{-1}, OD_{max} = 0.3). The growth pattern followed a linear growth in this case.

For *B. longum,* the absence or presence of SCFA in both media types had a strong impact on its growth kinetics (Fig. 13 C). In contrast to *B. producta* and *B. thetaiotaomicron*, the growth of *B. longum* was reduced in YCFA without SCFA, where mainly the biomass formation was decreased. The maximum OD was 0.36, which is 1.6 times less compared to the biomass formation of bacteria grown in standard YCFA medium (OD_{max} = 0.59). In this case as well, the standard YCFA medium provides optimal growth conditions for *B. longum*. Here, the bacteria showed a short lag phase, had a growth rate of 3.66 h^{-1} and a doubling time of 11 min. Similar or same growth kinetics could be observed for bacteria grown in BHI media and BHI media with yeast extract or LPS as additives. Generally, a slower growth rate with 1.0 - 1.5 h^{-1} could be observed and the maximum OD was around half as high compared to bacteria grown in standard YCFA medium. Replicates of *B. longum* grown in BHI with SCFA showed ambiguous growth patterns.

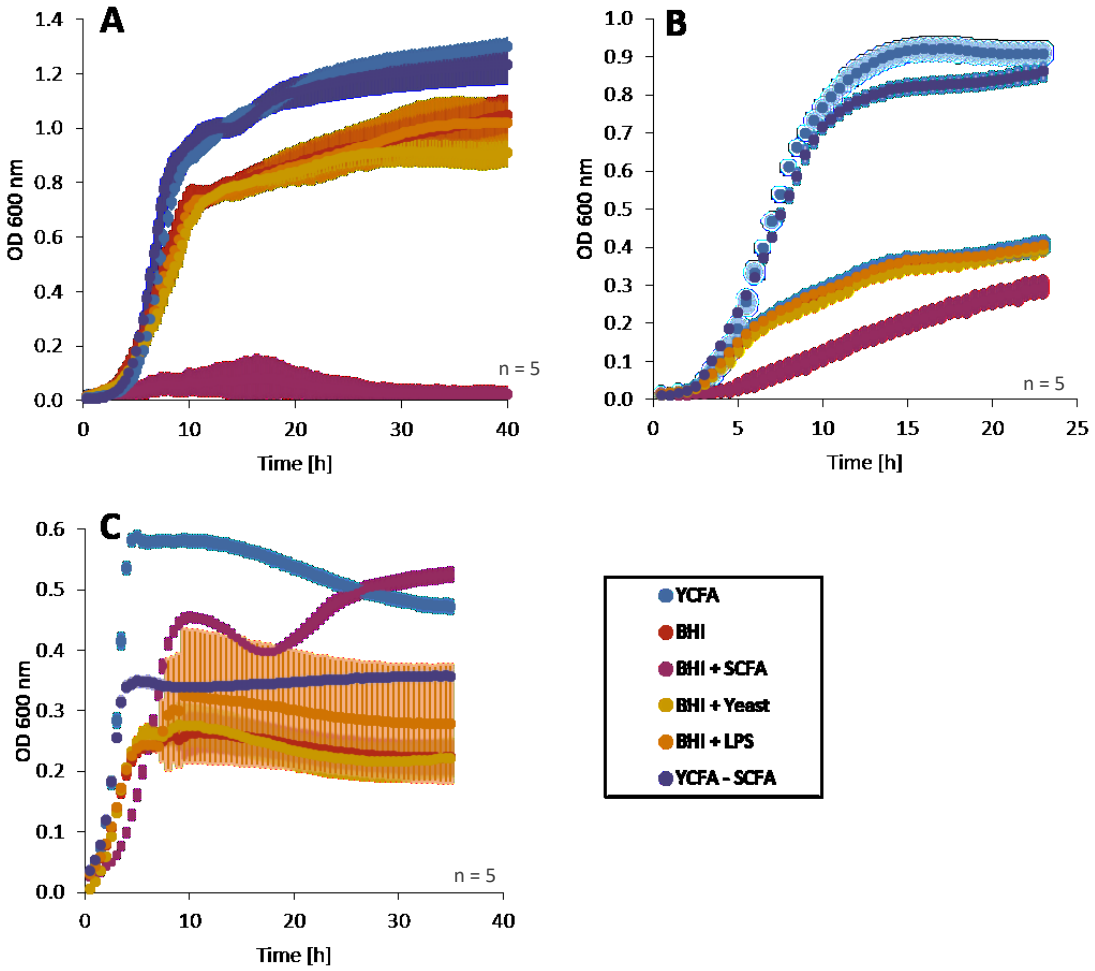

Figure 13: Growth dynamics of gut bacteria in two different media with various additives. All conditions were tested with n= 5 technical replicates. The mean value with the standard deviation of the replicates is displayed. (A) For *B. producta* the absence or presence of SCFA in YCFA medium (blue and dark purple) showed no influence on growth behaviour. The presence of SCFA in BHI slowed down the growth (plum red), here almost no biomass formation was detected, while other additives (Yeast extract: yellow, LPS: orange) did not influence the growth compared to replicates grown in standard BHI media (red) (B) Cultures of *B. thetaiotaomicron* grew similar in YCFA with and without SCFA (blue and dark purple). For replicates grown in BHI with SCFA reduced growth was detected (plum red), whereas other additives (Yeast extract: yellow, LPS: orange) did not influence the growth compared to replicates grown in standard BHI media (red). (C) Standard YCFA media good growth conditions for *B. longum* (blue). In YCFA media without SCFA reduced biomass formation can be observed (purple). In standard BHI media (red) and BHI media with LPS (orange) and yeast extract (yellow) the growth of the replicated were similar, while cultures grown in BHI with SCFA (plum red) had higher biomass formation in comparison.

3.1.4 Media composition affects sORF-encoded peptides production in B. producta

While analysing the monoculture of *B. producta* grown in standard YFCA medium, short open reading frame (sORF) encoded peptides (SEP) could be detected using bottom-up proteomics. Those SEP were previously described to be produced by this bacterium only in SIHUMIx community using bioreactors. Hence, the production of SEP was investigated in this project, exposing this bacterium to different media, which allows to identify triggers for SEP production and elucidate potential functions. For the qualitative detection of SEPs, *B. producta* was grown in n= 2 biological replicates; except for bacteria grown at pH 6, where n= 5 biological replicates were used, as these cultures were also used in another experimental approach for quantitative proteome analysis. In this thesis, the bottom-up proteome analysis discovering SEPs are shown, associated growth curves were addressed in the results section above.

Across all different growth conditions, SEPs were produced by *B. producta* in monoculture. In total 45 SEPs were identified (Fig. 14 A). 11 of the SEPs were found produced by bacteria grown in all the seven media types. Seven SEP were identified in all culture conditions except for the acidic YCFA condition, while five of them were observed to be produced by *B. producta* only under acidic conditions. Some SEPs were only identified in the presence of cellular components such as yeast extract or lipopolysaccharide. The bottom-up proteome analysis detected previously described SEPs, with the exception of BP15. Five of the detected SEPs were previously identified only during co-culture with SIHUMIx (Fig. 14 B).

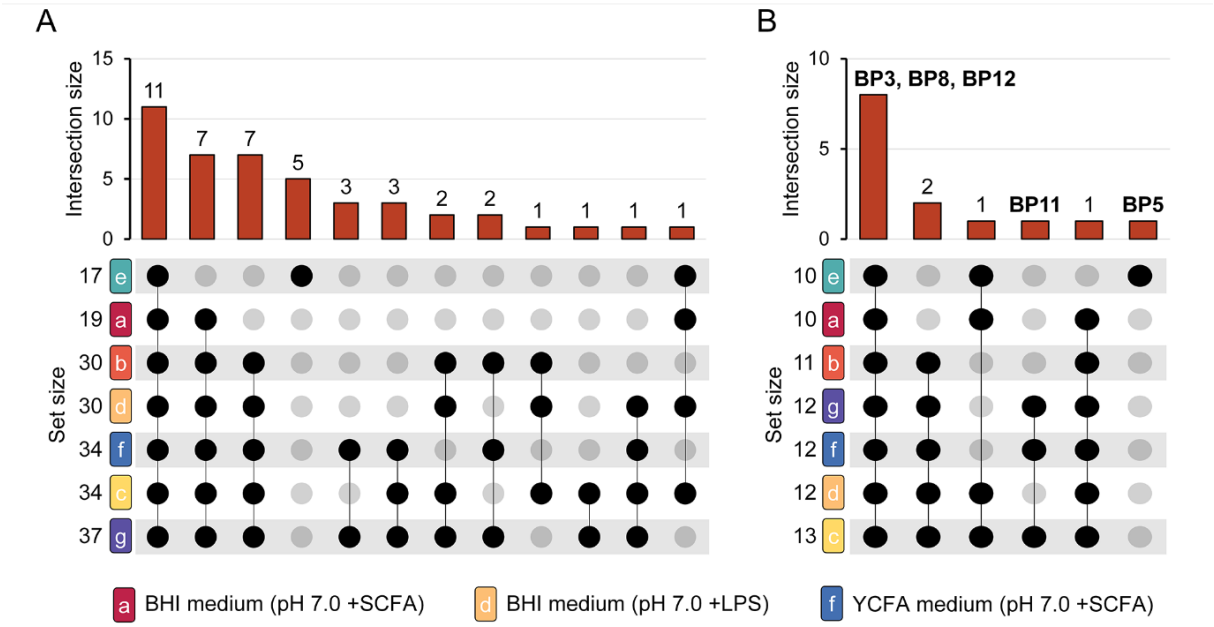

Figure 14: SEP detection from *B. producta* grown in different media using bottom-up proteomics. All bacteria were grown in n= 2 biological replicates, except for bacteria grown in pH 6 were n= 5 biological replicates. (A) Upset plot analysis of novel SEP identified within this project. (B) Plot analysis of described SEP, those previously reported to be produced within the microbiome community are highlighted. (Genth et al., 2023a).

3.2 Bacteria show morphological diversity in acidic environments

Electron microscopy (EM) pictures of the three gut bacteria were taken to observe their morphology in different pH conditions in YCFA media during end of exponential phase / start of stationary phase. Pictures from *B. producta* cultured in pH 6 and pH 7, from *B. thetaiotaomicron* cultured in pH 5.5, pH 6 and pH 7. From *B. longum* grown in pH 6, pH 7 and pH8 were taken, since this bacterium showed growth differences in pH 8 as well.

B. producta cell shape was not affected in the different conditions (Fig. 15). Cells of *B. producta* grown in pH 6 appeared to be mostly cocci and diplococci shaped, approximately 1-2 µm in length. A plethora of the bacterial cells seems to be in the process of dividing. Similar observations can be made for *B. producta* grown in pH 7. In contrast, the bacterial morphology of *B. thetaiotaomicron* was affected drastically by acidic conditions (Fig. 16). Cells grown in pH 5.5 and pH 6 showed different shapes within one monoculture. Some of the cells were elongated, whereas others were shaped as small cocci. In pH 5.5, some cells appeared to have protuberances or buds. In some pictures of *B. thetaiotaomicron* grown in pH 6, bacteria showed a rough surface (Fig. 16 B). Under physiological conditions (pH 7), bacterial cells of *B. thetaiotaomicron* were mostly rod shaped, with a wide range of size and length of 2 µm and more (Fig. 16 D + E). For the growth of *B. longum* in different pH, no clear morphological patterns were observed (Fig. 17). In acidic environments, *B. longum* has a straight and branched morphology, occasionally “bloated” cells and bacteria with buds or protuberances were observed. In pH 7 *B. longum* showed a similar phenotype, with “bloated” cells and cells which are mostly irregularly shaped and in the process of dividing. On some pictures, small vesicle-like structures appeared on the mostly rough bacterial surface (Fig. 17 D). *B. longum* grown in pH 8 showed more consistently straight, slim and branched cells with a smoother surface compared to the other growth conditions.

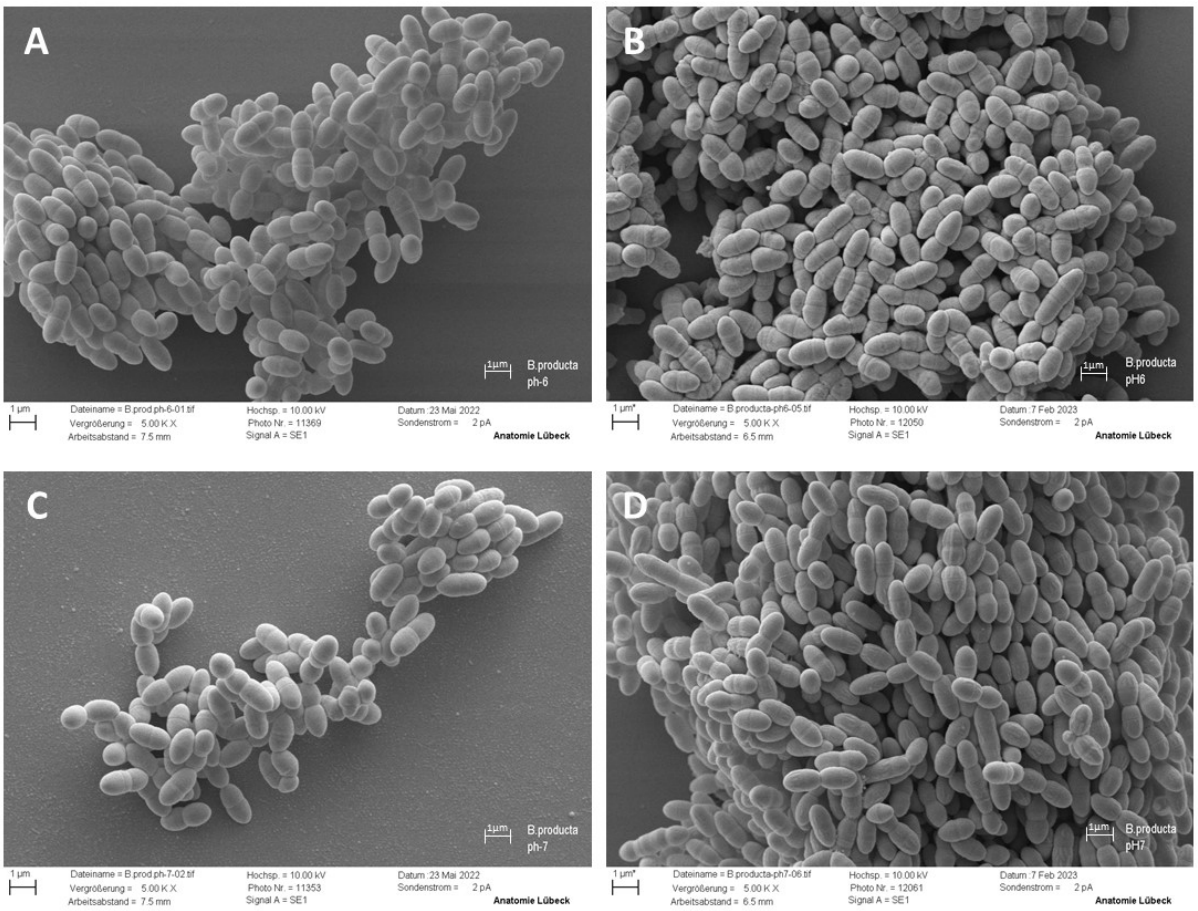

Figure 15: EM pictures of B. producta grown in pH 6 and pH 7 with no visible change in morphology. (A) + (B) B. producta grown in pH6 (representative pictures of n= 4 biological replicates). (C) + (D) B. producta grown in pH 7 (representative pictures out of n= 4 biological replicates).

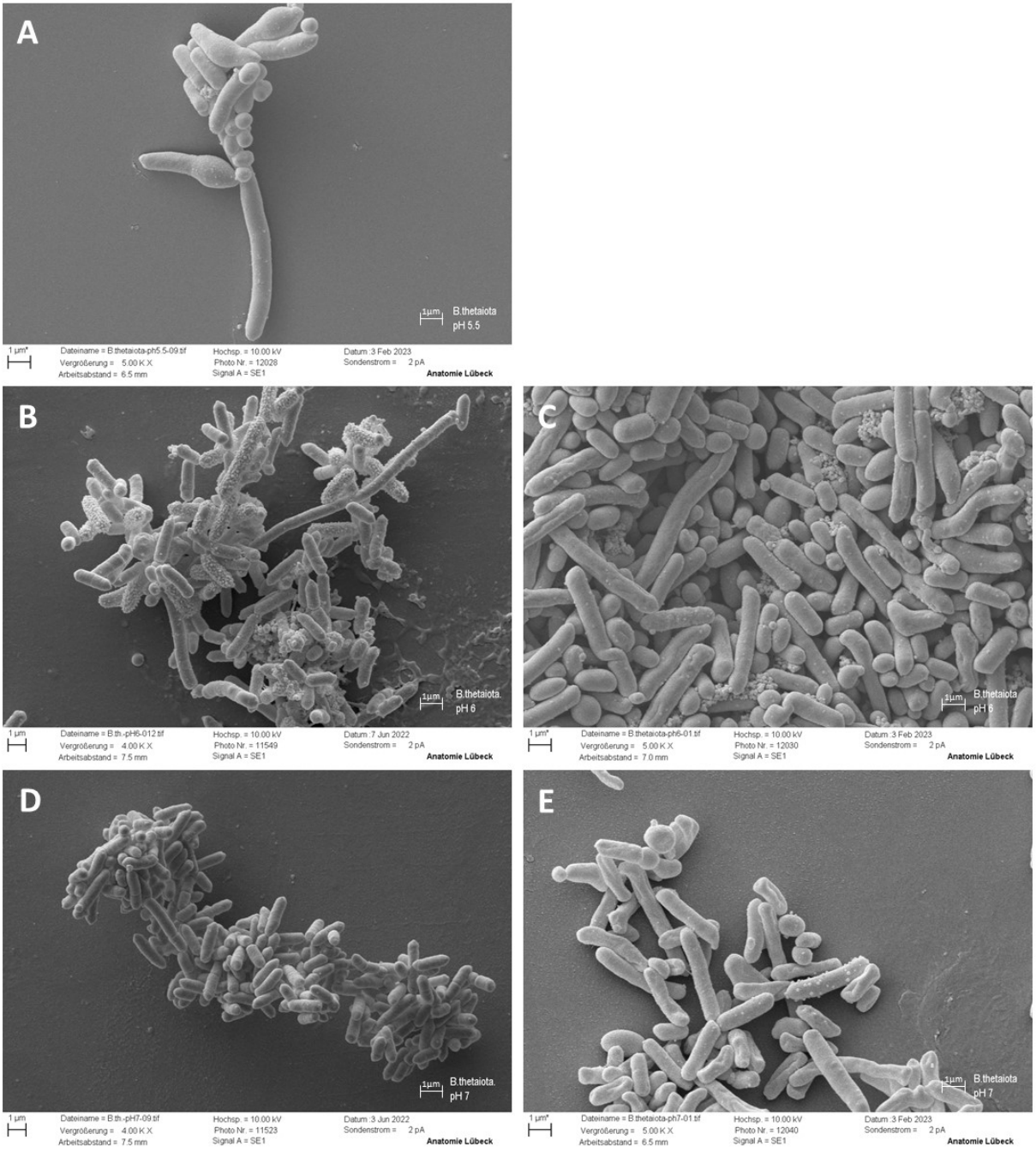

Figure 16: EM pictures of B. thetaiotaomicron grown in pH 5.5, pH 6 and pH 7 with polymorphic shapes. (A) B. thetaiotaomicron grown in pH 5.5 has heterogenic phenotype (n= 2 biological replicates, representative picture). (B) B. thetaiotaomicron grown in pH6, elongated bacteria and bacteria with a rough surface are observed and (C) diverse morphologies can be observed. (n= 4 biological replicates , representative pictures). (D) B. thetaiotaomicron grown in pH 7 appears mostly rod shaped or (E) showed divers shapes (representative pictures, n= 4 biological replicates).

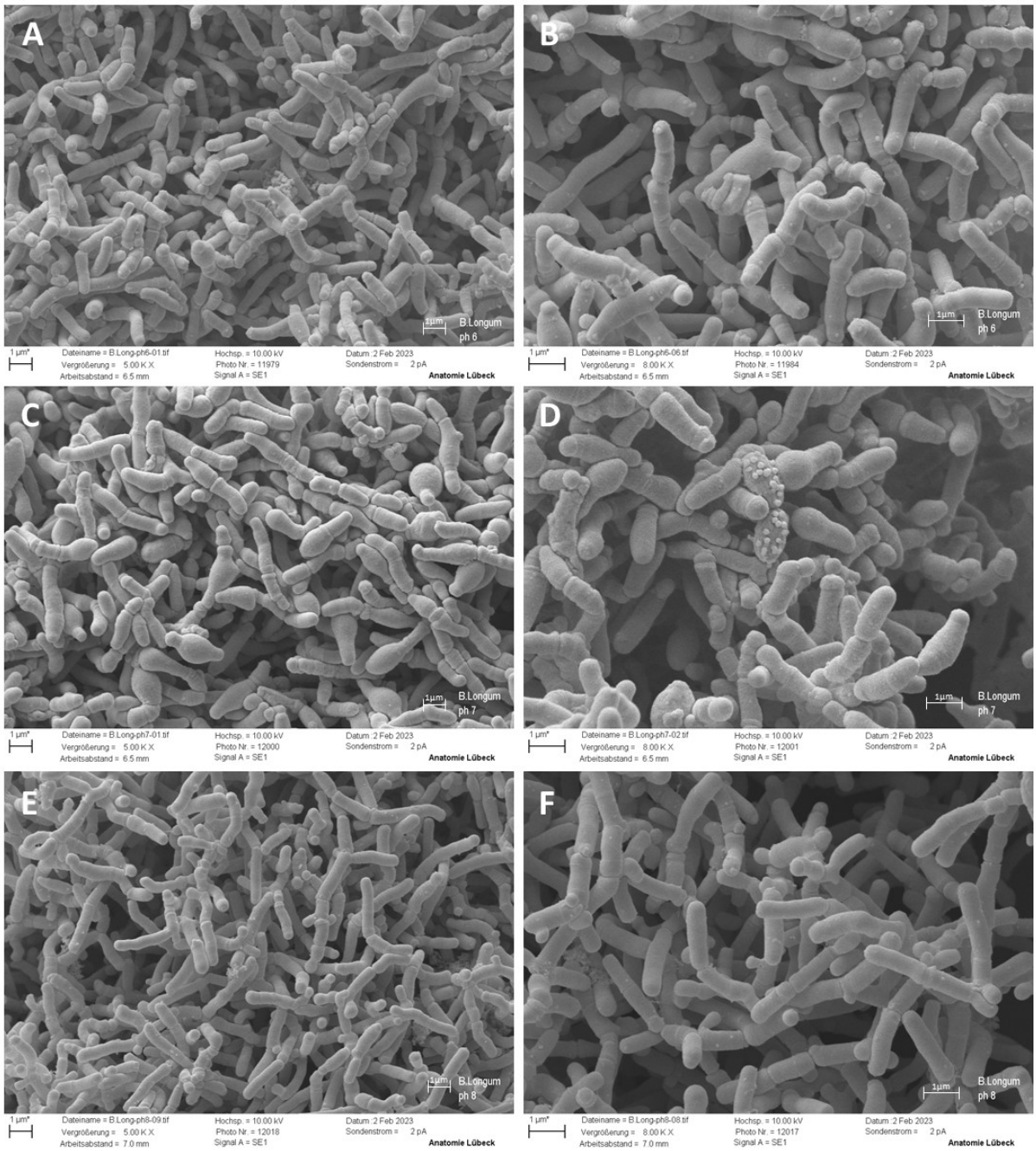

Figure 17: EM pictures of B. longum grown in pH 6, pH 7 and pH 8 showing a heterogenous morphology. Representative pictures of each condition, bacteria grown in n= 2 biological replicates. (A) & (B) Representative pictures of B. longum gown in pH 6. (C) & (D) B. longum grown in pH 7. (E) & (F) B. longum grown in pH 8.

3.3 Transcriptome analysis of *B. producta* and *B. thetaiotaomicron* grown in pH 6 vs pH 7

The transcriptomic analysis was performed to reveal upregulated genes in grown in pH 6 compared to pH7. For *B. longum* transcriptome analysis were not possible, since there were complications with the RNA isolation. A heatmap and the comparison of the technical triplicates of *B. producta* and *B. thetaiotaomicron* grown in either pH 6 or pH 7 can be found in the appendix (Fig. 36 - 38). For *B. producta* one of the pH 6 triplicates appears to be an outlier and hence was excluded for further analysis. Only small perceptible differences in the transcriptome were detected for *B. producta* grown under the different pH conditions, whereas for *B. thetaiotaomicron* the differences were slightly more pronounced (Fig. 18). The corresponding significant genes shown in the MA plot of each respective bacterium can be found in the appendix (Tab. 13 - 16). To regroups the genes into functional groups using the FACoP.v2 for functional annotation and the FUNAGE-Pro V1 for functional analysis, for *B. producta* no pathways that are over/under regulated could be identified. Moreover, for *B. thetaiotaomicron* grown in pH 7 no pathways could be detected by the FUNAGE-Pro web server. Therefore, this thesis focuses on the functional groups and pathways that are up regulated in *B. thetaiotaomicron* grown at pH 6.

For *B. thetaiotaomicron* grown in acidic conditions, several genes involved in iron acquisition, (membrane) transporter, membrane synthesis and DNA synthesis are upregulated in this condition, identified by using Gene Ontology (GO) (Fig. 19) and Protein Families (Pfam) (Fig. 20) for functional classification. The genes involved in iron acquisition are genes responsible for iron ion homeostasis, siderophore-iron transmembrane transporter activity, siderophore uptake transmembrane transporter activity, siderophore transmembrane transport, 4Fe-4S binding domain or the TonB dependent receptor. Genes involved in transporter activity and membrane associated processes can be recognized, such as colicin transmembrane transporter activity, transmembrane transporter complex and CDP-glycerol glycerophosphotransferase activity. Additionally, there are genes upregulated encoding enzymes which are involved in DNA methylation and DNA repair, such as DNA-methyltransferase domain and the enzyme N-6 DNA Methylase or UvrD/REP helicase N-terminal domain, UvrD-like helicase C-terminal domain, PD-(D/E)XK nuclease superfamily and DNA-directed 5'-3' RNA polymerase. Other upregulated genes encoding enzymes for pyruvate and pyruvate-derivate metabolism and reactions can be identified, such as indolepyruvate ferredoxin oxidoreductase activity, pyruvate ferredoxin/flavodoxin oxidoreductase and pyruvate flavodoxin/ferredoxin oxidoreductase. Further, upregulated genes encoding sugar metabolisms can be detected, such as the Repressor-ORF-Kinase (ROK) family, sugar kinases and enzymes involved in rhamnose catabolic process or acetylxylan esterase activity. Genes concerning acetylation processes such as acetyltransferase (GNAT) family and acetyltransferase activity were as well upregulated in bacteria grown in acidic conditions.

Information on gene expression of genes regarding inositol can be found in the appendix in table 12 and table 13. None of them were significantly upregulated in *B. producta* and *B. thetaiotaomicron*, but are considered in the discussion part of this thesis.

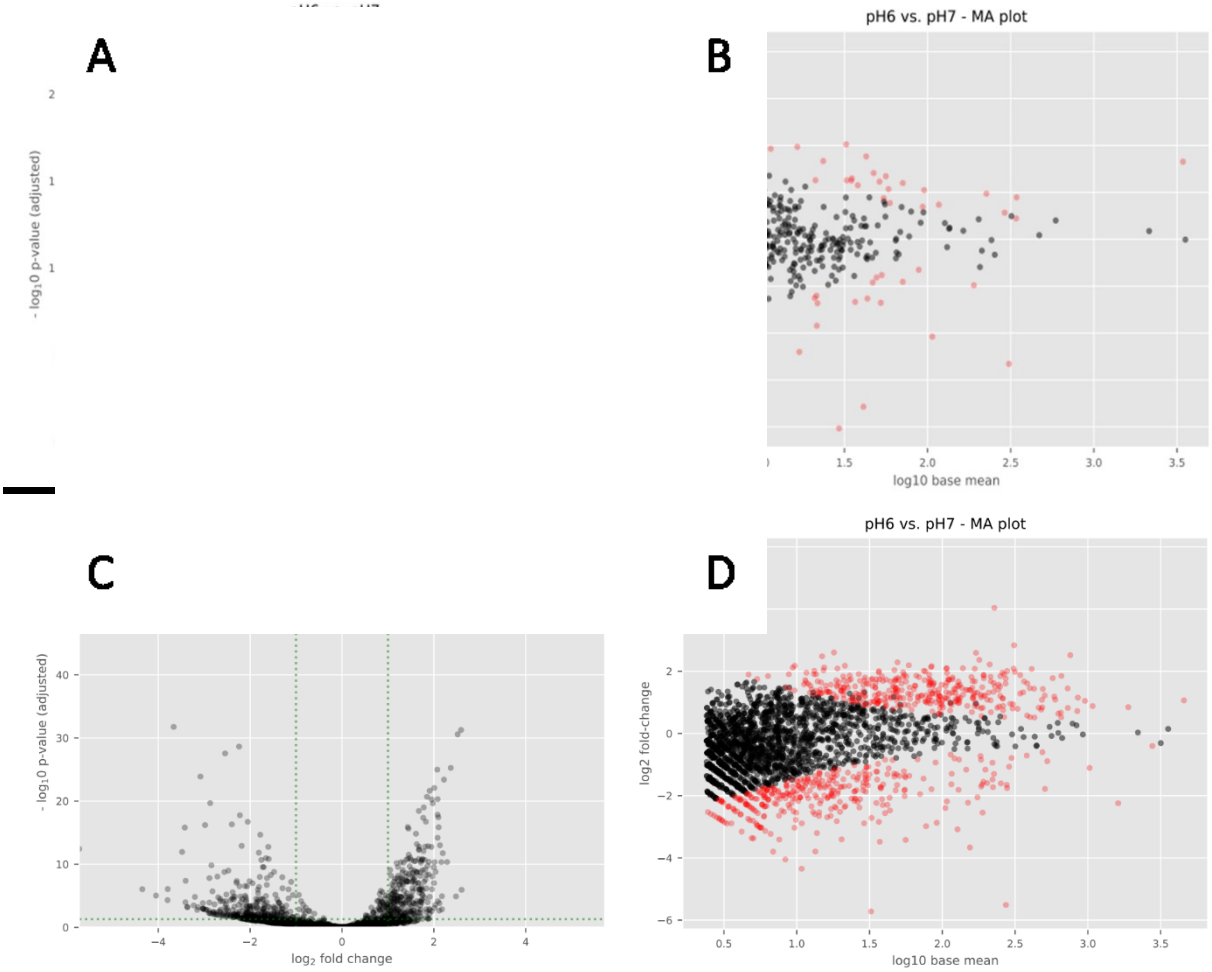

Figure 18: Overview transcriptomic analysis. (A) Volcano plot with log2 fold change vs adjusted p-value of *B. producta* grown in YCFA medium with pH6 (n= 2 biological replicates) compared to pH7 (n= 3 biological replicates) and (B) the respective MA-plot with a log10 base mean vs log2 fold-change for this bacterium. (C) Volcano plot with log2 fold change vs adjusted p-value *B. thetaiotaomicron* grown in YCFA medium with pH6 (n= 3) compared to pH7 (n= 3 biological replicates) and (D) the respective MA-plot with a log10 base mean vs log2 fold-change for this bacterium.

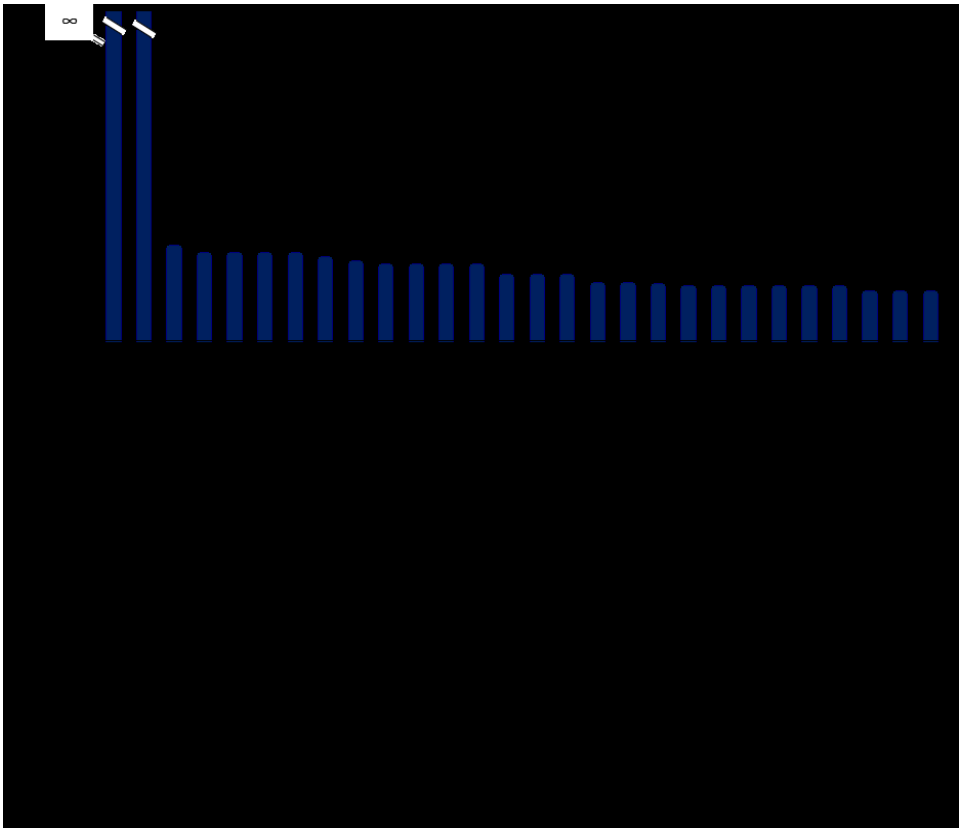

Figure 19: Differently expressed pathways in *B. thetaiotaomicron* grown in pH 6 searching Gene Ontology (GO) data base. The x-axis shows the name of the upregulated enzyme or the connected activity and the significant p-values (y-axis) for this bacterium in acidic stress conditions.

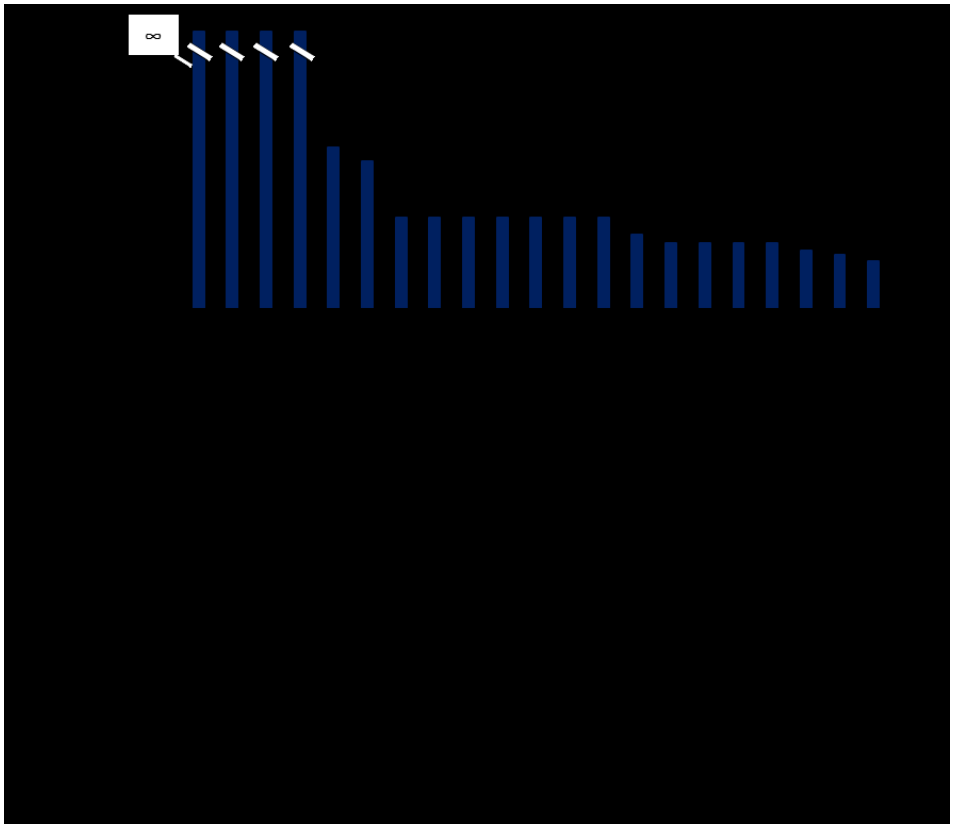

Figure 20: Differently expressed pathways in *B. thetaiotaomicron* grown in pH 6 using Protein Families (Pfam) data base. The x-axis shows the name of the upregulated protein/pathway or functional group and the significant p-values (y-axis) for this bacterium in acidic stress conditions.

3.4 Metabolome analysis reveals strain dependent metabolite production in acidic environments

3.4.1 Metabolome analysis of bacteria grown in YCFA medium with pH 6 and pH 7

The intracellular metabolomes of the 3 commensal gut bacteria grown in acidic stress at pH 6 and the physiological pH 7 were analysed, additionally *B. longum* grown on pH 8 was investigated, since in this case a more basic environment appeared to be also a stressor. For each condition n= 5 biological replicates were grown of the respective bacterium. The results revealed strain and condition dependent differences in metabolite production. While high differences of metabolite production could be observed for *B. producta* and *B. thetaiotaomicron* grown in different pH, the differences to *B. longum* were less distinct (Fig. 21). No single metabolite could be observed to be either produced or consumed same direction in all three strains grown in pH 6 and pH 7.

For each bacterium different levels of certain metabolites could be detected when grown in acidic conditions (Fig. 22, Appendix Fig. 33-35). *B. producta* grown in pH 6 showed low levels of fatty acid acetate and amino acids, such as glycine, glutamate, alanine, aspartate, arginine and threonine in its intracellular metabolome. Other metabolites such as ethanol, succinate, some amino acids and taurine were more abundant. In *B. thetaiotaomicron* several amino acids and metabolites involves in the cofactor metabolism are more abundant when grown in acidic conditions. Lower abundant in this condition in this bacterium were the metabolites alanine and propionate. For *B. longum* several pH-specific effects could be observed, in pH 6 an increased abundance of propionate, formate, pyruvate, succinate and amino acids like aspartate, arginine and lysine. In this bacterium grown at pH 6, metabolites such as Taurine, some sugars and lactated were less found.

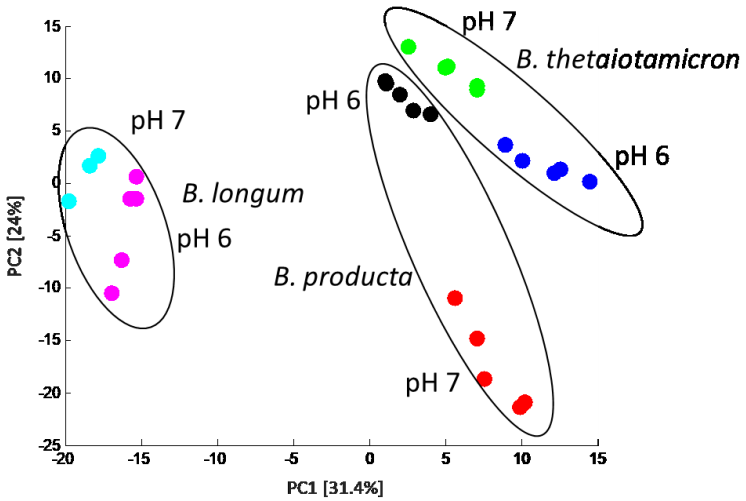

Figure 21: PCA shows strain and condition dependent metabolite production of *B. producta*, *B. thetaiotaomicron* and *B. longum* grown in pH 6 and pH 7 in n= 5 biological replicates. The data was reduced to 418 datapoints and normalized to the internal standard sodium trimethylsilyl propionate (TSP) and OD of the bacterial replicates. PCA1= 31.4 %, PCA2= 24.0 %.

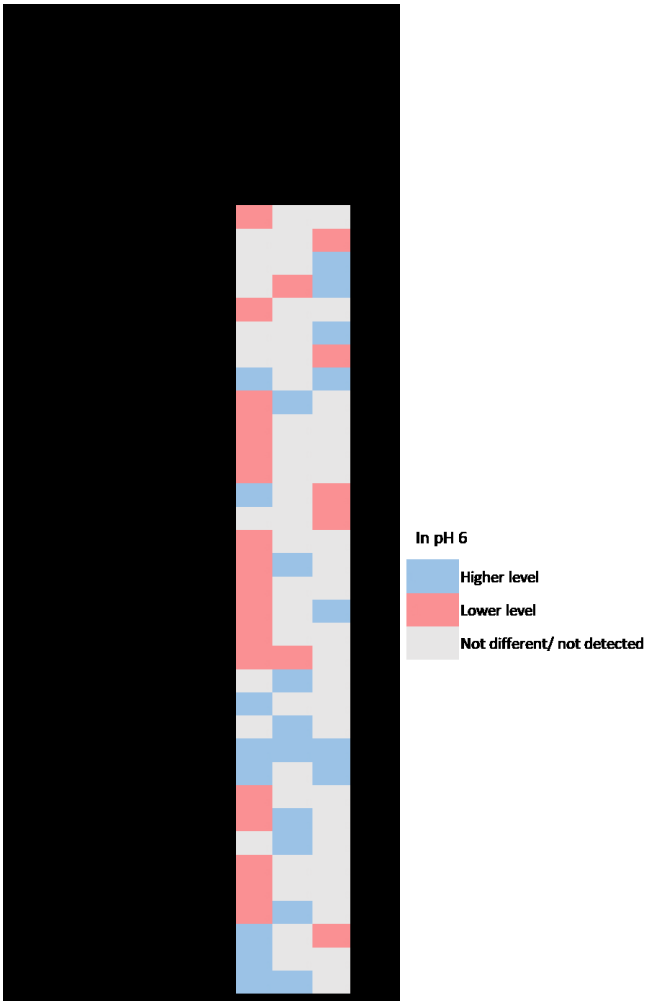

Figure 22: Graphic summary of the detected intracellular metabolites from the gut bacteria grown in pH 6 compared to pH 7. For all three bacteria several metabolites were less abundant (red) when grown in pH 6; for example, *B. producta* had a lower intracellular abundance of several metabolites involved in the amino acid metabolism. For some metabolites a higher level (blue) could be detected as well, especially for *B. thetaiotaomicron* concerning the cofactor metabolism.

3.5 Biological interactions of *B. producta* and *B. thetaiotaomicron*

3.5.1 Co-culture experiments provide insights into potential bacterial interactions

To evaluate potential biological interactions between the bacteria, co-cultures were established for *B. producta* and *B. thetaiotaomicron* analysing their relation qualitatively and quantitatively. In total 12 biological experiments were conducted for qPCR analysis; each qPCR was performed using 3 technical replicates for each primer of each bacterium. The qPCR results to determine the dominant member of the co-culture with *B. thetaiotaomicron* and *B. producta* appeared inconclusive. Observing the first co-culture experiments using qPCR, it was indicated that *B. thetaiotaomicron* was the dominant part of this bacterial interaction (Fig. 23 A and B). Repeating the experiments, *B. producta* was more abundant concerning the DNA amount over time (Fig. 23 C, D, H and I). In some cases, the amount of DNA from *B. producta* was only slightly increased compared to *B. thetaiotaomicron* or the DNA concentration of the two bacteria was relatively similar (Fig. 23 E, F, G). Conducting the experiments with the microbiome DNA-isolation kit revealed once more results, with DNA of either *B. producta* or *B. thetaiotaomicron* rarely present and the respective other bacterium as dominant member (Fig. 24).

In addition to the quantitative analysis of the bacterial ratio over time, qualitative approaches to examine to co-culture were conducted. Knowing the different morphological shape of the two bacteria, EM pictures of the co-culture at different times were made. Directly after inoculation with an expected ratio of 50:50, the EM picture after 0 h cultivation time showed rod shaped bacteria and shrivelled cocci-like shaped bacteria (Fig. 25). The shrivelled shape is a result of the method that was used for taking the pictures. After 6 h of cultivation time, it appeared that there are mostly rod-shaped bacteria present (Fig. 25 B). Zooming in at bacteria grown 24 h in co-culture, in some cases pili formation between bacteria was noticed (Fig. 25 C). On PVX plates, *B. thetaiotaomicron* appears in white-creamy and smooth big colonies, while *B. producta* forms dry and beige smaller colonies. Streaking out the bacterial co-culture on Agar plates during the later cultivation times like 24 h and 40 h (Fig. 25 D and E), it appeared that more creamy-white bigger colonies were formed, indicating *B. thetaiotaomicron* being more present at later time points.

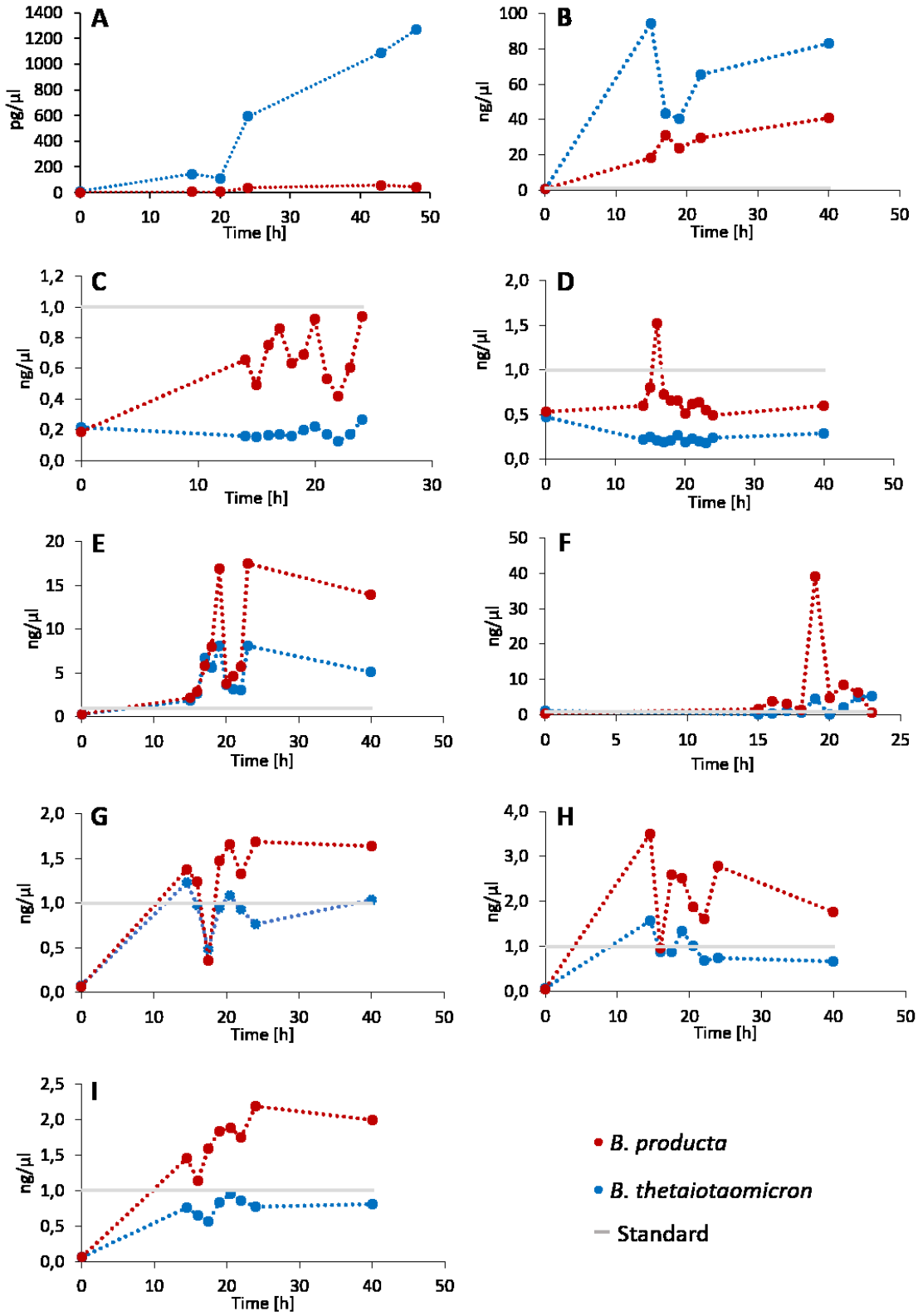

Figure 23: qPCR results of *B. producta*/*B. thetaiotaomicron* co-cultures. The NEBioCalculator uses the value average mean Cq of n= 3 technical replicates of the qPCR to calculate the amount of DNA in the sample. (A) + (B) *B. thetaiotaomicron* emerges as dominant member with more DNA formation over time. In experiments (C), (D), (H) and (I) *B. producta* build more DNA and appears to be the dominant member of this culture. For experiments (E), (F) and (G) slightly more DNA of *B. producta* or similar amount of DNA from both bacteria could be detected, no clear dominant member could be determined.

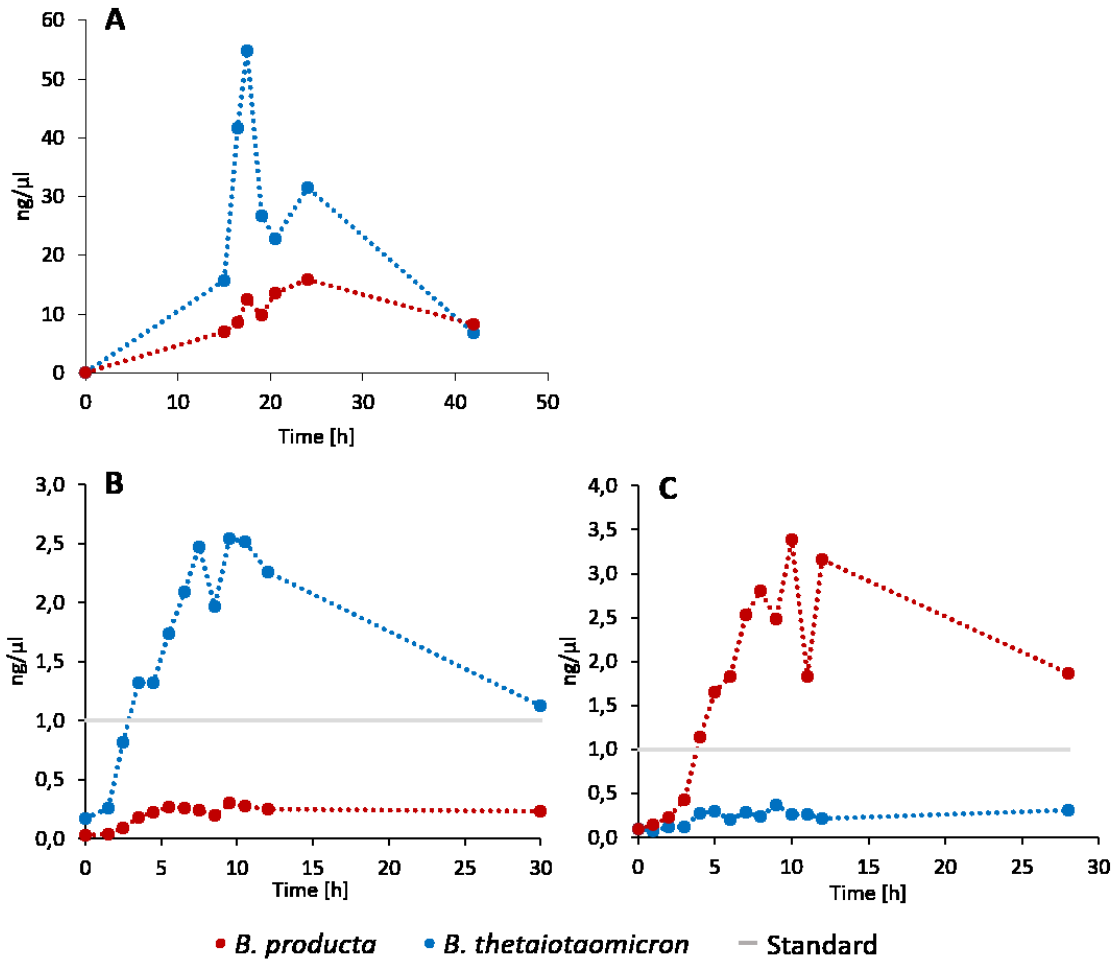

Figure 24: qPCR results of *B. producta*/*B. thetaiotaomicron* co-cultures after the use of Microbiome kit for DNA isolation. The NEBioCalculator uses the value average mean Cq of n= 3 technical replicates of the qPCR to calculate the amount of DNA in the sample. (A) *B. thetaiotaomicron* emerges as dominant member of the co-culture, while *B. producta* displayed a reduced growth (02.11.22, no standard was added in this experiment). (B) *B. thetaiotaomicron* emerges as dominant member of the co-culture, while *B. producta* appears to not be able to grow well (02.12.22). (C) In this experiment, *B. producta* is the dominant member, while *B. thetaiotaomicron* had no major DNA increase over time (16.01.23).

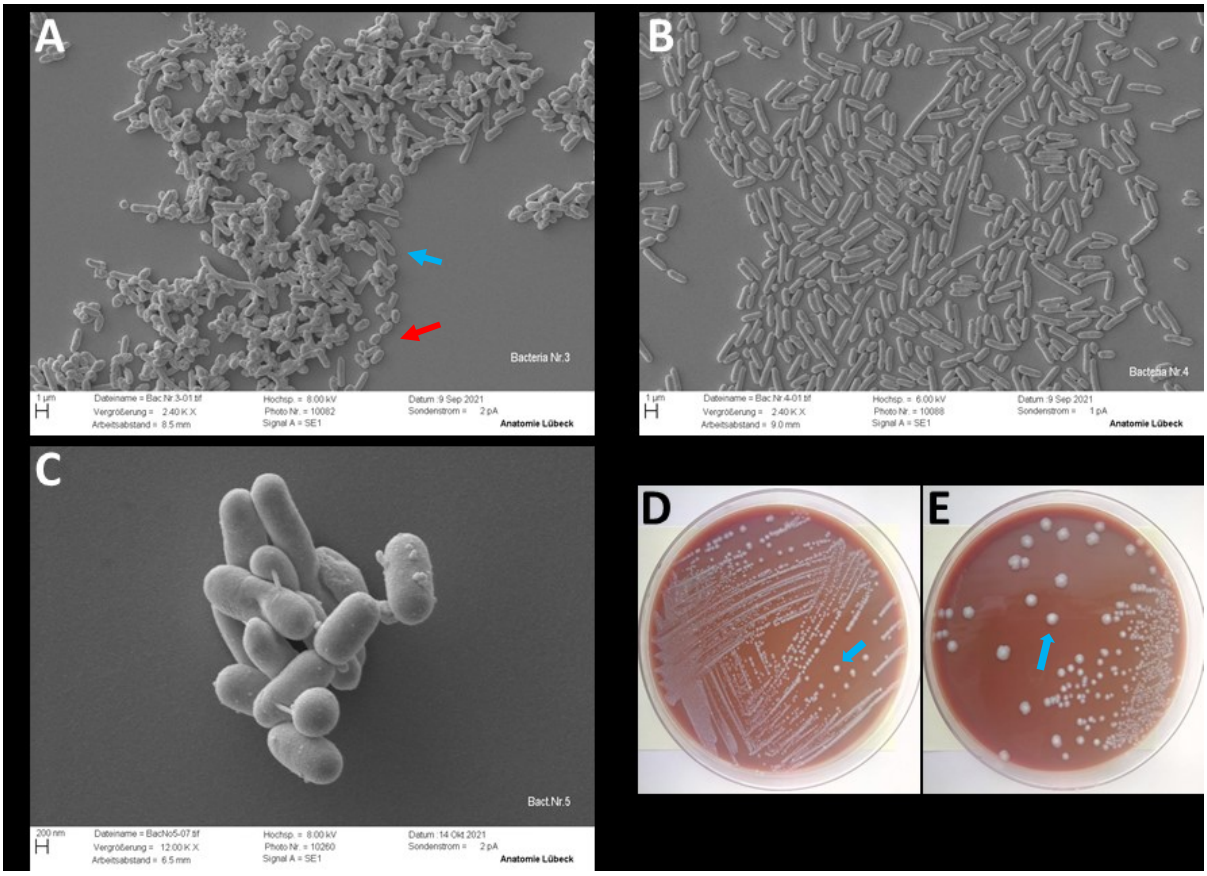

Figure 25: Images of co-culture. (A) EM picture after directly inoculation the two bacteria (cultivation time 0 h). Rod shaped bacterium *B. thetaiotaomicron* (blue arrow) and cocci shaped bacterium *B. producta* (red arrow) can be noticed. (B) EM picture after 6 h of cultivation time (C) EM picture after 24 h of cultivation time, for some bacteria pili formation is visible. (D) Co-culture streaked out on PVX agar after 24 h of cultivation time, the small and bigger smooth, white cultures indicate the primarily presence of *B. thetaiotaomicron*. (E) Co-culture streaked out on PVX plate after 40 h of cultivation time. Mainly big, smooth and creamy-white coloured colonies of *B. thetaiotaomicron* are visible.

3.5.2 Intact cell measurements provide new workflow for co-culture experiments

In all of the experiments, the OD was used to inoculate the bacteria. While for comparing the growth within one bacterial species under different conditions this was a suitable parameter, the OD appears to be not reliable inoculating 2 different bacterial species. Using the same culture of each, *B. thetaiotaomicron* and *B. producta* grown in standard YCFA medium, the OD and measurements with the BactoBox providing intact and total cell numbers were compared over time. For *B. producta*, the OD and the cell number followed the same growth patterns and the intact cell number was comparably close to the total cell number (Fig. 26 A). Correlating the OD to intact cell numbers and total cell numbers, it was noticed, that the total cell number correlated more strongly with the measured OD (Fig. 26 B and C). For *B. thetaiotaomicron* the OD and total cell number followed the same growth patterns, while the intact cell number showed lower values and a flat growth pattern (Fig. 27 A). Hence, the correlation of OD and total cell number was stronger than the one with OD and the intact cell number (Fig. 27 B and C).

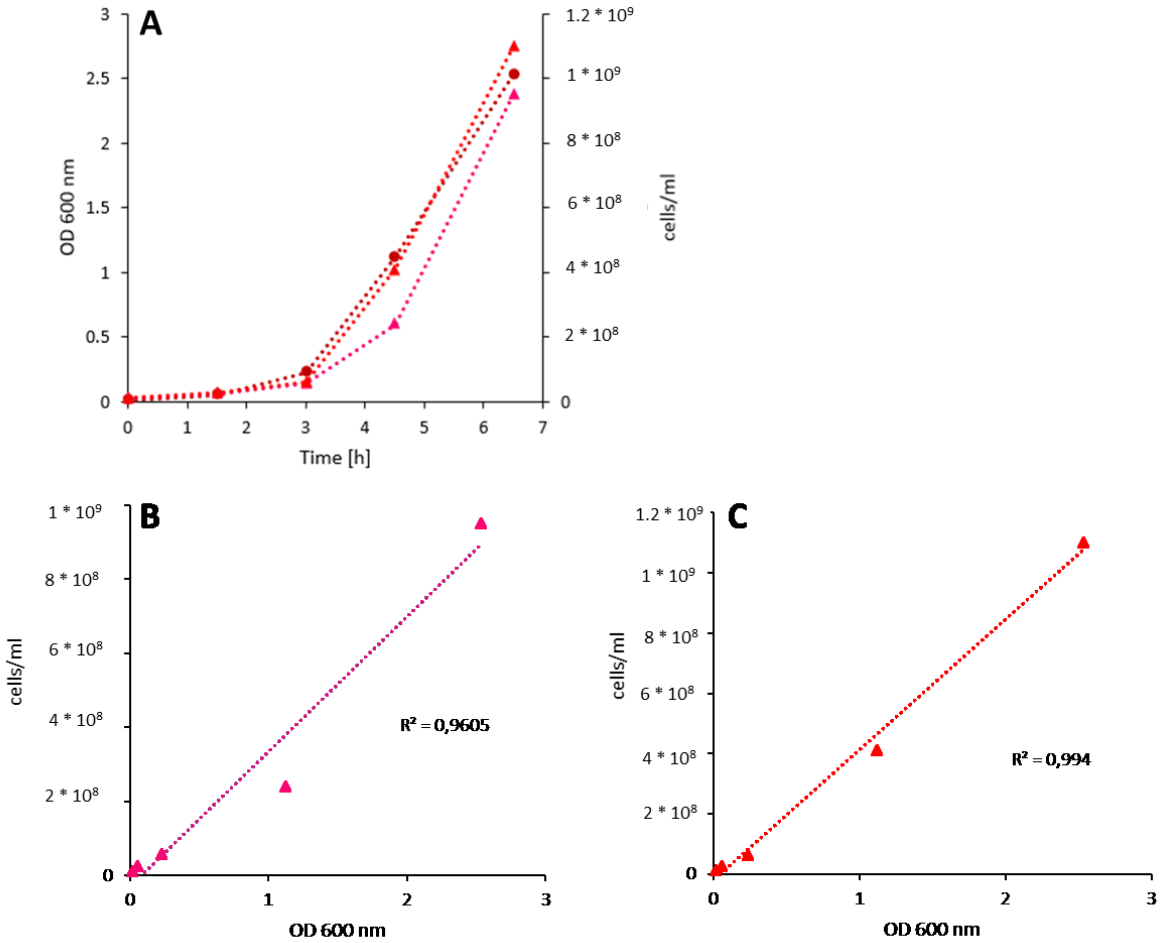

Figure 26: BactoBox vs Photometer measurements for *B. producta* (n=1). (A) OD and BactoBox measurements with intact and total cell numbers of the same culture. The OD (y_1-axis), the intact and total cell number (both on the second y-axis) are plotted against time (x-axis) and displayed typical bacterial growth with a lag-phase and exponential growth. (B) Correlation with R^2= 0.9605 of OD vs intact cells. (C) Correlation with R^2= 0.994 of OD and total cell number showed a stronger correlation compared to OD vs intact cells.

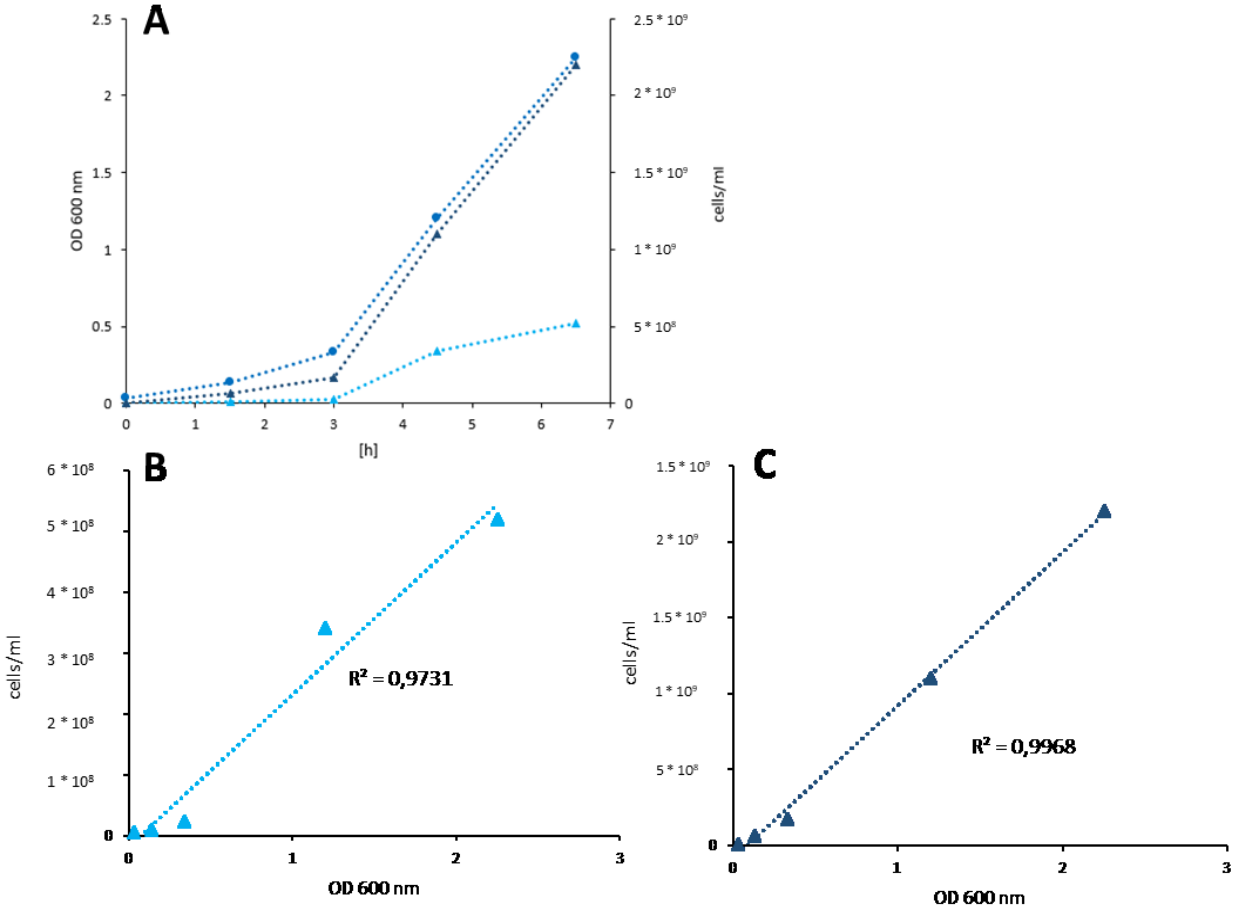

Figure 27: BactoBox vs Photometer measurements for *B. thetaiotaomicron* (n= 1). (A) OD and BactoBox measurements with intact and total cell numbers of the same culture. OD and BactoBox measurements with intact and total cell numbers of the same culture. The OD (y_1-axis), the intact and total cell number (both on the second y-axis) are plotted against time (x-axis) and displayed the growth of *B. thetaiotaomicron* with a lag-phase and afterwards mostly linear growth. (B) Correlation with R^2= 0.9731 of OD and intact cells. (C) A stronger correlation with R^2= 0.9968 of OD and total cell numbers can be determined.

3.6 The ARTE assay elucidates T-cell reaction to different bacteria

The Antigen-reactive T-cell enrichment (ARTE) assay was conducted for bacterial lysates of pathogenic *E. coli* species grown in different conditions, as well as for *B. thetaiotaomicron* grown in pH 7 and pH 6 to investigate the specific T-cell reaction to the bacteria grown in stressful conditions. Each lysate was tested once per donor. To compare multiple bacteria and conditions the Kruskal-Wallis with Dunn's post hoc was applied, for direct comparison between the two conditions pH6 and pH7, the Mann-Whitney test was applied. The T-cell frequency was higher for the pathogenic bacteria compared to the commensal bacteria (Fig. 28 A-C). The inflammatory cytokines were increased when T-cells were exposed to the pathogenic *E. coli*, but not when exposed to *B. thetaiotaomicron.* No differences in the number of cytokines can be detected for *B. thetaiotaomicron* grown in pH 6 and pH 7 (Fig. 28 D-F). Other tested parameters of the ARTE assay are as well not significantly different for *B. thetaiotaomicron* grown in pH 6 or pH 7 (Fig. 28 G-M).

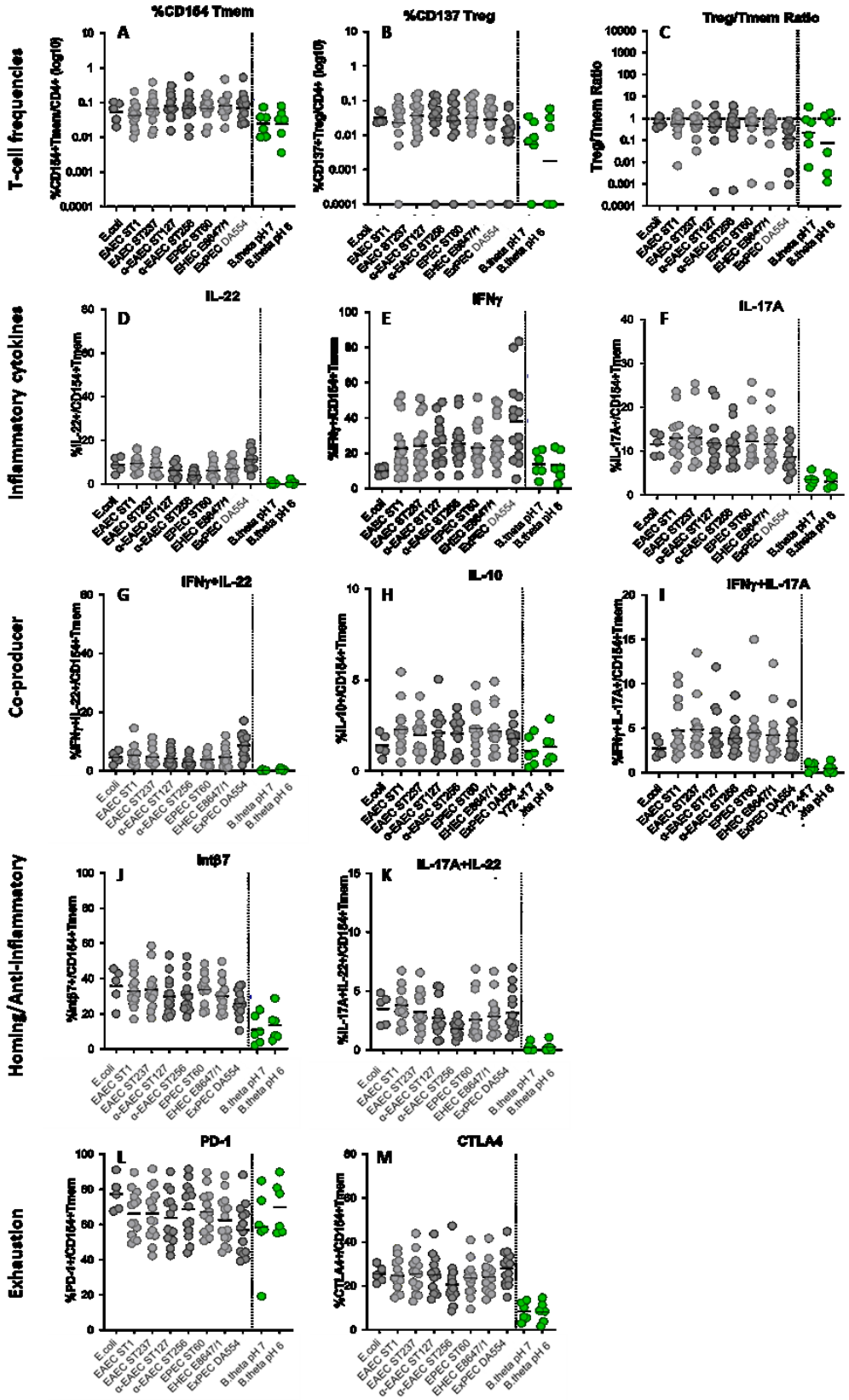

Figure 28: ARTE assay of pathogenic *E. coli* strains and *B. thetaiotaomicron* grown in pH 7 and pH 6. (A) - (C) T-cells had higher frequencies to *E. coli* strains compared to *B. thetaiotaomicron* grown in pH 6 and pH 7. (D)-(F) Inflammatory cytokines were more present with *E. coli* strains and no differences between *B. thetaiotaomicron* grown in pH 6 and pH 7 can be observed. (G) – (I) Observing Co-producer and (J) + (K) Homing/Anti-Inflammatory it can be noticed, that the *E. coli* strains provoked a stronger reaction compared to *B. thetaiotaomicron* grown in both conditions. (L) + (M) Exhaustion assay showed as well mostly a stronger reaction to *E. coli* strains compared to *B. thetaiotaomicron*. Each lysate was tested once per donor. In cooperation with Prof. P. Bacher and S. Schneiders (modified).

4. Discussion

4.1 Phenotypic plasticity of single bacterial isolation during changing environments

The three gut bacteria *B. producta*, *B. thetaiotaomicron* and *B. longum* were tested for their phenotypic plasticity to different pH, various saccharides as main carbon source and in two media with different additives. Investigating single bacterial isolates under various physiological and IBD-relevant stress conditions provides important insights to decipher their plasticity and discover the functional potential.

4.1.1 Alterations in pH reduces biomass of common gut bacteria, potentially opening niches for pathogen during inflammation

For the Gram-positive Bacillota (formerly Firmicute) *B. producta* changing conditions to the more basic environment had no impact on the growth. After inoculating from a pre-culture grown in standard YCFA (pH 6.8), cultures grown in media with pH 6 had an elongated lag phase. This longer adaptation to the acidic conditions indicates a longer time to adjust the metabolism accordingly, most likely to prepare for optimal exponential growth (Rolfe et al., 2012). Hence, *B. producta* appears to be sensitive to environmental changes to more acidic conditions. The Gram-negative *B. thetaiotaomicron* showed similar growth behaviour under acidic conditions compared to *B. producta*, having an elongated adaptation phase, slower growth and less biomass formation in the more acidic conditions.

In patients with IBD, a disruption of the intestinal pH can be noticed. Studies showed a decrease in the colonic luminal pH for both, CD and UC patients. The low pH values might be caused by an increased concentrations of SCFAs or the disturbed SCFAs absorption (Barkas et al., 2013). The influence of SCFA itself on the bacterial growth will be addressed later on in this thesis in chapter 4.1.3. Only limited results regarding the pH values within the GIT are given for patients with CD (Nugent, 2001), while extreme acidification was observed in the proximal colon with a pH down to 2.3 - 3.4 for patients during active UC (Fallingborg et al., 1993). Since the two bacteria *B. producta* and *B. thetaiotaomicron* showed only low biomass formation in acidic environments *in vitro* in this project, the acidic conditions during inflammation might affect their abundance in the gut as well. Microbiome analysis confirmed a reduction in bacteria of this genera in patients with IBD. It can be observed, that a loss of normal anaerobic bacteria such as *Bacteroides* species (like *B. thetaiotaomicron*), Eubacteriales (like *B. producta*), and *Lactobacillus* species in the diseased gut (Ott, 2004). The reduction of biomass from these bacteria can potentially open the possibility for pathogens, leading to a (further) change in the bacterial community. Pathogens are bacteria with proinflammatory properties and low-pH tolerant microorganism that might invade the vacant niche. Furthermore, the absence of specific bacteria conclusively leads to an absence of beneficial proteins and metabolites.

For *B. producta* only little information about their abundance in IBD can be found, and the results indicate partially contrary information. For example, one study analysed faecal and mucosal microbial

communities in IBD patients and healthy people. It revealed that *Blautia* abundance is significantly reduced in the mucosal microbiota of patients with CD (X. Liu et al., 2021), while in another study, *B. producta* was more abundant during IBD (Fornelos et al., 2020). This stresses the fact that more research and investigation of single bacterial isolates, Culturomics and microbiome analysis in this field is necessary to completely understand the role of single bacterial species in these diseases. This thesis helps to understand the potential functional properties and phenotypic plasticity to IBD-relevant conditions of *B. producta* as single bacterium, which can be put into a greater context, e.g. by investigating the produced proteins (SEPs) of this bacterium, which were found during this project (3.1.4) and are discussed later on.

While the beneficial role of *B. thetaiotaomicron* in IBD has been described by several studies using mouse models (Delday et al., 2019) (K. Li et al., 2021), the effect of different pH on this bacterium in the context of IBD was not investigated yet. Since *B. thetaiotaomicron* had inhibited growth in lower pH environment *in vitro*, it can be assumed that this bacterium also will have a reduced biomass formation in the inflamed gut. A reduced Bacteroidetes species diversity in patients with UC was already reported (Nomura et al., 2021). Additionally, a difference in gene expression and metabolite production can be expected by this bacterium grown in stressful environmental conditions compared to the optimal growth conditions, which will be addressed later in this thesis.

The results for *B. longum* grown in pH 6 and pH 8 differed compared to *B. producta* and *B. thetaiotaomicron*. In contrast to the other species, *B. longum* seems to endure acidic environments, but showed reduced growth in pH 8. Hence, *B. longum* could potentially endure the more acidic environments during inflammation flares in IBD. On the other hand, in a healthy gut this bacterium might be inhibited to grow well in the slightly more alkalic environments of the colon and rectum. Based on current information, *B. longum* is a well-known probiotic gut bacterium, which is capable of modulating the intestinal environment and having physiological effects, such as anti-allergy effects, or is involved in the reduction of harmful bacteria (Sugahara et al., 2015). Although further studies are necessary, *B. longum* strains also showed great potential in reducing inflammation in mouse models (Lin et al., 2023).

4.1.2 The hosts sugar intake could influence single bacterial species differently

In vitro, all three bacteria showed generally better growth with monosaccharides compared to growth in media with polysaccharides provided as main carbon source.

For *B. producta* it was observed that growth was not sufficient when providing starch as polysaccharide, while it grew well on the polysaccharide beta-glucan. Both polysaccharides consist of the monomer D-glucose. However, barley beta-glucan has mainly linear β-1,3/β-1,4-glyosidic bonds,

while starch is a mixture of amylase with α-1,4-glycosidic bonds and amylopectin with α-1,4-glycosidic bonds, which are additionally α-1,6-glycosidic queerly linked. Despite consisting of the same building block, the growth of *B. producta* appears to be strongly influenced by the different glycosidic interconnections. Hence, it appears that this bacterium generally can use polysaccharides, but the linkage of the sugars is crucial for the metabolic exploitability. For modulating bacteria growth by diet, not only the molecular length of the saccharide is crucial, but also the linkage in between the monomers needs to be considered. Furthermore, the location of bacteria in gut and the resulting environmental conditions, connected with the stage of the hosts digestion and broken-down saccharides, might influence the bacterial abundance of *B. producta* quiet strongly. In addition, the presence of other bacteria which are able to metabolize interconnected saccharides, might become important for the growth of *B. producta*, demonstrating the need for symbiotic relations within the gut microbiota. It needs to be kept in mind, that there is also always great competition for easy to metabolize nutrient sources. Those competitions with other bacteria or even the host means a reduction of nutrients in the direct environment, displaying a threat for sufficient growth of *B. producta*, especially when only providing certain polysaccharides.

B. thetaiotaomicron growth was tested with more polysaccharides, and no growth differences between the provided polysaccharides and their concentrations could be observed. Since *B. thetaiotaomicron* is known for its capability to degrade various polysaccharides (Vinke et al., 2017), these observations could be confirmed in YCFA grown monocultures. Nevertheless, the best growth of this bacterium was observed providing short sugars such as glucose and sucrose, which are most likely easy to metabolize, since no further cleavage is needed. This observation was also confirmed on the protein level. Proteome analysis revealed that the protein production of *B. thetaiotaomicron* is mostly unaffected providing a monosaccharide or a disaccharide. The intracellular proteome maintains similar comparing the two growth conditions and only the mechanisms for metabolizing the provided carbon source was adjusted (Genth et al., 2022). The similar growth and the unaffected proteome of *B. thetaiotaomicron* providing two different saccharides indicates its potential for adapting effortless to minor dietary changes.

Observing the growth of *B. longum*, the growth kinetics vary quite drastically. Nevertheless, the best growth conditions were consistently provided by YCFA with sucrose as carbon source in these experiments. Sucrose consists of the monosaccharides glucose and fructose and it was expected, that providing the monosaccharides individually, the growth would be as good or better than with sucrose itself. Surprisingly, the growth with glucose or fructose as main carbon source was not as efficient compared to sucrose or even non-existent. In this case, a close look into the genome, metabolome and proteome would be necessary to complement the phenotypic observations. Potentially, *B. longum* did not grow well in regard of biomass formation, but other metabolic pathways may be activated while

being cultivated in sucrose, glucose or fructose. Since those sugars a relatively common in the Western Diet, it would be important to gain further insight into the bacterial metabolic plasticity regarding short sugars. In most cases, *B. longum* did not grow well providing polysaccharides as main carbon source. While it was discovered, that *B. longum* harbours a high amount of genes which are associated with the oligosaccharide metabolism (Schell et al., 2002), this bacterium seems to be not efficiently capable of degrading longer saccharides in this project. This opens up an opportunity for a potential interaction between the tested bacteria in this thesis. It is known that *B. longum* has good importing system for simple sugars, especially comparing it to the one from *B. thetaiotaomicron* (Wexler, 2007). On the other hand, *B. thetaiotaomicron* can break down a large variety of glycosidic bonds and polysaccharides as described above. Hence, *B. thetaiotaomicron* could provide the metabolic products, which can be used by *B. longum*, enabling a symbiotic interaction between these two considered beneficial bacteria in the competitive environment of the human GIT.

The plasticity of the three tested bacteria *in vitro* in YCFA monoculture could lead to the assumption that the optimal growth conditions to nurture bacteria would be a diet providing them with high amounts of monosaccharides. *In vivo,* the opposite is actually the case: in mouse models it was shown that a high intake of short sugars aggravates inflammation and the consumption of polysaccharides, such as oat beta-glucans, is connected with an improvement of colitis (Khan et al., 2020) (Żyła et al., 2021). A high consumption of simple sugar can modulate the microbiota and shift the balance to bacteria with pro-inflammatory properties (Satokari, 2020). Therefore, potentially harmful bacteria often profit from a high intake of simple sugars. Additionally, the presence of simple sugars has a higher influence on bacteria than just on growth and biomass formation. Monosaccharides, such as fructose and glucose, which are often consumed in the Western diet, can inhibit the „regulator of colonization" *roc* in the commensal gut bacterium *B. thetaiotaomicron*, by influencing the production of the protein necessary for the murine gut colonization (Townsend et al., 2019). Therefore, this beneficial gut bacterium cannot settle in the hosts intestine. Furthermore, in most cases mono- and disaccharides consumed by the host are absorbed in the small intestine and only the relatively indigestible plant polysaccharides can be utilized by microorganisms that inhabit this environment. Alternatively, they have to scavenge the short saccharides hydrolysed by other bacteria to win competition and acquire nutrients (Comstock and Coyne, 2003). Since complex carbohydrates such as resistant starch and beta-glucan can reach the colon, they potentially promote the growth of certain beneficial bacteria and support improvements of clinical remission in patients (Vinke et al., 2017). *B. thetaiotaomicron* grew with both complex carbohydrates and *B. producta* grew well with beta-glucan in this project. In later stages of digestion in the colon, where potentially more polysaccharides are present, the two bacteria are more likely to grow well and enable beneficial symbiotic interaction, compared to *B. longum,* which appeared to be mostly not able to use complex carbohydrates in experiments for this thesis.

Diet, and especially the consumption of various saccharides, is critical for the hosts health and disease due to the influence on the resident gut microbiota. The project shows, that bacteria reacted very differently not only to the length of the provided saccharide (mono-, di-, or polysaccharide), but also the interconnection within the molecule and the composition appeared to be relevant. By integrating more conditions, for example varying the nutrient supply or additionally introduce bacterial competition, the bacterial plasticity and microbial ecology can be further explored, which will promote our understanding of how different saccharides shape bacterial communities and consequently influence the hosts health or disease.

4.1.3 SCFA influencing bacterial growth and inflammation in the gut

While *B. producta* and *B. thetaiotaomicron* mainly seem to be negatively affected by the presence of SCFA in BHI media, *B. longum* showed a higher biomass formation in both tested media when SCFAs were present. Those findings address two topics: how the media composition impacts the experimental outcome and the role of SCFA as environmental factor for the single bacterial isolates in IBD.

The choice of media is critical for the outcome and interpretation of bacterial experiments. For example: The discovery of novel SEPs. In the experimental set up of Petrushke et al., single strain bacteria were cultivated in BHI medium with additives, while for the community experiments in the bioreactor the complex intestinal medium (CIM) with pH 6.7 and constant gassing with N_2 was used (Petruschke et al., 2021). Despite creating different environmental conditions, the production of SEPs by *B. producta* was interpreted as community effect. In contrast, experiments from this project could confirm the production of SEPs in single bacterial cultures grown in YCFA. Suspecting SCFA as relevant trigger for SEPs production, experiments omitting SCFA from YCFA and adding SCFA to BHI media were performed (3.1.3, Fig. 12). Additionally, BHI was modified with yeast extract and LPS to mimic the presence of other microorganisms. SEPs were found to be produced by *B. producta* monoculture across all the tested conditions (Fig. 13), indicating that they potentially harbour an universal role in those single bacterial isolates, completely independent from the presence of a bacterial community. On the other hand, extracellular stressors, such as pH or the presence/absence of endotoxins (i.e., LPS), appear to influence the production of SEPs as well. Hence, the biosynthesis of these SEPs is not exclusively dependent on interspecies interactions or communication within the microbiome, but also on other environmental stressors such as the presence of SCFA and low pH. SEPs only detected at pH 6 (BP5), potentially function in the acid stress response in *B. producta* from monocultures. Nevertheless due to technical limitations, the presence of SEP at low concentrations cannot be excluded (Genth et al., 2023) and further examination of these hard to detect SEPs is necessary to completely understand

their biological function. Regulatory functions of sORFs and their encoded SEPs in humans and bacteria are proposed by several scientists (Leong et al., 2022) (Yadavalli and Yuan, 2022), but more investigation especially concerning community functions and their role in host diseases are needed. Another example illustrating the importance to precisely define the experimental conditions and the biological interpretation of experiments is the influence of SCFA to bacterial growth. In this project, no growth differences could be observed for *B. thetaiotaomicron* grown in YCFA with and without SCFA using the multiplate reader. There was also no significant difference in the growth kinetics in the presence or absence of SCFA for *B. thetaiotaomicron* grown in RUM medium (Rangarajan et al., 2020). These findings would lead to the interpretation, that *B. thetaiotaomicron* in monoculture is not affected by the presence or absence of SCFA. However, the presence of SCFA in BHI medium inhibited its growth drastically in this project, hence this bacterium seems to be negatively affected by the presence of SCFA under certain conditions. This emphasized that experimental interpretations are very context dependent and different experimental outcomes need to be compared cautiously, especially when environmental conditions are different. In regards to IBD it might also mean, that the influence of SCFA on bacteria can vary, making them either a harmful or beneficial factor for bacterial growth depending on other present environmental parameters.

The presence of SCFA is not only an influencing factor on bacterial growth, but SCFA is as well a crucial parameter for IBD and shaping the microenvironment by decreasing the pH. Previously in this thesis (4.1.1.), the negative influence of an acidic pH to the growth of two gut bacteria were addressed. One possible reason for the decreased pH in the GIT of IBD patients might be an increased concentration of SCFAs, caused by a disturbed SCFAs absorption and utilization. This was reported in patients with active UC, conclusively leading to a decreased colonic pH (Barkas et al., 2013). Alterations of SCFAs were generally found in IBD patients. The SCFA butyrate was considered to potentially serve as a biomarker for predicting the disease activity for UC activity (Zhuang et al., 2019). Later studies confirmed the altered SCFA profile in active CD and UC (Kaczmarczyk et al., 2022). Once more, butyric acid was detected as potential biomarker of active IBD, since it was lower abundant in both, patients with active CD and active UC (Kaczmarczyk et al., 2022). In DSS-induced mouse models, it was shown that supplementation of SCFA promoted regulatory T-cell and IL17-producing T-cell expression, which increased the abundance of both, protective and harmful gut bacteria, causing a neutral effect on the inflamed colon (Lee et al., 2022). Hence, SCFA are an indicator for the assessment of IBD and the beneficial effects of SCFAs have been confirmed in patients with IBD (Zhuang et al., 2019).

4.2 Morphological plasticity as an adaptation strategy

Using electron microscopy, the bacterial shape was investigated. While *B. thetaiotaomicron* showed drastic morphological changes in acidic environments, the shape of *B. producta* did not seem to be affected at pH 6. *B. longum* showed overall a polymorphic appearance in the tested pH conditions.

Bacterial shape is genetically determined, but physical forces can also have a considerable influence in bacterial morphogenesis (Fig. 29) (Van Teeseling et al., 2017). Conclusively, genetically identical bacterial cells have the possibility to display different phenotypes; this morphological plasticity might also reflect different functional properties. Phenotypic heterogeneity is known as a coping mechanism for changing environments, protecting against unpredictable environmental conditions, but interestingly different phenotypic variants of bacteria also are manifested independently of environmental contexts (Shen and Chou, 2016) (Choudhary et al., 2023). Besides symmetrical binary fission, any bacterial species has the capability to divide by alternative mechanisms. But so far, there seem to be no universal pathway to induce morphological plasticity, and the precise mechanism of the development of bacterial morphology in response to specific environmental conditions remain mostly unknown (Shen and Chou, 2016). The bacterial morphology contributes to surviving selective pressures. As an example: the spherical shape of a coccoid bacterium has a nearly maximal cytoplasmic volume relative to the membrane surface area while a rod-shaped bacterium has a lower cytoplasmic volume relative to the membrane, which results in a different surface-volume ratio and allows a different nutrient exchange with the environment. Plenty of Gram-negative pathogens change under stressful conditions from rod to coccoid forms. These morphological shifts are sometimes connected with the regulation of the expression of cell envelope and cell wall genes (Van Teeseling et al., 2017). Becoming small and coccoid allows energy conservation during nutritional depletion and prevents to be captured by predators (Young, 2007). Furthermore, a smaller cell surface of the coccoid bacteria might as well reduce attacks from the hosts immune system, since morphological shape might influence the detection of theses bacteria by the immune system (Van Teeseling et al., 2017).

For *B. producta,* the described coccobacillus shape (Liu et al., 2008) could be confirmed in this project. While acidic conditions influence the growth kinetics of this bacterium negatively, the cell shape remains consistently stable. Either this cell shape is already the optimal morphology for this bacterium to cope with changing and stressful environments and there is simply no need to adjust the shape or *B. producta* is not capable to adapt the cell shape. Since the thick peptidoglycan layer of Gram-positive bacteria presumably impedes quick shape shifting as well, developing other mechanisms to overcome stress conditions might be necessary. In this case, other methods such as metabolomics and proteomics are urgently necessary to elucidate adaptation strategies.

Already decades ago, pleomorphism, which is per definition "to exist in a number of morphological forms" (Joshi and Toleti, 2009), was observed in various *Bacteroides* strains, for which large round and fusiform bodies or a unusual granular growth could be noticed (Dienes and Smith, 1944). In another study, it was observed that *Bacteroides* species grown in tryptic soy broth displayed an increase in cell size and extreme polymorphism. Observed under a light microscope, some *Bacteroides* species showed spheroidal and filamentous forms, while others had cocci-bacillary shapes (Okuda et al., 1984). In more recent studies, *B. thetaiotaomicron* showed an elongated phenotype in a sugar-reduced environments and in the presence of sodium. The presence of sodium carbonate potentially changes the membrane potential of the cell wall, resulting in this elongation (Rangarajan et al., 2020). Morphological change appears to be a universal stress reaction of *B. thetaiotaomicron* to environmental challenges. However, the effect of pH stress on bacterial morphology was not examined so far. In this project, an elongation of bacterial cells and polymorphism of *B. thetaiotaomicron* grown in acidic environments could be observed as stress reaction. One potential mechanism for microbes to resist acid stress is to reconstruct their membranes (Hu et al., 2023), this strategy seems to be valid for *B. thetaiotaomicron* and might be used in acidic conditions in patients with IBD as well. Potentially, the different bacterial shapes of the monoculture, could harbour different tasks within the community to overcome the stress condition as an intraspecies community.

In fact, only very few *Bifidobacterium* species display a bifid shape, but there are some polymorphic rod-shaped and bifid-shaped species. *B. longum* was described by Dhanashree et al. as elongated rod-shaped bacterium. It has pleomorphic morphology, which was demonstrated by its change of morphology into a short rod or a bifid shape, exposing it to different conditions such as different salts, amino acids, or higher temperatures, but was not tested for pH changes (Dhanashree et al., 2017). *Bifidobacterium longum* subsp. *longum* strains isolated from fresh faeces samples of healthy infants were cultivated in various media, displayed also pleomorphism such as dumbbell-, V- and Y-shaped in light microscopy as well as in scanning electron microscopy (Zhao et al., 2021). Those observations align with the findings in this project, where *B. longum* showed a heterogeneous cell shape in all tested pH conditions. Especially concerning the pH 6 condition, this bacterium displays as acid resistant in this project, having sufficient growth and no specific morphological adaptation. Either there is no adaptation needed for this bacterium at lower pH or the mechanisms are very effective, so that the adaptation is phenotypical not visible, but potentially present on a molecular level. Hence, solely observing the morphology of this bacterium cannot be used as indication for stress reaction or adaptations, rather growth kinetics and especially -omics methods should be used to identify mechanisms of this bacterium to cope with stress.

Regarding bacterial morphology and pleomorphism during different environmental conditions little to no information is available, like for *B. producta*. In other cases, the studies are relatively old and

possibly outdated, like for *Bacteroides spp.* from the year 1944 and 1984 (Dienes and Smith, 1944) (Okuda et al., 1984). Only a limited number of studies dealing with environmental pH and its influence on bacterial morphology can be found, no further information considering pH changes, host, IBD and bacterial morphology could be retrieved. This stresses the fact, that whole and intensive bacterial characterization, including morphological investigations, are needed in the future, since bacterial shape does not only have implications for bacterial metabolism and adaptation to changing environments, but also influence the host and immune system reaction by changing their size. This project offers insights into that important topic, especially regarding the morphological change in *B. thetaiotaomicron* grown in stressful IBD- relevant conditions. Due to this project, a first effort to close the data gap of morphological changes in potentially IBD-beneficial bacteria grown in acidic conditions is made.

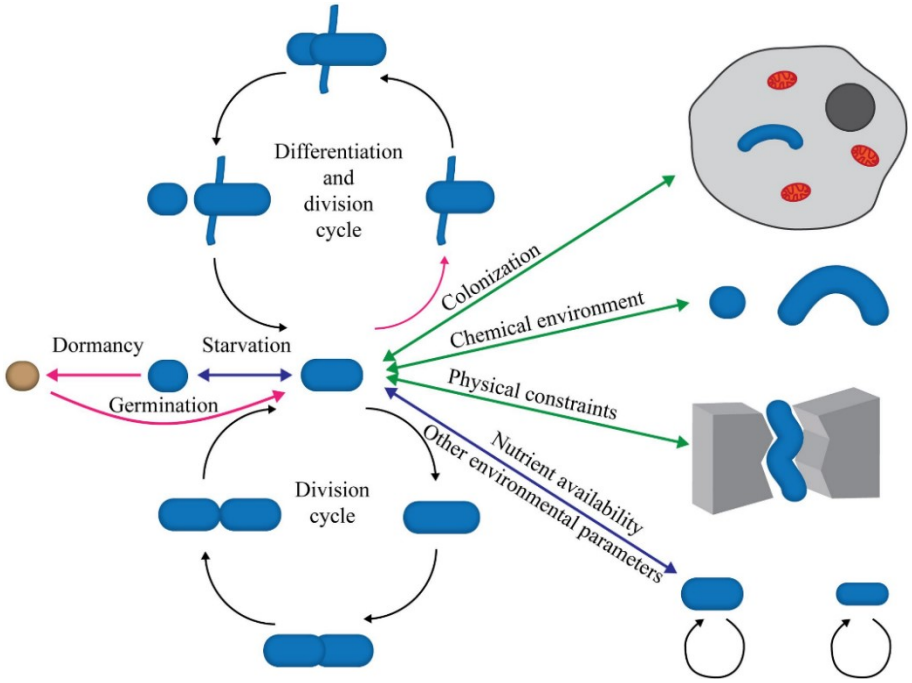

Figure 29: Parameters effecting bacterial shape and size , resulting in different morphologies of bacteria (Van Teeseling et al. 2017).

4.3 Transcriptome data indicate potential genes of interest, especially in *B. thetaiotaomicron* grown in acidic stress conditions

For *B. thetaiotaomicron* grown in pH 6, several genes involved were upregulated, while for *B. producta* in both conditions and for *B. thetaiotaomicron* grown in pH 7 only few significantly expressed genes could be detected and none of them could be regrouped by the FUNAGE server to assign them into pathway or functional groups. Therefore, all further evaluations and assumptions about the role of the up-regulated genes in relation to stress responses refer to *B. thetaiotaomicron* grown at pH 6.

A great number of genes involved in iron acquisition were upregulated, especially siderophore uptake transmembrane genes. Siderophores are low molecular weight Fe(III)-chelating molecules, which are secreted by some bacteria in low iron conditions and are transported via the membrane (Schwyn and Neilands, 1987). The respective TonB-dependent transporters are bacterial outer membrane proteins of Gram-negative bacteria, which are needed to bind and transport these siderophores into the bacterial cell. Additionally, 4Fe-4S binding domains could be detected in *B. thetaiotaomicron* in this project, which contains domains to bind iron-sulphur clusters. It needs to be considered, that all found upregulated genes are membrane associated molecules for iron acquisition. *Bacteroides spp.* itself are not capable of producing siderophores, but uses siderophores produced by other bacteria (Rocha and Krykunivsky, 2017) (Zhu et al., 2020). Since it was grown in monoculture, *B. thetaiotaomicron* potentially unsuccessfully tried to cheat for iron-bound siderophores to overcome the stressful condition. Iron is needed by a huge variety of organisms; in nature and in the host, the concentration of bioavailable iron is always rare and a competitive resource (Skaar, 2010). During inflammation, the availability of iron is even decreased by the host. While some pathogens are able to scavenge this rare iron using siderophores, *B. thetaiotaomicron* survives these low iron conditions during colitis by utilizing siderophores produced by members of the *Enterobacteriaceae* family (Zhu et al., 2020). It is hypothesized by Zhu et al., that this is one possible mechanism of interphylum iron metabolism and its impact gut microbiota resilience against colitis.

Other genes involved in transporter activity and membrane associated processes were detected. An elevated expression of genes encoding for transmembrane transporter complexes and involved in colicin transmembrane transporter activity were found. Colicins are a group of bacteriocins produced by *E. coli* (Cascales et al., 2007). In the experimental setup of *B. thetaiotaomicron* monoculture, presumably no colicin should be present. Apparently, there was a need to modify membrane transporters for this bacterium in acidic conditions, to eventually improve nutrient uptake, toxin excretion or to maintain pH homeostasis inside the bacterial cell by regulating the flow of protons into and outside of the cell. To secure proper molecular and metabolic functions, it is essential for the bacterium to maintain the intracellular pH, which might be difficult to maintain during acidic stress and more transporters or cell wall modification is needed.

Increased expression of genes involved in the CDP-glycerol glycerophosphotransferase activity and in the metabolic pathways of teichoic acid biosynthesis were detected as well. The CDP-glycerol glycerophosphotransferase controls the polymerisation of the main chain of the teichoic acid (Fitzgerald and Foster, 2000). The cell wall-associated teichoic acids are phosphate-rich polymers, which are linked to the cell wall peptidoglycan of Gram-positive bacteria (Fitzgerald and Foster, 2000). Interestingly, *B. thetaiotaomicron* belongs to the Gram-negative bacteria. Additionally, transcription of a predicted AAA-ATPase gene were found to be upregulated, which participate in diverse cellular

processes including membrane fusion and is involved in the lytic endotransglucosylase activity, which is responsible for the cleavage of the peptidoglycan structures of the bacterial cell wall (Das and Bajpai, 2023). Those genes could be indications for the morphology change on *B. thetaiotaomicron* grown in pH 6, which was visible on the EM pictures (chapter 3.2) and lead to possible molecular mechanisms. Changning morphology can assist overcoming stressful conditions by changing the surface to volume ration for maximum nutrient acquisition, improve the attachment to surfaces, influence the active motility or the biofilm formation (Van Teeseling et al., 2017a).

Genes connected to metabolic pathways such as DNA repair, synthesis and methylation are upregulated in *B. thetaiotaomicron* grown in pH 6 in this project. Effectively protecting the DNA against external factors in stressful conditions, such as low pH, is a necessary process for survival. Methylation, for example, protects against DNA degradation by restriction enzymes modifying the DNA chemically (Cheng, 1995). Although in pH 6 *B. thetaiotaomicron* had reduced growth and biomass formation, the upregulation of corresponding genes indicates the possibility of this bacterium to protect its DNA against acidic conditions. Nevertheless, the low pH in an inflamed gut potentially influences the DNA repair of commensal gut bacteria, displaying another factor to cope with for the already stressed and less abundant bacteria. On the other hand, the acid tolerant human pathogen *E. coli* O157:H7 harbours the DNA-binding protein in starved cells (Dps) to resist acidic conditions by binding to DNA and forming secondary structures. If this protein is knocked out, the acid stress results in DNA damage that is more pronounced in these mutants (Jeong et al., 2008). Hence, this leads to the assumption that in IBD, if bacteria that do not harbour this protein or other protection mechanisms, will undergo more severe DNA damage and have a reduced growth compared to acidic tolerant pathogens, leading to a further dysbiosis in the gut.

Furthermore, elevated gene expression concerning pyruvate and pyruvate-derivate metabolism and reactions were discovered under lower pH. It is reported, that pyruvate-associated acid resistance mechanisms occurring in *E. coli* strains grown in glucose-rich medium (Wu et al., 2014). This project revealed first indications of similar acidic resistance mechanism potentially present in *B. thetaiotaomicron*, although its growth in acidic conditions was slower and with less biomass formation compared to the growth in pH 7 and pH 8. Hence, the resistance mechanisms are potentially at the expense of good growth in order to survive. Nevertheless, growth would be possibly even more inhibited, if mechanisms like this would be not activated.

Additionally, upregulated transcription of enzymes involved in sugar metabolisms were detected, such as from the ROK (Repressor, ORF, Kinase) family, a group of proteins connected to transcriptional repressors, sugar kinases and yet uncharacterised open reading frames (Kazanov et al., 2013). Although the standard YCFA media does not directly provide other sugars than glucose, genes were

upregulated which encode chemical reactions for rhamnose catabolic process, lactose catabolism and acetylxylan esterase activity, the latter is responsible for the deacetylation of xylans/xylo-oligosaccharides. The only potential source for those plant- and milk derived sugars, might originate from the yeast extract or the casitone in the complex YCFA media. Since those genes are not upregulated in bacteria grown in pH 7, there appears to be a need of further energy source under acidic stress at pH 6. In low pH conditions during IBD, that this adjustment exhaust energy capacities for the bacterial growth or it is possible that the bacteria are not capable of suppling the need of additional sugars, reducing their abundance in the dysbiotic gut even more.

Genes encoding for the acetyltransferase (GNAT family) and involved in their activity were upregulated. Acetyltransferases are enzymes that use acetyl coenzyme A (CoA) to transfer an acetyl group to a substrate (Galdieri et al., 2014). So far, it is reported for Gram-negative bacteria, that (protein) acetylation is a mechanism to endure low pH conditions and modulate the bacterial virulence (Ren et al., 2016) (Ren et al., 2019). Genes contributing to protein production and folding were found upregulated under acidic stress in *B. thetaiotaomicron*. Further evaluation by proteome analysis could elucidate the protein modification as stress resistance mechanisms for bacteria grown in pH 6.

The transcriptome of *B. thetaiotaomicron* grown in acidic conditions revealed several genes encoding for enzymes, which are potentially involved acid resistance mechanisms, such as DNA repair, transporter activities or iron acquisition. Those findings can be as well relevant for IBD conditions, where the pH is low and iron is reduced and these insights could be furthermore important for potential interspecies interactions in stressful environments. In regard to the data, it needs to be considered, that the overall repetition numbers for the experiments are small. To support the results of this project, the experiments need to be repeated with an increased sample size. The here discovered over-expressed genes already provide great insights and a further experimental validation would be the next step to securely determine if the encoded enzymes, proteins and metabolites are actually produced and optimally going back into (bacterial) cell culture experiments in the future.

4.4 Metabolite production as an adaption strategy in acidic environments for bacteria influencing IBD

Grown in acidic conditions, a general reduction of metabolites in *B. producta* and *B. thetaiotaomicron* especially considering amino acids and cofactors can be noticed. Ejecting produced metabolites and proteins out of the cell could be a potential mechanism to maintain homeostasis. Slowing down metabolic and cellular processes might be a stress compensation, so that bacteria conserve energy to recover quickly when conditions become beneficial again (Czech et al., 2022). If less metabolites are

produced, less metabolites can be transferred or transported, resulting in limited interactions with environment and host cells during the stressful acidic conditions in an inflamed gut.

B. producta grown in pH 6 showed low levels of acetate and amino acids in its intracellular metabolome. Some amino acids, including glycine, threonine, glutamate, lysine, ornithine, and aspartate, can be metabolized by anaerobic bacteria to acetate (Fotschki et al., 2020). A low level of these amino acids results subsequently in a low level of that fatty acid. Gut bacteria are able to either provide amino acids for the host or obtain them by utilizing them, hence they are able to alter the bioavailability of amino acids (Neis et al., 2015). This opens opportunities for interactions and cross feeding not only with other bacteria, but also with the host. The amino acid tryptophan is strongly increased in acidic grown *B. producta*. *Blautia* spp. are reported to biosynthesize aromatic amino acids such as tryptophan (Maturana and Cárdenas, 2021). If the excessive amount of intracellular tryptophan is released into the surrounding, it could have a beneficial effect against host inflammation. In the human gut, tryptophan is an essential amino acid for the mucosal cells and a deficiency is associated with intestinal inflammation. A tryptophan depletion was reported to contribute to the development of IBD and provoke the disease activity (X. Li et al., 2021) (Nikolaus et al., 2017). Besides the amino acids, several cofactors are lower abundant for *B. producta* in acidic conditions. Uridine monophosphate is a second messengers and an intermediate in pyrimidine biosynthesis, which is important for de novo synthesis of ribonucleotides (Seifert, 2015) (Moffatt and Ashihara, 2002). Moreover, a decreased intracellular amount of the cofactor metabolisms associated ADP/ATP and NADP can be detected in *B. producta*. All these parameters potentially point towards less energy generation, slower RNA synthesis and reduced metabolic activity during stressful conditions, which explains the lower biomass formation and slower growth observed in pH 6. Hence, in the diseased gut both the growth and metabolism of *B. producta* is most likely negatively affected by the inflammation associated reduced pH.

Additionally, low intracellular inositol is detected for *B. producta* grown in pH 6. Shown by the transcriptome, this bacterium harbours genes coding for inositol 2-dehydrogenase and myo-inosose-2 dehydrogenase, which are linked to the inositol phosphate metabolisms, but are not significantly up or down regulated. Inositol and its derivatives are potential key metabolites in connection to IBD. The absence of inositol influences bacterial growth and hosts inflammation. Mainly found in eukaryotic cells, myo-inositol displays an essential nutrient to build phosphatidylinositol, an important compound in lipid homeostasis. In mouse models, the absence of the enzyme Src homology 2 (SH2)-containing inositol-5-phosphatase (SHIP), resulted in a further damaging inflammation of the distal ileum (Kerr et al., 2011). It was proposed that eukaryotic cells require an enzymatically active SHIP for sufficient immune function and homeostasis in the small intestine, suggesting that inositol plays a major role in IBD-like inflammation (Kerr et al., 2011). Another study verified the anti-inflammatory/antioxidant

effect of myo-inositol in human cellular models in the context of diabetes, attributing this inositol derivative with a protective action against chronic inflammation (Baldassarre et al., 2021). In this project, no inositol or its derivatives could be metabolically detected in *B. longum* and *B. thetaiotaomicron*, but for *B. thetaiotaomicron* it was described to produce inositol lipids and sphingolipids (Heaver et al., 2022). While during *in vitro* experiments, the loss of inositol lipid production altered the capsule expression and antimicrobial peptide resistance in this bacterium, *in vivo* mouse models revealed that the loss of inositol lipids decreased the bacterial fitness. These findings point out that inositol and the inositol lipids are important for the bacterial resistance to host immune defences and for general fitness in the mammalian gut, also fostering the cross-kingdom communication between the bacteria and the host (Heaver et al., 2022). Metabolites can be very unstable, and in this project, the metabolic analysis only provide a snap shot of the intracellular metabolome. Hence, it still might be possible to detect inositol in *B. thetaiotaomicron* by repeating the experiments and choosing different time points conducting metabolome lysates for analysis. Nevertheless, in this project genes encoding inositol monophosphate 1-phosphatase and inositol-3-phosphate synthetase are slightly, but not significantly, upregulated in the transcriptome of *B. thetaiotaomicron* grown on pH 6. Consequently, this bacterium is theoretically capable of producing inositol or its derivatives.

The increased abundance of the amino acid valine in *B. thetaiotaomicron* during acidic conditions could be connected to biofilm formation. It is reported that biofilms of the Gram-negative *E. coli* secrete great amounts of valine, when carbon sources are not limited. Additionally, elevated valine concentrations due to changes in the amino acid biosynthetic pathways have been reported caused by acidic stress (Valle et al., 2008). Therefore, the increased amounts of intracellular valine in *B. thetaiotaomicron* could be an indication for biofilm formation to increase survival chances and as a mechanism to survive acidic stress. Uridine diphosphate is a transporter of monosaccharides (Bhagavan, 2002), which could indicate for an increased need for effective sugar transport in *B. thetaiotaomicron* grown in pH 6. In the transcriptome analysis, genes encoding enzymes for the utilization of casitone and yeast extract derived sugars are upregulated in pH 6 complementing this indication. Furthermore, in the transcriptome of *B. thetaiotaomicron* in acidic conditions genes coding NADH dehydrogenase are upregulated, which is reflected in an intracellular enrichment in NAD observing the corresponding metabolome data. The regeneration of NAD+ from NADH is needed for glycolysis, which is connected to energy generation. Additionally, the amount of PEP is increased. The metabolism of PEP to pyruvic acid by the pyruvate kinase generates ATP, which is also increased in the intracellular metabolome. It appears that more energy generation is needed to adapt to these stressful conditions, for example to modify the membrane and morphology. Ethanol could be also detected intracellularly in *B. thetaiotaomicron*, potentially derived from sugar fermentation. It was reported

that *B. thetaiotaomicron* is indeed capable of producing small amounts of ethanol when grown in MCB medium at low pH 4-5 (Elshaghabee et al., 2016). While it could be a bacterial byproduct of *B. thetaiotaomicron* produced in acidic conditions, if the ethanol is released into the environment, it can cause health problems for the host, especially when being predisposed like during inflammation in IBD. Ethanol alone can be intrarectally applied in mouse models to induce colitis. The animals developed a severe inflammation affecting the mucosa and submucosa of colon (Andrade et al., 2003). Compliant with this, in most cases alcohol consumption in patients with IBD is associated with a higher risk of relapse and more pronounced symptoms (Piovezani Ramos and Kane, 2021).

An increased amount of SCFA can be detected in *B. longum* grown at pH 6. Those could derived either from a bacterial production since *Bifidobacterium* species are known to produce various SCFA (Yoon et al., 2023), or they were acquired from the YCFA medium, but are not further metabolized. Most likely, the glucose of the medium was metabolized to SCFA, since Bifidobacteria have the ability to change monosaccharides into intermediates of the hexose fermentation pathway, and later on are converted to SCFAs (Pokusaeva et al., 2011), which could result in the accumulation of SCFA. For some bacterial species, citrate is an important metabolite, since it can be utilized as a carbon source and plays a role in resistance against low pH. While for *Lactococcus lactis* it is published that the citrate cometabolism with glucose, compared to growth on glucose alone, provided an advantage during low pH conditions (Magni et al., 1999), on the other hand for *Streptococcus mutans* grown in acidic conditions, intracellular citrate inhibited its growth (Korithoski et al., 2005). The decrease of citrate in *B. longum* grown in pH 6 could potentially indicate either a use of citrate as an additionally needed carbon source or a discard of citrate as a protection mechanism. Further pyruvate was found intracellular in this bacterium grown in pH6. It is reported, that some bacteria protect themselves from acidic stress by regulating the glucose-derived production of pyruvate, pyruvate-acetate efflux, or reversion from acetate to pyruvate (Wu et al., 2014). Hence, regulating the abundance of pyruvate can be assigned to acidic stress resistance in *B. longum*. Arginine is intracellularly decreased in *B. longum*, equally to *B. thetaiotaomicron*. Arginine is a crucial amino acid for sustaining bacterial growth and can be used as both, carbon and nitrogen source (Scribani Rossi et al., 2022). Additionally, for some bacteria the arginine metabolism is linked to bacterial pathogenesis, since they can target arginine for self-preservation. Here, the arginase produced by bacteria can compete for arginine and therefore inhibit the NO production of the host, which is important for the innate immunity (Xiong et al., 2016). Arginine is also involved in the synthesis of bacterial metabolites and it was shown that the supplementation of dietary arginine is protective in colitis models (Singh et al., 2019). *B. longum* grew well in pH 6 but apparently lack the possibility to synthesize arginine in this condition, while *B. producta* had an enhanced level of arginine in low pH, but did not build sufficient biomass. The absence or presence of arginine in low pH conditions is not only crucial for the bacterium itself, but also fosters

possible cross feeding and plays a crucial role during inflammation. On the other hand, the amino acid aspartate was increased in *B. longum*. This amino acid can be utilized by *B. longum* in stressful conditions as a nutrient source to secure sufficient growth even at low pH and potentially also during inflammation, since it can be used as a component of cell wall peptidoglycan and could be also probably used for cell wall modification or as nitrogen source (Kajitani et al., 2022) (Schubert et al., 2021). Taurine is decreased in *B. longum*, while being increased in *B. producta*. This amino acids has various important functions, for example it can prevent inflammation, it can be utilized as a modulator to restore a favourable microenvironment and to prevent gut dysbiosis (Qian et al., 2023). In the low pH environment during inflammation*, B. longum* probably shows more sufficient growth compared to the other in this project tested bacteria, but produced less taurine and subsequently less of this amino acid could be released, which would potentially lead to less inflammation prevention in a diseased gut.

In the low pH conditions of an inflamed gut, the two bacteria *B. producta* and *B. thetaiotaomicron* are potentially lower in biomass and therefore are not able to provide as much useful metabolites, contributing to the maintenance of a healthy gut. Additionally, the production or consumption of beneficial metabolites is altered in the bacteria, demonstrated for example by the absence of inositol in *B. producta* or taurine in *B. longum*. On the other hand, metabolites aggravating inflammation like ethanol are produced. Nevertheless, potentially helpful metabolites such as tryptophane or probably SCFA are produced as well in acidic conditions, which have an anti-inflammatory effect. This project shows that, in most cases the bacterial metabolome is altered to adjust and survive the stressful conditions. Analysing the intracellular metabolome is important to fully investigate the functional potential within single bacterial isolates, especially bringing it into context with the transcriptome data. It needs to be considered, that the metabolomic data of this project cover a snap shot. A time series of produced metabolites and also the secretome would elucidate results of the metabolome more intensively, providing more opportunities to discover key metabolites, particularly taken together with transcriptome and proteome analysis.

4.5 Biological interactions shape the bacterial community and the host

To obtain further insights into the functional potential of bacteria, biological interactions need to be taken into account. Conducting co-cultures of *B. producta* and *B. thetaiotaomicron* comprised unexpected challenges and hitherto indistinct results. While improving inoculation of the two bacteria starting the co-culture, the results revealed *B. thetaiotaomicron* as dominant member at that time. Repeating the experiments to determine the best time point for sampling for proteome lysis, the results were not reproducible. In later qPCR analysis, *B. producta* appeared to be the dominant member.

Other co-culture studies investigating *B. thetaiotaomicron* with another member of the *Blautia* genus, *Blautia hydrogenotrophica* (*B. hydrogenotrophica*), in *in vivo* gnotobiotic mouse experiments and also *in vitro* experiments demonstrated that *B. hydrogenotrophica* was able to exploit the hydrogen produced by *B. thetaiotaomicron* (Rey et al., 2010). In return *B. thetaiotaomicron* was therefore enabled to regenerate NAD+ which is needed for glycolysis, otherwise the reoxidation of NADH to NAD+ would be inhibited by the accumulation of H_2. *B. hydrogenotrophica* benefited greatly from the presence of *B. thetaiotaomicron* in those experiments. In another *in vitro* co-culture experiment from *B. thetaiotaomicron* with the beneficial gut bacterium *Roseburia intestinalis (R. intestinalis),* the symbiotic potential of *B. thetaiotaomicron* was shown as well. While *B. thetaiotaomicron* is capable of acquiring several mucin monosaccharides due to its central carbon/energy metabolism, the presence of mucin inhibits the growth of *R. intestinalis. R. intestinalis* uses carbon chain elongation to generate additional energy and maintain a redox balance, as well as change its energy source to acetate and lactate, which are generated by *B. thetaiotaomicron* (Liu et al., 2023). On the other hand, during acidic stress *B. thetaiotaomicron* potentially release toxins that are connected to the loss of viability of *R. intestinalis* during that co-culture experiments (Liu et al., 2023)*,* stressing the importance of further investigating those complex interactions. Besides the capability of direct biological interactions with some gut bacteria community members, *B. thetaiotaomicron* has the possibility to interact via outer membrane vesicles (OMVs) with other bacteria or the hosts immune system (Valguarnera et al., 2018). Hence, including pure OMVs or supernatants of *B. thetaiotaomicron* into bacterial cultures or cell cultures would be a nice opportunity to investigate further their biological functions.

Biological interactions from members of the genus *Blautia* are reported, such as the cross-feeding relationships from *B. hydrogenotrophica* with other members of the gut microbiota (Plichta et al., 2016) and *B. coccoides* producing SCFAs, which act as relevant metabolic mediators between the microbiota and the host (X. Liu et al., 2021). For the species *B. producta* little information can be retrieved. Consequently, more research of this commensal bacterial species is needed, especially since during this thesis novel SEPs were discovered (4.3.1), which have the potential to interact with the host and other bacterial members, probably acting as antimicrobial peptides. In this project, it was as well discovered that *B. producta* produces SEPs independent of the community. Regarding the role of *B. producta* in bacterial interactions and its produced SEPs, the interpretation of other experiments is essentially influenced by this finding.

Regarding the co-culture experiments in this project, one potential source of error lay within the selection of primers used for qPCR. The primer efficiency was similar for both bacteria, but not identical. Additionally, the primers for *B. thetaiotaomicron* and *B. producta* had slightly different annealing temperatures, providing for one primer potentially more optimal conditions and therefore influencing the results. It is necessary to search more intensively for efficient primers with identical

annealing temperatures. First measures were made to improve the general co-culture work flow. The DNA extraction method is different for Gram-negative and Gram-positive bacteria, hence it was firstly decided to choose to follow the Gram-positive extraction protocol, before switching to the microbiome kit. This kit covers the extraction of more diverse bacterial species, successfully improving the overall DNA amount after isolation. Nevertheless, results were still not optimally reproduceable. Further, the cell shape can influence the OD measurements strongly and lead to inaccurate starting ratios. Since the BactoBox is able to measure the intact cells in a suspension, the inoculation of the start inoculum could be improved compared to using the OD. Besides that, with the BactoBox it might be possible to distinguish two different cell types. Since *B. producta* is cocci shaped and *B. thetaiotaomicron* is mainly rod shaped, a customized approach using BactoBoxExplorer would be a possibility to differentiate the two species and allows an accurate measurement of the cell ratio in the co-culture.

Besides using the quantitative approach via real-time PCR to investigate the outcome of bacterial interspecies competition, another method could be streaking out the co-cultures on selective agar. Streaking out *B. thetaiotaomicron* monocultures over time and *B. thetaiotaomicron*/*B. producta* co-cultures for the same timepoints on MacConkey, which selects for Gram-negative organisms by inhibiting Gram-positive organisms, can help to discover whether the presence of another bacterium had enhancing or inhibiting effects on the growth of *B. thetaiotaomicron* compared to its growth in monoculture.

In the future, observing more bacterial partners, including pathogens such as adhesive *E. coli*, whole bacterial communities like SIHUMIx or including even host cells would considerably contribute to the investigation of the plasticity from different bacteria and their functional potential. For the biological context and the ecological function within the gut, it would be insightful to observe, if and how pathogens or other commensal bacteria inhibit or promote each other's growth. Firstly, cultivating bacteria together providing an environment with optimal conditions would be necessary to investigate their potential to interact, including proteomic and metabolomic analysis. Afterwards including IBD relevant stressors, such as low pH, would allow to elucidate whether the relation and interaction of bacteria change with the environmental changes. This could help to identify key bacterial species and environmental conditions which could act as "adjusting screw", concerning community dynamics and maintaining the hosts health. Including -omics methods would be needed to even further characterize bacterial functions and identify key metabolites or proteins.

4.6 Stress reaction of beneficial gut bacteria do not cause T-cell activation

Commensal bacteria are capable of regulating the development of T-helper 17 (Th17) and regulatory T-cells (Treg). While Treg cells are generally connected to immune homeostasis by maintaining the unresponsiveness to self-antigens or inhibiting an exaggerated immune response (Rocamora-Reverte et al., 2021), Th17 cells, a CD4+ T-cell subset, are able to produce the proinflammatory interleukin-17 (IL-17) (Tesmer et al., 2008). Those T-cells harbour also a connection to the immunological homeostasis in the human gut and T-cells play a crucial role in IBD. In patients with IBD a dysfunctional interaction between gut microbiota and the mucosal immune system is observed, characterized by an exaggerated reaction of effector T-cells against common bacterial antigens or deficient Treg cell function, leading to an overproduction of proinflammatory cytokines (Silva et al., 2016). In addition, the Th17 cells may play an significant role in the development and persistence of IBD (Silva et al., 2016) (Mirsepasi-Lauridsen et al., 2019). In this project, while all the pathogenic *E. coli* species provoked a T-cell reaction, *B. thetaiotaomicron* grown in stressful low pH conditions did not provoke increased frequencies of antigen-specific T cells or a stronger cytokine release compared to the one grown under neutral pH. This aligns with the fact, that healthy T-cells react to pathogens, but not to commensal bacteria.

A low pH in the environment found at inflammatory site additionally influences the immune response by suppressing the T cell-mediated immunity and cytotoxic response (Erra Díaz et al., 2018). The environmental influence of pH on immune reaction and the reduced growth of stressed bacteria might be a driving factor in IBD. For *B. thetaiotaomicron* as well as *B. producta* the low pH displays as stressor and inhibits their growth (3.1.1). While proposing that stressed bacteria might produce (harmful) byproducts in order to their physiological adaptation, the ARTE assay provides indications that for the immune system there is no discrimination between stressed and non-stressed commensal bacteria. Hence, the stressed commensal bacteria remain beneficial, independent of the environmental pH. The cell shape, which is altered in *B. thetaiotaomicron* and *B. longum* in low pH, potentially influences the immune cell reaction and facilitate a reduced detection by the immune system (Veyrier et al., 2015). *B. producta* might provoke no further immune reaction when grown in acidic conditions as well, since its shape was not affected by pH 6 and the reduced cell surface of the coccoid bacteria lower attacks and detection from the hosts immune system (Van Teeseling et al., 2017). The observations of this thesis need to be verified by further ARTE assays and other host related experiments, for example with using a triple cell model that incorporate the classical Caco-2 cell model with mucin-secreting HT29-MTX-E12 goblet cells and exposing them differently shaped bacteria. Generally, it would be interesting to further investigate the effect of acidic conditions on the morphologies of pathogenic bacteria, and subsequently the impact on immune system reaction to further elucidate the influence of stress reactions of already harmful bacteria on human health and disease, especially in the context of predisposed patients. In *E. coli,* several regulatory systems which control acid resistance, enabling the

bacterium to survive under acidic conditions without actually displaying growth (Xu et al., 2020). This could be a relevant fact for the acidified GIT of patients with IBD, as *E. coli*, and potentially pathogenic *E. coli* species as well, do have the ability to persist those unfavourable conditions.

The intestinal microbiome of patients with IBD shows an enrichment in *Enterobacteriaceae*, possessing a higher amount of virulence factors (Moustafa et al., 2018). Pathogenic strains of the common gut bacterium *E. coli,* belonging to that bacterial family, might be a potential reason for the outbreak of IBD or disease relapses in IBD patients, due to its capability to potentially adhere and invade epithelial cells and multiply within macrophages (Mirsepasi-Lauridsen et al., 2019). *E. coli* was associated with both CD and UC, the isolated species from IBD patients showed adhesive properties, similar to those of other pathogenic intestinal *E. coli* (Burke and Axon, 1988). Generally, pathogenic *E. coli* are associated with GIT related diseases and cause symptoms such as acute or persistent bloody or watery diarrhoea (Kaur et al., 2010) (Nguyen and Sperandio, 2012) (Clarke et al., 2003). For this project, the T- cell reaction to pathogenic enterohemorrhagic *E. coli* (EHEC), enteroaggregative *E. coli* (EAEC) and enteropathogenic *E. coli* (EPEC) were investigated, all isolated from stool samples from the routine Diagnostic. Another important pathogenic *E. coli* in IBD is the adherent invasive *E. coli* (AIEC). The increased abundance of AIEC was discovered to be disease-related in patients with both, CD and UC (Kamali Dolatabadi et al., 2021). Furthermore, animal models showed that specific AIEC phenotypes are pathologically relevant, having an increased capability to cause colitis in comparison to other commensal *E. coli* strains. Moreover, it was observed that *E. coli* strains without virulence factors can prevent inflammation (Kittana et al., 2023). Therefore, it would be interesting to include AIEC in further projects and investigate the T-cell reaction after grown in different IBD relevant conditions, e.g. testing pathogenic *E. coli* grown in anaerobe and low pH conditions to evaluate potentially different T cell reactions.

Observing T-cell reactions to different bacteria is important since the immune reaction in a dysbiotic gut is connected to the inflammation in IBD. Generally, it would be crucial to test more potentially beneficial bacteria and bacterial communities, for example mix of several bacteria such as SIHUMIx together. Additionally, the ARTE assay with pathogens grown in different conditions would be important to elucidate if the T-cell reaction is increased or decreased when culturing potentially harmful bacteria differently. With this, specific beneficial conditions or even risk factors could be discovered, which could be a modulator in IBD, for the gut microbiome and the hosts immune reaction. So far, the ARTE assay for this project was conducted with blood from healthy donors. It would be interesting to investigate the T-cell reaction of blood from IBD-diseased donors to the differently grown bacteria as well, to discover if the T-cells from a diseased host are reacting differently to the stressed and non-stressed commensals and pathogens.

4.7 Strengths, weaknesses and importance of investigating single bacterial isolates

This thesis provides deep insight into the characterization and investigation of the functional potential of single bacterial isolates. This is important, because there is still little information regarding several human associated bacterial species, their properties and their function in the microbial community or in the host; in this case especially for *B. producta*. Microbiome analysis and Culturomics provide intriguing possibilities to get insight into the community dynamics and abundances of specific bacteria, but do not provide information about the functional potential of a single bacterium. A thorough characterization of single bacterial isolates, which are known to be absent or present during health and disease, might help to recognize and understand general patterns and relate them to a whole system. This opens the possibility to detect key molecules, proteins or metabolites, which otherwise would have been neglected. The discovery of key species and bacterial products can be an important complement as a therapeutic target or approach to already existing once. Additionally, identifying changes in single bacteria regarding their metabolome or proteome could potentially have community-wide impacts and implications on gut microbiome function and shaping the gut microbial composition. Nevertheless, one should be cautious of generalization and transferring from artificial *in vitro* results into complex and multifactorial *in vivo* settings. In this project for example, the *in vitro* experiments imply that the optimal saccharides to promote growth of the investigated bacteria are monosaccharides and hence consuming such would be favourable for the hosts health, while the literature and *in vivo* studies showed the opposite.

The conducted microbial growth experiments for this thesis were generally quick and plausible; those experiments can be applied and further developed quickly. The culturing of bacteria in defined conditions provides many options to identify stressors and capture the bacterial mechanisms to overcome them by adjusting their metabolism or protein production. In combination with -omics methods such as metabolomics, proteomics or transcriptomics, the bacterial cultivation becomes a strong tool in (medical) research to gain unique insights into bacteria and their potential benefits for the host. Furthermore, identifying optimal growth conditions might help to produce sufficient biomass for further investigations, such as for the ARTE assay to investigate T-cell reaction to bacterial lysates. Also, identifying conditions that trigger certain behaviour, or e.g. induce SEPs production in bacteria as a stress reaction, allows further important investigations regarding bacteria-bacteria and bacteria-host interaction.

Bacterial growth experiments provide a great insight into plasticity to environmental conditions and are certainly helpful as described above. However, a high growth diversity and difficulty in reproducibility within the experiments can be noticed. This might be due to bacterial aggregate formation, different fitness of overnight cultures and the complex YCFA medium. Aggregate formation could be avoided by vortexing or shaking over time, while the fitness of the overnight cultures is hard

to influence. In this study, the OD was primarily used to determine bacterial growth. This method itself harbours some limitations, which should be considered carefully: the OD does not discriminate between dead and living cells, aggregate formation can lead to false absorption values, and bacterial cells of different size and shape can have different OD values, giving no reliable results on the actual vital cell count. In this project, the rod-shaped bacterium *B. thetaiotaomicron* had generally a higher OD compared to the cocci-shaped bacterium *B. producta* after the same cultivation time. Using the BactoBox it could be noticed that after the same cultivation time in the same medium, *B. producta* had a higher cell count compared to *B. thetaiotaomicron*. Hence, using the OD as measurement for growth is suitable to compare bacterial growth within one species, but it should be cautiously used when comparing growth of different bacteria with each other. To minimize the human error, measurements and media preparation should be conducted, if possible, by the same person with the same equipment and under the same conditions. Depending on the media, this could be acquired by purchase, and ideally, the same provider should be used. To limit pipetting error, it can be considered using a pipette robot.

4.8 Conclusion

This thesis provides insights to elucidate the plasticity and potential role of single bacteria and connecting parameters in IBD. In an inflamed gut a low pH can be observed; in this project *in vitro* experiments revealed the impact of low pH to bacterial growth, morphology, metabolite production and gene expression in certain gut bacteria. *B. producta* and *B. thetaiotaomicron* showed a lower biomass formation, hence potentially allowing harmful bacteria to invade the vacant niche. For *B. producta* novel SEPs were discovered grown in acidic conditions and in different media with and without SCFA. While *B. longum* showed more acidic resistance, it did not grow sufficient in some diet related conditions e.g. with polysaccharides. Especially for *B. thetaiotaomicron*, drastic morphological shifts can be observed at low pH, which could result in bacteria harbouring different tasks within the community to overcome the stress conditions. First transcriptome results show, that *B. thetaiotaomicron* is not only phenotypically affected by acidic conditions, but this also can be reflected the differentially expressed genes. In most cases the bacterial metabolome of the three tested bacteria is adjusted to survive the stress conditions, but the absence of production of certain metabolites, such as inositol, or the production of potentially harmful metabolites might aggravate the inflammation during IBD. In this project, investigating biological interactions via co-culture revealed unexpected difficulties, but also enforced the need for further method development to elucidate this important topic. Regarding host interactions, in this project *B. thetaiotaomicron* did not activate a further T-cell

reaction when grown in stressful acidic conditions. The GIT is a complex environment and understanding the presence of certain bacteria, their plasticity and their functional potential is needed to elucidate single most important mechanisms, key species and metabolites, interconnecting other parameters and their influence on diseases like IBD (Fig. 30).

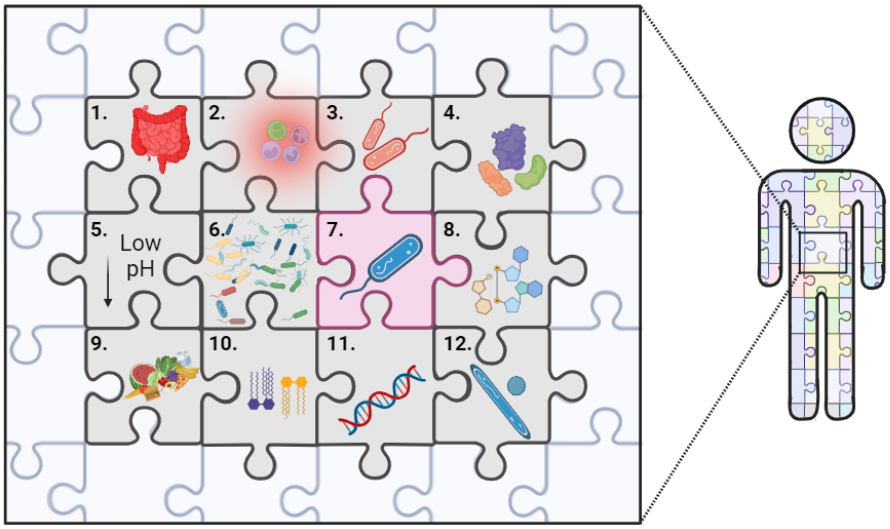

Figure 30: Single bacteria affected by biotic and abiotic factors, influencing other bacteria, host and environment and indicating the complex connections inside a host with IBD 1.) Inflamed gut 2.) Reacting T-cells 3.) (opportunistic) pathogens/harmful bacteria. 4) (Altered) protein production. 5) A low pH can be observed in patients with IBD. 6) Changing microbiome. 7) Understanding the functional potential and phenotypic plasticity of single bacterial strains is crucial for the complete understanding of their role in the host and during disease. 8) (Changed) metabolite production. 9) The hosts diet has influence. 10) The presence of SCFA is crucial for some bacteria and influence the environmental conditions. 11) DNA and gene expression. 12) Bacterial morphology is influenced by the microenvironment

4.9 Outlook

Observing and comparing the bacterial growth in different environmental conditions, with investigating the metabolite and protein production and the gene expression in a time series during different growth phases, would benefit this project greatly. To fully assess the functional potential of bacteria in various phases of growth, metabolomics, proteomics and transcriptomic changes over time are necessary to obtain the full potential of single bacteria in all of their life stages and hence, their full plasticity resisting, adapting and overcoming certain IBD relevant stressors. A special focus could be on the role of SCFA on bacterial growth. Since in IBD the SCFA absorption of epithelia cells is altered and the concentration of SCFA in the gut environment could directly influencing the bacteria, it would be important to have further investigations of the single bacteria regarding the absence or presence of SCFA in different media. It would be interesting to observe the metabolome/secretome, proteome, and transcriptome of YCFA -SCFA grown cultures to evaluate the role of SCFA on single bacteria.

Especially the secretome is of great relevance, since the components of bacteria secreted to the environment provide direct conclusions of interactions with other bacteria and the host.

It is important to continue observing the bacterial morphology, since it provides complementary insights and unique possibilities for a more comprehensive understanding of bacterial adaptation to different environments. The different bacterial cell populations and conspicuous cells within a monoculture observed in this project could be distinguished using flow cytometry. This would allow the quantification and separation of different cell types providing the possibility for further statements and experiments. Additionally, the EM pictures could be used for co-culture experiments. First experiments were conducted in this thesis, but improvement for bacterial discrimination is necessary. Therefore, the bacterial species need to be labelled with fluorescence in situ hybridization (FISH) to allow clear assignment of the bacterial species and their ratio present in the co-culture.

Moreover, bacterial co-cultures could be investigated by streaking them out on selective agar. This would work adequately with *B. thetaiotaomicron* and *B. producta* and other Gram-positive bacteria of SHIUMIx or pathogens on McConkey agar plates, which select for Gram-negative bacteria. Comparing the growth of *B. thetaiotaomicron* monocultures and co-cultured with other bacteria plated on McConkey would allow first indications of symbiotic partners inhibiting or promoting growth for this beneficial gut bacterium. Improving the qPCR work flow further on would afterwards allow quantitative results complementing the qualitatively gained observations. Obtaining precise ratios of bacteria and performing proteome lysis at specific timepoints would enable the possibility to discover key proteins and elucidate proteome changes inside of the bacteria grown in co-culture compared to monocultures.

Complementary to the co-culture experiments, growth experiments using bacterial supernatants and products on beneficial and harmful bacteria could be conducted. Comparing standard bacterial growth and the growth exposing the chosen bacteria to supernatants could indicate positive or negative interactions. If bacteria produce SEPs with potential antimicrobial functions in certain conditions, their effect on other bacteria could be investigated further by designing peptides or working with bacterial supernatants. Beneficial bacteria could potentially provide produced metabolites or proteins for other bacteria, for example via OMVs. While extracted OMVs themselves could be isolated for further growth experiments, promising metabolites such as inositol, could be introduced into the medium of other bacteria.

Additionally, host-bacteria interactions should be analysed with IBD relevant bacteria and their products. With an epithelial cell model and bacteria, OMVs or supernatants the cells fitness could be investigated in the presence of differently cultivated bacteria or their metabolites. This would help to asses if considerably beneficial bacteria grown in stressful conditions, such as low pH, or harmful

bacteria have different effects on the cells compared to bacteria grown in physiological optimal conditions. Moreover, the T-cell reaction to stressed single bacteria, the OMVs or whole bacterial communities could be further investigated using the ARTE assay, to assess and confirm the immunogenic potential of commensal gut bacteria or pathogens grown under IBD relevant stress conditions. In addition, conducting the ARTE assay with blood from IBD patients would give additional insights into the host-driven mechanisms against harmful and beneficial bacteria in healthy and diseased patients.

5. References

Alam, M.T., Amos, G.C.A., Murphy, A.R.J., Murch, S., Wellington, E.M.H., Arasaradnam, R.P., 2020. Microbial imbalance in inflammatory bowel disease patients at different taxonomic levels. Gut Pathog. 12, 1. https://doi.org/10.1186/s13099-019-0341-6

Andrade, M.C., Vaz, N.M., Faria, A.M.C., 2003. Ethanol-induced colitis prevents oral tolerance induction in mice. Braz. J. Med. Biol. Res. 36, 1227–1232. https://doi.org/10.1590/S0100-879X2003000900013

Armstrong, H., Alipour, M., Valcheva, R., Bording-Jorgensen, M., Jovel, J., Zaidi, D., Shah, P., Lou, Y., Ebeling, C., Mason, A.L., Lafleur, D., Jerasi, J., Wong, G.K.-S., Madsen, K., Carroll, M.W., Huynh, H.Q., Dieleman, L.A., Wine, E., 2019. Host immunoglobulin G selectively identifies pathobionts in pediatric inflammatory bowel diseases. Microbiome 7, 1. https://doi.org/10.1186/s40168-018-0604-3

Baldassarre, M.P.A., Di Tomo, P., Centorame, G., Pandolfi, A., Di Pietro, N., Consoli, A., Formoso, G., 2021. Myoinositol Reduces Inflammation and Oxidative Stress in Human Endothelial Cells Exposed In Vivo to Chronic Hyperglycemia. Nutrients 13, 2210. https://doi.org/10.3390/nu13072210

Barkas, F., Liberopoulos, E., Kei, A., Elisaf, M., 2013. Electrolyte and acid-base disorders in inflammatory bowel disease. Ann. Gastroenterol. 26, 23–28.

Bernstein, C.N., 2019. Is Antibiotic Use a Cause of IBD Worldwide? Inflamm. Bowel Dis. izz138. https://doi.org/10.1093/ibd/izz138

Bhagavan, N.V., 2002. Enzymes I: General Properties, Kinetics, and Inhibition, in: Medical Biochemistry. Elsevier, pp. 85–108. https://doi.org/10.1016/B978-012095440-7/50008-1

Blackwell, J., Saxena, S., Jayasooriya, N., Petersen, I., Hotopf, M., Creese, H., Bottle, A., Pollok, R.C.G., 2022. Stoma Formation in Crohn's Disease and the Likelihood of Antidepressant Use: A Population-Based Cohort Study. Clin. Gastroenterol. Hepatol. 20, e703–e710. https://doi.org/10.1016/j.cgh.2020.12.026

Bokemeyer, B., Hardt, J., Hüppe, D., Prenzler, A., Conrad, S., Düffelmeyer, M., Hartmann, P., Hoffstadt, M., Klugmann, T., Schmidt, C., Weismüller, J., Mittendorf, T., Raspe, H., 2013. Clinical status, psychosocial impairments, medical treatment and health care costs for patients with inflammatory bowel disease (IBD) in Germany: An online IBD registry. J. Crohns Colitis 7, 355–368. https://doi.org/10.1016/j.crohns.2012.02.014

Bose, S., Aggarwal, S., Singh, D.V., Acharya, N., 2020. Extracellular vesicles: An emerging platform in gram-positive bacteria. Microb. Cell 7, 312–322. https://doi.org/10.15698/mic2020.12.737

Bravo, J.A., Forsythe, P., Chew, M.V., Escaravage, E., Savignac, H.M., Dinan, T.G., Bienenstock, J., Cryan, J.F., 2011. Ingestion of *Lactobacillus* strain regulates emotional behavior and central GABA receptor expression in a mouse via the vagus nerve. Proc. Natl. Acad. Sci. 108, 16050–16055. https://doi.org/10.1073/pnas.1102999108

Bull, M.J., Plummer, N.T., 2014. Part 1: The Human Gut Microbiome in Health and Disease. Integr. Med. Encinitas Calif 13, 17–22.

Burke, D.A., Axon, A.T., 1988. Adhesive Escherichia coli in inflammatory bowel disease and infective diarrhoea. BMJ 297, 102–104. https://doi.org/10.1136/bmj.297.6641.102

Burke, D.A., Axon, A.T., 1987. Ulcerative colitis and Escherichia coli with adhesive properties. J. Clin. Pathol. 40, 782–786. https://doi.org/10.1136/jcp.40.7.782

Carabotti, M., Scirocco, A., Maselli, M.A., Severi, C., 2015. The gut-brain axis: interactions between enteric microbiota, central and enteric nervous systems. Ann. Gastroenterol. 28, 203–209.

Card, T., 2004. Antibiotic use and the development of Crohn's disease. Gut 53, 246–250. https://doi.org/10.1136/gut.2003.025239

Cascales, E., Buchanan, S.K., Duché, D., Kleanthous, C., Lloubès, R., Postle, K., Riley, M., Slatin, S., Cavard, D., 2007. Colicin Biology. Microbiol. Mol. Biol. Rev. 71, 158–229. https://doi.org/10.1128/MMBR.00036-06

Chen, L., Zhang, Y.-H., Huang, T., Cai, Y.-D., 2016. Gene expression profiling gut microbiota in different races of humans. Sci. Rep. 6, 23075. https://doi.org/10.1038/srep23075

Cheng, X., 1995. Structure and Function of DNA Methyltransferases. Annu. Rev. Biophys. Biomol. Struct. 24, 293–318. https://doi.org/10.1146/annurev.bb.24.060195.001453

Clark, A., Mach, N., 2017. The Crosstalk between the Gut Microbiota and Mitochondria during Exercise. Front. Physiol. 8, 319. https://doi.org/10.3389/fphys.2017.00319

Clarke, S.C., Haigh, R.D., Freestone, P.P.E., Williams, P.H., 2003. Virulence of Enteropathogenic *Escherichia coli* , a Global Pathogen. Clin. Microbiol. Rev. 16, 365–378. https://doi.org/10.1128/CMR.16.3.365-378.2003

Comstock, L.E., Coyne, M.J., 2003. Bacteroides thetaiotaomicron: a dynamic, niche-adapted human symbiont. BioEssays 25, 926–929. https://doi.org/10.1002/bies.10350

Cordain, L., Eaton, S.B., Sebastian, A., Mann, N., Lindeberg, S., Watkins, B.A., O'Keefe, J.H., Brand-Miller, J., 2005. Origins and evolution of the Western diet: health implications for the 21st century1,2. Am. J. Clin. Nutr. 81, 341–354. https://doi.org/10.1093/ajcn.81.2.341

Czech, L., Mais, C.-N., Kratzat, H., Sarmah, P., Giammarinaro, P., Freibert, S.-A., Esser, H.F., Musial, J., Berninghausen, O., Steinchen, W., Beckmann, R., Koch, H.-G., Bange, G., 2022. Inhibition of SRP-dependent protein secretion by the bacterial alarmone (p)ppGpp. Nat. Commun. 13, 1069. https://doi.org/10.1038/s41467-022-28675-0

Das, R., Bajpai, U., 2023. Functional characterization of a DNA-dependent AAA ATPase in a F-cluster mycobacteriophage. Virus Res. 323, 198957. https://doi.org/10.1016/j.virusres.2022.198957

David, L.A., Maurice, C.F., Carmody, R.N., Gootenberg, D.B., Button, J.E., Wolfe, B.E., Ling, A.V., Devlin, A.S., Varma, Y., Fischbach, M.A., Biddinger, S.B., Dutton, R.J., Turnbaugh, P.J., 2014. Diet rapidly and reproducibly alters the human gut microbiome. Nature 505, 559–563. https://doi.org/10.1038/nature12820

De Pessemier, B., Grine, L., Debaere, M., Maes, A., Paetzold, B., Callewaert, C., 2021. Gut–Skin Axis: Current Knowledge of the Interrelationship between Microbial Dysbiosis and Skin Conditions. Microorganisms 9, 353. https://doi.org/10.3390/microorganisms9020353

Delday, M., Mulder, I., Logan, E.T., Grant, G., 2019a. *Bacteroides thetaiotaomicron* Ameliorates Colon Inflammation in Preclinical Models of Crohn's Disease. Inflamm. Bowel Dis. 25, 85–96. https://doi.org/10.1093/ibd/izy281

De Vadder, F., Kovatcheva-Datchary, P., Goncalves, D., Vinera, J., Zitoun, C., Duchampt, A., Bäckhed, F., Mithieux, G., 2014. Microbiota-Generated Metabolites Promote Metabolic Benefits via Gut-Brain Neural Circuits. Cell 156, 84–96. https://doi.org/10.1016/j.cell.2013.12.016

Diakite, A., Dubourg, G., Dione, N., Afouda, P., Bellali, S., Ngom, I.I., Valles, C., Tall, M.L., Lagier, J.-C., Raoult, D., 2020. Optimization and standardization of the culturomics technique for human microbiome exploration. Sci. Rep. 10, 9674. https://doi.org/10.1038/s41598-020-66738-8

Dienes, L., Smith, W.E., 1944a. The Significance of Pleomorphism in *Bacteroides* Strains. J. Bacteriol. 48, 125–153. https://doi.org/10.1128/jb.48.2.125-153.1944

Doecke, J.D., Simms, L.A., Zhao, Z.Z., Huang, N., Hanigan, K., Krishnaprasad, K., Roberts, R.L., Andrews, J.M., Mahy, G., Bampton, P., Lewindon, P., Florin, T., Lawrance, I.C., Gearry, R.B., Montgomery, G.W., Radford-Smith, G.L., 2013. Genetic Susceptibility in IBD: Overlap Between Ulcerative Colitis and Crohn's Disease. Inflamm. Bowel Dis. 19, 240–245. https://doi.org/10.1097/MIB.0b013e3182810041

Dubinsky, V., Reshef, L., Rabinowitz, K., Wasserberg, N., Dotan, I., Gophna, U., 2022. *Escherichia coli* Strains from Patients with Inflammatory Bowel Diseases have Disease-specific Genomic Adaptations. J. Crohns Colitis 16, 1584–1597. https://doi.org/10.1093/ecco-jcc/jjac071

Durant, L., Stentz, R., Noble, A., Brooks, J., Gicheva, N., Reddi, D., O'Connor, M.J., Hoyles, L., McCartney, A.L., Man, R., Pring, E.T., Dilke, S., Hendy, P., Segal, J.P., Lim, D.N.F., Misra, R., Hart, A.L., Arebi, N., Carding, S.R., Knight, S.C., 2020. Bacteroides thetaiotaomicron-derived outer membrane vesicles promote regulatory dendritic cell responses in health but not in inflammatory bowel disease. Microbiome 8, 88. https://doi.org/10.1186/s40168-020-00868-z

Elshaghabee, F.M.F., Bockelmann, W., Meske, D., De Vrese, M., Walte, H.-G., Schrezenmeir, J., Heller, K.J., 2016. Ethanol Production by Selected Intestinal Microorganisms and Lactic Acid Bacteria Growing under Different Nutritional Conditions. Front. Microbiol. 7. https://doi.org/10.3389/fmicb.2016.00047

Enaud, R., Prevel, R., Ciarlo, E., Beaufils, F., Wieërs, G., Guery, B., Delhaes, L., 2020. The Gut-Lung Axis in Health and Respiratory Diseases: A Place for Inter-Organ and Inter-Kingdom Crosstalks. Front. Cell. Infect. Microbiol. 10, 9. https://doi.org/10.3389/fcimb.2020.00009

Erridge, C., 2010. Lysozyme promotes the release of toll-like receptor-2 stimulants from Gram-positive but not Gram-negative intestinal bacteria. Gut Microbes 1, 383–387. https://doi.org/10.4161/gmic.1.6.13726

Evans, D.F., Pye, G., Bramley, R., Clark, A.G., Dyson, T.J., Hardcastle, J.D., 1988. Measurement of gastrointestinal pH profiles in normal ambulant human subjects. Gut 29, 1035–1041. https://doi.org/10.1136/gut.29.8.1035

Ezaki, T., Li, N., Hashimoto, Y., Miura, H., Yamamoto, H., 1994. 16S Ribosomal DNA Sequences of Anaerobic Cocci and Proposal of Ruminococcus hansenii comb. nov. and Ruminococcus productus comb. nov. Int. J. Syst. Bacteriol. 44, 130–136. https://doi.org/10.1099/00207713-44-1-130

Fallingborg, J., Christensen, L.A., Jacobsen, B.A., Rasmussen, S.N., 1993a. Very low intraluminal colonic pH in patients with active ulcerative colitis. Dig. Dis. Sci. 38, 1989–1993. https://doi.org/10.1007/BF01297074

Fitzgerald, S.N., Foster, T.J., 2000. Molecular Analysis of the *tagF* Gene, Encoding CDP-Glycerol:Poly(glycerophosphate) Glycerophosphotransferase of *Staphylococcus epidermidis* ATCC 14990. J. Bacteriol. 182, 1046–1052. https://doi.org/10.1128/JB.182.4.1046-1052.2000

Fornelos, N., Franzosa, E.A., Bishai, J., Annand, J.W., Oka, A., Lloyd-Price, J., Arthur, T.D., Garner, A., Avila-Pacheco, J., Haiser, H.J., Tolonen, A.C., Porter, J.A., Clish, C.B., Sartor, R.B., Huttenhower, C., Vlamakis, H., Xavier, R.J., 2020. Growth effects of N-acylethanolamines on gut bacteria reflect altered bacterial abundances in inflammatory bowel disease. Nat. Microbiol. 5, 486–497. https://doi.org/10.1038/s41564-019-0655-7

Fotschki, B., Juśkiewicz, J., Jurgoński, A., Amarowicz, R., Opyd, P., Bez, J., Muranyi, I., Lykke Petersen, I., Laparra Llopis, M., 2020. Protein-Rich Flours from Quinoa and Buckwheat Favourably Affect the Growth Parameters, Intestinal Microbial Activity and Plasma Lipid Profile of Rats. Nutrients 12, 2781. https://doi.org/10.3390/nu12092781

Galdieri, L., Zhang, T., Rogerson, D., Lleshi, R., Vancura, A., 2014. Protein Acetylation and Acetyl Coenzyme A Metabolism in Budding Yeast. Eukaryot. Cell 13, 1472–1483. https://doi.org/10.1128/EC.00189-14

Genth, J., Kaleja, P., Treitz, C., Schäfer, K., Graspeuntner, S., Rupp, J., Tholey, A., 2022. The intracellular proteome of the gut bacterium *Bacteroides thetaiotaomicron* is widely unaffected by a switch from glucose to sucrose as main carbohydrate source. PROTEOMICS 22, 2200189. https://doi.org/10.1002/pmic.202200189

Genth, J., Schäfer, K., Cassidy, L., Graspeuntner, S., Rupp, J., Tholey, A., 2023. Identification of proteoforms of short open reading frame-encoded peptides in *Blautia producta* under different cultivation conditions. Microbiol. Spectr. e02528-23. https://doi.org/10.1128/spectrum.02528-23

Gill, S.R., Pop, M., DeBoy, R.T., Eckburg, P.B., Turnbaugh, P.J., Samuel, B.S., Gordon, J.I., Relman, D.A., Fraser-Liggett, C.M., Nelson, K.E., 2006. Metagenomic Analysis of the Human Distal Gut Microbiome. Science 312, 1355–1359. https://doi.org/10.1126/science.1124234

Gray, T., Storz, G., Papenfort, K., 2022. Small Proteins; Big Questions. J. Bacteriol. 204, e00341-21. https://doi.org/10.1128/JB.00341-21

Greub, G., 2012. Culturomics: a new approach to study the human microbiome. Clin. Microbiol. Infect. 18, 1157–1159. https://doi.org/10.1111/1469-0691.12032

Heaver, S.L., Le, H.H., Tang, P., Baslé, A., Mirretta Barone, C., Vu, D.L., Waters, J.L., Marles-Wright, J., Johnson, E.L., Campopiano, D.J., Ley, R.E., 2022. Characterization of inositol lipid metabolism in gut-associated Bacteroidetes. Nat. Microbiol. 7, 986–1000. https://doi.org/10.1038/s41564-022-01152-6

Hviid, A., Svanstrom, H., Frisch, M., 2011. Antibiotic use and inflammatory bowel diseases in childhood. Gut 60, 49–54. https://doi.org/10.1136/gut.2010.219683

Jeong, K.C., Hung, K.F., Baumler, D.J., Byrd, J.J., Kaspar, C.W., 2008. Acid stress damage of DNA is prevented by Dps binding in Escherichia coliO157:H7. BMC Microbiol. 8, 181. https://doi.org/10.1186/1471-2180-8-181

Jess, T., Rungoe, C., Peyrin–Biroulet, L., 2012. Risk of Colorectal Cancer in Patients With Ulcerative Colitis: A Meta-analysis of Population-Based Cohort Studies. Clin. Gastroenterol. Hepatol. 10, 639–645. https://doi.org/10.1016/j.cgh.2012.01.010

Jones, E.J., Booth, C., Fonseca, S., Parker, A., Cross, K., Miquel-Clopés, A., Hautefort, I., Mayer, U., Wileman, T., Stentz, R., Carding, S.R., 2020. The Uptake, Trafficking, and Biodistribution of Bacteroides thetaiotaomicron Generated Outer Membrane Vesicles. Front. Microbiol. 11, 57. https://doi.org/10.3389/fmicb.2020.00057

Joshi, H.M., Toleti, R.S., 2009. Nutrition induced pleomorphism and budding mode of reproduction in Deinococcus radiodurans. BMC Res. Notes 2, 123. https://doi.org/10.1186/1756-0500-2-123

Kaczmarczyk, O., Dąbek-Drobny, A., Woźniakiewicz, M., Paśko, P., Piątek-Guziewicz, A., Zwolińska-Wcisło, M., 2022. Altered fecal short-chain fatty acid profile as a potential marker of disease activity in patients with ulcerative colitis and Crohn's disease: a pilot study. Pol. Arch. Intern. Med. https://doi.org/10.20452/pamw.16254

Kajitani, K., Ishikawa, T., Kobayashi, T., Asato, M., Shibata, K., Kouya, T., Takahashi, S., 2022. Mechanism of high d-aspartate production in the lactic acid bacterium Latilactobacillus sp. strain WDN19. Appl. Microbiol. Biotechnol. 106, 2651–2663. https://doi.org/10.1007/s00253-022-11870-w

Kamali Dolatabadi, R., Feizi, A., Halaji, M., Fazeli, H., Adibi, P., 2021. The Prevalence of Adherent-Invasive Escherichia coli and Its Association With Inflammatory Bowel Diseases: A Systematic Review and Meta-Analysis. Front. Med. 8, 730243. https://doi.org/10.3389/fmed.2021.730243

Kaur, P., Chakraborti, A., Asea, A., 2010. Enteroaggregative *Escherichia coli* : An Emerging Enteric Food Borne Pathogen. Interdiscip. Perspect. Infect. Dis. 2010, 1–10. https://doi.org/10.1155/2010/254159

Kazanov, M.D., Li, X., Gelfand, M.S., Osterman, A.L., Rodionov, D.A., 2013. Functional diversification of ROK-family transcriptional regulators of sugar catabolism in the Thermotogae phylum. Nucleic Acids Res. 41, 790–803. https://doi.org/10.1093/nar/gks1184

Kerr, W.G., Park, M.-Y., Maubert, M., Engelman, R.W., 2011. SHIP deficiency causes Crohn's disease-like ileitis. Gut 60, 177–188. https://doi.org/10.1136/gut.2009.202283

Khan, S., Waliullah, S., Godfrey, V., Khan, M.A.W., Ramachandran, R.A., Cantarel, B.L., Behrendt, C., Peng, L., Hooper, L.V., Zaki, H., 2020. Dietary simple sugars alter microbial ecology in the gut and promote colitis in mice. Sci. Transl. Med. 12, eaay6218. https://doi.org/10.1126/scitranslmed.aay6218

Kim, J.H., Lee, J., Park, J., Gho, Y.S., 2015. Gram-negative and Gram-positive bacterial extracellular vesicles. Semin. Cell Dev. Biol. 40, 97–104. https://doi.org/10.1016/j.semcdb.2015.02.006

Kittana, H., Gomes-Neto, J.C., Heck, K., Juritsch, A.F., Sughroue, J., Xian, Y., Mantz, S., Segura Muñoz, R.R., Cody, L.A., Schmaltz, R.J., Anderson, C.L., Moxley, R.A., Hostetter, J.M., Fernando, S.C., Clarke, J., Kachman, S.D., Cressler, C.E., Benson, A.K., Walter, J., Ramer-Tait, A.E., 2023. Evidence for a Causal Role for Escherichia coli Strains Identified as Adherent-Invasive (AIEC) in Intestinal Inflammation. mSphere 8, e00478-22. https://doi.org/10.1128/msphere.00478-22

Korithoski, B., Krastel, K., Cvitkovitch, D.G., 2005. Transport and Metabolism of Citrate by *Streptococcus mutans*. J. Bacteriol. 187, 4451–4456. https://doi.org/10.1128/JB.187.13.4451-4456.2005

Kunde, S., Pham, A., Bonczyk, S., Crumb, T., Duba, M., Conrad, H., Cloney, D., Kugathasan, S., 2013. Safety, Tolerability, and Clinical Response After Fecal Transplantation in Children and Young Adults With Ulcerative Colitis. J. Pediatr. Gastroenterol. Nutr. 56, 597–601. https://doi.org/10.1097/MPG.0b013e318292fa0d

Lagier, J.-C., Armougom, F., Million, M., Hugon, P., Pagnier, I., Robert, C., Bittar, F., Fournous, G., Gimenez, G., Maraninchi, M., Trape, J.-F., Koonin, E.V., La Scola, B., Raoult, D., 2012. Microbial culturomics: paradigm shift in the human gut microbiome study. Clin. Microbiol. Infect. 18, 1185–1193. https://doi.org/10.1111/1469-0691.12023

Lagier, J.-C., Edouard, S., Pagnier, I., Mediannikov, O., Drancourt, M., Raoult, D., 2015. Current and Past Strategies for Bacterial Culture in Clinical Microbiology. Clin. Microbiol. Rev. 28, 208–236. https://doi.org/10.1128/CMR.00110-14

Lee, J.G., Lee, J., Lee, A., Jo, S.V., Park, C.H., Han, D.S., Eun, C.S., 2022. Impact of short-chain fatty acid supplementation on gut inflammation and microbiota composition in a murine colitis model. J. Nutr. Biochem. 101, 108926. https://doi.org/10.1016/j.jnutbio.2021.108926

Leong, A.Z.-X., Lee, P.Y., Mohtar, M.A., Syafruddin, S.E., Pung, Y.-F., Low, T.Y., 2022. Short open reading frames (sORFs) and microproteins: an update on their identification and validation measures. J. Biomed. Sci. 29, 19. https://doi.org/10.1186/s12929-022-00802-5

Ley, R.E., Bäckhed, F., Turnbaugh, P., Lozupone, C.A., Knight, R.D., Gordon, J.I., 2005. Obesity alters gut microbial ecology. Proc. Natl. Acad. Sci. 102, 11070–11075. https://doi.org/10.1073/pnas.0504978102

Li, K., Hao, Z., Du, J., Gao, Y., Yang, S., Zhou, Y., 2021. Bacteroides thetaiotaomicron relieves colon inflammation by activating aryl hydrocarbon receptor and modulating CD4+T cell homeostasis. Int. Immunopharmacol. 90, 107183. https://doi.org/10.1016/j.intimp.2020.107183

Li, X., Zhang, Z., Zabed, H.M., Yun, J., Zhang, G., Qi, X., 2021. An Insight into the Roles of Dietary Tryptophan and Its Metabolites in Intestinal Inflammation and Inflammatory Bowel Disease. Mol. Nutr. Food Res. 65, 2000461. https://doi.org/10.1002/mnfr.202000461

Lin, Q., Hao, W.-J., Zhou, R.-M., Huang, C.-L., Wang, X.-Y., Liu, Y.-S., Li, X.-Z., 2023. Pretreatment with Bifidobacterium longum BAA2573 ameliorates dextran sulfate sodium (DSS)-induced colitis by modulating gut microbiota. Front. Microbiol. 14, 1211259. https://doi.org/10.3389/fmicb.2023.1211259

Liu, B., Garza, D.R., Gonze, D., Krzynowek, A., Simoens, K., Bernaerts, K., Geirnaert, A., Faust, K., 2023. Starvation responses impact interaction dynamics of human gut bacteria *Bacteroides thetaiotaomicron* and *Roseburia intestinalis*. ISME J. 17, 1940–1952. https://doi.org/10.1038/s41396-023-01501-1

Liu, C., Du, M.-X., Abuduaini, R., Yu, H.-Y., Li, D.-H., Wang, Y.-J., Zhou, N., Jiang, M.-Z., Niu, P.-X., Han, S.-S., Chen, H.-H., Shi, W.-Y., Wu, L., Xin, Y.-H., Ma, J., Zhou, Y., Jiang, C.-Y., Liu, H.-W., Liu, S.-J., 2021. Enlightening the taxonomy darkness of human gut microbiomes with a cultured biobank. Microbiome 9, 119. https://doi.org/10.1186/s40168-021-01064-3

Liu, C., Finegold, S.M., Song, Y., Lawson, P.A., 2008a. Reclassification of Clostridium coccoides, Ruminococcus hansenii, Ruminococcus hydrogenotrophicus, Ruminococcus luti, Ruminococcus productus and Ruminococcus schinkii as Blautia coccoides gen. nov., comb. nov., Blautia hansenii comb. nov., Blautia hydrogenotrophica comb. nov., Blautia luti comb. nov., Blautia producta comb. nov., Blautia schinkii comb. nov. and description of Blautia wexlerae sp. nov., isolated from human faeces. Int. J. Syst. Evol. Microbiol. 58, 1896–1902. https://doi.org/10.1099/ijs.0.65208-0

Liu, X., Guo, W., Cui, S., Tang, X., Zhao, J., Zhang, H., Mao, B., Chen, W., 2021a. A Comprehensive Assessment of the Safety of Blautia producta DSM 2950. Microorganisms 9, 908. https://doi.org/10.3390/microorganisms9050908

Liu, X., Mao, B., Gu, J., Wu, J., Cui, S., Wang, G., Zhao, J., Zhang, H., Chen, W., 2021b. *Blautia* —a new functional genus with potential probiotic properties? Gut Microbes 13, 1875796. https://doi.org/10.1080/19490976.2021.1875796

Loh, G., Blaut, M., 2012a. Role of commensal gut bacteria in inflammatory bowel diseases. Gut Microbes 3, 544–555. https://doi.org/10.4161/gmic.22156

Madsen, Doyle, J.S., Jewell, L.D., Tavernini, M.M., Fedorak, R.N., 1999. Lactobacillus Species Prevents Colitis in Interleukin 10 Gene–Deficient Mice. GASTROENTEROLOGY.

Magni, C., De Mendoza, D., Konings, W.N., Lolkema, J.S., 1999. Mechanism of Citrate Metabolism in *Lactococcus lactis* : Resistance against Lactate Toxicity at Low pH. J. Bacteriol. 181, 1451–1457. https://doi.org/10.1128/JB.181.5.1451-1457.1999

Mao, B., Guo, W., Cui, S., Zhang, Q., Zhao, J., Tang, X., Zhang, H., 2023. *Blautia producta* displays potential probiotic properties against dextran sulfate sodium-induced colitis in mice. Food Sci. Hum. Wellness 1–18. https://doi.org/10.26599/FSHW.2022.9250060

Maturana, J.L., Cárdenas, J.P., 2021. Insights on the Evolutionary Genomics of the Blautia Genus: Potential New Species and Genetic Content Among Lineages. Front. Microbiol. 12, 660920. https://doi.org/10.3389/fmicb.2021.660920

Mirsepasi-Lauridsen, H.C., Vallance, B.A., Krogfelt, K.A., Petersen, A.M., 2019. *Escherichia coli* Pathobionts Associated with Inflammatory Bowel Disease. Clin. Microbiol. Rev. 32, e00060-18. https://doi.org/10.1128/CMR.00060-18

Moffatt, B.A., Ashihara, H., 2002. Purine and Pyrimidine Nucleotide Synthesis and Metabolism. Arab. Book 1, e0018. https://doi.org/10.1199/tab.0018

Moller, F.T., Andersen, V., Wohlfahrt, J., Jess, T., 2015. Familial Risk of Inflammatory Bowel Disease: A Population-Based Cohort Study 1977–2011. Am. J. Gastroenterol. 110, 564–571. https://doi.org/10.1038/ajg.2015.50

Moustafa, A., Li, W., Anderson, E.L., Wong, E.H.M., Dulai, P.S., Sandborn, W.J., Biggs, W., Yooseph, S., Jones, M.B., Venter, C.J., Nelson, K.E., Chang, J.T., Telenti, A., Boland, B.S., 2018. Genetic risk, dysbiosis, and treatment stratification using host genome and gut microbiome in inflammatory bowel disease. Clin. Transl. Gastroenterol. 9, e132. https://doi.org/10.1038/ctg.2017.58

Neis, E., Dejong, C., Rensen, S., 2015. The Role of Microbial Amino Acid Metabolism in Host Metabolism. Nutrients 7, 2930–2946. https://doi.org/10.3390/nu7042930

Nguyen, Y., Sperandio, V., 2012. Enterohemorrhagic E. coli (EHEC) pathogenesis. Front. Cell. Infect. Microbiol. 2. https://doi.org/10.3389/fcimb.2012.00090

Nikolaus, S., Schulte, B., Al-Massad, N., Thieme, F., Schulte, D.M., Bethge, J., Rehman, A., Tran, F., Aden, K., Häsler, R., Moll, N., Schütze, G., Schwarz, M.J., Waetzig, G.H., Rosenstiel, P., Krawczak, M., Szymczak, S., Schreiber, S., 2017. Increased Tryptophan Metabolism Is Associated With Activity of Inflammatory Bowel Diseases. Gastroenterology 153, 1504-1516.e2. https://doi.org/10.1053/j.gastro.2017.08.028

Nomura, K., Ishikawa, D., Okahara, K., Ito, S., Haga, K., Takahashi, M., Arakawa, A., Shibuya, T., Osada, T., Kuwahara-Arai, K., Kirikae, T., Nagahara, A., 2021a. Bacteroidetes Species Are Correlated with Disease Activity in Ulcerative Colitis. J. Clin. Med. 10, 1749. https://doi.org/10.3390/jcm10081749

Nugent, S.G., 2001. Intestinal luminal pH in inflammatory bowel disease: possible determinants and implications for therapy with aminosalicylates and other drugs. Gut 48, 571–577. https://doi.org/10.1136/gut.48.4.571

Okuda, K., Ohta, K., Sasaki, T., Takazoe, I., 1984. Morphological changes in the bacterium Bacteroides melaninogenicus subspecies melaninogenicus isolated from the human mouth and grown in culture without added blood components. Arch. Oral Biol. 29, 81–85. https://doi.org/10.1016/0003-9969(84)90048-7

Olén, O., Erichsen, R., Sachs, M.C., Pedersen, L., Halfvarson, J., Askling, J., Ekbom, A., Sørensen, H.T., Ludvigsson, J.F., 2020. Colorectal cancer in Crohn's disease: a Scandinavian population-based cohort study. Lancet Gastroenterol. Hepatol. 5, 475–484. https://doi.org/10.1016/S2468-1253(20)30005-4

Oliphant, K., Parreira, V.R., Cochrane, K., Allen-Vercoe, E., 2019. Drivers of human gut microbial community assembly: coadaptation, determinism and stochasticity. ISME J. 13, 3080–3092. https://doi.org/10.1038/s41396-019-0498-5

Ott, S.J., 2004a. Reduction in diversity of the colonic mucosa associated bacterial microflora in patients with active inflammatory bowel disease. Gut 53, 685–693. https://doi.org/10.1136/gut.2003.025403

Perler, B.K., Ungaro, R., Baird, G., Mallette, M., Bright, R., Shah, S., Shapiro, J., Sands, B.E., 2019. Presenting symptoms in inflammatory bowel disease: descriptive analysis of a community-based inception cohort. BMC Gastroenterol. 19, 47. https://doi.org/10.1186/s12876-019-0963-7

Petruschke, H., Anders, J., Stadler, P.F., Jehmlich, N., Von Bergen, M., 2020. Enrichment and identification of small proteins in a simplified human gut microbiome. J. Proteomics 213, 103604. https://doi.org/10.1016/j.jprot.2019.103604

Petruschke, H., Schori, C., Canzler, S., Riesbeck, S., Poehlein, A., Daniel, R., Frei, D., Segessemann, T., Zimmerman, J., Marinos, G., Kaleta, C., Jehmlich, N., Ahrens, C.H., Von Bergen, M., 2021a. Discovery of novel community-relevant small proteins in a simplified human intestinal microbiome. Microbiome 9, 55. https://doi.org/10.1186/s40168-020-00981-z

Piovezani Ramos, G., Kane, S., 2021. Alcohol Use in Patients With Inflammatory Bowel Disease. Gastroenterol. Hepatol. 17, 211–225.

Plichta, D.R., Juncker, A.S., Bertalan, M., Rettedal, E., Gautier, L., Varela, E., Manichanh, C., Fouqueray, C., Levenez, F., Nielsen, T., Doré, J., Machado, A.M.D., De Evgrafov, M.C.R., Hansen, T., Jørgensen, T., Bork, P., Guarner, F., Pedersen, O., Metagenomics of the Human Intestinal Tract (MetaHIT) Consortium, Sommer, M.O.A., Ehrlich, S.D., Sicheritz-Pontén, T., Brunak, S., Nielsen, H.B., 2016. Transcriptional interactions suggest niche segregation among microorganisms in the human gut. Nat. Microbiol. 1, 16152. https://doi.org/10.1038/nmicrobiol.2016.152

Pokusaeva, K., Fitzgerald, G.F., Van Sinderen, D., 2011. Carbohydrate metabolism in Bifidobacteria. Genes Nutr. 6, 285–306. https://doi.org/10.1007/s12263-010-0206-6

Prenzler, A., Bokemeyer, B., Von Der Schulenburg, J.-M., Mittendorf, T., 2011. Health care costs and their predictors of inflammatory bowel diseases in Germany. Eur. J. Health Econ. 12, 273–283. https://doi.org/10.1007/s10198-010-0281-z

Press, Hauptmann, Hauptmann, Fuchs, Fuchs, Ewe, Ramadori, 1998. Gastrointestinal pH profiles in patients with inflammatory bowel disease: GASTROINTESTINAL pH IN INFLAMMATORY BOWEL DISEASE. Aliment. Pharmacol. Ther. 12, 673–678. https://doi.org/10.1046/j.1365-2036.1998.00358.x

Probert, C.S., Jayanthi, V., Hughes, A.O., Thompson, J.R., Wicks, A.C., Mayberry, J.F., 1993. Prevalence and family risk of ulcerative colitis and Crohn's disease: an epidemiological study among Europeans and south Asians in Leicestershire. Gut 34, 1547–1551. https://doi.org/10.1136/gut.34.11.1547

Qian, W., Li, M., Yu, L., Tian, F., Zhao, J., Zhai, Q., 2023. Effects of Taurine on Gut Microbiota Homeostasis: An Evaluation Based on Two Models of Gut Dysbiosis. Biomedicines 11, 1048. https://doi.org/10.3390/biomedicines11041048

Rangarajan, A.A., Koropatkin, N.M., Biteen, J.S., 2020. Nutrient-dependent morphological variability of Bacteroides thetaiotaomicron. Microbiology 166, 624–628. https://doi.org/10.1099/mic.0.000924

Ren, J., Sang, Y., Qin, R., Su, Y., Cui, Z., Mang, Z., Li, H., Lu, S., Zhang, J., Cheng, S., Liu, X., Li, J., Lu, J., Wu, W., Zhao, G.-P., Shao, F., Yao, Y.-F., 2019. Metabolic intermediate acetyl phosphate modulates bacterial virulence *via* acetylation. Emerg. Microbes Infect. 8, 55–69. https://doi.org/10.1080/22221751.2018.1558963

Ren, J., Sang, Y., Tan, Y., Tao, J., Ni, J., Liu, S., Fan, X., Zhao, W., Lu, J., Wu, W., Yao, Y.-F., 2016. Acetylation of Lysine 201 Inhibits the DNA-Binding Ability of PhoP to Regulate Salmonella Virulence. PLOS Pathog. 12, e1005458. https://doi.org/10.1371/journal.ppat.1005458

Rey, F.E., Faith, J.J., Bain, J., Muehlbauer, M.J., Stevens, R.D., Newgard, C.B., Gordon, J.I., 2010. Dissecting the in Vivo Metabolic Potential of Two Human Gut Acetogens. J. Biol. Chem. 285, 22082–22090. https://doi.org/10.1074/jbc.M110.117713

Rinninella, E., Raoul, P., Cintoni, M., Franceschi, F., Miggiano, G., Gasbarrini, A., Mele, M., 2019a. What is the Healthy Gut Microbiota Composition? A Changing Ecosystem across Age, Environment, Diet, and Diseases. Microorganisms 7, 14. https://doi.org/10.3390/microorganisms7010014

Rocamora-Reverte, L., Melzer, F.L., Würzner, R., Weinberger, B., 2021. The Complex Role of Regulatory T Cells in Immunity and Aging. Front. Immunol. 11, 616949. https://doi.org/10.3389/fimmu.2020.616949

Rocha, E.R., Krykunivsky, A.S., 2017. Anaerobic utilization of Fe(III)-xenosiderophores among *Bacteroides* species and the distinct assimilation of Fe(III)-ferrichrome by *Bacteroides fragilis* within the genus. MicrobiologyOpen 6, e00479. https://doi.org/10.1002/mbo3.479

Rodríguez, J.M., Murphy, K., Stanton, C., Ross, R.P., Kober, O.I., Juge, N., Avershina, E., Rudi, K., Narbad, A., Jenmalm, M.C., Marchesi, J.R., Collado, M.C., 2015. The composition of the gut microbiota throughout life, with an emphasis on early life. Microb. Ecol. Health Dis. 26. https://doi.org/10.3402/mehd.v26.26050

Rolfe, M.D., Rice, C.J., Lucchini, S., Pin, C., Thompson, A., Cameron, A.D.S., Alston, M., Stringer, M.F., Betts, R.P., Baranyi, J., Peck, M.W., Hinton, J.C.D., 2012. Lag Phase Is a Distinct Growth Phase That Prepares Bacteria for Exponential Growth and Involves Transient Metal Accumulation. J. Bacteriol. 194, 686–701. https://doi.org/10.1128/JB.06112-11

Rosati, E., Rios Martini, G., Pogorelyy, M.V., Minervina, A.A., Degenhardt, F., Wendorff, M., Sari, S., Mayr, G., Fazio, A., Dowds, C.M., Hauser, C., Tran, F., Von Schönfels, W., Pochhammer, J., Salnikova, M.A., Jaeckel, C., Gigla, J.B., Sabet, S.S., Hübenthal, M., Schiminsky, E., Schreiber, S., Rosenstiel, P.C., Scheffold, A., Thomas, P.G., Lieb, W., Bokemeyer, B., Wite, M., Aden, K., Hendricks, A., Schafmayer, C., Egberts, J.-H., Mamedov, I.Z., Bacher, P., Franke, A., 2022. A novel unconventional T cell population enriched in Crohn's disease. Gut 71, 2194–2204. https://doi.org/10.1136/gutjnl-2021-325373

Rothfuss, K.S., Stange, E.F., Herrlinger, K.R., 2006. Extraintestinal manifestations and complications in inflammatory bowel diseases. World J. Gastroenterol. 12, 4819. https://doi.org/10.3748/wjg.v12.i30.4819

Rui Wang, Zhaoqi Li, Shaojun Liu, Decai Zhang, 2023. Global, regional and national burden of inflammatory bowel disease in 204 countries and territories from 1990 to 2019: a systematic analysis based on the Global Burden of Disease Study 2019. BMJ Open 13, e065186. https://doi.org/10.1136/bmjopen-2022-065186

Saez-Lara, M.J., Gomez-Llorente, C., Plaza-Diaz, J., Gil, A., 2015. The Role of Probiotic Lactic Acid Bacteria and Bifidobacteria in the Prevention and Treatment of Inflammatory Bowel Disease and Other Related Diseases: A Systematic Review of Randomized Human Clinical Trials. BioMed Res. Int. 2015, 1–15. https://doi.org/10.1155/2015/505878

Sarkar, A., Harty, S., Lehto, S.M., Moeller, A.H., Dinan, T.G., Dunbar, R.I.M., Cryan, J.F., Burnet, P.W.J., 2018. The Microbiome in Psychology and Cognitive Neuroscience. Trends Cogn. Sci. 22, 611–636. https://doi.org/10.1016/j.tics.2018.04.006

Sasaki, Y., Hada, R., Nakajima, H., Fukuda, S., Munakata, A., 1997. Improved localizing method of radiopill in measurement of entire gastrointestinal pH profiles: colonic luminal pH in normal subjects and patients with Crohn's disease. Am. J. Gastroenterol. 92, 114–118.

Satokari, R., 2020. High Intake of Sugar and the Balance between Pro- and Anti-Inflammatory Gut Bacteria. Nutrients 12, 1348. https://doi.org/10.3390/nu12051348

Schell, M.A., Karmirantzou, M., Snel, B., Vilanova, D., Berger, B., Pessi, G., Zwahlen, M.-C., Desiere, F., Bork, P., Delley, M., Pridmore, R.D., Arigoni, F., 2002. The genome sequence of *Bifidobacterium longum* reflects its adaptation to the human gastrointestinal tract. Proc. Natl. Acad. Sci. 99, 14422–14427. https://doi.org/10.1073/pnas.212527599

Schneiders, Stephan-Maurus, 2024. Detection and characterization of microbe-reactive CD4+ T cells in individuals at high risk for inflammatory bowel disease. Doctoral thesis. Mathematisch-Naturwissenschaftlichen Fakultät der Christian-Albrechts-Universität Kiel.

Schubert, C., Zedler, S., Strecker, A., Unden, G., 2021. L-Aspartate as a high-quality nitrogen source in *Escherichia coli* : Regulation of L-aspartase by the nitrogen regulatory system and interaction of L-aspartase with GlnB. Mol. Microbiol. 115, 526–538. https://doi.org/10.1111/mmi.14620

Schwyn, B., Neilands, J.B., 1987. Universal chemical assay for the detection and determination of siderophores. Anal. Biochem. 160, 47–56. https://doi.org/10.1016/0003-2697(87)90612-9

Scribani Rossi, C., Barrientos-Moreno, L., Paone, A., Cutruzzolà, F., Paiardini, A., Espinosa-Urgel, M., Rinaldo, S., 2022. Nutrient Sensing and Biofilm Modulation: The Example of L-arginine in Pseudomonas. Int. J. Mol. Sci. 23, 4386. https://doi.org/10.3390/ijms23084386

Segura Munoz, R.R., Mantz, S., Martínez, I., Li, F., Schmaltz, R.J., Pudlo, N.A., Urs, K., Martens, E.C., Walter, J., Ramer-Tait, A.E., 2022. Experimental evaluation of ecological principles to

understand and modulate the outcome of bacterial strain competition in gut microbiomes. ISME J. 16, 1594–1604. https://doi.org/10.1038/s41396-022-01208-9

Seifert, R., 2015. cCMP and cUMP: emerging second messengers. Trends Biochem. Sci. 40, 8–15. https://doi.org/10.1016/j.tibs.2014.10.008

Seksik, P., 2003. Alterations of the dominant faecal bacterial groups in patients with Crohn's disease of the colon. Gut 52, 237–242. https://doi.org/10.1136/gut.52.2.237

Sender, R., Fuchs, S., Milo, R., 2016. Revised Estimates for the Number of Human and Bacteria Cells in the Body. PLOS Biol. 14, e1002533. https://doi.org/10.1371/journal.pbio.1002533

Silva, F.A.R., Rodrigues, B.L., Ayrizono, M.D.L.S., Leal, R.F., 2016. The Immunological Basis of Inflammatory Bowel Disease. Gastroenterol. Res. Pract. 2016, 1–11. https://doi.org/10.1155/2016/2097274

Singh, K., Gobert, A.P., Coburn, L.A., Barry, D.P., Allaman, M., Asim, M., Luis, P.B., Schneider, C., Milne, G.L., Boone, H.H., Shilts, M.H., Washington, M.K., Das, S.R., Piazuelo, M.B., Wilson, K.T., 2019. Dietary Arginine Regulates Severity of Experimental Colitis and Affects the Colonic Microbiome. Front. Cell. Infect. Microbiol. 9, 66. https://doi.org/10.3389/fcimb.2019.00066

Skaar, E.P., 2010. The Battle for Iron between Bacterial Pathogens and Their Vertebrate Hosts. PLoS Pathog. 6, e1000949. https://doi.org/10.1371/journal.ppat.1000949

Steinberg, R., Koch, H., 2021. The largely unexplored biology of small proteins in pro- and eukaryotes. FEBS J. 288, 7002–7024. https://doi.org/10.1111/febs.15845

Strauch, U.G., 2005. Influence of intestinal bacteria on induction of regulatory T cells: lessons from a transfer model of colitis. Gut 54, 1546–1552. https://doi.org/10.1136/gut.2004.059451

Sugahara, H., Odamaki, T., Fukuda, S., Kato, T., Xiao, J., Abe, F., Kikuchi, J., Ohno, H., 2015. Probiotic Bifidobacterium longum alters gut luminal metabolism through modification of the gut microbial community. Sci. Rep. 5, 13548. https://doi.org/10.1038/srep13548

Swidsinski, A., 2005. Spatial organization of bacterial flora in normal and inflamed intestine: A fluorescence *in situ* hybridization study in mice. World J. Gastroenterol. 11, 1131. https://doi.org/10.3748/wjg.v11.i8.1131

Syromyatnikov, M., Nesterova, E., Gladkikh, M., Smirnova, Y., Gryaznova, M., Popov, V., 2022. Characteristics of the Gut Bacterial Composition in People of Different Nationalities and Religions. Microorganisms 10, 1866. https://doi.org/10.3390/microorganisms10091866

Teofani, A., Marafini, I., Laudisi, F., Pietrucci, D., Salvatori, S., Unida, V., Biocca, S., Monteleone, G., Desideri, A., 2022. Intestinal Taxa Abundance and Diversity in Inflammatory Bowel Disease Patients: An Analysis including Covariates and Confounders. Nutrients 14, 260. https://doi.org/10.3390/nu14020260

Tesmer, L.A., Lundy, S.K., Sarkar, S., Fox, D.A., 2008. Th17 cells in human disease. Immunol. Rev. 223, 87–113. https://doi.org/10.1111/j.1600-065X.2008.00628.x

Thursby, E., Juge, N., 2017. Introduction to the human gut microbiota. Biochem. J. 474, 1823–1836. https://doi.org/10.1042/BCJ20160510

Townsend, G.E., Han, W., Schwalm, N.D., Raghavan, V., Barry, N.A., Goodman, A.L., Groisman, E.A., 2019. Dietary sugar silences a colonization factor in a mammalian gut symbiont. Proc. Natl. Acad. Sci. 116, 233–238. https://doi.org/10.1073/pnas.1813780115

Turnbaugh, P.J., Bäckhed, F., Fulton, L., Gordon, J.I., 2008. Diet-Induced Obesity Is Linked to Marked but Reversible Alterations in the Mouse Distal Gut Microbiome. Cell Host Microbe 3, 213–223. https://doi.org/10.1016/j.chom.2008.02.015

Valguarnera, E., Scott, N.E., Azimzadeh, P., Feldman, M.F., 2018a. Surface Exposure and Packing of Lipoproteins into Outer Membrane Vesicles Are Coupled Processes in *Bacteroides*. mSphere 3, e00559-18. https://doi.org/10.1128/mSphere.00559-18

Valle, J., Da Re, S., Schmid, S., Skurnik, D., D'Ari, R., Ghigo, J.-M., 2008. The Amino Acid Valine Is Secreted in Continuous-Flow Bacterial Biofilms. J. Bacteriol. 190, 264–274. https://doi.org/10.1128/JB.01405-07

Van Teeseling, M.C.F., De Pedro, M.A., Cava, F., 2017a. Determinants of Bacterial Morphology: From Fundamentals to Possibilities for Antimicrobial Targeting. Front. Microbiol. 8, 1264. https://doi.org/10.3389/fmicb.2017.01264

Vernia, P., Caprilli, R., Latella, G., Barbetti, F., Magliocca, F.M., Cittadini, M., 1988. Fecal Lactate and Ulcerative Colitis. Gastroenterology 95, 1564–1568. https://doi.org/10.1016/S0016-5085(88)80078-7

Victoria Pascal, Marta Pozuelo, Natalia Borruel, Francesc Casellas, David Campos, Alba Santiago, Xavier Martinez, Encarna Varela, Guillaume Sarrabayrouse, Kathleen Machiels, Severine Vermeire, Harry Sokol, Francisco Guarner, Chaysavanh Manichanh, 2017. A microbial signature for Crohn's disease. Gut 66, 813. https://doi.org/10.1136/gutjnl-2016-313235

Vinke, P.C., El Aidy, S., Van Dijk, G., 2017. The Role of Supplemental Complex Dietary Carbohydrates and Gut Microbiota in Promoting Cardiometabolic and Immunological Health in Obesity: Lessons from Healthy Non-Obese Individuals. Front. Nutr. 4, 34. https://doi.org/10.3389/fnut.2017.00034

Visconti, A., Le Roy, C.I., Rosa, F., Rossi, N., Martin, T.C., Mohney, R.P., Li, W., De Rinaldis, E., Bell, J.T., Venter, J.C., Nelson, K.E., Spector, T.D., Falchi, M., 2019. Interplay between the human gut microbiome and host metabolism. Nat. Commun. 10, 4505. https://doi.org/10.1038/s41467-019-12476-z

Wexler, H.M., 2007. *Bacteroides* : the Good, the Bad, and the Nitty-Gritty. Clin. Microbiol. Rev. 20, 593–621. https://doi.org/10.1128/CMR.00008-07

Wong, J.M.W., De Souza, R., Kendall, C.W.C., Emam, A., Jenkins, D.J.A., 2006. Colonic Health: Fermentation and Short Chain Fatty Acids: J. Clin. Gastroenterol. 40, 235–243. https://doi.org/10.1097/00004836-200603000-00015

Wu, H.-J., Wu, E., 2012. The role of gut microbiota in immune homeostasis and autoimmunity. Gut Microbes 3, 4–14. https://doi.org/10.4161/gmic.19320

Wu, J., Li, Y., Cai, Z., Jin, Y., 2014. Pyruvate-Associated Acid Resistance in Bacteria. Appl. Environ. Microbiol. 80, 4108–4113. https://doi.org/10.1128/AEM.01001-14

Xiong, L., Teng, J., Botelho, M., Lo, R., Lau, S., Woo, P., 2016. Arginine Metabolism in Bacterial Pathogenesis and Cancer Therapy. Int. J. Mol. Sci. 17, 363. https://doi.org/10.3390/ijms17030363

Xu, J., Bjursell, M.K., Himrod, J., Deng, S., Carmichael, L.K., Chiang, H.C., Hooper, L.V., Gordon, J.I., 2003. A Genomic View of the Human- *Bacteroides thetaiotaomicron* Symbiosis. Science 299, 2074–2076. https://doi.org/10.1126/science.1080029

Xu, Y., Zhao, Z., Tong, W., Ding, Y., Liu, B., Shi, Y., Wang, J., Sun, S., Liu, M., Wang, Y., Qi, Q., Xian, M., Zhao, G., 2020. An acid-tolerance response system protecting exponentially growing Escherichia coli. Nat. Commun. 11, 1496. https://doi.org/10.1038/s41467-020-15350-5

Yadavalli, S.S., Yuan, J., 2022. Bacterial Small Membrane Proteins: the Swiss Army Knife of Regulators at the Lipid Bilayer. J. Bacteriol. 204, e00344-21. https://doi.org/10.1128/JB.00344-21

Yang, L., Tang, S., Baker, S.S., Arijs, I., Liu, W., Alkhouri, R., Lan, P., Baker, R.D., Tang, Z., Ji, G., Rutgeerts, P., Vermeire, S., Zhu, R., Zhu, L., 2019. Difference in Pathomechanism Between Crohn's Disease and Ulcerative Colitis Revealed by Colon Transcriptome. Inflamm. Bowel Dis. 25, 722–731. https://doi.org/10.1093/ibd/izy359

Yao, S., Zhao, Z., Wang, W., Liu, X., 2021. Bifidobacterium Longum: Protection against Inflammatory Bowel Disease. J. Immunol. Res. 2021, 1–11. https://doi.org/10.1155/2021/8030297

Yoon, S.J., Yu, J.S., Min, B.H., Gupta, H., Won, S.-M., Park, H.J., Han, S.H., Kim, B.-Y., Kim, K.H., Kim, B.K., Joung, H.C., Park, T.-S., Ham, Y.L., Lee, D.Y., Suk, K.T., 2023. Bifidobacterium-derived short-chain fatty acids and indole compounds attenuate nonalcoholic fatty liver disease by modulating gut-liver axis. Front. Microbiol. 14, 1129904. https://doi.org/10.3389/fmicb.2023.1129904

Young Park, S., Lee, D.K., Mi An, H., Gyeong Cha, M., Baek, E.H., Rae Kim, J., Lee, S.W., Kim, M.J., Lee, K.O., Joo Ha, N., 2011. Phenotypic and genotypic characterization of Bifidobacterium isolates from healthy adult Koreans. Iran. J. Biotechnol. 9, 173–180.

Yuan, J., Zhu, L., Liu, X., Li, T., Zhang, Y., Ying, T., Wang, B., Wang, Junjun, Dong, H., Feng, E., Li, Q., Wang, Jie, Wang, Hongxia, Wei, K., Zhang, X., Huang, C., Huang, P., Huang, L., Zeng, M., Wang, Hengliang, 2006. A Proteome Reference Map and Proteomic Analysis of Bifidobacterium

longum NCC2705. Mol. Cell. Proteomics 5, 1105–1118. https://doi.org/10.1074/mcp.M500410-MCP200

Zhang, Y., Chen, R., Zhang, D., Qi, S., Liu, Y., 2023. Metabolite interactions between host and microbiota during health and disease: Which feeds the other? Biomed. Pharmacother. 160, 114295. https://doi.org/10.1016/j.biopha.2023.114295

Zhu, W., Winter, M.G., Spiga, L., Hughes, E.R., Chanin, R., Mulgaonkar, A., Pennington, J., Maas, M., Behrendt, C.L., Kim, J., Sun, X., Beiting, D.P., Hooper, L.V., Winter, S.E., 2020. Xenosiderophore Utilization Promotes Bacteroides thetaiotaomicron Resilience during Colitis. Cell Host Microbe 27, 376-388.e8. https://doi.org/10.1016/j.chom.2020.01.010

Zhuang, X., Li, T., Li, M., Huang, S., Qiu, Y., Feng, R., Zhang, S., Chen, M., Xiong, L., Zeng, Z., 2019. Systematic Review and Meta-analysis: Short-Chain Fatty Acid Characterization in Patients With Inflammatory Bowel Disease. Inflamm. Bowel Dis. 25, 1751–1763. https://doi.org/10.1093/ibd/izz188

Żyła, E., Dziendzikowska, K., Kamola, D., Wilczak, J., Sapierzyński, R., Harasym, J., Gromadzka-Ostrowska, J., 2021. Anti-Inflammatory Activity of Oat Beta-Glucans in a Crohn's Disease Model: Time- and Molar Mass-Dependent Effects. Int. J. Mol. Sci. 22, 4485. https://doi.org/10.3390/ijms22094485

6. Appendix

Tables from growth experiments 3.1.1 - 3.1.3

Table 4: Growth of three gut bacteria in YCFA media with pH 6, pH 7 and pH 8

	Lag-Time [h]	Max V [h^{-1}]	Time at Max V [h]	Linear Regression	Doubling time [min]	Max OD
(A) *B. producta*						
pH 6	24.3 ± 9.2	0.57 ± 0.39	35 ± 16.5	0.999 ± 0.001	73.1 ± 71.4	/
pH 7	8.6 ± 0.1	2.21 ± 0.09	11 ± 0.0	0.984 ± 0.002	18.8 ± 0.7	0.69 ± 0.01
pH 8	8.4 ± 0.2	2.77 ± 0.27	11 ± 0.0	0.975 ± 0.003	15.0 ± 1.3	0.69 ± 0.08
(B) *B. thetaiotaomicron*						
pH 6	10.1 ± 0.8	0.768 ± 0.07	14.8 ± 0.4	0.997 ± 0.003	54.2 ± 5.3	0.62 ± 0.01
pH 7	6.9 ± 0.3	2.279 ± 0.00	10.0 ± 0.0	0.989 ± 0.002	18.2 ± 0.8	0.94 ± 0.00
pH 8	6.9 ± 0.1	2.447 ± 0.13	10.6 ± 0.5	0.993 ± 0.001	17.0 ± 0.9	0.83 ± 0.03
(C) *B. longum*						
pH 6	3.05 ± 0.04	1.62 ± 0.03	5.99 ± 0	0.997 ± 0.000	25.6 ± 0.5	0.73 ± 0.013
pH 7	2.75 ± 0.05	2.28 ± 0.11	4.99 ± 0	0.991 ± 0.001	18.3 ± 0.9	0.58 ± 0.027
pH 8	2.34 ± 0.02	0.98 ± 0.07	4.99 ± 0	0.989 ± 0.003	42.3 ± 3	0.49 ± 0.017

Table 5: Calculation of growth parameters of *B. producta* grown with different saccharides as main carbon source

	Lag-Time [h]	Max V	Time at Max V [h]	Linear Regression	Doubling time [min]	OD max
13.08.2021						
Glucose	13.3 ± 3.4	1.18 ± 0.13	17.2 ± 3.7	0.899 ± 0.039	35.1 ± 3.7	0.41 ± 0.02
Fructose	17.7 ± 0.9	0.89 ± 0.14	22.4 ± 1.5	0.960 ± 0.013	46.6 ± 7.3	0.38 ± 0.03
Sucrose	8.9 ± 2.9	1.30 ± 0.05	12.8 ± 2.7	0.947 ± 0.011	32.1 ± 1.2	0.54 ± 0.03
Starch	12.2 ± 7.0	0.44 ± 0.20	19.2 ± 12.5	0.969 ± 0.014	95.0 ± 132.1	0.19 ± 0.01
Beta-glucan	13.0 ± 3.5	0.88 ± 0.30	16.8 ± 3.7	0.955 ± 0.011	47.4 ± 29.7	0.37 ± 0.13
15.11.2021 A						
Glucose	5.0 ± 0.2	0.89 ±0.12	9.6 ±0.8	0.973 ±0.007	46.7 ±5.4	0.43 ±0.04
Fructose	3.0 ± 0.0	1.01 ±0.03	6.0 ±0.0	0.893 ±0.003	41.4 ±1.2	0.44 ±0.01
Sucrose	4.5 ± 0.0	1.42 ±0.08	8.0 ±0.0	0.944 ±0.005	29.3 ±1.5	0.64 ±0.03
Fru + Glu	3.0 ± 0.0	1.15 ±0.04	6.0 ±0.0	0.909 ±0.006	36.0 ±1.3	0.48 ±0.02
Starch	2.1 ± 0.0	0.19 ±0.01	6.0 ±0.0	0.957 ±0.004	222.6 ±7.3	0.08 ±0.01
Beta-glucan	3.6 ± 0.3	0.92 ±0.04	7.6 ±0.8	0.905 ±0.012	45.2 ±1.8	0.41 ±0.02
15.11.2021 B						
Glucose	4.9 ±0.2	0.84 ±0.01	9.6 ±0.8	0.960 ±0.003	49.6 ±0.6	0.40 ±0.00
Fructose	3.7 ±0.0	0.95 ±0.01	8.0 ±0.0	0.902 ±0.006	43.7 ±0.7	0.41 ±0.01
Sucrose	4.7 ±0.1	1.33 ±0.09	8.0 ±0.0	0.933 ±0.004	31.2 ±2.3	0.60 ±0.04
Starch	2.7 ±0.2	0.20 ±0.01	7.6 ±0.8	0.968 ±0.003	209.4 ±7.2	0.22 ±0.02
Beta-glucan	4.1 ±0.1	0.89 ±0.06	8.0 ±0.0	0.937 ±0.004	46.5 ±3.4	0.38 ±0.03
Without	3.1 ±0.2	0.22 ±0.01	8.8 ±1.0	0.973 ±0.003	186.3 ±10.1	0.23 ±0.02

Table 6: Calculation of growth parameters of *B. thetaiotaomicron* grown with different saccharides as main carbon source

	Lag-Time [h]		Max V		Time at Max V [h]		Linear Regression		Doubling time [min]		OD max	
17.05.2021												
Beta-glucan 0.1%	4.83	±0.34	0.25	±0.01	12.39	±0.80	0.999	±0.000	163.22	±5.13	0.29	±0.01
Mucin 0.1%	3.75	±0.17	0.31	±0.01	10.39	±0.80	0.998	±0.001	136.09	±5.06	0.32	±0.01
Mucin 1%	2.79	±0.31	0.28	±0.01	9.99	±2.19	0.991	±0.008	148.74	±7.51	0.30	±0.01
Laminarin 0.1%	3.44	±0.16	0.25	±0.01	11.99	±0.00	0.998	±0.000	167.16	±4.52	0.29	±0.01
Glucose 0.01%	3.48	±0.11	0.44	±0.01	7.99	±0.00	0.996	±0.001	94.31	±2.11	0.35	±0.01
Glucose 0.1%	3.49	±0.31	0.91	±0.00	7.19	±0.98	0.909	±0.002	45.76	±0.04	0.63	±0.01
12.05.2021												
Mucin 0.1%	2.07	±0.03	0.26	±0.04	5.99	±0.00	0.967	±0.016	160.33	±26.69	0.27	±0.01
Mucin 1%	n.A.	n.A.	0.32	±0.01	5.99	±0.00	0.970	±0.011	130.13	±2.80	0.29	±0.01
Laminarin 0.1%	n.A.	n.A.	0.24	±0.04	5.99	±0.00	0.979	±0.007	175.33	±36.76	0.23	±0.09
Beta-glucan 0.1%	2.36	±0.39	0.23	±0.03	6.79	±1.60	0.979	±0.007	179.57	±21.59	0.23	±0.01
Glucose 0.01%	2.58	±0.38	0.35	±0.03	6.39	±0.80	0.981	±0.013	119.85	±11.20	0.29	±0.11
Glucose 0.1%	n.A.	n.A.	1.26	±0.08	5.99	±0.00	0.826	±0.062	33.00	±0.55	0.66	±0.04
12.09.2021												
Glucose	3.87	±0.09	0.53	±0.06	7.79	±0.40	0.997	±0.003	78.86	±7.84	0.35	±0.01
Sucrose	5.15	±0.31	0.59	±0.01	10.19	±0.40	0.998	±0.001	70.87	±0.76	0.40	±0.01
Beta-glucan	3.82	±0.30	0.29	±0.04	8.59	±1.74	0.996	±0.004	142.72	±20.09	0.29	±0.02
Starch	2.73	±0.91	0.26	±0.01	6.99	±1.90	0.996	±0.005	157.89	±8.49	0.29	±0.03
Fructose	3.84	±0.70	0.44	±0.02	8.19	±1.47	0.997	±0.002	95.43	±4.73	0.34	±0.01
Fru + Gluc	3.11	±0.23	0.49	±0.03	6.19	±0.40	0.995	±0.002	84.46	±0.07	0.34	±0.02
08.07.2022												
Without	6.54	±0.41	0.38	±0.03	10.59	±0.49	0.991	±0.006	108.36	±8.25	0.26	±0.01
Glucose 27.8	4.45	±0.15	1.90	±0.03	7.19	±0.40	0.995	±0.002	21.89	±0.33	0.85	±0.01
Glucose 55.6	4.46	±0.13	1.93	±0.06	7.19	±0.40	0.994	±0.002	21.53	±0.62	0.88	±0.01
Sucrose 27.8	4.33	±0.08	1.79	±0.03	7.19	±0.40	0.997	±0.001	23.27	±0.33	0.91	±0.01
Sucrose 255.6	4.17	±0.11	1.71	±0.06	6.99	±0.00	0.998	±0.001	24.39	±0.83	0.94	±0.01

Table 7: Calculated growth parameters of *B. longum* grown with different saccharides as main carbon source

	Lag-Time [h]		Max V		Time at Max V [h]		Linear Regression		Doubling time [min]		OD max	
19.07.2022												
Glucose	1.27	±0.04	0.83	±0.07	2.99	±0.00	0.967	±0.005	50.40	±5.37	0.23	±0.04
Sucrose	2.43	±0.10	0.91	±0.02	4.99	±0.00	0.993	±0.001	45.81	±1.18	0.44	±0.01
Fructose	1.79	±0.31	0.09	±0.02	5.19	±1.83	0.993	±0.006	485.85	±1.51	0.09	±0.02
Starch	2.44	±0.63	0.07	±0.00	7.19	±0.75	0.999	±0.001	571.28	±1.27	0.07	±0.01
Beta-glucan	2.24	±0.57	0.09	±0.00	7.19	±1.17	0.999	±0.000	480.24	±7.34	0.08	±0.00
without	3.37	±0.41	0.06	±0.01	8.99	±0.00	0.998	±0.002	745.32	±1.81	0.06	±0.01
21.07.2022												
Glucose	1.96	±0.03	0.76	±0.02	3.99	±0.00	0.971	±0.001	55.04	±5.37	0.20	±0.04
Sucrose	3.53	±0.03	1.15	±0.02	5.99	±0.00	0.993	±0.001	36.06	±1.18	0.40	±0.01
Fructose	9.80	±3.28	0.32	±0.15	17.39	±4.59	0.999	±0.001	130.45	±1.51	0.19	±0.06
Strach	1.58	±0.62	0.09	±0.01	4.19	±0.40	0.997	±0.002	479.13	±1.27	0.08	±0.04
Beta-glucan	1.08	±0.09	0.11	±0.00	3.99	±0.00	0.995	±0.002	385.80	±7.34	0.07	±0.00
Without	1.23	±0.05	0.12	±0.00	3.99	±0.00	0.997	±0.001	359.76	±1.81	0.04	±0.00
25.07.2022												
Glucose	1.65	±0.13	0.96	±0.04	3.59	±0.20	0.995	±0.001	43.29	±5.37	0.18	±0.01
Sucrose	3.25	±0.03	1.34	±0.01	5.49	±0.00	0.999	±0.000	31.10	±1.18	0.44	±0.01
Fructose	10.59	±2.62	0.32	±0.12	17.49	±4.55	0.999	±0.001	131.78	±1.51	0.21	±0.00
Starch	3.21	±0.01	1.32	±0.02	5.49	±0.00	1.000	±0.000	31.43	±1.27	0.42	±0.01
Beta-glucan	0.78	±0.17	0.10	±0.01	2.89	±1.16	0.998	±0.001	417.56	±7.34	0.04	±0.01
0.5% Glucose	4.69	±0.98	1.54	±0.13	8.19	±1.03	0.996	±0.001	26.94	±1.81	0.50	±0.03

Table 8: Growth parameters of bacteria grown in different media types

	Lag-Time [h]	Max V	Time at Max V [h]	Linear Regression	Doubling time [min]	OD max
B. producta						
YCFA	4.9 ± 0.2	3.78 ± 0.15	7.1 ± 0.2	1 ± 0.000	11 ± 0.5	1.30± 0.05
YCFA-SCFA	4.8 ± 2.0	4.2 ± 0.12	7.0 ± 0.0	0.999 ± 0.00	9.9 ± 0.3	1.23 ± 0.08
BHI	4.4 ± 0.8	2.33 ± 0.33	4.8 ± 2.7	0.998 ± 0.002	17.8 ± 2.3	1.05 ± 0.06
BHI + SCFA	12.9 ± 2.2	/	13.3 ± 8.0	0.878 ± 0.085	/	0.09 ± 0.06
BHI + Yeast	4.7 ± 0.7	2.14 ± 0.23	8.1 ± 1.0	0.996 ± 0.001	19.5 ± 1.9	0.91 ± 0.04
BHI + LPS	4.4 ± 0.3	2.28 ± 0.26	23.8 ± 0.1	0.994 ± 0.003	18.3 ± 1.9	1.02 ± 0.08
B. thetaiotaomicron						
YCFA	3.7 ± 0.2	2.44 ± 0.15	6.2 ± 0.4	0.999 ± 0.001	17.1 ± 1.1	0.92 ± 0.01
YCFA -SCFA	3.1 ± 0.1	1.89 ± 0.08	23.9 ± 0.0	0.999 ± 0.000	22 ± 1	0.86 ± 0.02
BHI	2.4 ± 1.2	0.85 ± 0.04	4.2 ± 0.5	0.998 ± 0.002	49.1 ± 2.2	0.40 ± 0.01
BHI + SCFA	4.8 ± 1.2	0.34 ± 0.02	3.3 ± 1.5	0.998 ± 0.002	121.7 ± 7.1	0.30 ± 0.02
BHI + Yeast	2.5 ± 2.5	0.80 ± 0.02	4.5 ± 0.3	0.995 ± 0.005	51.7 ± 1.1	0.40 ± 0.01
BHI + LPS	2.3 ± 0.1	0.88 ± 0.03	4.1 ± 0.2	0.999 ± 0.000	47.9 ± 1.6	0.41 ± 0.01
B. longum						
YCFA	1.7 ± 0.0	3.66± 0.03	3.1 ± 0.2	0.987 ± 0.003	11.4 ± 0.1	0.59 ± 0.01
YCFA -SCFA	1.2 ± 0.0	2.11 ± 0.05	23.8 ± 0.0	0.992 ± 0.000	19.7 ± 0.5	0.36 ± 0.01
BHI	1.1 ± 0.0	1.01 ± 0.03	2.99 ± 0.0	0.999 ± 0.000	41.3 ± 1.4	0.26 ± 0.03
BHI + SCFA	3.5 ± 0.1	1.46 ± 0.02	2.6 ± 0.5	0.999 ± 0.000	28.4 ± 0.5	0.53 ± 0.01
BHI + Yeast	1.3 ± 1.3	1.24 ± 0.02	3 ± 0.00	0.999 ± 0.000	33.5 ± 0.7	0.28 ± 0.03
BHI + LPS	3.0 ± 2.3	1.49 ± 0.55	5.1 ± 2.6	0.934 ± 0.089	27.9 ± 9.8	0.33 ± 0.11

SEPs Lysates OD

Table 9: Optical Density of *B. producta* for SEPs lysates

Inoculated with OD 0.1 of a preculture OD 2.408

		YCFA		YCFA -SCFA		BHI		BHI + SCFA		BHI + LPS		BHI + YEAST	
Date and time	[h]	A	B	A	B	A	B	A	B	A	B	A	B
31.08.2022 08:15	0	0.1	0.1	0.1	0.1	0.1	0.1	0.1	0.1	0.1	0.1	0.1	0.1
31.08.2022 10:00	1.8	0.088	0.127	0.102	0.112	0.092	0.103	0.077	0.084	0.093	0.1	0.099	0.114
31.08.2022 12:30	4.3	0.47	0.49	0.31	0.45	0.39	0.5	0.123	0.124	0.38	0.43	0.4	0.47
31.08.2022 14:15	6	1.27	1.57	1.34	1.74	0.94	0.99	0.167	0.169	0.81	0.98	0.94	0.89
31.08.2022 15:30	7.3	2.15	2.34	2.42	2.71	1.31	1.32	0.23	0.202	1.28	1.28	1.27	1.3

Metabolome Lysis final OD, growth curves and metabolome results overview

Table 10: Metabolome lysis OD from *B. producta* and *B. thetaiotaomicron* grown in pH 6 and pH 7

Time	[h]	A	B	C	D	E	Average
B. producta pH 6							
28.09.2022 15:30	0.0	0.05	0.05	0.05	0.05	0.05	0.05
29.09.2022 08:30	17.0	1.85	1.59	1.42	1.56	1.58	1.6
29.09.2022 09:10	17.7	2.08	1.91	1.85	1.8	1.7	1.9
29.09.2022 09:35	18.1	2.13	2.03	1.94	1.85	2.05	2.0
29.09.2022 10:05	18.6	2.37	2.25	2.56	2.36	2.17	2.3
B. producta pH 7							
14.09.2022 08:00	0	0.05	0.05	0.05	0.05	0.05	0.05
14.09.2022 10:30	2.5	0.189	0.171	0.169	0.176	0.188	0.179
14.09.2022 12:00	4	0.5	0.52	0.5	0.57	0.49	0.516
14.09.2022 14:00	6	1.79	1.88	2.11	1.87	2.08	1.946
B. thetaiotaomicron pH 6							
15.09.2022 07:00	0	0.05	0.05	0.05	0.05	0.05	0.05
15.09.2022 10:00	3	0.087	0.09	0.082	0.09	0.091	0.088
15.09.2022 12:00	5	0.194	0.197	0.199	0.207	0.201	0.200
15.09.2022 15:15	8.3	0.59	0.66	0.63	0.6	0.6	0.616
15.09.2022 15:45	8.8	0.69	0.72	0.58	0.71	0.68	0.676
B. thetaiotaomicron pH 7							
15.09.2022 07:00	0	0.05	0.05	0.05	0.05	0.05	0.05
15.09.2022 10:00	3	0.178	0.182	0.175	0.188	0.196	0.184
15.09.2022 12:00	5	0.69	0.75	0.77	0.74	0.76	0.742
15.09.2022 15:15	8.3	2.77	2.5	2.73	2.23	2.48	2.542

Table 11: Metabolome lysis of *B. longum* grown in pH 6, pH 7 and pH 8. Replicates A - B were used for lysates, the replicate "OD" was continued to be measured to complete the growth curve

Zeit	[h]	A	B	C	D	E	OD
pH 6							
25.08.2022 09:15	0	0.1	0.1	0.1	0.1	0.1	0.1
25.08.2022 10:00	0.75						0.177
25.08.2022 10:45	1.5	0.252	0.264	0.248	0.274	0.256	0.277
25.08.2022 11:30	2.25						0.418
25.08.2022 12:15	3						0.66
25.08.2022 12:45	3.5	0.82	0.82	0.88	0.85	0.88	0.88
25.08.2022 13:30	4.25						1.22
25.08.2022 14:00	4.75						1.45
25.08.2022 14:30	5.25	1.62	1.63	1.59	1.63	1.64	1.7
25.08.2022 15:15	6.0						1.92
25.08.2022 16:40	7.4						2.05
pH 7							
24.08.2022 09:00	0	0.1	0.1	0.1	0.1	0.1	0.1
24.08.2022 10:00	1						0.221
24.08.2022 10:30	1.5	0.3	0.373	0.302	0.338	0.345	0.348
24.08.2022 11:00	2						0.497
24.08.2022 11:45	2.8	0.75	0.72	0.67	0.75	0.64	0.69
24.08.2022 12:30	3.5						1.26
24.08.2022 13:00	4.0						1.79
24.08.2022 13:15	4.3						2.07
24.08.2022 13:20	4.3	2.31	2.27	2.21	2.22	2.16	
24.08.2022 14:10	5.2						2.68
24.08.2022 15:00	6.0						2.42
24.08.2022 16:30	7.5						2.55
pH 8							
05.07.2022 08:15	0	0.05	0.05	0.05	0.05	0.05	0.05
05.07.2022 09:45	1.5						0.108
05.07.2022 10:45	2.5						0.211
05.07.2022 11:45	3.5	0.407	0.401	0.423	0.446	0.435	0.37
05.07.2022 12:45	4.5						0.92
05.07.2022 13:45	5.5	1.69	1.81	1.74	1.62	1.64	1.59
05.07.2022 14:15	6.0						2.02
05.07.2022 15:00	6.8	2.92	2.27	2.8	4.2	3.06	3.07
05.07.2022 15:55	7.7						2.49
05.07.2022 17:00	8.8						2.94

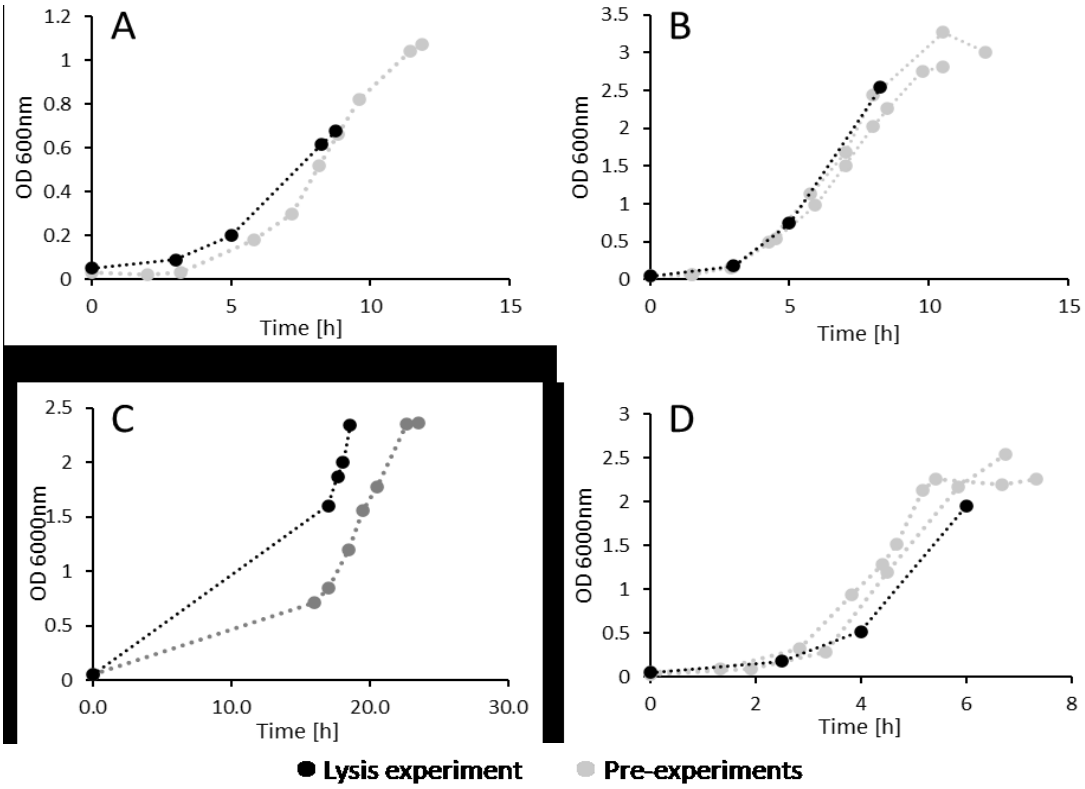

Figure 31: Growth curves of metabolome lysis. Black dots display the lysate experiment, the last displayed point is the time point of the lysis. The grey dots show growth curves from pre-experiments, to determine the lysis timepoint more reliably. (A) *B. producta* grown in YCFA with pH 6. (B) *B. producta* grown in YCFA pH 7. (C) *B. thetaiotaomicron* grown in YCFA with pH 6. (D) *B. thetaiotaomicron* grown in YCFA with pH 7.

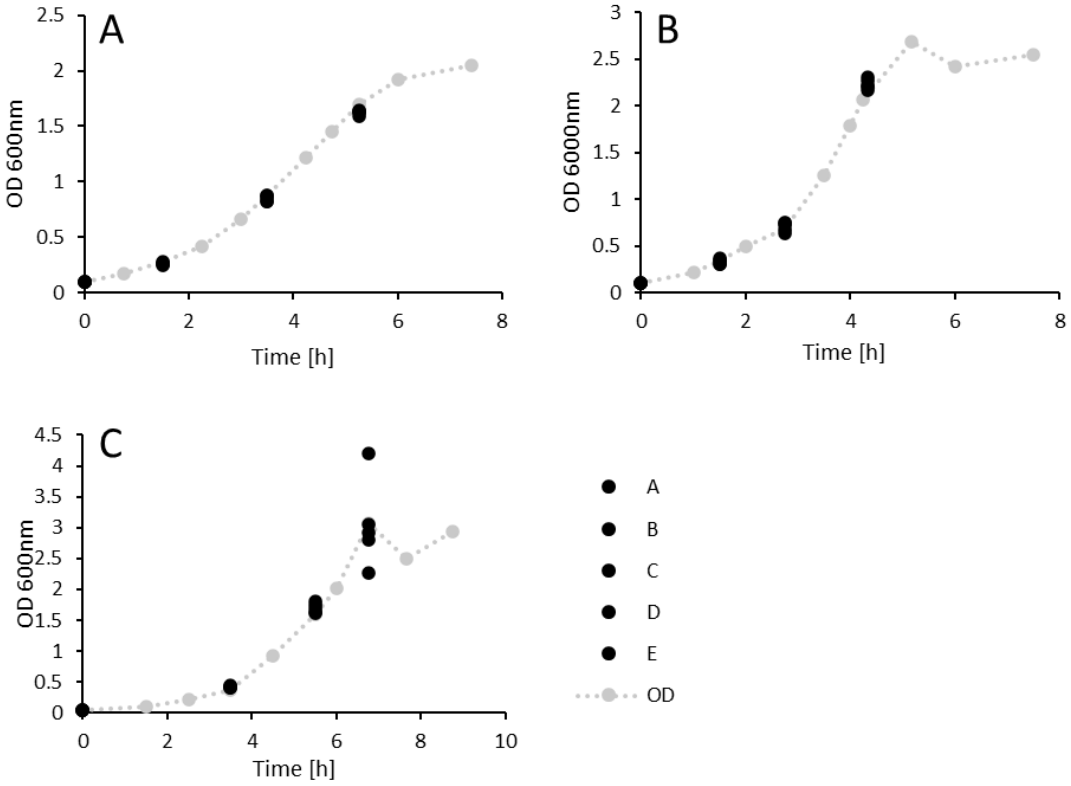

Figure 32: Growth curves of metabolome lysis of B. longum. The black dots display the replicates for lysis, the grey dot is an additional replicate for completion of the growth curves. (A) Growth in YCFA pH 6. (B) Growth in YCFA with pH 7. (C) Growth in YCFA with PH 8.

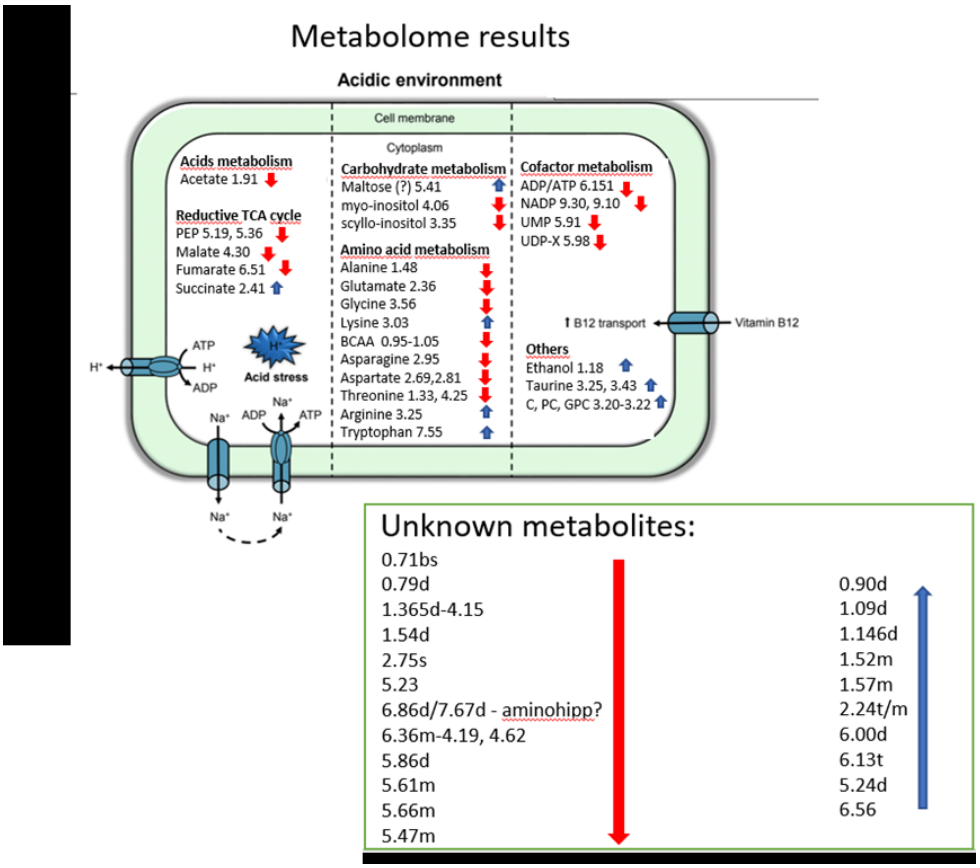

Figure 33: Metabolome results for *B. producta* grown in pH6 normalized to OD and TSP. The numbers indicate the chemical shifts of the NMR signals. The original raw data can be found on the institute server (IFIM), the digital lab book or in Dr. Silke Heinzmann Lab, Helmholtz Munich (miTarget PZ).

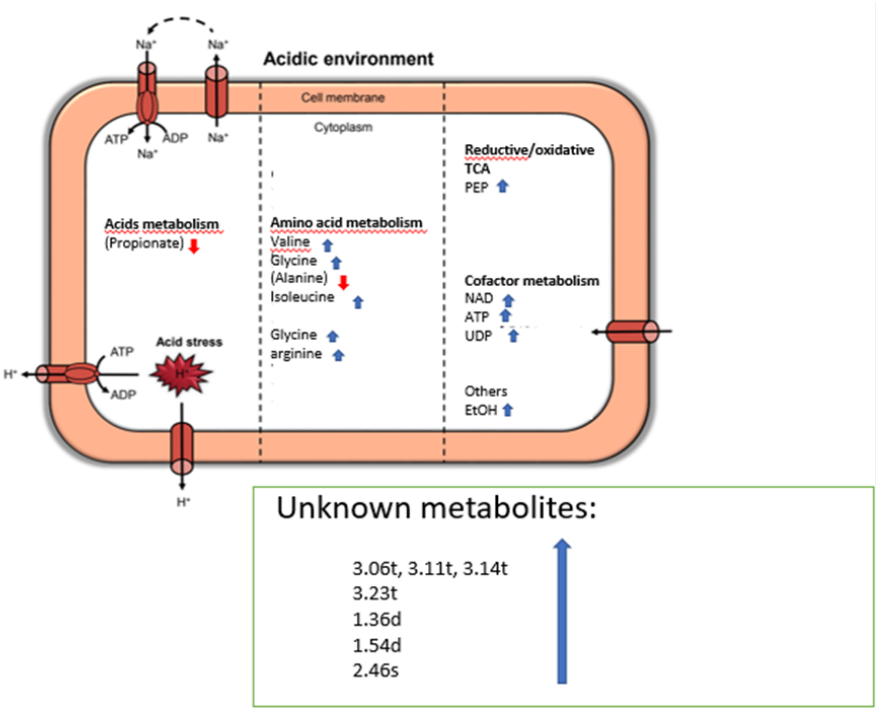

Figure 34: Metabolome results for *B. thetaiotaomicron* grown in pH6 normalized to OD and TSP. The numbers indicate the chemical shifts of the NMR signals. The original raw data can be found on the institute server (IFIM), the digital lab book or in Dr. Silke Heinzmann Lab, Helmholtz Munich (miTarget PZ).

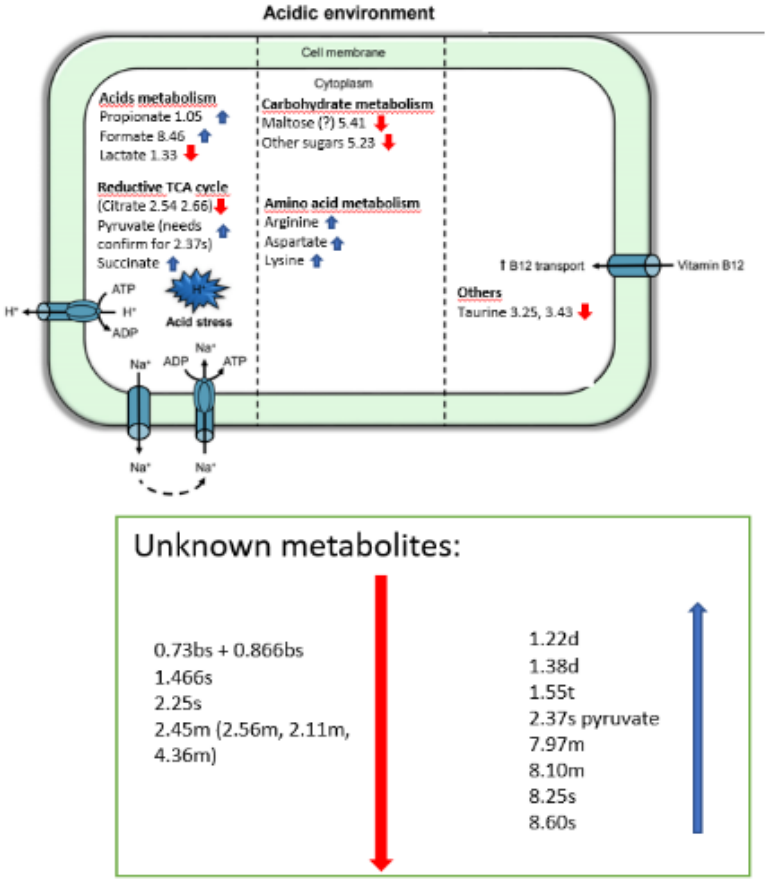

Figure 35: Metabolome results for *B. longum* grown in pH 6 normalized to OD and TSP. The numbers indicate the chemical shifts of the NMR signals. The original raw data can be found on the institute server (IFIM), the digital lab book or in Dr. Silke Heinzmann Lab, Helmholtz Munich (miTarget PZ).

RNA concentration of lysates for transcriptomics and PCA transcriptome

Table 12: RNA isolation of the three gut bacteria grown on pH 6, pH 7 and respectively pH 8. For *B. longum* no reliable RNA concentration could be isolated, hence this bacterium was excluded for further transcriptome analysis, 12.05.2023

Bacterium/Condition	RNA Concentration [ng/µl]	A260/280	A260/230
B. longum pH6 I	-	-	-
B. longum pH6 II	-	-	-
B. longum pH6 III	6.759	1.700	0.321
B. longum pH7 I	-	-	
B. longum pH7 II	6.368	1.728	0.615
B. longum pH7 III	17.1	1.654	0.489
B. longum pH8 I	-	-	-
B. longum pH8 II	3.579	1.800	0.750
B. longum pH8 III	-	-	-
B. producta pH6 I	7.157	2.000	1.500
B. producta pH6 II	6.759	2.125	0.213
B. producta pH6 III	6.362	2.000	1.600
B. producta pH7 I	365	2.132	2.511
B. producta pH7 II	179	2.128	2.467
B. producta pH7 III	317	2.108	2.522
B. thetaiotaomicron pH6 I	165	2.108	2.015
B. thetaiotaomicron pH6 II	134	2.086	2.112
B. thetaiotaomicron pH6 III	140	2.120	1.751
B. thetaiotaomicron pH7 I	196	1.992	1.563
B. thetaiotaomicron pH7 II	128	1.640	2.084
B. thetaiotaomicron pH7 III	143	2.094	1.821

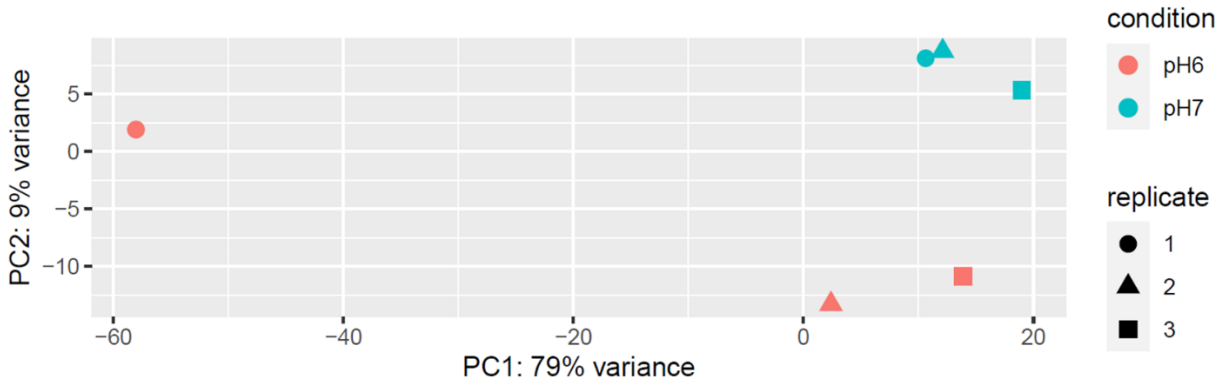

Figure 36: PCA transcriptome *B. producta* pH 6 vs pH 7 sample comparison. For pH6, sample one (red circle) is an outlier. Hence, for further evaluation this replicate was excluded.

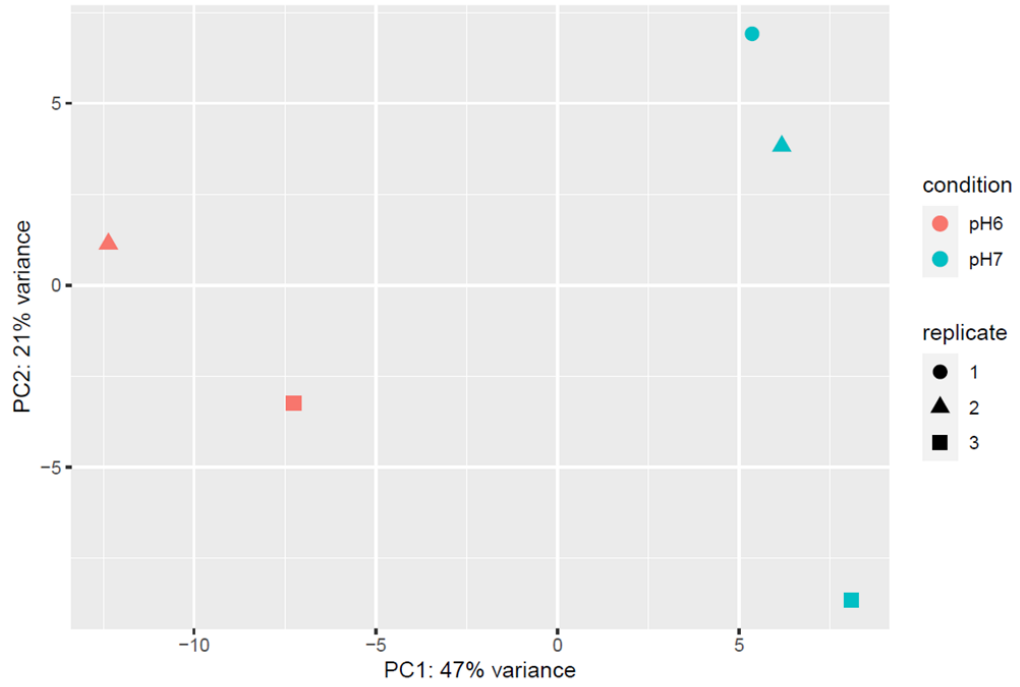

Figure 37: PCA transcriptome *B. producta* pH 6 vs pH 7 sample comparison without the outlier.

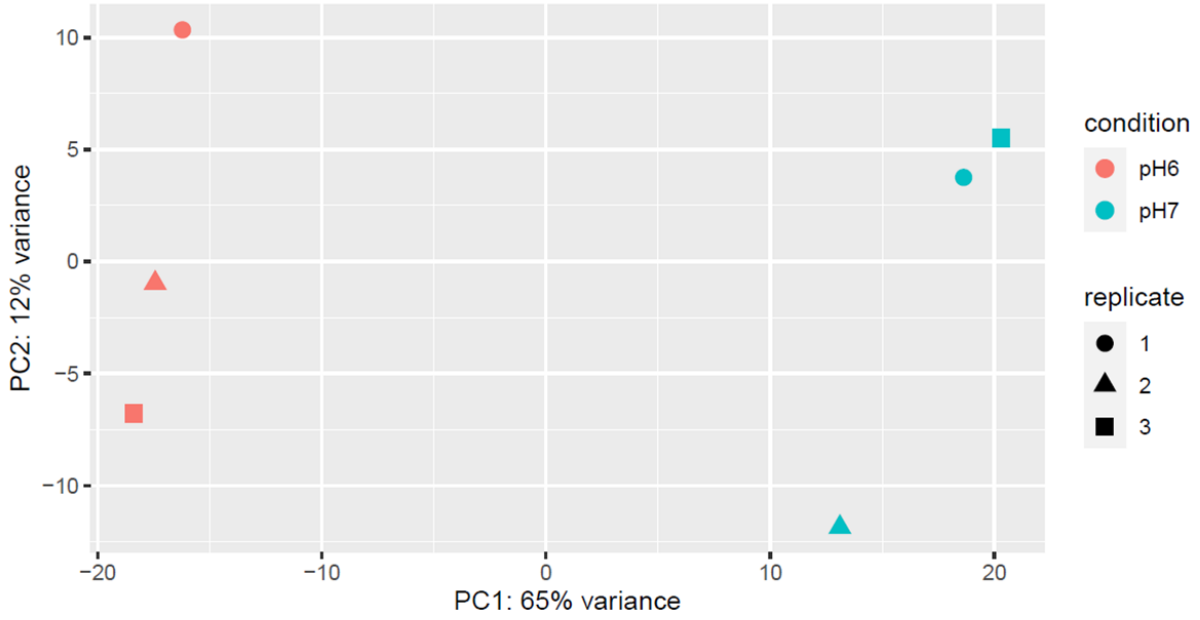

Figure 38: PCA transcriptome *B. thetaiotaomicron* pH 6 vs pH 7 sample comparison.

Tables of significant expressed genes of *B. producta* and *B. thetaiotaomicron* pH 6 vs. pH 7

Table 13: Transcripts with negative fold change corresponding to MA Plot of *B. thetaiotaomicron* comparing pH 6 vs. pH7. shows upregulated genes when grown in pH 6. Cut-off was made for padjust of <0.05 and log2 foldChance at >2. log2FoldChange is the log2 fold change between the groups, Pvalue: Wald test p-value, padj: Benjamini-Hochberg adjusted p-value. The sequence name is "NC_004663.1"

Locus Tag	Source	Feature	Start	End	Strand	Potential attribute, product or function	log2FoldChange	pvalue	padj
BT_RS08860	Protein Homology	CDS	2159537	2159725	+	hypothetical protein	-5,512	4,1E-66	1,0E-62
BT_RS03020	Protein Homology	CDS	757320	758273	+	polysaccharide biosynthesis/export family protein	-3,665	2,8E-35	1,8E-32
BT_RS07820	Protein Homology	CDS	1907242	1908417	+	DUF418 domain-containing protein	-2,240	6,4E-32	2,3E-29
BT_RS12180	Protein Homology	CDS	3010413	3010538	-	helix-turn-helix domain-containing protein	-2,544	8,9E-31	2,8E-28
BT_RS12685	Protein Homology	CDS	3131786	3132496	+	hypothetical protein	-3,081	5,6E-27	1,3E-24
BT_RS23165	Protein Homology	CDS	6016568	6016816	+	hypothetical protein	-2,870	1,4E-22	2,0E-20
BT_RS14565	Protein Homology	CDS	3592634	3593575	-	capsular polysaccharide synthesis protein	-2,223	1,6E-20	1,8E-18
BT_RS03685	Protein Homology	CDS	914067	915734	+	formate--tetrahydrofolate ligase	-2,051	2,0E-19	1,9E-17
BT_RS08700	Protein Homology	CDS	2112269	2113528	-	CDP-glycerol glycerophosphotransferase family protein	-2,398	5,3E-19	4,8E-17
BT_RS21325	Protein Homology	CDS	5566091	5567371	-	Mfa1 family fimbria major subunit	-2,981	7,2E-19	6,2E-17
BT_RS11830	Protein Homology	CDS	2921339	2921611	+	TfoX/Sxy family protein	-3,422	2,0E-18	1,6E-16
BT_RS01320	Protein Homology	CDS	304251	307184	+	SusC/RagA family TonB-linked outer membrane protein	-2,183	1,9E-15	1,2E-13
BT_RS19595	Protein Homology	CDS	5052447	5054124	+	DUF5686 family protein	-5,721	6,6E-15	3,7E-13
BT_RS13655	Protein Homology	CDS	3365374	3365979	-	30S ribosomal protein S4	-3,481	2,2E-14	1,1E-12
BT_RS15455	Protein Homology	CDS	3861603	3864290	-	hypothetical protein	-2,842	4,4E-12	1,5E-10
BT_RS13675	Protein Homology	CDS	3367037	3367255	-	translation initiation factor IF-1	-2,473	3,6E-11	1,0E-09
BT_RS13670	Protein Homology	CDS	3366911	3367027	-	type B 50S ribosomal protein L36	-2,561	6,4E-11	1,7E-09
BT_RS16695	Protein Homology	CDS	4222532	4224556	-	RagB/SusD family nutrient uptake outer membrane protein	-2,712	3,9E-10	9,1E-09
BT_RS20615	Protein Homology	CDS	5329091	5330422	+	DUF5005 domain-containing protein	-2,886	7,1E-10	1,6E-08
BT_RS23440	Protein Homology	CDS	6085860	6088481	-	DUF4962 domain-containing protein	-3,404	2,1E-09	4,2E-08
BT_RS17100	Protein Homology	CDS	4354001	4354906	+	beta-1%2C6-N-acetylglucosaminyltransferase	-2,291	2,2E-09	4,4E-08
BT_RS11780	Protein Homology	CDS	2910596	2911315	-	DUF6088 family protein	-2,011	2,4E-09	4,8E-08
BT_RS20875	Protein Homology	CDS	5427009	5428826	-	alpha-L-fucosidase	-2,298	4,7E-09	8,6E-08
BT_RS02985	Protein Homology	CDS	749938	751098	+	glycosyltransferase family 4 protein	-2,111	1,7E-08	2,9E-07

BT_RS03870	Protein Homology	CDS	963212	964909	-	alpha-amylase family protein	-2,233	1,8E-08	3,0E-07
BT_RS18185	Protein Homology	CDS	4669160	4672315	-	TonB-dependent receptor	-2,063	1,9E-08	3,1E-07
BT_RS02110	Protein Homology	CDS	519272	520150	-	DNA/RNA non-specific endonuclease	-3,794	5,5E-08	8,5E-07
BT_RS19605	Protein Homology	CDS	5054875	5055489	+	fumarylacetoacetate hydrolase family protein	-4,347	5,8E-08	8,9E-07
BT_RS06845	Protein Homology	CDS	1676856	1678025	-	glycosyltransferase	-2,820	1,4E-07	1,9E-06
BT_RS08035	Protein Homology	CDS	1948868	1949620	-	GNAT family N-acetyltransferase	-2,381	1,9E-07	2,7E-06
BT_RS12590	Protein Homology	CDS	3108332	3111382	-	PL29 family lyase N-terminal domain-containing protein	-2,518	4,7E-07	6,3E-06
BT_RS02695	Protein Homology	CDS	676005	676766	-	glycerophosphodiester phosphodiesterase	-4,048	7,1E-07	9,0E-06
BT_RS05615	Protein Homology	CDS	1400017	1400442	-	flavodoxin	-2,108	7,6E-07	9,6E-06
BT_RS17885	GeneMarkS-2+	CDS	4578739	4580307	+	transglutaminase domain-containing protein	-2,208	1,0E-06	1,3E-05
BT_RS20760	Protein Homology	CDS	5382882	5384741	-	RagB/SusD family nutrient uptake outer membrane protein	-2,333	1,1E-06	1,3E-05
BT_RS08505	Protein Homology	CDS	2070593	2071114	-	HAD-IIIA family hydrolase	-3,202	1,3E-06	1,5E-05
BT_RS13810	Protein Homology	CDS	3382099	3382404	-	DUF3467 domain-containing protein	-2,368	1,3E-06	1,5E-05
BT_RS22865	Protein Homology	CDS	5952578	5955406	+	type I restriction endonuclease subunit R	-2,694	1,5E-06	1,7E-05
BT_RS12020	Protein Homology	CDS	2966907	2967641	-	alpha/beta hydrolase	-2,095	1,6E-06	1,8E-05
BT_RS14550	Protein Homology	CDS	3589800	3590903	-	acyltransferase	-2,390	2,6E-06	2,8E-05
BT_RS06810	Protein Homology	CDS	1670820	1671713	-	ATP-grasp fold amidoligase family protein	-2,648	2,9E-06	3,1E-05
BT_RS19655	Protein Homology	CDS	5064686	5065444	+	tRNA (guanosine(46)-N7)-methyltransferase TrmB	-2,168	3,0E-06	3,2E-05
BT_RS10580	Protein Homology	CDS	2615821	2617983	-	DNA topoisomerase 3	-2,354	3,7E-06	3,8E-05
BT_RS20715	Protein Homology	CDS	5363539	5366913	+	AAA domain-containing protein	-2,086	4,4E-06	4,4E-05
BT_RS02625	Protein Homology	CDS	656402	657586	-	tryptophan synthase subunit beta	-3,798	4,8E-06	4,8E-05
BT_RS20880	Protein Homology	CDS	5429325	5433257	+	hybrid sensor histidine kinase/response regulator transcription factor	-2,427	4,9E-06	5,0E-05
BT_RS02150	Protein Homology	CDS	530005	533124	+	TonB-dependent receptor	-2,532	6,9E-06	6,7E-05
BT_RS20350	Protein Homology	CDS	5244897	5245373	+	HU family DNA-binding protein	-2,652	7,3E-06	7,1E-05
BT_RS10620	Protein Homology	CDS	2629926	2631989	+	glycoside hydrolase family 127 protein	-2,596	8,1E-06	7,7E-05
BT_RS11450	Protein Homology	CDS	2841589	2844543	-	SusC/RagA family TonB-linked outer membrane protein	-2,197	9,7E-06	9,1E-05
BT_RS15030	Protein Homology	CDS	3737421	3738668	-	DUF5126 domain-containing protein	-2,088	9,8E-06	9,2E-05
BT_RS19600	Protein Homology	CDS	5054213	5054875	+	redox-sensing transcriptional repressor Rex	-3,408	1,2E-05	0,00011
BT_RS22205	Protein Homology	CDS	5798923	5799474	+	RNA polymerase sigma-70 factor	-2,888	1,3E-05	0,00012
BT_RS02105	Protein Homology	CDS	518130	519167	-	endolytic transglycosylase MltG	-3,030	1,6E-05	0,00014
BT_RS04855	Protein Homology	CDS	1179380	1182006	-	carboxypeptidase regulatory-like domain-containing protein	-2,524	2,6E-05	0,00022
BT_RS10625	Protein Homology	CDS	2632182	2633321	+	ABC transporter substrate-binding protein	-2,776	2,8E-05	0,00023
BT_RS01905	GeneMarkS-2+	CDS	478981	480345	+	O-antigen export protein	-2,251	3,4E-05	0,00027
BT_RS19610	Protein Homology	CDS	5055529	5056008	+	2-C-methyl-D-erythritol 2%2C4-cyclodiphosphate synthase	-3,228	4,1E-05	0,00033
BT_RS08290	Protein Homology	CDS	2021666	2025631	+	response regulator	-2,018	5,0E-05	0,00039
BT_RS02585	Protein Homology	CDS	647028	649490	-	LruC domain-containing protein	-2,079	5,5E-05	0,00043
BT_RS24690	Protein Homology	CDS	3675806	3676534	-	hypothetical protein	-2,020	6,2E-05	0,00047
BT_RS02575	Protein Homology	CDS	645248	646408	-	sugar transferase	-2,056	6,3E-05	0,00049
BT_RS02315	Protein Homology	CDS	582758	583972	+	glycosyltransferase family 4 protein	-2,341	6,6E-05	0,00050
BT_RS21435	Protein Homology	CDS	5599443	5600096	-	FecR family protein	-2,159	6,8E-05	0,00052
BT_RS23445	Protein Homology	CDS	6088483	6089748	-	sugar MFS transporter	-3,370	8,1E-05	0,00060
BT_RS20985	Protein Homology	CDS	5464630	5466291	+	glycoside hydrolase family protein	-3,364	8,1E-05	0,00060
BT_RS05595	Protein Homology	CDS	1397337	1397546	-	hypothetical protein	-2,545	8,4E-05	0,00061
BT_RS14005	Protein Homology	CDS	3424923	3425258	-	hypothetical protein	-3,133	8,4E-05	0,00061
BT_RS20345	Protein Homology	CDS	5243999	5244502	+	N-acetylmuramoyl-L-alanine amidase	-2,501	0,00012	0,00086
BT_RS15965	Protein Homology	CDS	4017138	4017353	-	helix-turn-helix transcriptional regulator	-3,036	0,00015	0,00104
BT_RS16950	Protein Homology	CDS	4316255	4317457	+	glycoside hydrolase family 88 protein	-2,056	0,00015	0,00104
BT_RS22370	Protein Homology	CDS	5842110	5842817	+	hypothetical protein	-3,026	0,00016	0,00112
BT_RS08810	Protein Homology	CDS	2142214	2144133	-	HAMP domain-containing sensor histidine kinase	-3,010	0,00017	0,00116
BT_RS23455	Protein Homology	CDS	6090900	6092528	-	hypothetical protein	-3,020	0,00017	0,00116
BT_RS02580	Protein Homology	CDS	646421	646786	-	response regulator	-2,643	0,00023	0,00150
BT_RS07270	Protein Homology	CDS	1766226	1766513	-	YtxH domain-containing protein	-2,964	0,00024	0,00155
BT_RS00360	Protein Homology	CDS	73184	74416	+	site-specific integrase	-2,954	0,00024	0,00158
BT_RS17090	Protein Homology	CDS	4351512	4352672	-	aminotransferase class I/II-fold pyridoxal phosphate-dependent enzyme	-2,520	0,00026	0,00169
BT_RS23450	Protein Homology	CDS	6089786	6090739	-	ROK family protein	-3,153	0,00027	0,00171
BT_RS10780	Protein Homology	CDS	2680909	2681946	+	aspartate--ammonia ligase	-2,385	0,00027	0,00173
BT_RS18975	Protein Homology	CDS	4883107	4884564	+	rhamnulokinase	-2,898	0,00035	0,00218
BT_RS01880	Protein Homology	CDS	474112	475272	+	polysaccharide pyruvyl transferase family protein	-2,477	0,00039	0,00243
BT_RS05440	Protein Homology	CDS	1367048	1367665	-	recombination mediator RecR	-2,079	0,00040	0,00248
BT_RS17895	Protein Homology	CDS	4581515	4583104	+	O-antigen ligase family protein	-2,173	0,00042	0,00259
BT_RS08190	Protein Homology	CDS	1984871	1986331	+	aminoacyl-histidine dipeptidase	-2,232	0,00048	0,00285
BT_RS08485	Protein Homology	CDS	2065707	2066678	+	ABC transporter substrate-binding protein	-2,674	0,00048	0,00289
BT_RS16940	Protein Homology	CDS	4311134	4314217	-	TonB-dependent receptor	-2,649	0,00055	0,00326
BT_RS07850	Protein Homology	CDS	1920134	1921462	+	RagB/SusD family nutrient uptake outer membrane protein	-2,054	0,00056	0,00331
BT_RS01825	Protein Homology	CDS	460448	461998	+	ATP-binding protein	-2,049	0,00061	0,00357
BT_RS11085	Protein Homology	CDS	2747782	2751363	-	glycoside hydrolase family 2 TIM barrel-domain containing protein	-2,792	0,00062	0,00358
BT_RS20340	Protein Homology	CDS	5243593	5243847	+	DUF4248 domain-containing protein	-2,805	0,00063	0,00364
BT_RS01890	GeneMarkS-2+	CDS	476462	477778	+	NADH dehydrogenase subunit 2	-2,052	0,00067	0,00385
BT_RS04535	Protein Homology	CDS	1113022	1113312	-	hypothetical protein	-2,293	0,00068	0,00390
BT_RS02100	Protein Homology	CDS	516457	518049	-	thiamine pyrophosphate-dependent enzyme	-2,097	0,00069	0,00391

BT_RS02095	Protein Homology	CDS	515869	516453	-	indolepyruvate oxidoreductase subunit beta	-2,738	0,00085	0,00471
BT_RS07550	Protein Homology	CDS	1840788	1841546	+	DUF4465 domain-containing protein	-2,892	0,00096	0,00528
BT_RS20180	Protein Homology	CDS	5211775	5213070	-	lytic transglycosylase domain-containing protein	-2,562	0,00098	0,00536
BT_RS12560	Protein Homology	CDS	3103699	3104073	-	hypothetical protein	-2,072	0,00100	0,00543
BT_RS17945	Protein Homology	CDS	4597363	4597830	+	CYTH domain-containing protein	-2,887	0,00102	0,00552
BT_RS19580	Protein Homology	CDS	5049972	5050808	+	30S ribosomal protein S2	-2,855	0,00113	0,00603
BT_RS23595	Protein Homology	CDS	6140802	6143240	-	glycoside hydrolase N-terminal domain-containing protein	-2,495	0,00130	0,00678
BT_RS12945	Protein Homology	CDS	3194382	3197753	-	TonB-dependent receptor	-2,083	0,00132	0,00686
BT_RS20270	Protein Homology	CDS	5234612	5235034	-	conjugal transfer protein MobA	-2,805	0,00142	0,00730
BT_RS05465	Protein Homology	CDS	1371733	1373721	+	oligopeptide transporter%2C OPT family	-2,354	0,00151	0,00774
BT_RS15830	Protein Homology	CDS	3981331	3982770	-	sialate O-acetylesterase	-2,240	0,00152	0,00774
BT_RS20330	Protein Homology	CDS	5242311	5242583	+	hypothetical protein	-2,786	0,00156	0,00790
BT_RS21430	Protein Homology	CDS	5596039	5599392	-	TonB-dependent receptor	-2,339	0,00156	0,00790
BT_RS18995	Protein Homology	CDS	4887821	4888975	+	lactaldehyde reductase	-2,614	0,00164	0,00829
BT_RS12185	Protein Homology	CDS	3010823	3011311	-	GNAT family N-acetyltransferase	-2,268	0,00166	0,00839
BT_RS13320	Protein Homology	CDS	3288975	3289967	-	tyrosine-type recombinase/integrase	-2,331	0,00178	0,00891
BT_RS18985	Protein Homology	CDS	4885884	4886903	+	L-rhamnose/proton symporter RhaT	-2,751	0,00180	0,00897
BT_RS20590	Protein Homology	CDS	5319485	5321245	+	hypothetical protein	-2,453	0,00185	0,00918
BT_RS08370	Protein Homology	CDS	2040648	2042009	-	bifunctional cytidylyltransferase/SDR family oxidoreductase	-2,590	0,00191	0,00944
BT_RS04245	GeneMarkS-2+	CDS	1039627	1039917	+	hypothetical protein	-2,287	0,00201	0,00991
BT_RS18035	Protein Homology	CDS	4626231	4626995	+	hypothetical protein	-2,724	0,00203	0,00997
BT_RS13255	Protein Homology	CDS	3264883	3266193	-	GDSL-type esterase/lipase family protein	-2,108	0,00206	0,01010
BT_RS10590	Protein Homology	CDS	2620284	2622185	-	methylmalonyl-CoA mutase small subunit	-2,414	0,00208	0,01018
BT_RS02120	Protein Homology	CDS	520419	521627	-	ROK family transcriptional regulator	-2,288	0,00222	0,01074
BT_RS13590	Protein Homology	CDS	3350059	3351405	-	TolC family protein	-2,698	0,00224	0,01080
BT_RS13815	Protein Homology	CDS	3382547	3386830	-	DNA-directed RNA polymerase subunit beta	-2,276	0,00225	0,01083
BT_RS09960	Protein Homology	CDS	2466692	2469889	-	efflux RND transporter permease subunit	-2,383	0,00242	0,01150
BT_RS09575	Protein Homology	CDS	2373541	2374614	-	nitronate monooxygenase	-2,132	0,00257	0,01216
BT_RS09835	Protein Homology	CDS	2437760	2440630	-	TonB-dependent receptor	-2,506	0,00270	0,01262
BT_RS20510	Protein Homology	CDS	5296978	5297466	-	4Fe-4S dicluster domain-containing protein	-2,066	0,00282	0,01313
BT_RS17575	Protein Homology	CDS	4475408	4478527	-	TonB-dependent receptor	-2,495	0,00287	0,01332
BT_RS06815	Protein Homology	CDS	1671731	1672756	-	CapA family protein	-2,638	0,00288	0,01335
BT_RS00010	Protein Homology	CDS	783	1778	+	hypothetical protein	-2,134	0,00305	0,01397
BT_RS11225	Protein Homology	CDS	2786924	2788333	-	C10 family peptidase	-2,341	0,00304	0,01397
BT_RS17970	Protein Homology	CDS	4602705	4603736	-	endonuclease	-2,590	0,00346	0,01574
BT_RS07220	Protein Homology	CDS	1757482	1758180	-	SIMPL domain-containing protein	-2,106	0,00352	0,01592
BT_RS15860	Protein Homology	CDS	3991841	3993997	-	alpha-galactosidase	-2,293	0,00376	0,01677
BT_RS19455	Protein Homology	CDS	5012927	5015488	+	hypothetical protein	-2,428	0,00377	0,01678
BT_RS11125	Protein Homology	CDS	2762989	2765265	-	GH92 family glycosyl hydrolase	-2,420	0,00395	0,01746
BT_RS14330	Protein Homology	CDS	3518178	3522095	-	two-component regulator propeller domain-containing protein	-2,278	0,00409	0,01806
BT_RS17570	Protein Homology	CDS	4473346	4475391	-	RagB/SusD family nutrient uptake outer membrane protein	-2,274	0,00410	0,01807
BT_RS09260	Protein Homology	CDS	2292185	2293747	-	ATP-binding protein	-2,064	0,00414	0,01816
BT_RS21615	Protein Homology	CDS	5640703	5641536	-	glycosyltransferase family 2 protein	-2,298	0,00414	0,01816
BT_RS02590	Protein Homology	CDS	649703	650743	-	asparaginase	-2,526	0,00445	0,01926
BT_RS08350	GeneMarkS-2+	CDS	2036422	2037720	-	hypothetical protein	-2,054	0,00454	0,01954
BT_RS14725	Protein Homology	CDS	3636030	3639233	-	TonB-dependent receptor	-2,261	0,00455	0,01954
BT_RS16310	Protein Homology	CDS	4114044	4114976	+	DUF4848 domain-containing protein	-2,362	0,00518	0,02196
BT_RS02620	Protein Homology	CDS	654951	656357	-	anthranilate synthase component I family protein	-2,356	0,00536	0,02264
BT_RS00840	Protein Homology	CDS	179107	180390	-	zinc-dependent metalloproteinase lipoprotein	-2,006	0,00547	0,02289
BT_RS08270	Protein Homology	CDS	2014035	2017394	-	TonB-dependent receptor	-2,332	0,00575	0,02379
BT_RS21425	Protein Homology	CDS	5594092	5596032	-	RagB/SusD family nutrient uptake outer membrane protein	-2,102	0,00609	0,02497
BT_RS00935	Protein Homology	CDS	200124	203564	+	TonB-dependent receptor	-2,097	0,00612	0,02506
BT_RS12200	Protein Homology	CDS	3014212	3015129	-	homoserine O-succinyltransferase	-2,181	0,00657	0,02650
BT_RS08355	Protein Homology	CDS	2037711	2038703	-	glycosyltransferase family 2 protein	-2,062	0,00679	0,02734
BT_RS10690	Protein Homology	CDS	2652976	2656104	+	GH92 family glycosyl hydrolase	-2,055	0,00716	0,02865
BT_RS18025	Protein Homology	CDS	4623903	4625528	+	tetratricopeptide repeat protein	-2,150	0,00747	0,02973
BT_RS16545	Protein Homology	CDS	4169331	4171160	-	excinuclease ABC subunit	-2,139	0,00802	0,03157
BT_RS18990	Protein Homology	CDS	4886916	4887725	+	rhamnulose-1-phosphate aldolase	-2,116	0,00835	0,03272
BT_RS02305	Protein Homology	CDS	580260	581522	+	O-antigen polymerase	-2,104	0,00910	0,03490
BT_RS09510	Protein Homology	CDS	2355408	2357366	-	RagB/SusD family nutrient uptake outer membrane protein	-2,222	0,00957	0,03624
BT_RS17290	GeneMarkS-2+	CDS	4399393	4399692	+	hypothetical protein	-2,074	0,01017	0,03797
BT_RS01550	Protein Homology	CDS	380228	381832	+	TonB-dependent receptor	-2,191	0,01020	0,03803
BT_RS23465	Protein Homology	CDS	6094272	6096272	-	heparinase II/III family protein	-2,188	0,01036	0,03851
BT_RS22255	Protein Homology	CDS	5814323	5817040	+	transglutaminase domain-containing protein	-2,068	0,01116	0,04108
BT_RS22420	Protein Homology	CDS	5855714	5857429	+	ATP-binding protein	-2,168	0,01122	0,04117
BT_RS23460	Protein Homology	CDS	6092550	6094160	-	sulfatase	-2,161	0,01170	0,04263
BT_RS23175	Protein Homology	CDS	6019688	6020272	+	DUF6621 family protein	-2,027	0,01240	0,04499
BT_RS02070	Protein Homology	CDS	512111	512308	+	50S ribosomal protein L35	-2,139	0,01286	0,04597
BT_RS02460	Protein Homology	CDS	620099	620455	+	hypothetical protein	-2,124	0,01315	0,04681

Table 14: Transcripts with positive fold change corresponding to MA Plot of *B. thetaiotaomicron* comparing pH 6 vs. pH7. shows upregulated genes when grown in pH 7. Cut-off was made for padjust of <0.05 and log2 foldChance at >2. log2FoldChange is the log2 fold change between the groups, Pvalue: Wald test p-value, padj: Benjamini-Hochberg adjusted p-value. The sequence name is "NC_004663.1"

Locus Tag	Source	Feature	Start	End	Strand	Potential function/product/attribute	log2Fold Change	pvalue	padj
BT_RS16160	Protein Homology	CDS	4081559	4082308	-	secondary active transmembrane transporter activity	4,039	1,1E-59	1,4E-56
BT_RS05765	Protein Homology	CDS	1425511	1426434	+	monoatomic cation transmembrane transporter activity	2,834	7,9E-51	6,7E-48
BT_RS01010	Protein Homology	CDS	220121	222046	-	NAD+ synthase (glutamine-hydrolyzing) activity	2,593	1,1E-34	5,5E-32
BT_RS10245	Protein Homology	CDS	2541785	2542450	-	hypothetical protein	2,518	6,4E-34	2,7E-31
BT_RS23860	Protein Homology	CDS	6213501	6213950	+	N-acetylmuramoyl-L-alanine amidase activity	2,367	2,0E-28	5,5E-26
BT_RS10855	Protein Homology	CDS	2698955	2699692	-	NADPH-dependent oxidoreductase	2,075	4,1E-28	1,0E-25
BT_RS22905	Protein Homology	CDS	5963411	5964556	-	DNA binding|0003677	2,220	1,9E-26	4,0E-24
BT_RS18740	Protein Homology	CDS	4826816	4827772	-	acetylornithine carbamoyltransferase	2,008	4,2E-25	8,2E-23
BT_RS05410	Protein Homology	CDS	1362814	1363593	+	DNA binding	2,083	3,2E-23	5,0E-21
BT_RS04025	Protein Homology	CDS	995222	996271	-	DUF2776 domain-containing protein	2,082	1,2E-20	1,4E-18
BT_RS20035	Protein Homology	CDS	5172133	5172675	+	glutathione peroxidase	2,098	3,5E-20	3,7E-18
BT_RS03475	Protein Homology	CDS	864533	866848	+	membrane	2,103	1,7E-18	1,4E-16
BT_RS06385	Protein Homology	CDS	1572150	1572950	-	DNA binding	2,082	9,2E-17	6,5E-15
BT_RS16885	Protein Homology	CDS	4293833	4294474	+	hydrolase activity%2C hydrolyzing O-glycosyl compounds	2,134	1,5E-15	9,9E-14
BT_RS23340	Protein Homology	CDS	6062271	6063833	-	arylsulfatase	2,194	3,5E-14	1,7E-12
BT_RS17070	Protein Homology	CDS	4347835	4348824	+	glycosyltransferase activity	2,289	1,2E-12	4,5E-11
BT_RS04860	Protein Homology	CDS	1182131	1183105	-	FecR domain-containing protein	2,163	1,3E-12	4,6E-11
BT_RS23185	Protein Homology	CDS	6021228	6022949	-	ATP-binding protein	2,016	1,3E-12	4,6E-11
BT_RS14380	tRNAscan-SE	tRNA	3537575	3537646	-	tRNA-Arg	2,037	5,8E-11	1,6E-09
BT_RS02905	Protein Homology	CDS	732978	733763	-	DUF4373 domain-containing protein	2,003	5,3E-09	9,6E-08
BT_RS20910	Protein Homology	CDS	5438918	5439598	+	epoxyqueuosine reductase	2,604	7,7E-08	1,1E-06
BT_RS05760	Protein Homology	CDS	1425327	1425506	+	hypothetical protein	2,176	9,4E-07	1,2E-05
BT_RS03435	Protein Homology	CDS	854378	856009	-	hydroxylamine reductase	2,482	1,0E-06	1,2E-05
BT_RS19385	Protein Homology	CDS	4994659	4995429	+	ATP binding	2,088	7,4E-06	0,0001
BT_RS08795	Protein Homology	CDS	2139397	2139954	+	chromate transmembrane transporter activity	2,122	1,8E-05	0,0002
BT_RS03380	Protein Homology	CDS	837499	838671	+	N-acetylglucosamine-6-phosphate deacetylase activity	2,030	3,4E-05	0,0003
BT_RS21195	Protein Homology	CDS	5539505	5539882	+	hypothetical protein	2,014	0,0001	0,0008
BT_RS04385	Protein Homology	CDS	1076614	1077498	-	carbon-nitrogen hydrolase	2,177	0,0002	0,0014
BT_RS21755	Protein Homology	CDS	5678656	5679009	+	aspartate 1-decarboxylase activity	2,117	0,0004	0,0023

Table 15: Transcripts with negative fold change corresponding to MA Plot of *B. producta* comparing pH 6 vs. pH7. This table shows the upregulated genes when grown in pH 6. The cut-off was made for padjust of <0.05. The log2FoldChange represents the log2 fold change between the groups. For the Pvalue the Wald test/Wald statistic was used. For padj represents the Benjamini-Hochberg adjusted p-value. The sequence name is „NZ_CP048626.1".

Locus Tag	Source	Start	End	Strand	Potential attribute, product or function	log2Fold Change	pvalue	padj
GXM18_RS21910	Protein Homology	4686859	4688133	-	family transposase	-3,572	2,30E-27	1,13E-24
GXM18_RS01620	Protein Homology	335398	335850	+	Hsp20/alpha crystallin family protein	-4,032	4,55E-23	1,12E-20
GXM18_RS22325	Protein Homology	4785378	4786508	-	product=ROK family protein	-1,844	0,0000033	1,48E-04
GXM18_RS23075	Protein Homology	4946544	4947788	-	product=MFS transporter	-1,265	0,0000075	2,64E-04
GXM18_RS20975	Protein Homology	4492207	4493187	-	product=AraC family transcriptional regulator	-0,983	0,0000109	3,41E-04
GXM18_RS15400	Protein Homology	3278289	3279821	-	product=helix-turn-helix domain-containing protein	-0,908	0,0000741	0,002
GXM18_RS24080	GeneMarkS-2+	5160768	5160905	+	hypothetical protein	-1,364	0,0003682	0,007
GXM18_RS16325	Protein Homology	3484013	3484215	-	transposase	-1,336	0,0005006	0,009
GXM18_RS23070	Protein Homology	4945641	4946522	-	LysR family transcriptional regulator	-0,924	0,0005529	0,009
GXM18_RS15205	Protein Homology	3220542	3222302	-	product=histidine kinase	-0,818	0,0010777	0,016
GXM18_RS18580	Protein Homology	3936903	3937151	-	hypothetical protein	-1,252	0,0015797	0,022
GXM18_RS05475	Protein Homology	1118129	1118800	-	Crp/Fnr family transcriptional regulator	-1,204	0,0017752	0,023
GXM18_RS00465	Protein Homology	97687	99354	+	nucleoside kinase	-2,015	0,0019531	0,024
GXM18_RS22265	Protein Homology	4771069	4771992	+	DUF1848 domain-containing protein	-0,764	0,0020821	0,025
GXM18_RS13380	Protein Homology	2782238	2782822	+	thiamine phosphate synthase	-0,652	0,0035253	0,039

Table 16: Transcripts with positive fold change corresponding to MA-Plot of *B. producta* comparing pH 6 vs. pH7. The table shows the upregulated genes when grown in pH 7. The cut-off was made for padjust of <0.05. The log2FoldChange represents the log2 fold change between the groups. For the Pvalue the Wald test/Wald statistic was used. For padj represents the Benjamini-Hochberg adjusted p-value. The sequence name is „NZ_CP048626.1“.

Gene Name/ Locus Tag	Source	Start	End	Strand	Potential attribute, product or function	Log2 FoldChange	pvalue	padj
GXM18_RS12850	Protein Homology	2668258	2669418	+	DNA-processing protein DprA	1,198	4,36E-06	0,00018
GXM18_RS13970	Protein Homology	2944566	2945969	-	glycoside-pentoside-hexuronide (GPH):cation symporter	1,412	4,90E-06	0,00019
GXM18_RS00015	Protein Homology	800	1102	+	cysteine-rich small domain-containing protein	1,229	0,00001	0,00034
GXM18_RS17555	Protein Homology	3775481	3776617	-	tyrosine-type recombinase/integrase	0,894	0,00003	0,00082
GXM18_RS24060	Protein Homology	5159048	5159245	+	helix-turn-helix transcriptional regulator	1,069	0,00005	0,00150
GXM18_RS08115	Protein Homology	1682017	1682187	-	helix-turn-helix transcriptional regulator	1,047	0,00006	0,00158
GXM18_RS17875	Protein Homology	3813894	3814073	+	hypothetical protein	1,344	0,00007	0,00171
GXM18_RS05325	Protein Homology	1087787	1088683	+	LysR family transcriptional regulator	1,299	0,00013	0,00284
GXM18_RS29125	Protein Homology	5171064	5171219	+	glycosyl hydrolase family 18 protein	1,970	0,00015	0,00322
GXM18_RS27220	GeneMarkS-2+	5874580	5874912	-	hypothetical protein	1,153	0,00025	0,00505
GXM18_RS16195	Protein Homology	3454703	3455983	-	carbohydrate metabolic process	1,257	0,00029	0,00563
GXM18_RS18860	Protein Homology	3990485	3991468	-	hypothetical protein	1,667	0,00055	0,00909
GXM18_RS24165	Protein Homology	5170585	5171067	+	class I SAM-dependent methyltransferase	1,930	0,00054	0,00909
GXM18_RS23125	Protein Homology	4959319	4959690	-	sigma factor-like helix-turn-helix DNA-binding protein	0,736	0,00070	0,01109
GXM18_RS12430	Protein Homology	2584654	2585721	+	undecaprenyldiphospho-muramoylpentapeptide beta-N-acetylglucosaminyltransferase	0,446	0,00109	0,01624
GXM18_RS17560	Protein Homology	3776769	3777503	-	DUF5067 domain-containing protein	0,690	0,00131	0,01849
GXM18_RS23800	Protein Homology	5102077	5103351	+	IS110 family transposase	0,873	0,00132	0,01849
GXM18_RS14665	Protein Homology	3132531	3133487	+	alpha/beta fold hydrolase	2,017	0,00168	0,02228
GXM18_RS18870	Protein Homology	3993618	3994121	+	DUF2798 domain-containing protein	1,258	0,00198	0,02440
GXM18_RS12445	Protein Homology	2586870	2587595	+	HAMP domain-containing sensor histidine kinase	0,566	0,00212	0,02479
GXM18_RS17030	Protein Homology	3655867	3657141	-	IS110 family transposase	0,773	0,00259	0,02959
GXM18_RS17590	GeneMarkS-2+	3780730	3780918	+	hypothetical protein	1,250	0,00327	0,03653
GXM18_RS08680	Protein Homology	1807360	1808225	+	IS3 family transposase	1,850	0,00376	0,04023

Inositol Genes in *B. producta* and *B. thetaiotaomicron*

Table 17: Excerpt of transcriptome table of *B. producta* pH 6 vs. pH 7 regarding genes found connected to inositol

Sequence name	Start	End	Strand	Potential Attributes	log2FoldChange	pvalue	padj
NZ_CP048626.1	2102541	2103440	-	product=myo-inososose-2 dehydratase	-0.14876671	0.84051956	NA
NZ_CP048626.1	2103499	2104509	-	product=inositol 2-dehydrogenase	0.34362925	0.60010295	NA
NZ_CP048626.1	2108838	2109737	-	product=myo-inososose-2 dehydratase	0.0486777	0.93187192	NA
NZ_CP048626.1	2120528	2122459	-	go_process=inositol catabolic processproduct=3D-trihydroxycyclohexane-dione acylhydrolase (decyclizing)	0.02524461	0.97317396	NA
NZ_CP048626.1	2122592	2123626	-	go_process=inositol catabolic process, product=5-dehydro-2-deoxygluconokinase	0.49219398	0.46675252	NA
NZ_CP048626.1	4742088	4743104	+	product=inositol 2-dehydrogenase	0.42127268	0.5280025	NA
NZ_CP048626.1	5337036	5337932	+	product=myo-inososose-2 dehydratase	0.0486777	0.93187192	NA

Table 18: Excerpt of transcriptome table of *B. thetaiotaomicron* pH 6 vs. pH 7 regarding genes found connected to inositol

Sequence name	Start	End	Strand	Potential Attributes	log2FoldChange	pvalue	padj
NC_004663.1	925432	926601	+	product=phosphatidylinositol-4-phosphate 5-kinase	0.88838363	0.30588924	NA
NC_004663.1	1880007	1881296	-	product=inositol-3-phosphate synthase	-1.69964825	0.02222954	0.07040284
NC_004663.1	3476031	3476834	-	product=inositol monophosphatase family protein	-1.87900941	0.01525405	0.05282344

Arte Assay FACS Analysis

Table 19: Sample stimulation for ARTE Assay at P. Bacher Lab , CAU/UKSH Kiel. All strains labelled with "SHxxxx" are *E. coli* strains from the routine diagnostic from AG Rupp, Department of Infectious Diseases and Microbiology, UKSH Lübeck. Strains labelled with "B. the" represents *B. thetaiotaomicron* grown in either YFCA medium with pH 6 or pH 7. The strains Y22 +Ca, Y22 -Ca and Y11 are *Yersinia* strains from another project. Each lysate was tested once per donor (Donor is identified by Leukocyte Reduction System (LRS) number). Table provided by Theresa Dittmers, AG Bacher, Kiel.

			Cell number CD154+													
Number	**Date**	**Name**	**w/o**	**Y72 +Ca**	**SH0038**	**SH0096**	**SH0103**	**B.the pH 7**	**E.coli**	**SH0006**	**Y72 - Ca**	**SH0114**	**SH0123**	**DA554**	**B.the pH 6**	**Y11**
1	20221025	LRS502	35	5312	6542	5402	5649	718		478	5881	3484	2768	3126	144	
2	20221025	LRS575	133	4175	4201	3494	2915	2500		1103	6239	3581	3289	2917	2483	
3	20221104	LRS849	113	9466	5577	6912	6070	3193		4912	12409	6105	6829	9345	3906	
4	20221104	LRS850	63	3380	1404	1249	1670	493		1643	5399	2566	2836	3597	1404	
5	20221108	LRS870	160	1439	1137	473	459	511		622	2592	1082	646	1011	575	
6	20221108	LRS872	200	5254	4792	4389	3901	1356		3020	6673	4728	4427	4934	1097	
7	20221122	LRS942*	54	1771	1676	1572	1638			1600	2134	1674	1737	1116		5160
8	20221129	LRS974*	41	689	1012	808	1146			812	743	938	1165	522		3011
9	20221129	LRS980*	149	4899	3292	4042	5864			2423	9060	4941	2332	5585		9337
10	20221209	LRS2055	94	1542	1119	1054	1292		2301	735	2360	1206	970	1599		2719
11	20221213	LRS2074	136	3664	2760	2407	2699		2943	1662	4490	2758	2709	3281		8003
12	20221213	LRS2077	156	984	1405	1224	1119		524	956	1117	1381	1066	709		2139
13	20221213	LRS2078	384	6103	5842	6002	4330		5227	4455	8064	6345	5528	3683		14223
14	20221213	LRS2079	100	6022	2124	2107	1904		2957	1512	6984	2315	2150	3846		11246

*w/o E.coli lysat

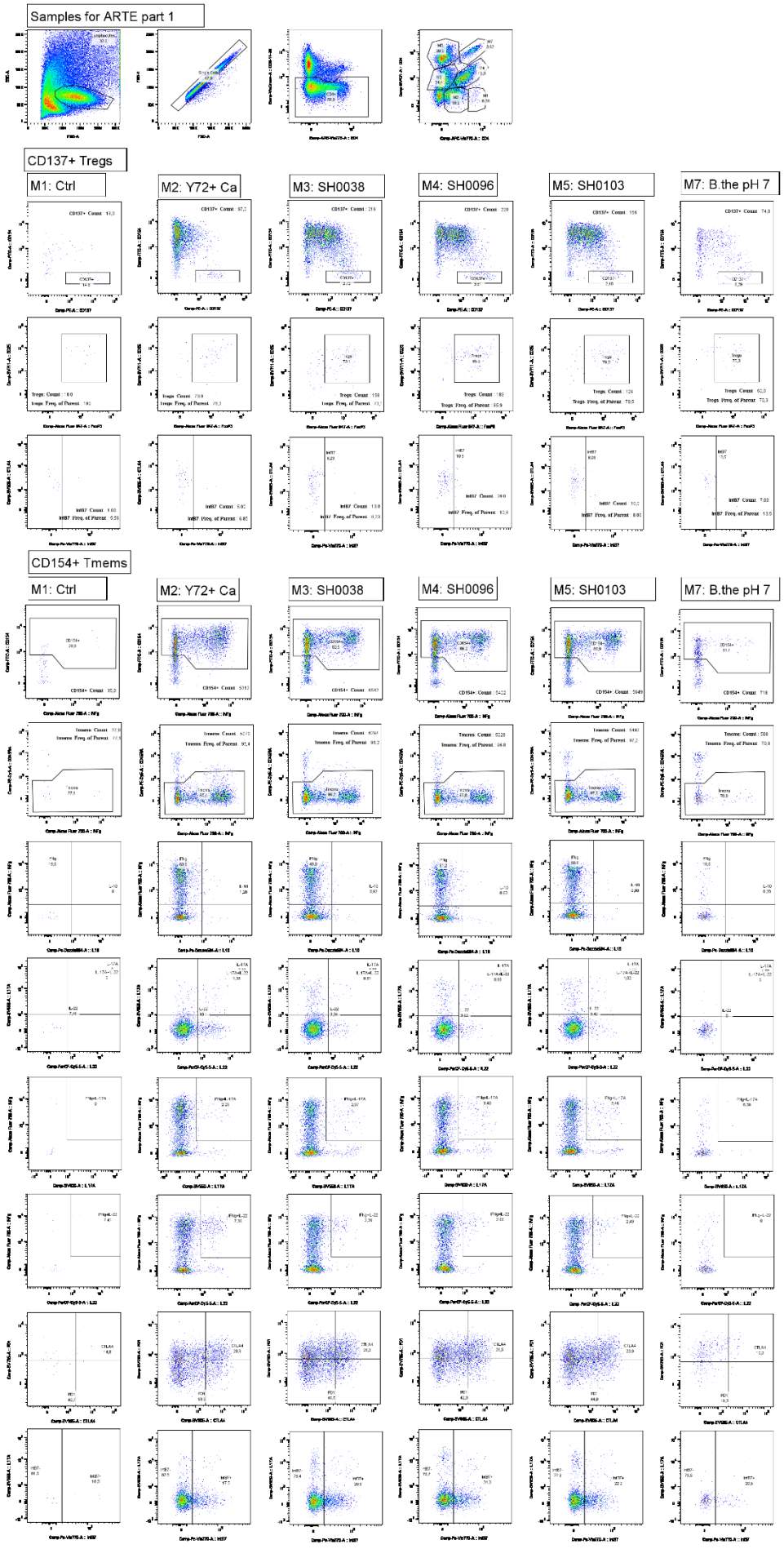

Figure 39: Dot plots ARTE Assay, Leukocyte Reduction System (LRS) Donor number 502 Part 1

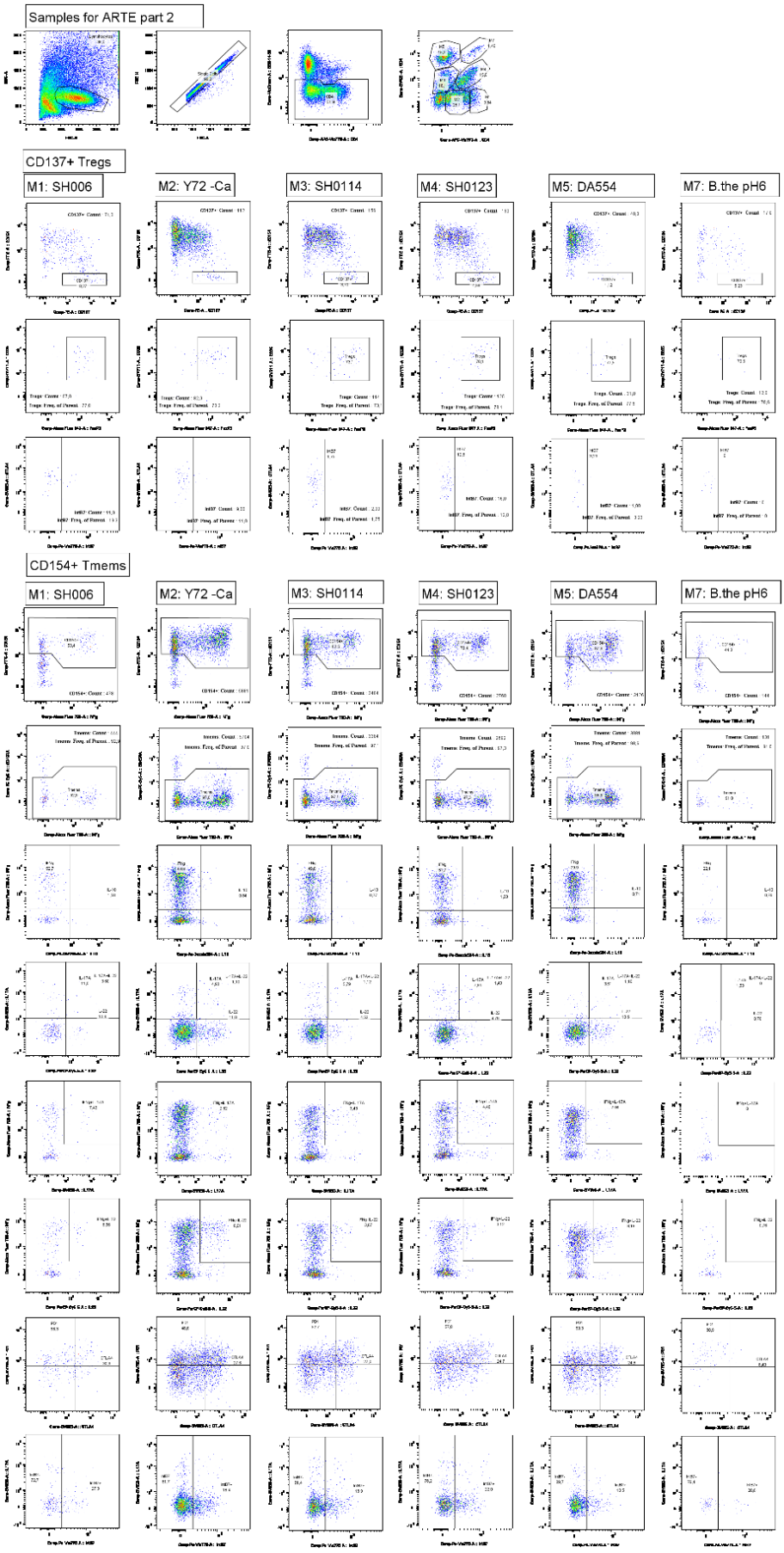

Figure 40: Dot plots ARTE Assay, Leukocyte Reduction System (LRS) Donor number 502 Part 2

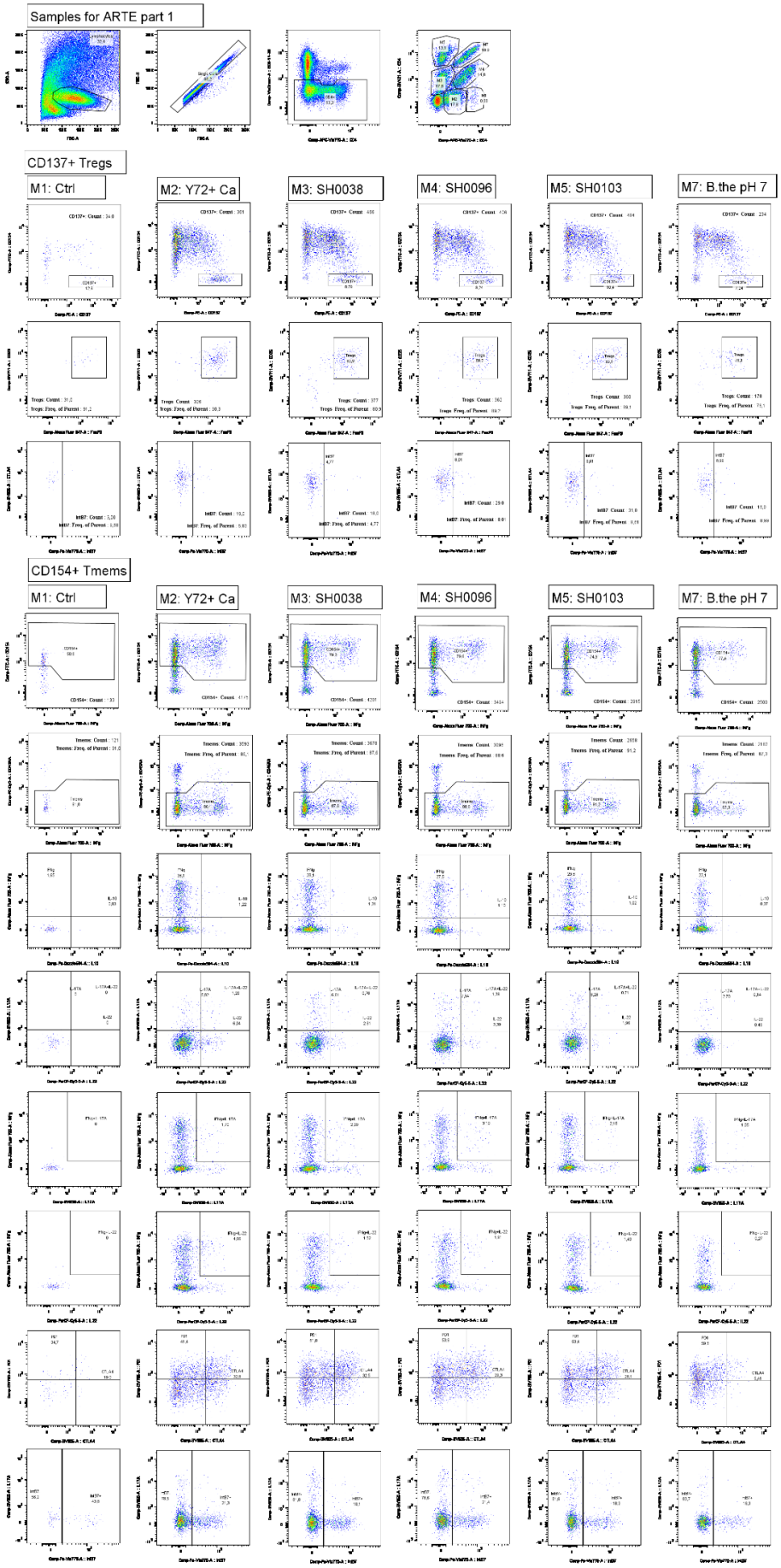

Figure 41: Dot plots ARTE Assay, Leukocyte Reduction System (LRS) Donor number 575 Part 1

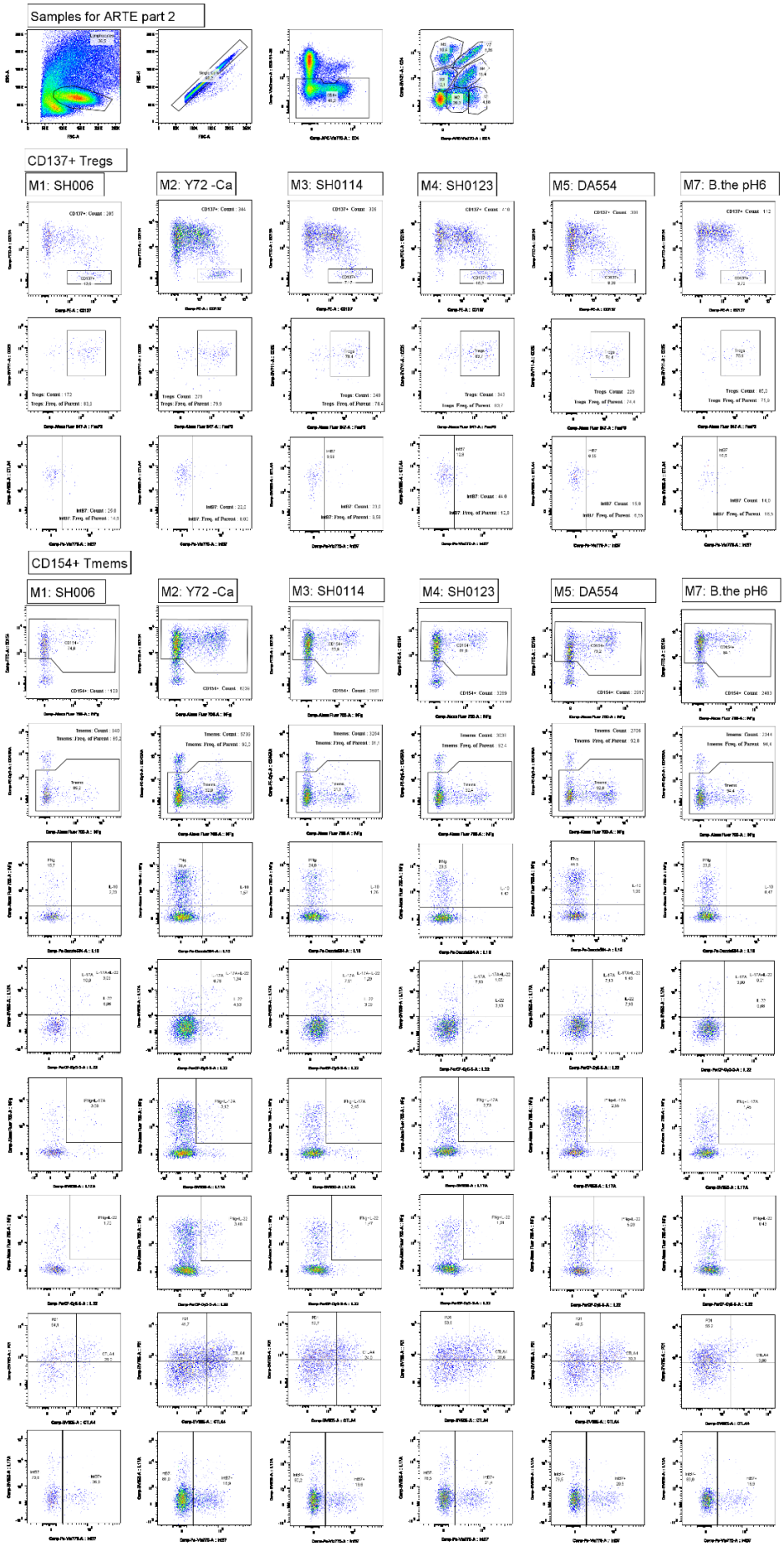

Figure 42: Dot plots ARTE Assay, Leukocyte Reduction System (LRS) Donor number 575 Part 2

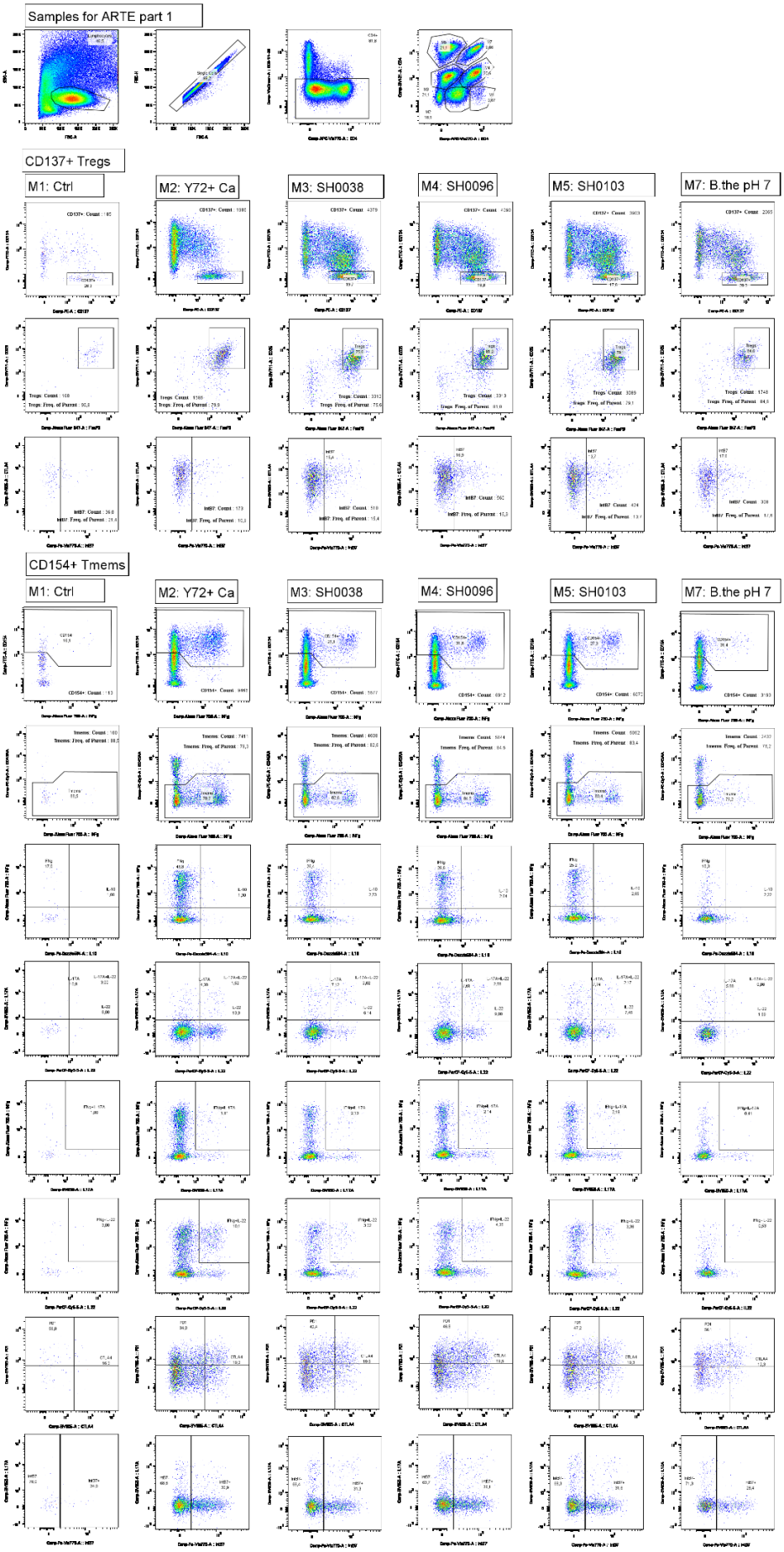

Figure 43: Dot plots ARTE Assay, Leukocyte Reduction System (LRS) Donor number 849 Part 1

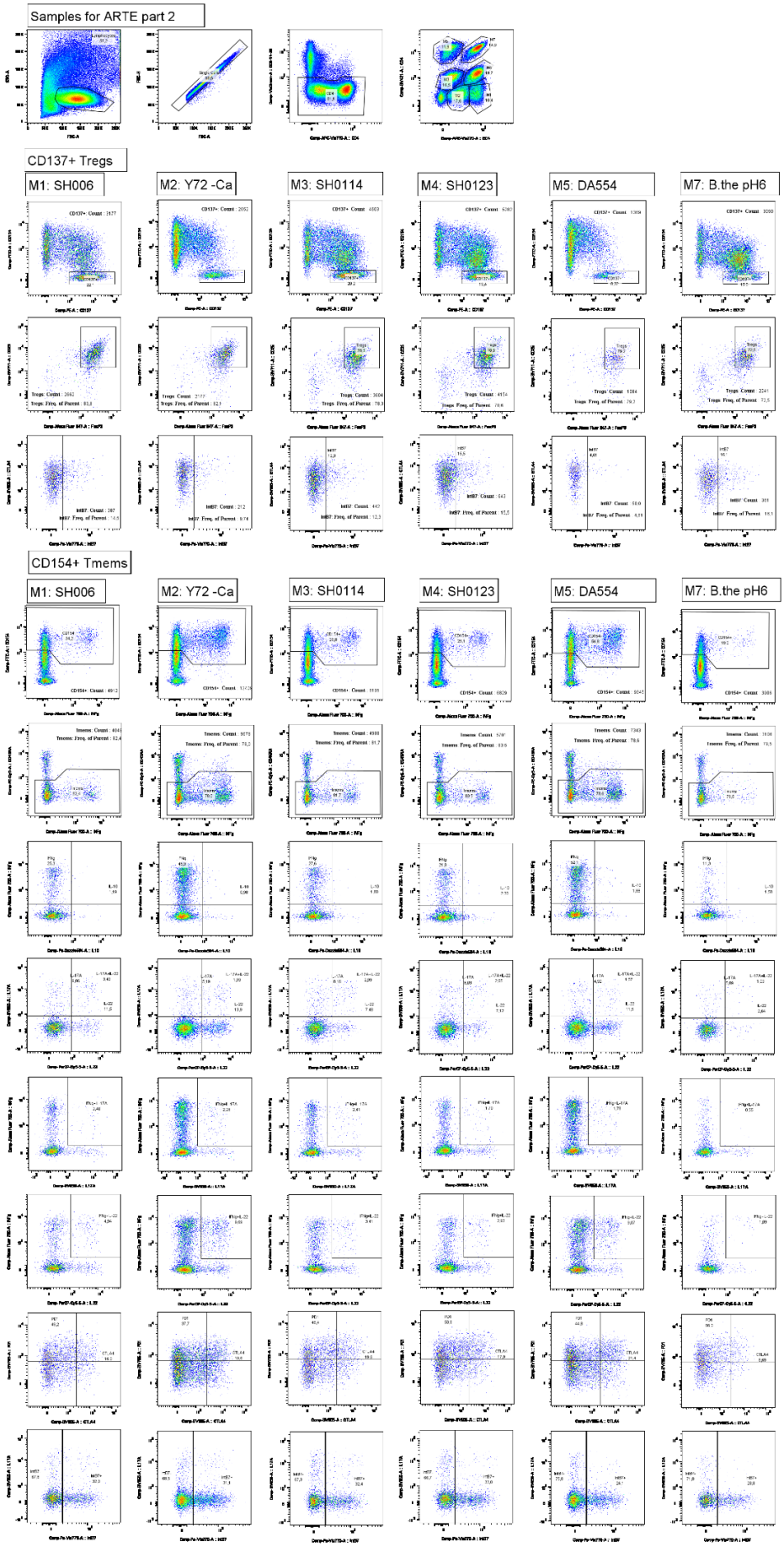

Figure 44: Dot plots ARTE Assay, Leukocyte Reduction System (LRS) Donor number 849 Part 2

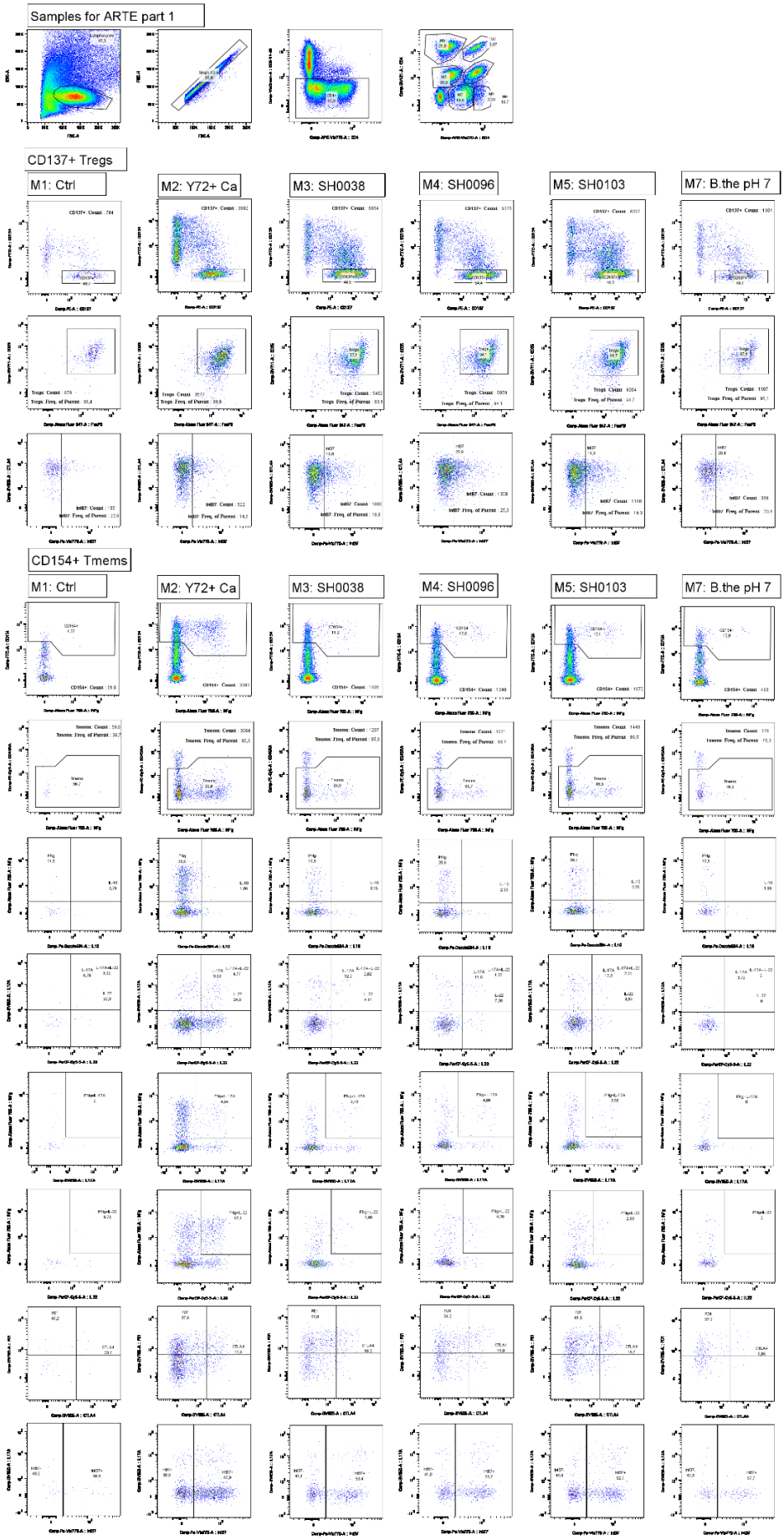

Figure 45: Dot plots ARTE Assay, Leukocyte Reduction System (LRS) Donor number 850 Part 1

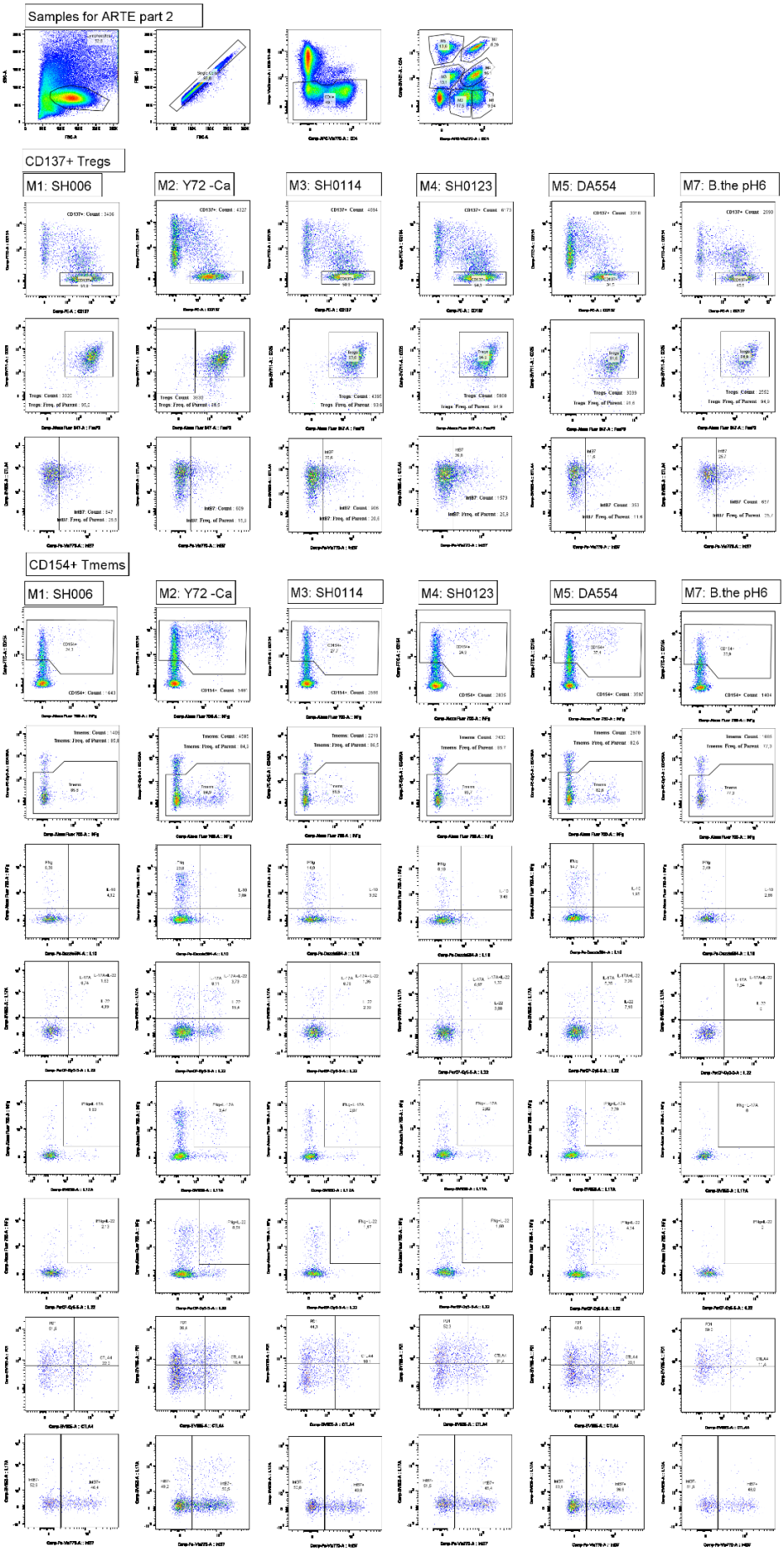

Figure 46: Dot plots ARTE Assay, Leukocyte Reduction System (LRS) Donor number 850 Part 2

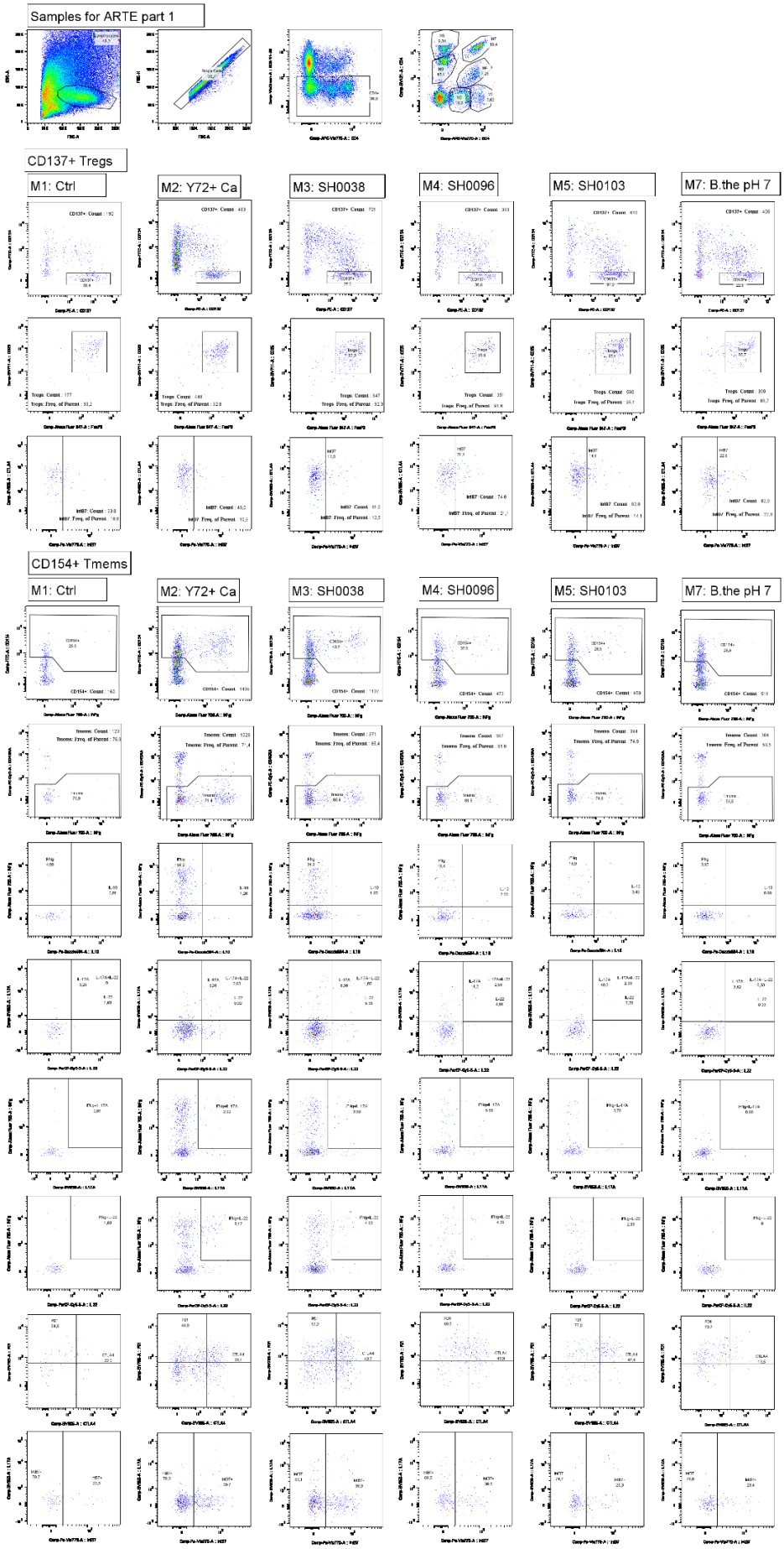

Figure 47: Dot plots ARTE Assay, Leukocyte Reduction System (LRS) Donor number 870 Part 1

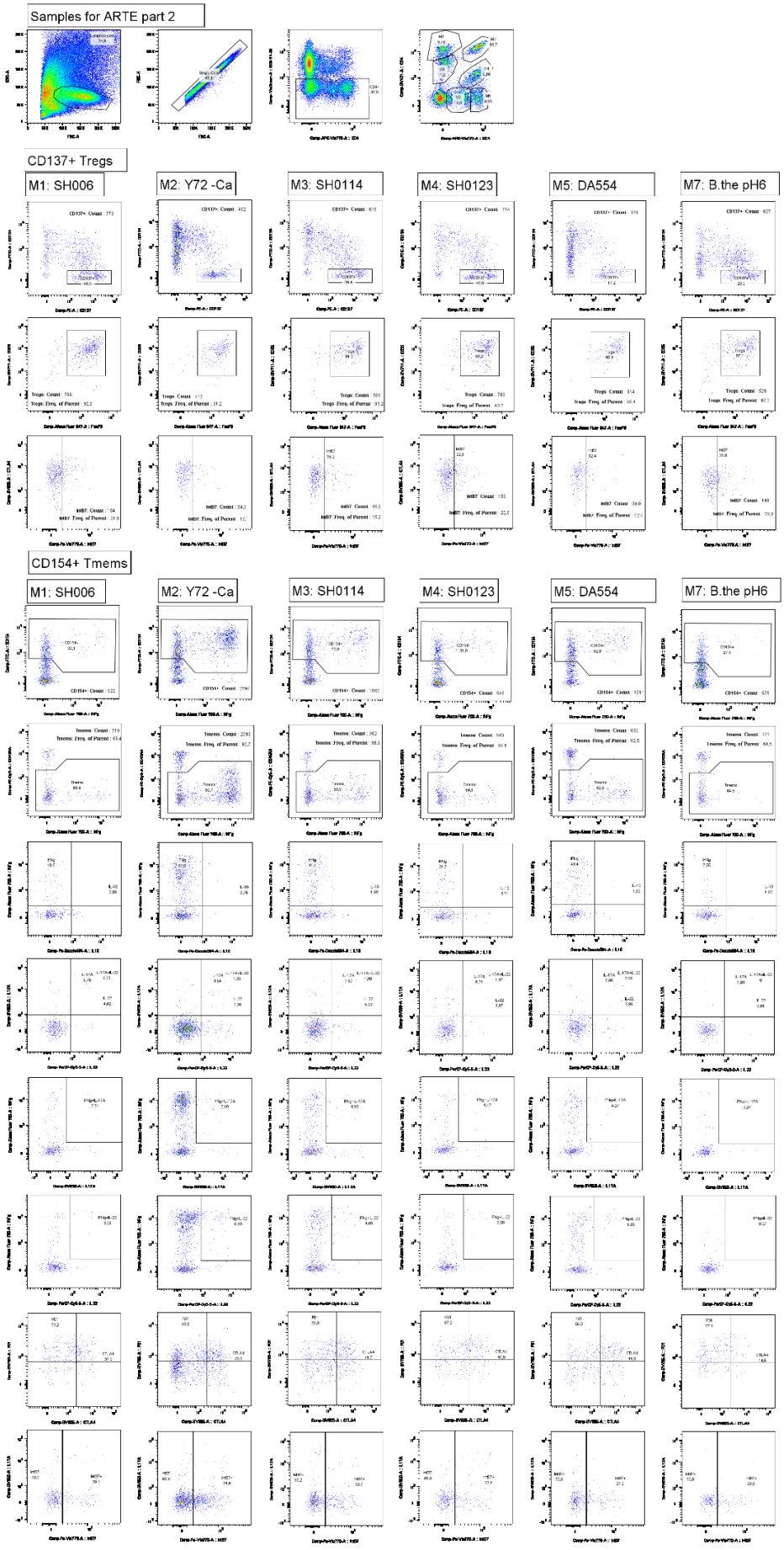

Figure 48: Dot plots ARTE Assay, Leukocyte Reduction System (LRS) Donor number 870 part 2

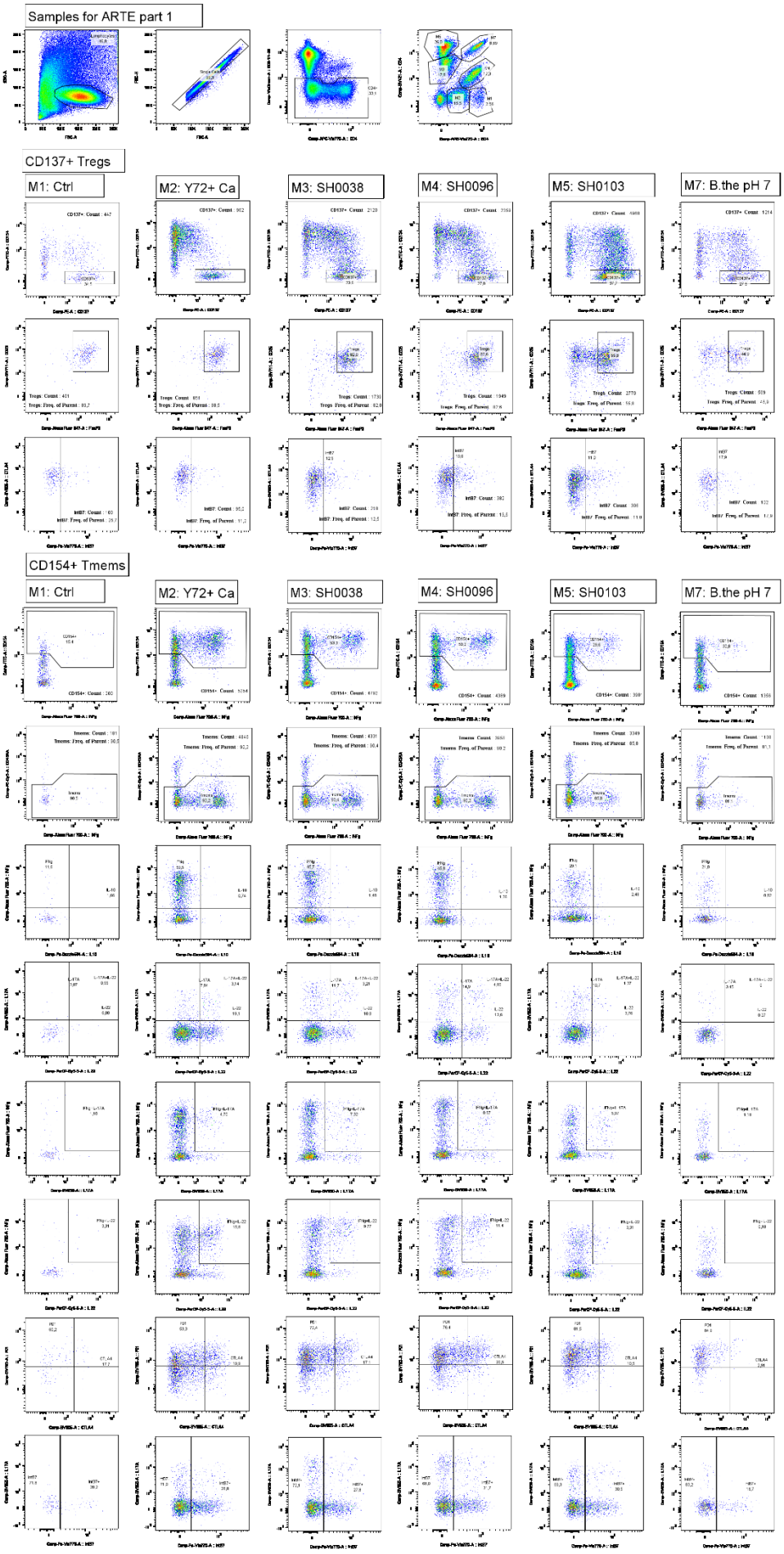

Figure 49: Dot plots ARTE Assay, Leukocyte Reduction System (LRS) Donor number 872 Part 1

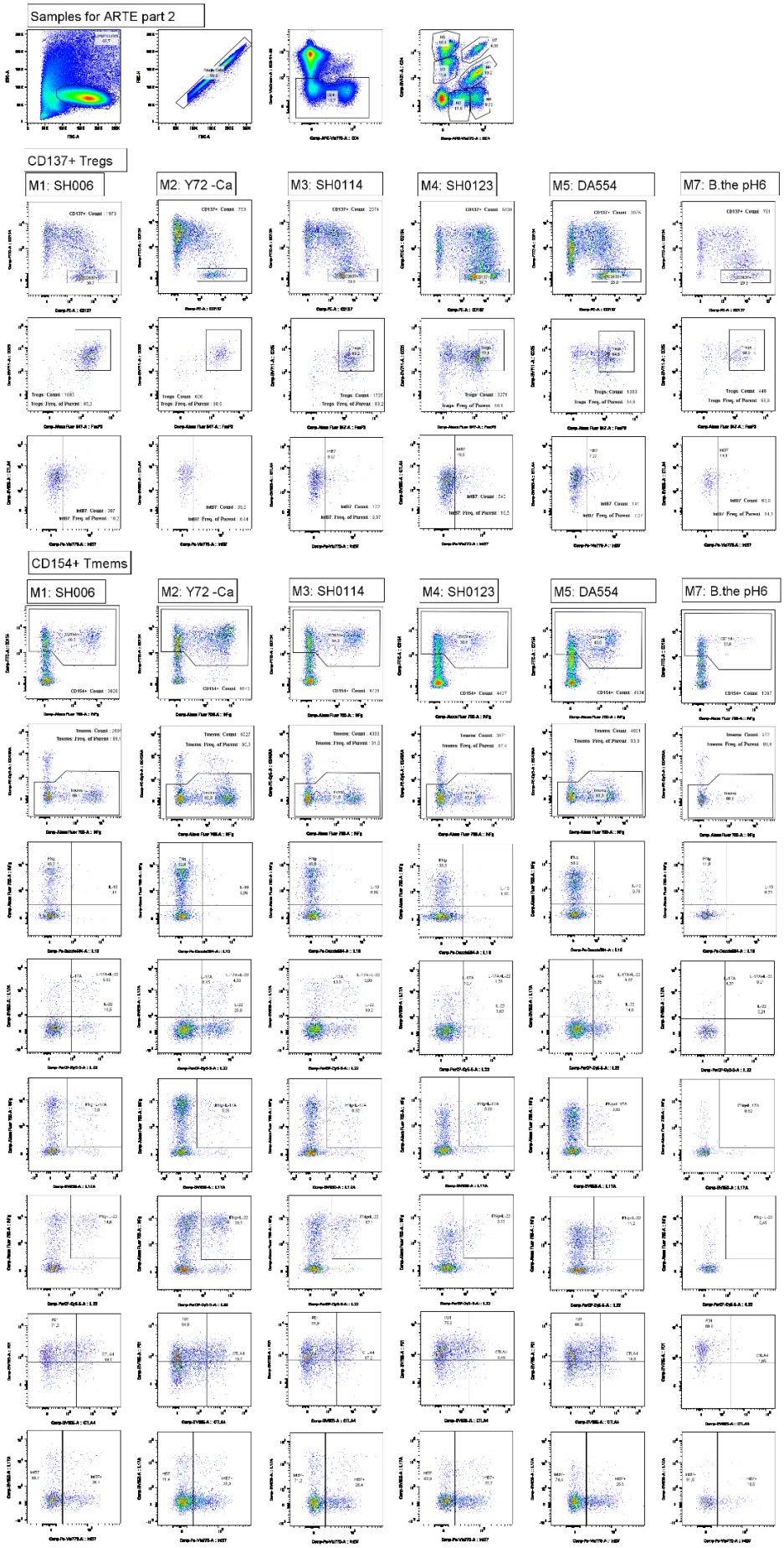

Figure 50: Dot plots ARTE Assay, Leukocyte Reduction System (LRS) Donor number 872 Part2

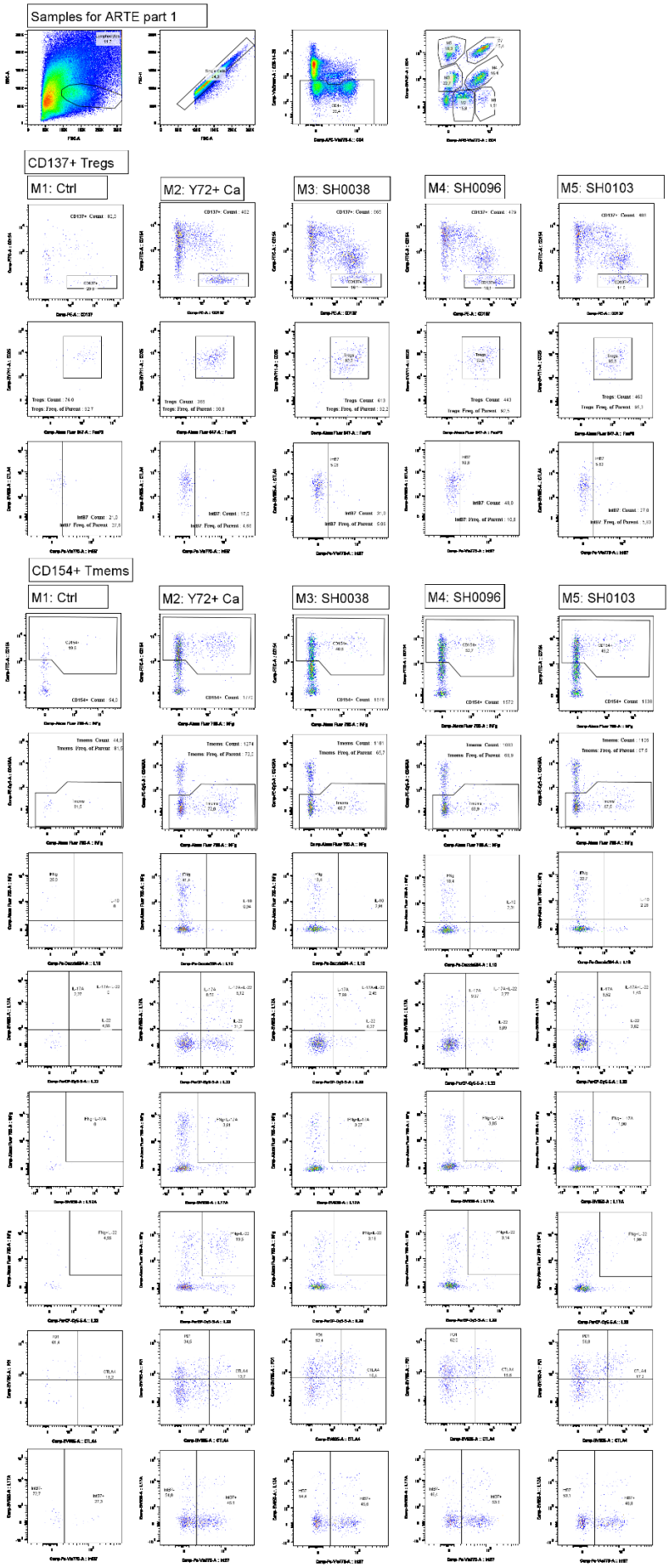

Figure 51: Dot plots ARTE Assay, Leukocyte Reduction System (LRS) Donor number 942 Part 1

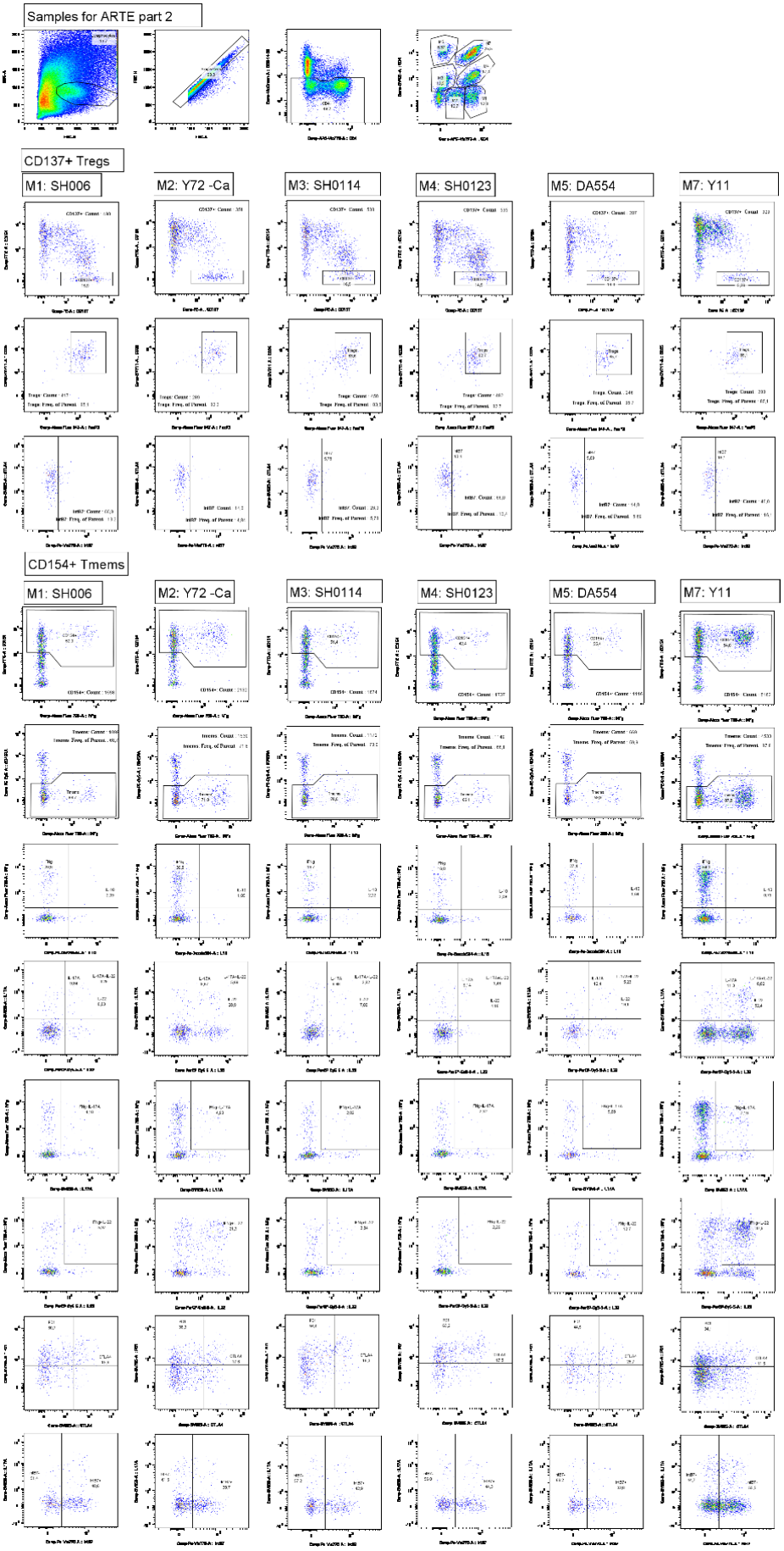

Figure 52: Dot plots ARTE Assay, Leukocyte Reduction System (LRS) Donor number 942 Part 2

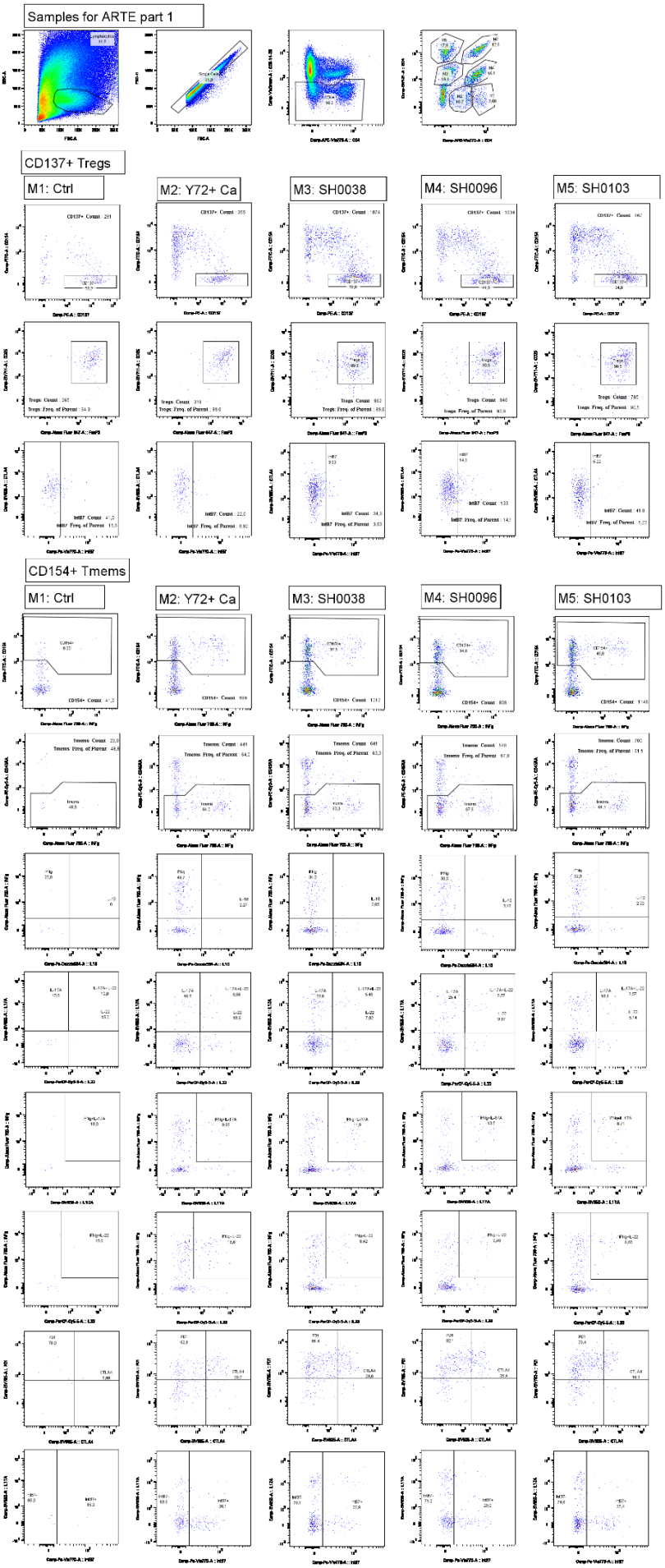

Figure 53: Dot plots ARTE Assay, Leukocyte Reduction System (LRS) Donor number 974 Part 1

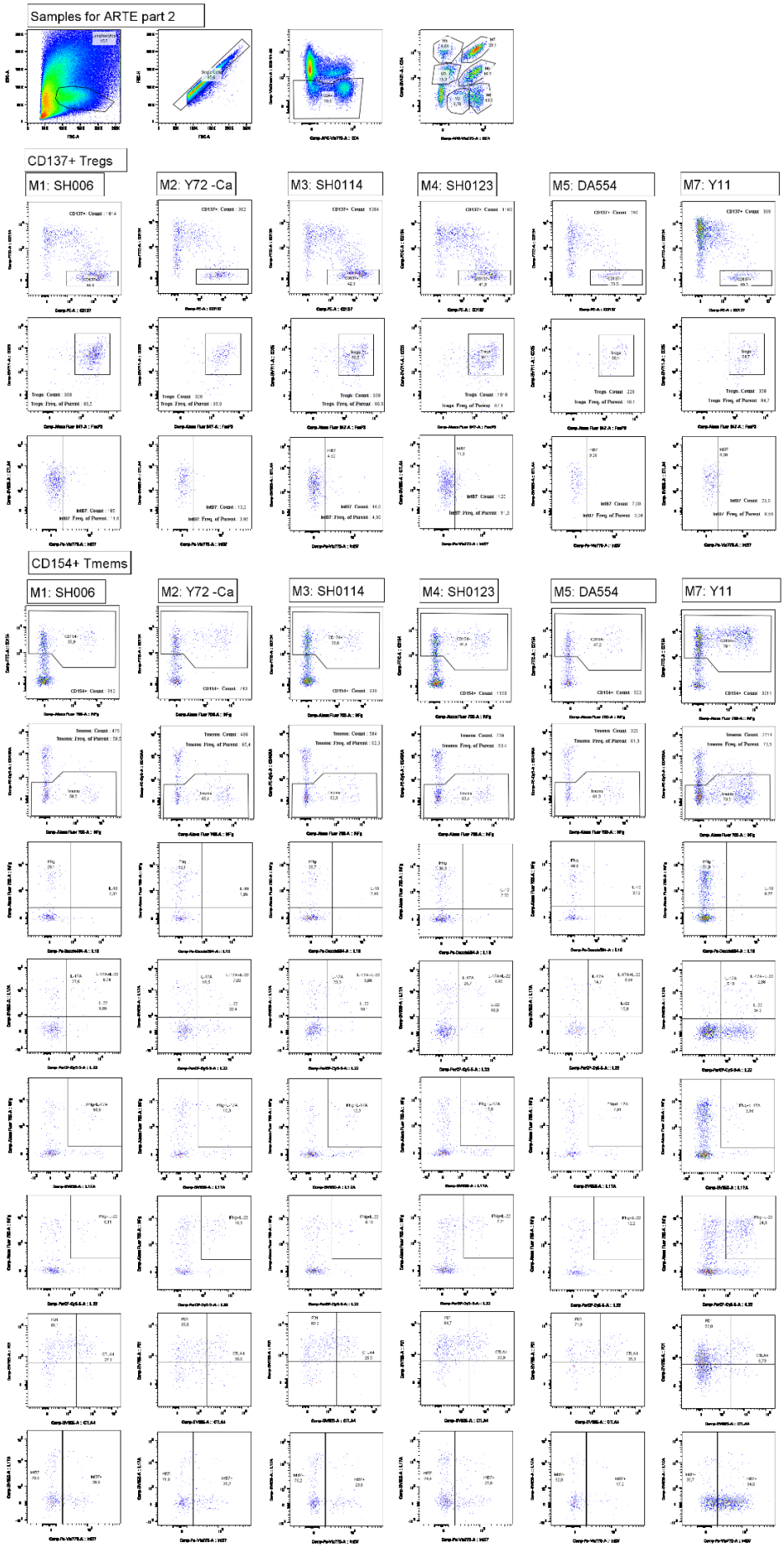

Figure 54: Dot plots ARTE Assay, Leukocyte Reduction System (LRS) Donor number 974 part2

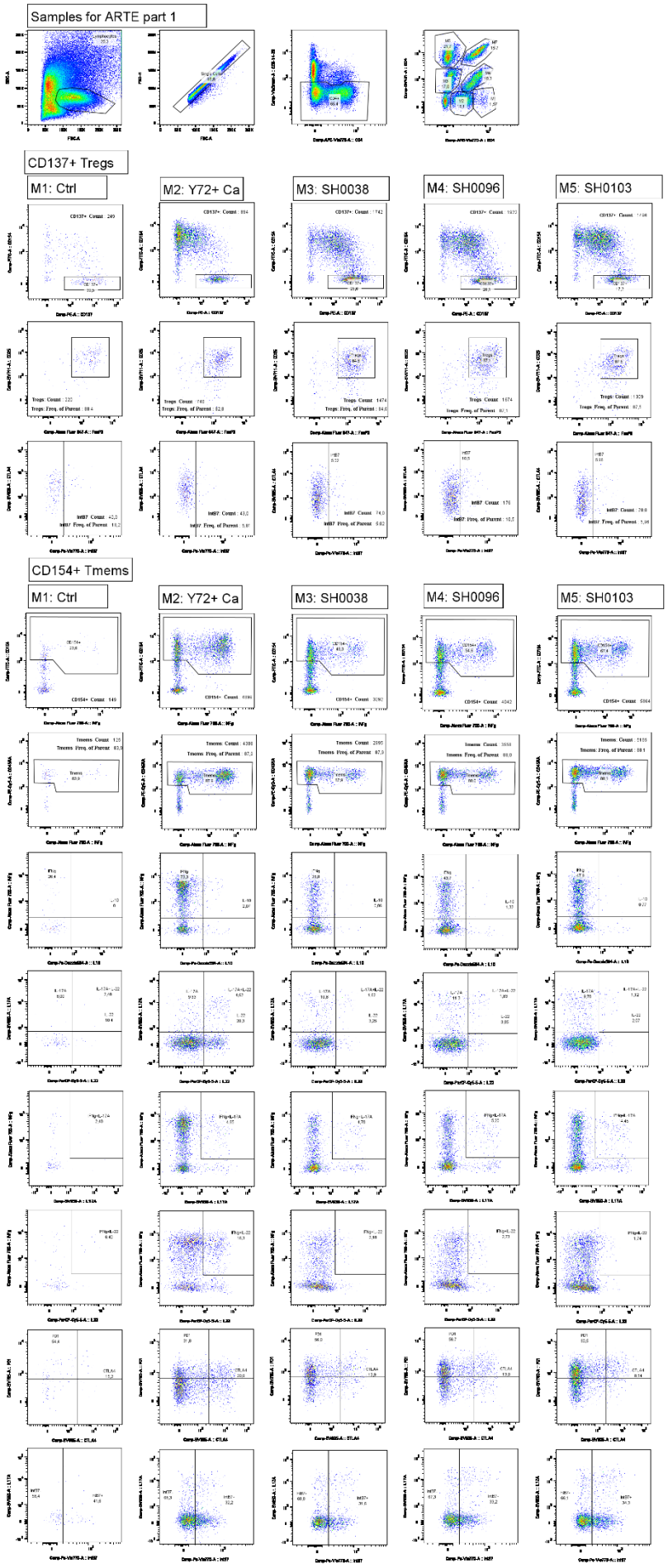

Figure 55: Dot plots ARTE Assay, Leukocyte Reduction System (LRS) Donor number 980 Part 1

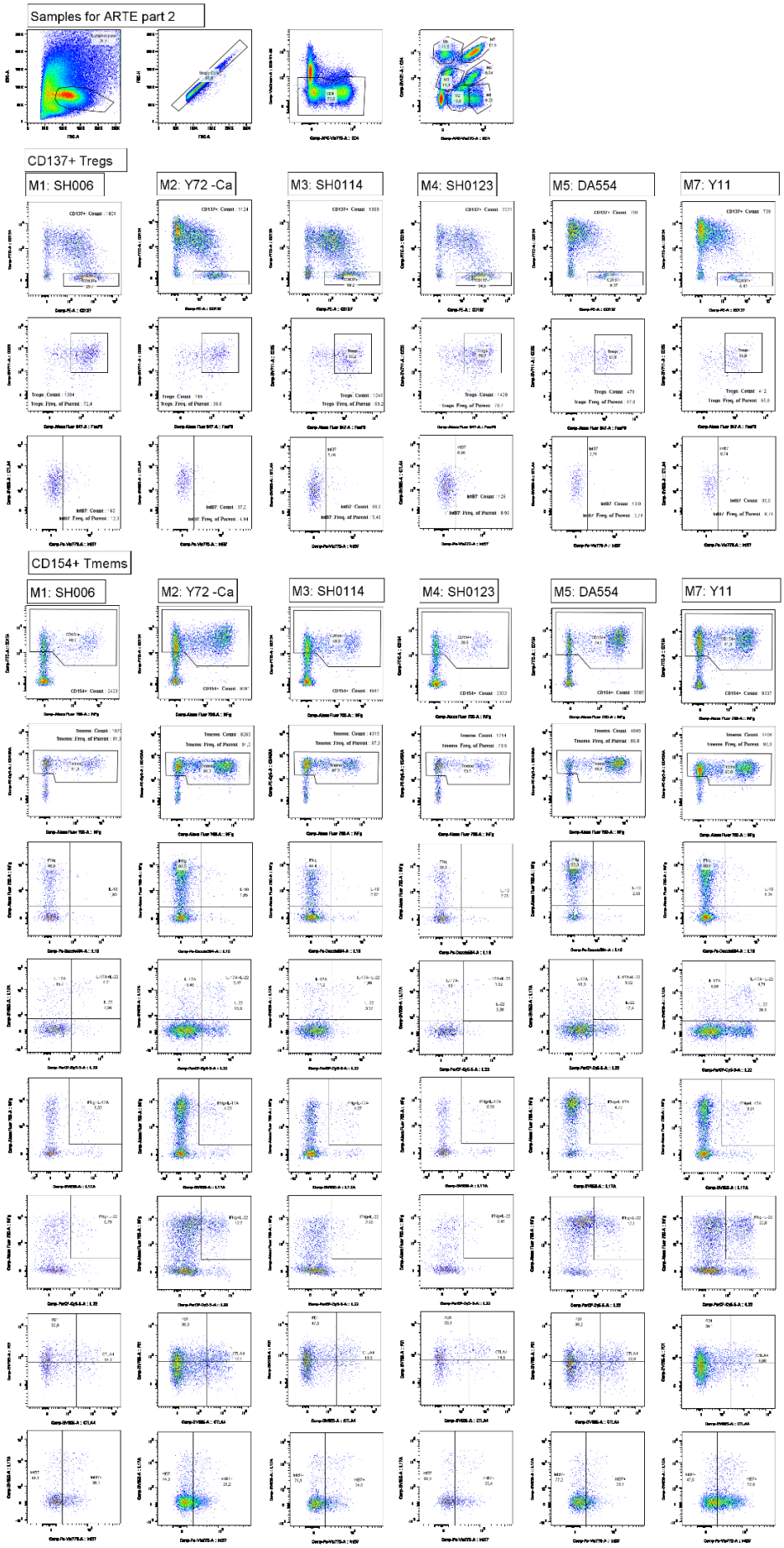

Figure 56: Dot plots ARTE Assay, Leukocyte Reduction System (LRS) Donor number 980 Part 2

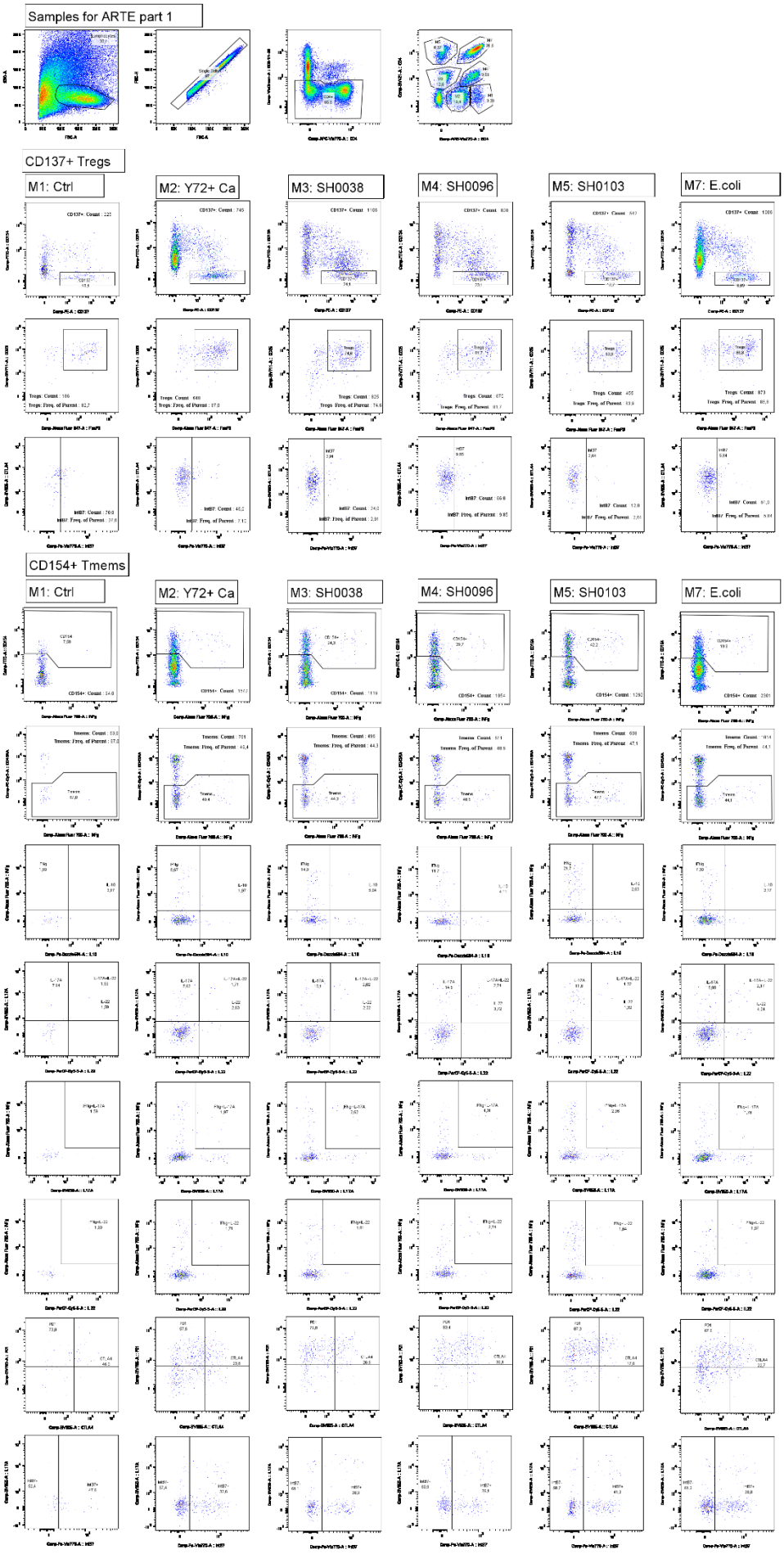

Figure 57: Dot plots ARTE Assay, Leukocyte Reduction System (LRS) Donor number 2055 Part 1

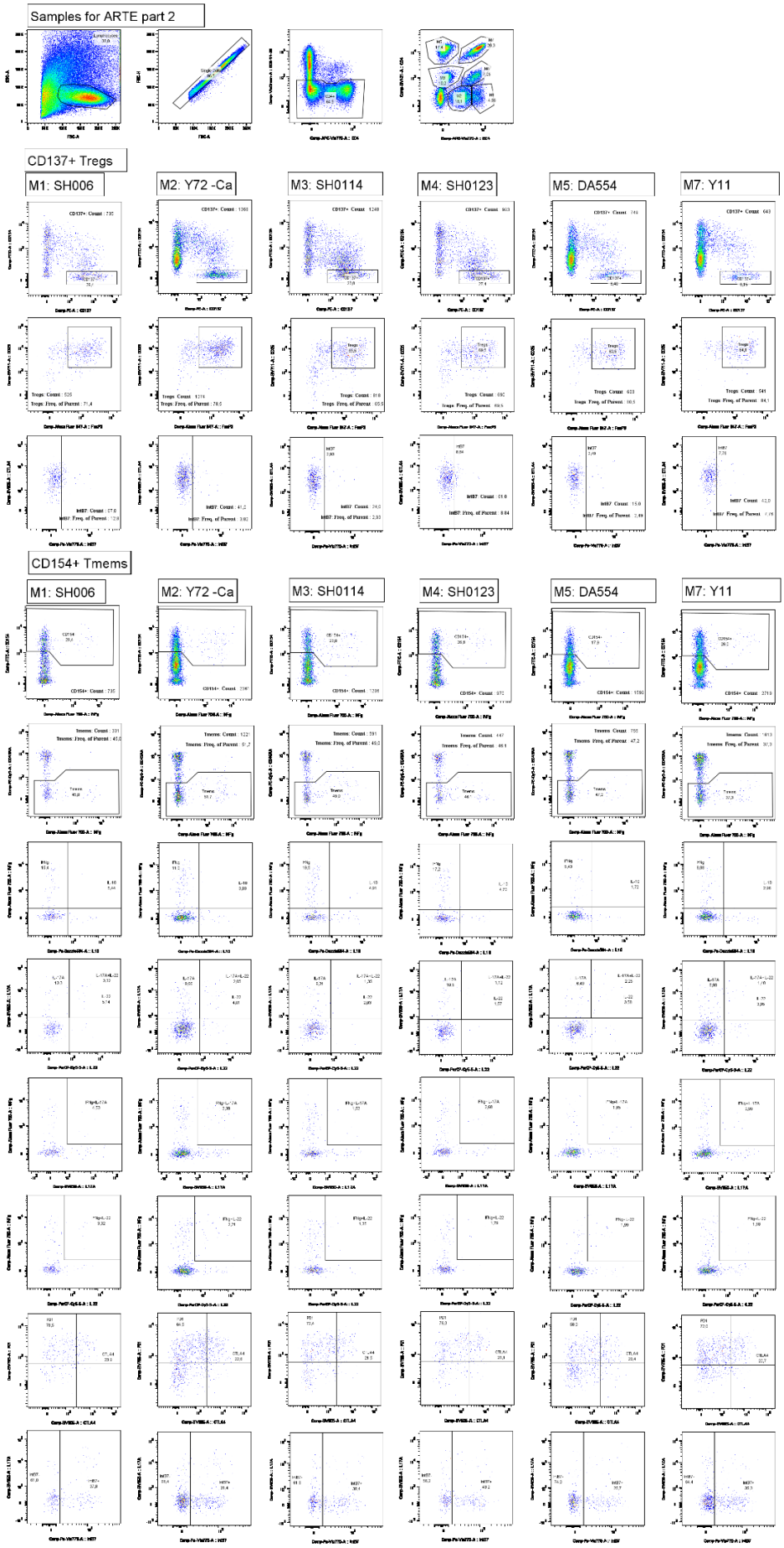

Figure 58: Dot plots ARTE Assay, Leukocyte Reduction System (LRS) Donor number 2055 Part 2

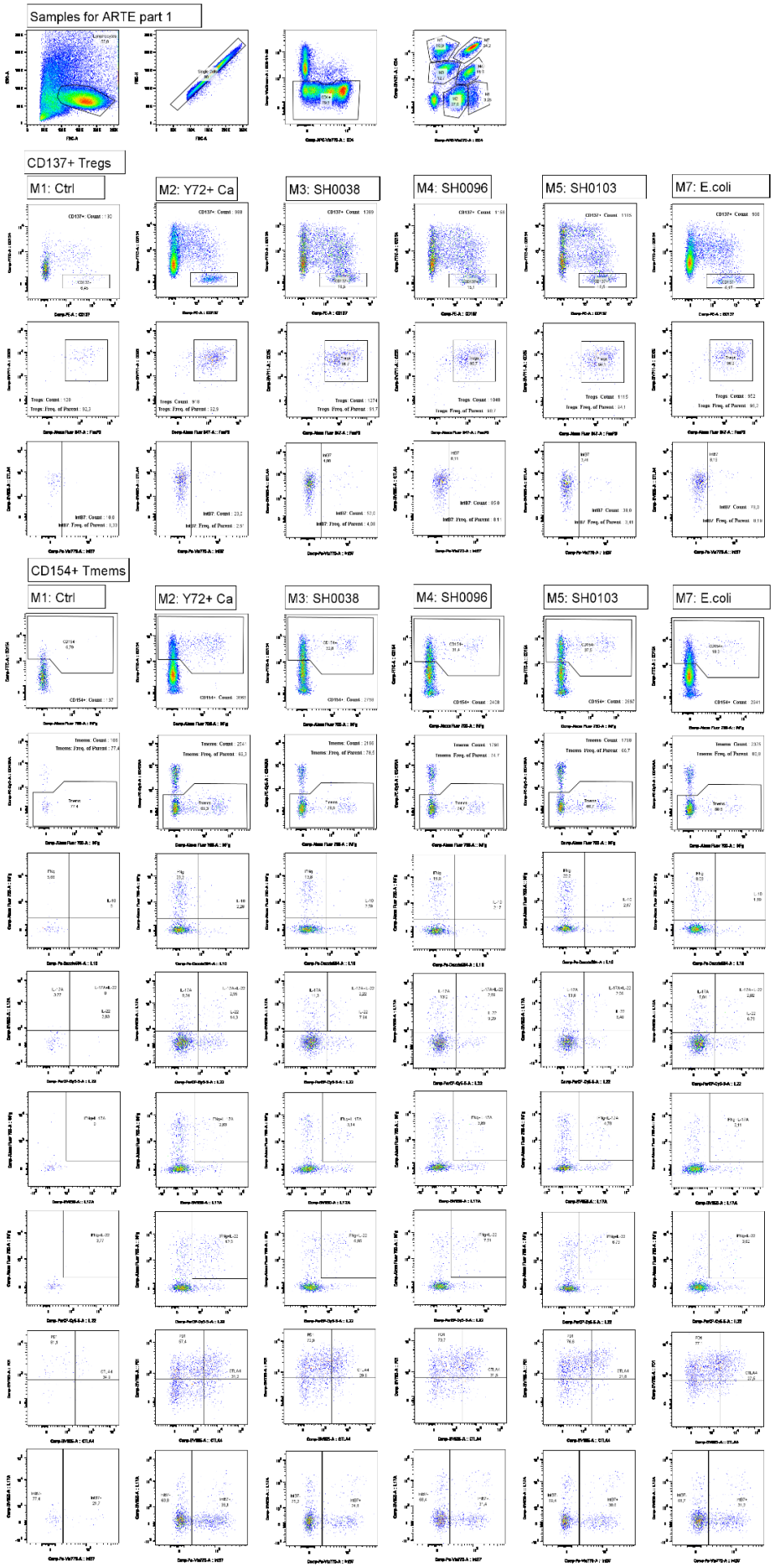

Figure 59: Dot plots ARTE Assay, Leukocyte Reduction System (LRS) Donor number 2074 Part 1

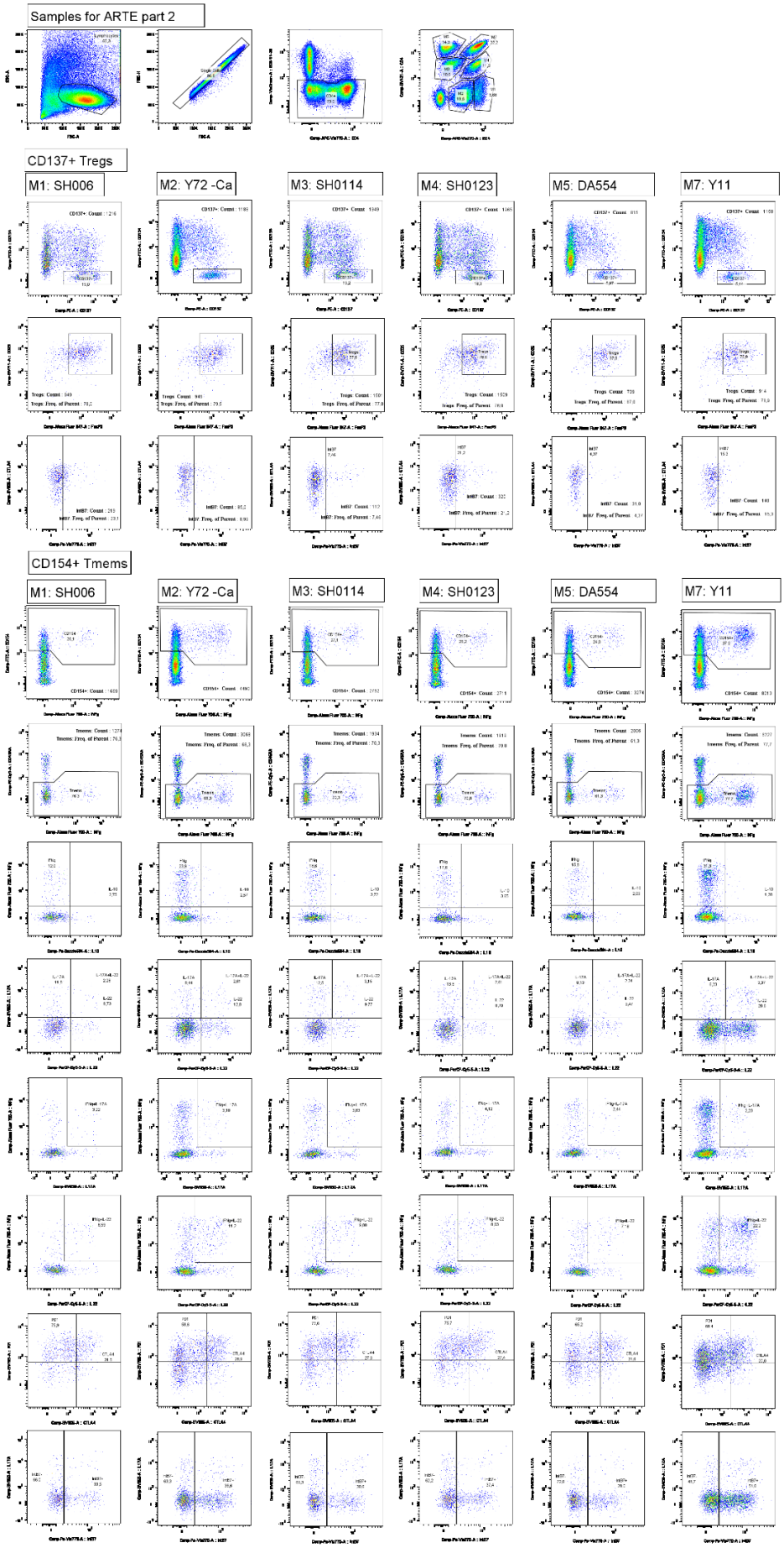

Figure 60: Dot plots ARTE Assay, Leukocyte Reduction System (LRS) Donor number 2074 Part 2

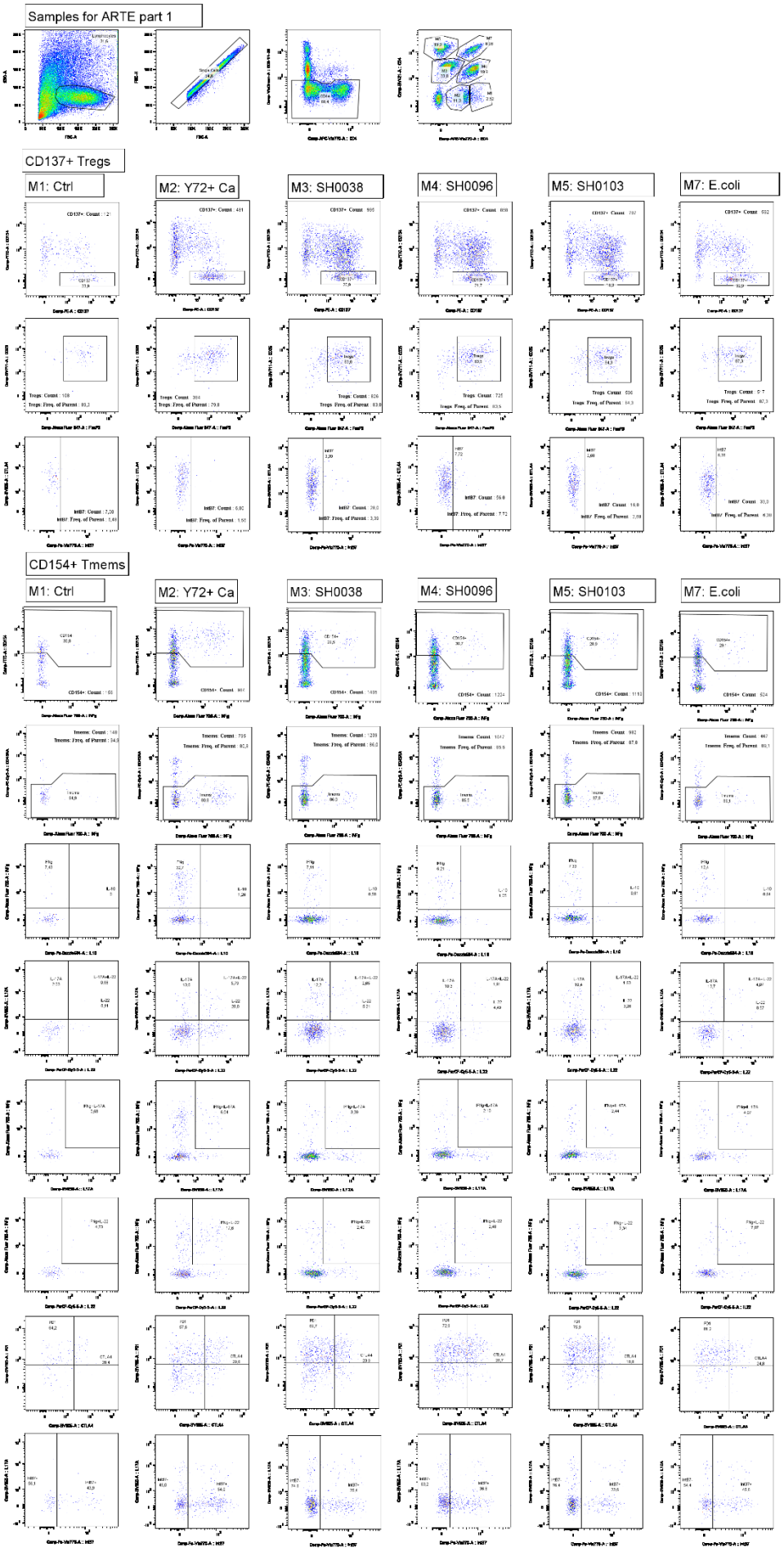

Figure 61: Dot plots ARTE Assay, Leukocyte Reduction System (LRS) Donor number 2077 Part 1

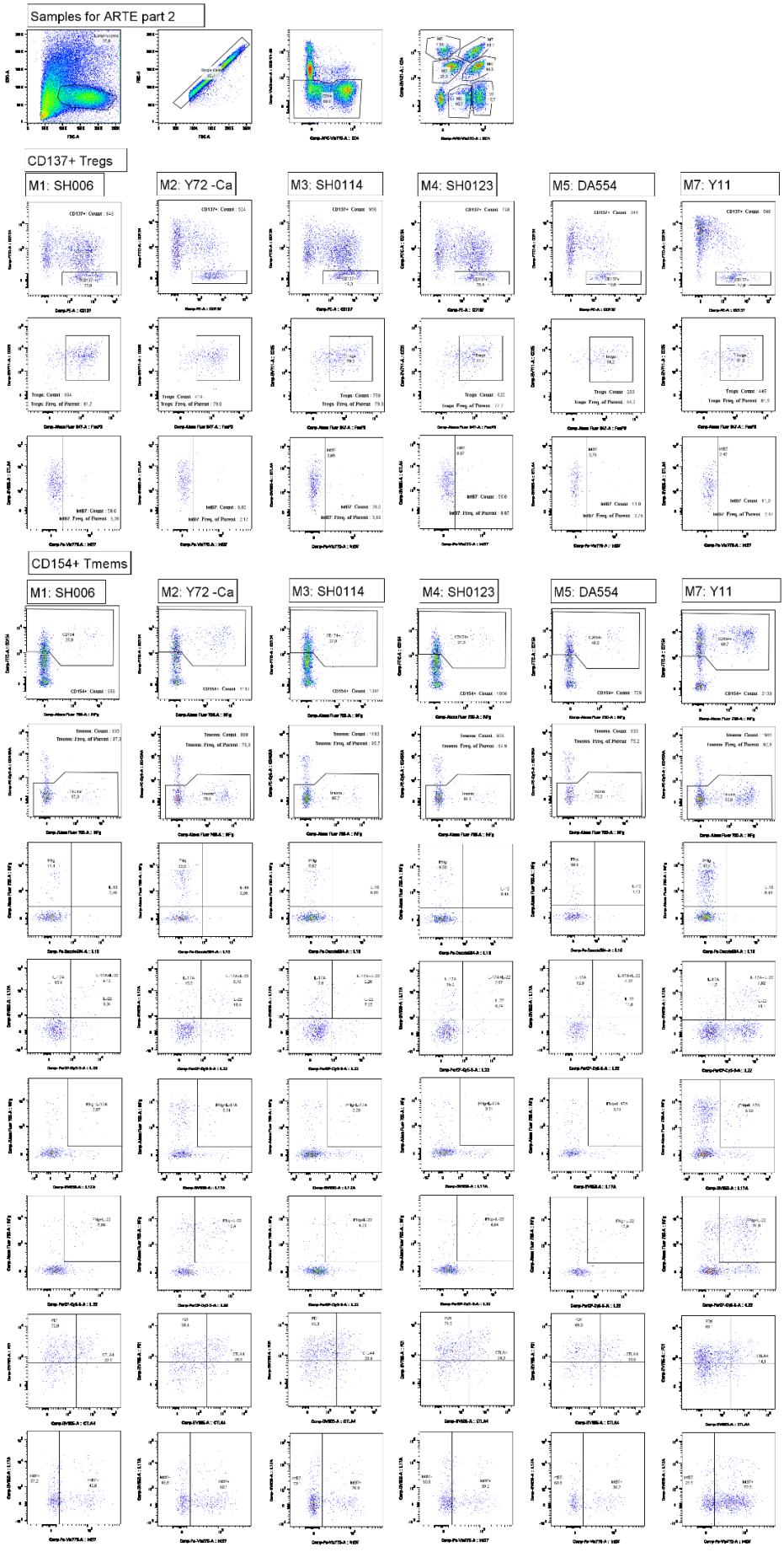

Figure 62: Dot plots ARTE Assay, Leukocyte Reduction System (LRS) Donor number 2077 Part 2

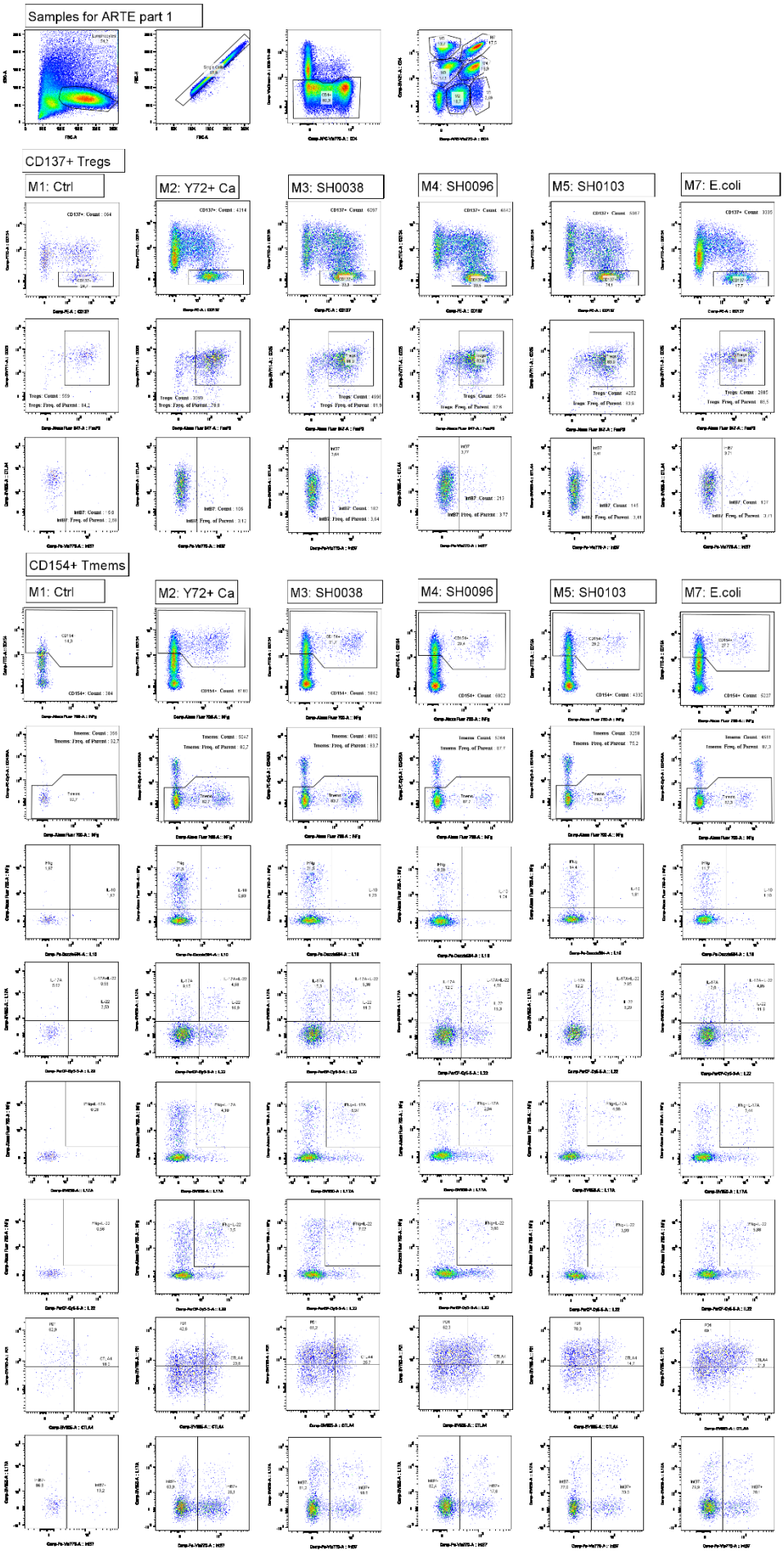

Figure 63: Dot plots ARTE Assay, Leukocyte Reduction System (LRS) Donor number 2078 Part 1

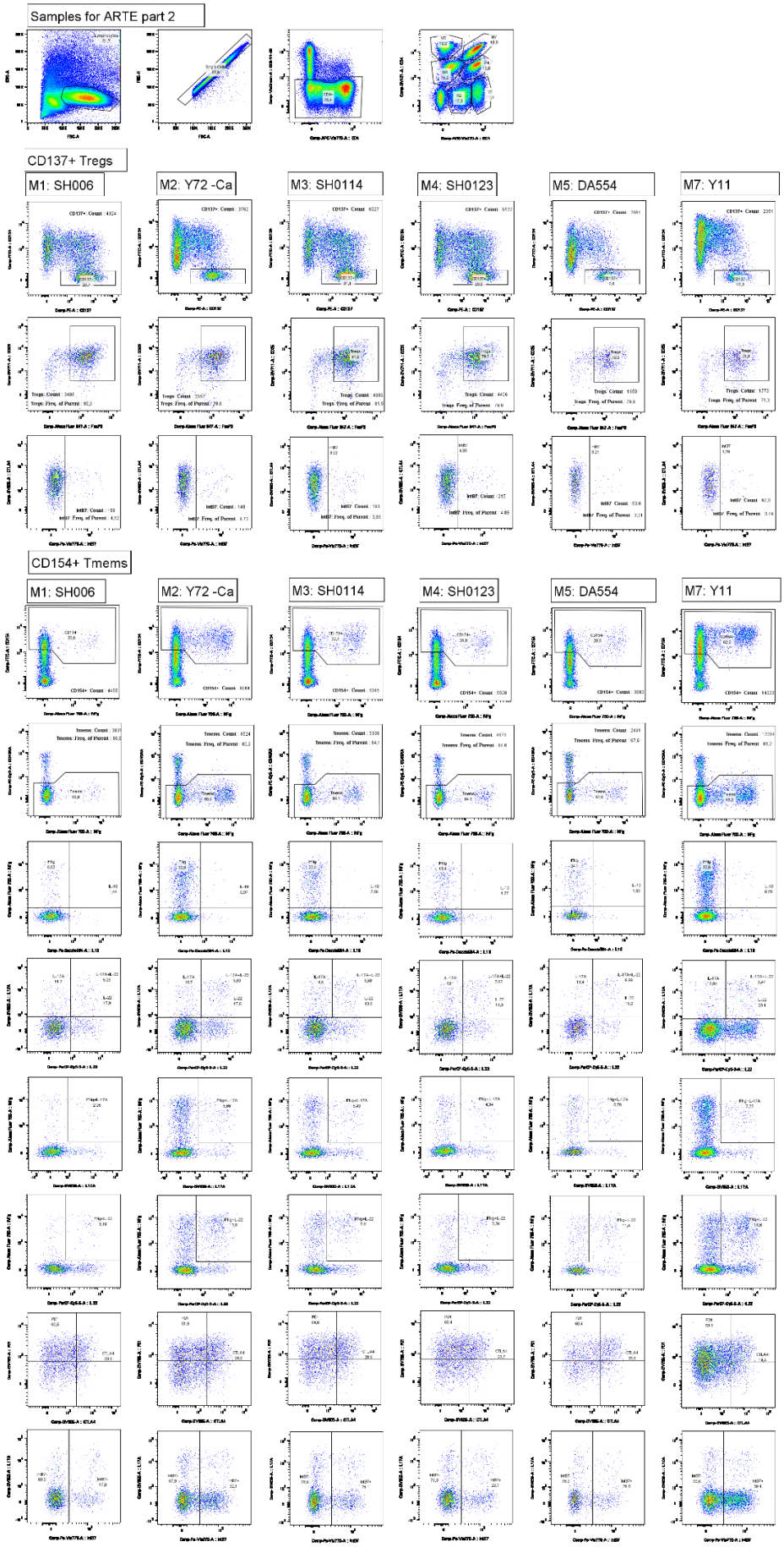

Figure 64: Dot plots ARTE Assay, Leukocyte Reduction System (LRS) Donor number 2078 Part 2

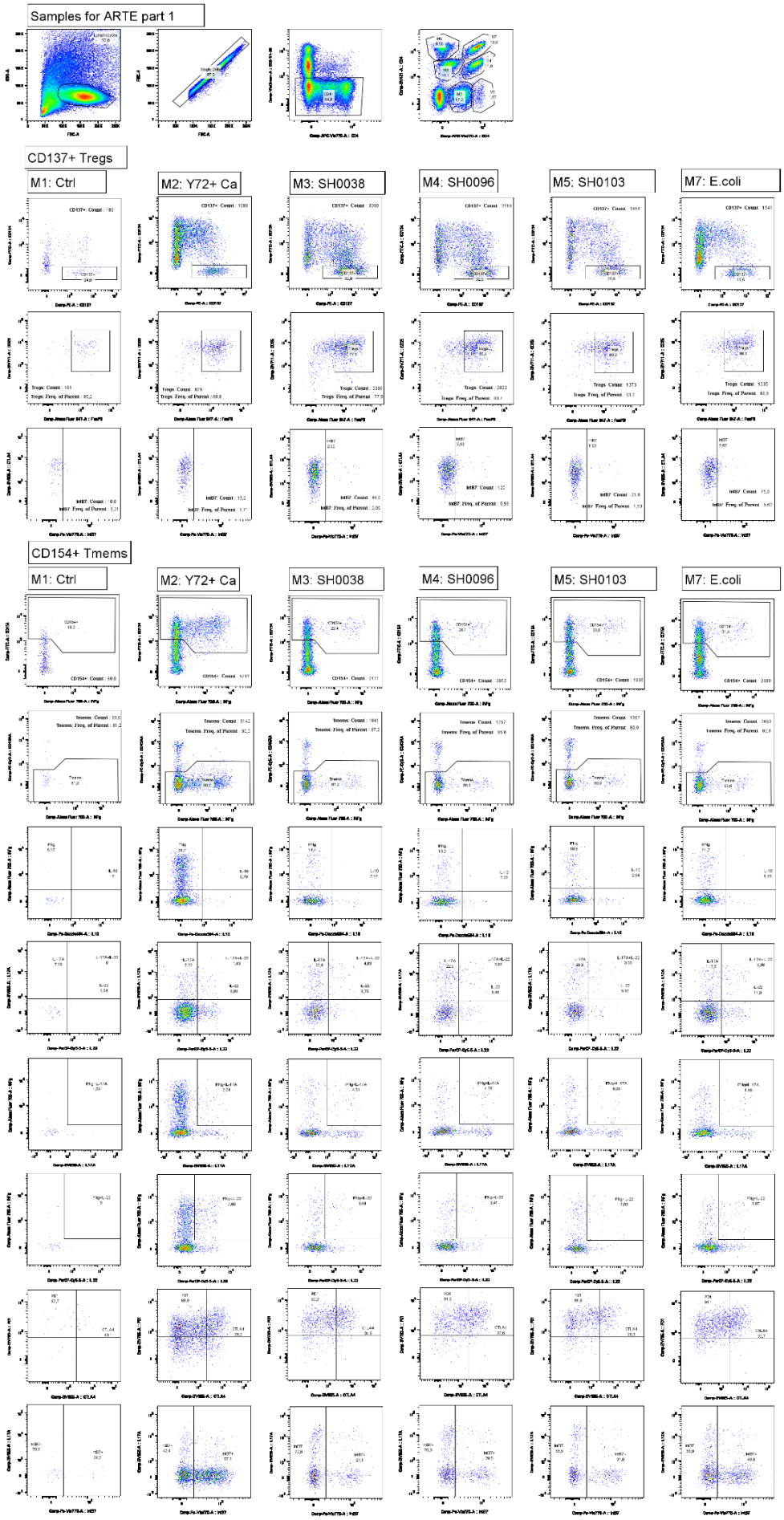

Figure 65: Dot plots ARTE Assay, Leukocyte Reduction System (LRS) Donor number 2079 Part 1

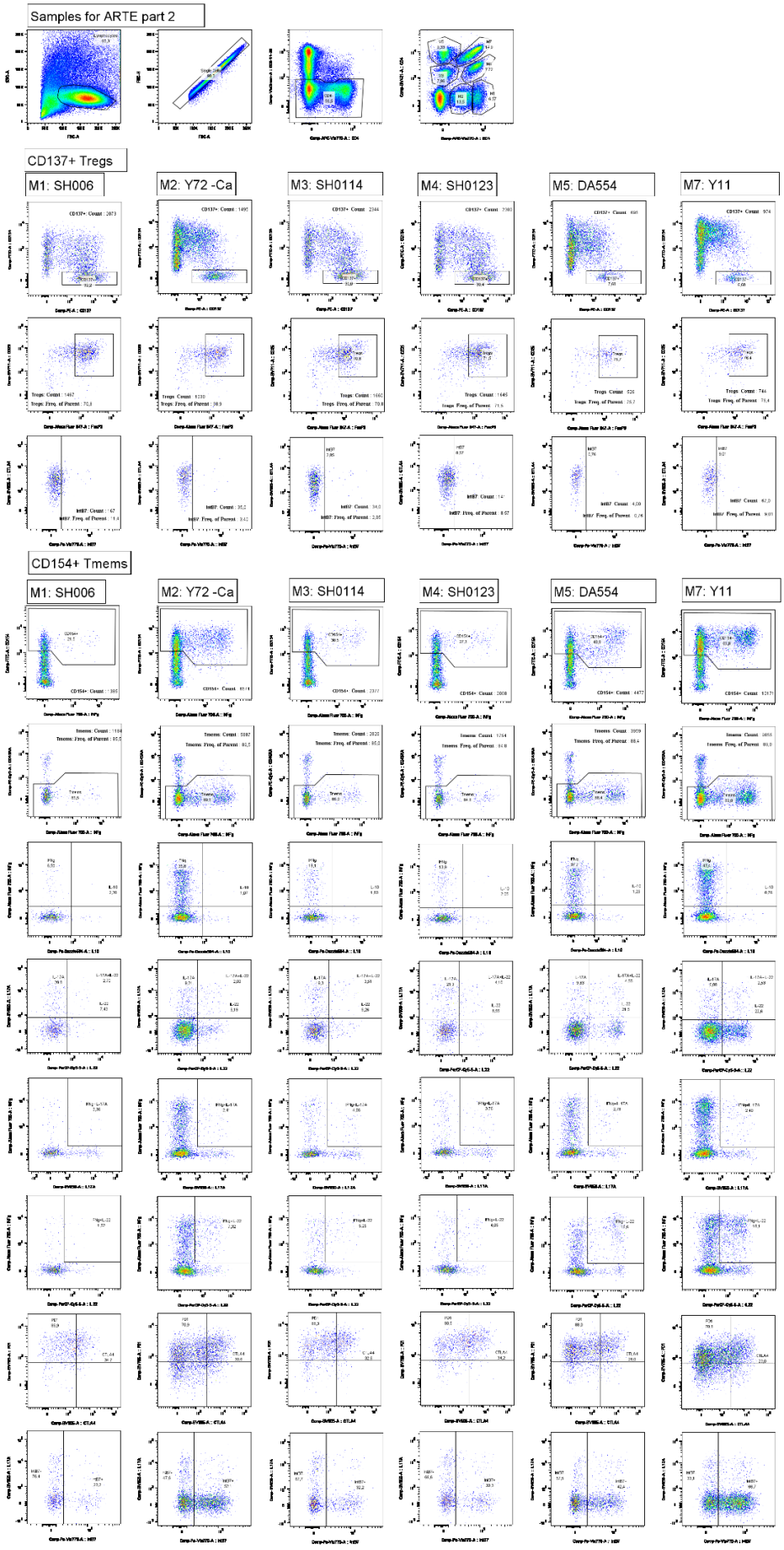

Figure 66: Dot plots ARTE Assay, Leukocyte Reduction System (LRS) Donor number 2079 Part 2

Consumables

Table 20: Table of consumables used for this project

Product	Supplier
96-Well Plates, flatt bottom	Greiner Bio-One GmbH,Kremsmünster, Austria
Amicon™ Ultra-15 Centrifugal Filter Units	Merck KGaA, Darmstadt, Germany
Bacillol	PAUL HARTMANN AG,Heidenheim an der Brenz, Germany
BTS Standard	Bruker Corporation, Massachusetts, USA
Cell spatula	TPP Techno Plastic Products AG, Switzerland
Chocolate agar PolyViteX	Biomérieux, Marcy-l'Étoile, Frankreich
Columbia agar + 5% sheep blood	Biomérieux, Marcy-l'Étoile, Frankreich
Cuvettes, semi-micro	Sarstedt AG & Co. KG, Nürnbrecht, Germany
CyroBank Tubes	Mast Diagnostica GmbH, Reinfeld, Germany
DNa Isolation Kit	Qiagen N.V., Venlo, Netherlands
DNeasy PowerSoil Pro Kit	Qiagen N.V., Venlo, Netherlands
Erlenmeyer Flasks 1000ml, 500ml	Thermo Fisher Scientific, Waltham, MA, USA
	Schott Duran AG, Mainz, Germany
	SOLAB Laborgeräte GmbH, Eschau, Germany
Flasks	Schott Duran AG, Mainz, Germany
Gas (85% N2, 10% CO2, 5% H2)	Air Liquide S.A, Paris, France
Gloves Nirtyl, Nitra-Tex	Ansell, Brussels, Belgium
Gloves Vinyl	Meditrade GmbH, UK
Hungate Tubes	VWR GmbH, Radnor, PA, USA
Injection bottles (empty)	Deltamedica, Reutlingen, Deutschland
Inoculation Loop	Sarstedt AG & Co. KG, Nürnbrecht, Germany
Isana Vaseline	Dirk Rossmann GmbH, Burgwedel, Germany
Kim wipe, precision wipes	Kimberly-Clark Worldwide, Inc, Neenah, WI, USA
LC 480 multiwell plate 96, white	Roche Holding AG, Basel, Schweiz
LC 480 Sealing Foil	Roche Holding AG, Basel, Schweiz
LightCycler 480 Instrument II	Roche Holding AG, Basel, Schweiz
PARAFILM® M Laboratory film	Pechiney Plastic Packaging Inc., Chicago, IL, USA
Pipett Tips 1-10µl, 10-100µl, 100-1000µl	Starlab International GmbH, Hamburg, Germany
	Sarstedt AG & Co. KG, Nürnbrecht, Germany
Protein LoBind Tube 1ml, 2ml	Eppendorf AG, Hamburg, Germany
Reaction Tube 1ml, 2ml	Sarstedt AG & Co. KG, Nürnbrecht, Germany
RNA Isolation Kit	Macherey-Nagel GmbH & Co. KG, Düren, Germany
serological pipettes	Greiner Bio-One GmbH,Kremsmünster, Austria
Stericup Quick Release 0.22µm, Millipore Express	Sigma-Aldrich, St. Louis, MO, USA
Sterillium	BODE Chemie GmbH, Hamburg, Germany
Syrringe 5ml, 20 ml	BD Chemicals, South Africa
Tissues	Tapira, GVS Group, Germany
	Abena, Zörbig, Germany
Transfer Pipette	Sarstedt AG & Co. KG, Nürnbrecht, Germany
Trash Bags	Th. Geyer Ingredients GmbH & Co. KG, Höxter, Germany

Tubes 15 ml, 50 ml	Sarstedt AG & Co. KG, Nürnbrecht, Germany
Whatman™ Filter 0.2µm	Cytiva, Massachusetts, USA

Chemicals

Table 21: Table of chemicals used for the experiments in this thesis

Chemical	Supplier
Acetic acid (glacial)	Merck KGaA, Darmstadt, Germany
Acetonitril 50%, Water 47.5% and TFA 2.5%	Honeywell, Riedel-de Haen
alpha-cyano-4-hydroxycinnamic acid	Sigma-Aldrich, St. Louis, MO, USA
Bacto Agar 454 g	Becton Dickinson Medical Systems, Franklin Lakes, NJ, USA
Beta-D-Glucan, from barley	Sigma-Aldrich, St. Louis, MO, USA
beta-Mercaptoethnol for molecular biology	AppliChem GmbH, Darmstadt, Germany
Biotin	Sigma-Aldrich, St. Louis, MO, USA
BTS Standard	Bruker Corporation, Massachusetts, USA
CaCl2 * 2H2O	Merck KGaA, Darmstadt, Germany
Casitone	Becton Dickinson Medical Systems, Franklin Lakes, NJ, USA
cOmplete Proteoase Inhibitor tablets, EDTA-free	Sigma-Aldrich, St. Louis, MO, USA
D-(-)-Frutcose	Sigma-Aldrich, St. Louis, MO, USA
D(+)-Glucose	Merck KGaA, Darmstadt, Germany
D-Ca-panthothenate	Sigma-Aldrich, St. Louis, MO, USA
Dulbecco's phosphate buffered saline (DPBS)	Gibco, Thermo Fisher Scientific, Waltham, MA, USA
Ethanol, >= 96% vergällt	Carl Roth GmbH, Karlsruhe, Germany
Ethanol, 80%	Th. Geyer Ingredients GmbH & Co. KG, Höxter, Germany
Folic Acid	Sigma-Aldrich, St. Louis, MO, USA
Formic Acid 98-100%	Sigma-Aldrich, St. Louis, MO, USA
Glycerol	Sigma-Aldrich, St. Louis, MO, USA
Guadinium Hydrochlorid	Sigma-Aldrich, St. Louis, MO, USA
HCL, 25%	Supelco, Merck KGaA, Darmstadt, Germany
Hemin, from Porcine	Sigma-Aldrich, St. Louis, MO, USA
Hepes	Sigma-Aldrich, St. Louis, MO, USA
Hirn-Herz-Glucose-Bouillon (BHI)	Carl Roth GmbH, Karlsruhe, Germany
Isobutyric acid, 99%	Sigma-Aldrich, St. Louis, MO, USA
Isovaleric acid, 99%	Sigma-Aldrich, St. Louis, MO, USA
K2HPO4	Merck KGaA, Darmstadt, Germany
KH2PO4	Sigma-Aldrich, St. Louis, MO, USA
Laminarin	Sigma-Aldrich, St. Louis, MO, USA
L-Cystein-HCl-H2O	SERVA Electrophoresis GmbH, Heidelberg, Germany
Lipoic acid	Sigma-Aldrich, St. Louis, MO, USA
Lysozyme from chicken egg white	Sigma-Aldrich, St. Louis, MO, USA

Magnesium Sulfate Hepta Hydrate	Merck KGaA, Darmstadt, Germany
Methanol	Merck KGaA, Darmstadt, Germany
Monti-Graziadei solution	Provided by C. Örün, Anatomie Lübeck
Mucin from porcine stomach, Type 2	Sigma-Aldrich, St. Louis, MO, USA
NaCl	Merck KGaA, Darmstadt, Germany
NaHCO3	Merck KGaA, Darmstadt, Germany
NaOH, 10mM	WTW, Xylem Analytics Germany Sales GmbH & Co. KG, Weilheim, Germany
Nicotinic acid >=98%	Sigma-Aldrich, St. Louis, MO, USA
p-aminobenzoic acid	Sigma-Aldrich, St. Louis, MO, USA
Peptone/Tryptone	Gibco, Thermo Fisher Scientific, Waltham, MA, USA
Propionic acid, >=99,5%	Sigma-Aldrich, St. Louis, MO, USA
Pyridoxine-HCL	Sigma-Aldrich, St. Louis, MO, USA
Resazurin	Sigma-Aldrich, St. Louis, MO, USA
Riboflavin	Sigma-Aldrich, St. Louis, MO, USA
Strach, soluble	Sigma-Aldrich, St. Louis, MO, USA
Sucrose	Sigma-Aldrich, St. Louis, MO, USA
TE Buffer pH8.0	Invitrogen, Thermo Fisher Scientific, Waltham, MA, USA
TFA	Merck KGaA, Darmstadt, Germany
Thiamine HCL	Sigma-Aldrich, St. Louis, MO, USA
Valeric acid, >=99%	Sigma-Aldrich, St. Louis, MO, USA
Vitamin B12	Sigma-Aldrich, St. Louis, MO, USA
Yeast Extract	Becton Dickinson Medical Systems, Franklin Lakes, NJ, USA

Devices

Table 22: Table of devices used for this project

Product	Version	Supplier
Anaerobe Workstation	H35	Don Whitley Scientific, Victoria St, UK
Autoclave	S1000	Matachana Germany GmbH, Selmsdorf, Germany
Centrifuges	5427 R	Eppendorf SE, Hamburg, Germany
	Rotina 38R	Hettich, Tuttlingen, Germany
	Biofuge fresco	Heraeus Instruments GmbH, Hanau, Deutschland
Diaphragm Vacuum pump	ME 2	Vacuumbrand GmbH + CoKG, Wertheim, Germany Werner Hassa GmbH, Lübeck, Germany
Fluorometer	Qubit 2.0	Invitrogen, Waltham, MA, Vereinigte Staaten
Freezers	Ultra low -80°C	Sanyo, Leicesterhsire, UK
	Ultra low -80°C	Thermo Fischer Scientifitc, Waltham, MA, USA
	-20°C	Liebherr, Biberach an der Riß, Germany
	-20°	Bosch, Munich, Germany
Fridge	Profiline	Liebherr, Biberach an der Riß, Germany
Heating plate	MR 3001 K	Heidolph, Schwabach, Germany

Inkubator (37°C)	H2200-H	Benchmark Scientific, Edison, USA
Light Cylcer	480	Roche Holding AG, Basel, Schweiz
Maldi Biotyper	MBT smart	Bruker Corporation, Massachusetts, USA
Microplate reader	Epoch 2	BioTek, Agilent, Santa Clara, USA
NanoPhotometer	P330	Implen, München, Germany
pH Meter	MP220	Mettler Toledo, Seeth-Ekholt. Germany
Pipettes	10µl, 100µl, 1000µl	Eppendorf SE, Hamburg, Germany
PowerLyzer	24 Homogenizer	Qiagen N.V., Venlo, Netherlands
Quick cooking pot	Perfect 6.5 l	WMF, D-73312 Geislingen/Steige
Scale	KB 600-2/ EMB 3.6	Kern, Ascuro Service GmbH, Lörrach, Germany
Shaker, Incubator	TH 30	Edmund Bühler GmbH, Bodelshausen, Germany
Sterile Workbench	EN 12469	Clean Air Techniek B.V. Woerden, Niederlande
	PCR workstation pro	Preqlab, Darmstadt, Germany
Ultrazentrifuge	Optima L70	Beckman Coulter GmbH, Krefeld, Germany
Vortexer	Reax Top	Heidolph, Schwabach, Germany

7. Acknowledgments

Firstly, I would like to thank my doctor father and first supervisor Prof. Dr. Jan Rupp making this project possible and for providing me the opportunity to carry out my thesis at his institute. His scientific input and experimental innovations were enormous helpful, important and insightful during this project.
Special thanks to my second referee and the chair person (third referee) for their time and help during the final steps of my thesis and the defence.
I would also like to thank Dr. Simon Graspeutner for his supervision, the brainstorming and troubleshooting during the project. A great thanks goes to the miTagret cooperation partners. Thanks to Prof. Dr. Andreas Tholey (Co-Supervisor) and Jerome Genth for the proteomic analysis and data support (Institute for experimental medicine, CAU/ UKSH Kiel). Thanks to Dr. Silke Heinzmann and Dr. Alesia Walker for the metabolome analysis and collaboration (Helmholtz Zentrum München GmbH, AG Analytical BioGeoChemistry). And special thanks to Prof. Dr. Petra Bacher and Stephan Schneiders for the immunophenotyping with the ARTE assay and to Theresa Dittmers for exporting all the data retrospectively (Institute of Clinical Molecular Biology, CAU/UKSH Kiel).

Thanks to Christi Orün (Institute of Anatomy, UzL) for the electron microscopy pictures, which provided great insight into the bacterial morphology. Many thanks to all members of AG Rupp and AG Nurjadi for the shared workspace, nice lunch breaks and all the support in the lab. A special thanks to Dr. Sebastien Boutin for the transcriptomics analysis and support, to Dr. Kensuke Shima for establishing the contact to C. Orün and providing consultation at any time and Erik Winzheim for the RNA isolation.
I am also very thankful having Gretchen Ruschman (University of Kentucky, USA) as my intern from the Rise Scholarship, she generated most of the data for *B. longum* in this thesis during her internship. I also would like to mention the organisers of the science communication certificate, which provided me the opportunity to develop additive skills. This opportunity was provided me, since I am a member of the RU miTarget in Kiel. miTarget also provided additional training, workshops, summer schools and symposium, which I am thankfully participated.
A big special thanks goes to my (former) office colleagues Celeste Scholz, Laura Kirchhoff, Lea Semmler und Lisa Göpel for the scientific advice on my posters and presentations, the warm teas, the cold ice-coffees and the encouraging talks during these pandemic-driven times. Likewise, thanks to Mariia Lupatsii for the great Anbox trouble shooting and Thanksgiving dinners. I'd like to specially thank Maria Hänel, Lea Semmler and Celeste Scholz, who read and corrected my thesis, for their input, their patients and time!
Another thanks goes to my friends from my home town (Alice, Anna, Annika, Christina, Daria, Ina, Irem, Jana, Julia, Jonas, Maria, Nicole and Vanessa). Having those friendships since school is not a matter of

course and staying in touch, updating on each other's life and celebrating the small or big success in life, helped me a lot. As well, thanks goes to my friends from my study times, who know my academic journey from the start and always helped me personally and my career on so many different levels (Fine, Franzi, Jesslyn, Jolena, Katrin, Louisa and Tristan). Thanks to Lisa, my former neighbour and dearest friend in Lübeck, and thanks to Juliana for the inspiring conversations during our car rides to Kiel. Lastly, I would like to thank my family. I am very grateful to have such pleasant relationships with my mum and dad, who always encouraged me to follow this path. I am also incredibly grateful to have my brother Nils, sister-in law Mel and my nephew Levin; it is always such a joy to spend time with them. Thanks to my grandma, who always send packages with food from my home town and thanks to my grandpa, who is sadly not able to see me finish this and is dearly missed.